AN INVESTGATION INTO THE POST IMPACT AND POST INDENTATION BEHAVIOUR OF AUXETIC COMPOSITES

Submitted in accordance with the requirements for the Degree of Doctor in Philosophy by:

SALMAN AZIZ

2016

Institute of Materials Research and Innovation (IMRI)

In the name of Allah the Most Gracious the Most Merciful

DECLARATION

This work has not been previously accepted in substance for any degree and is not concurrently submitted in candidature of any other higher degree.

Dedication

I would like to dedicate my thesis to my beloved mother.

ABSTRACT

Composites have been extensively used in high performance structural applications due their lightweight and better strength to weight ratio. A common defect in angle ply laminates is caused by the low velocity impacts, due to their poor resistance to accidental impact by foreign objects, and also the defect is barely visible. Actually contact zone between the target and the penetrating object is relatively large and the whole structure is affected even well away from the impact point. This type of interaction can generate large delaminations, which can reduce the strength under compressive loading. At present, allowance for the delamination induced strength reduction is given by maintaining the strain limits to the structures that prevent the failure due to delamination. If any damage is found in the structure, it is not easy to repair due to the larger damage area.

Carbon auxetic composites can be considered as good candidate materials with special properties required for today's modern technology. This thesis presents the study of auxetic laminates and their response to low velocity multiple impact events in order to assess the damage behaviour of the laminates. These materials are of great interest because the damage area created is smaller, which does not affect the whole structure as compared to the conventional carbon laminates.

As received unidirectional 12k tow fibre reinforced, high performance (IM7/8552), epoxy resin pre-preg, which one of the stiffest fibre matrix systems, was used to prepare 24-layers auxetic and positive Poisson's ratio laminates. This work focuses on four stacking sequences; all through-thickness auxetic and positive Poisson's ratio laminates were prepared with $[\pm 30]_s$ and [35/-20/25/40/-85/40/25/-

45/35/-15/25/40]$_s$ angles, respectively. Stacking angles for the in-plane auxetic and positive Poisson's ratio laminates were designed as [0/15/75/15]$_s$ and [0/-70/10/25]$_s$ respectively. These laminates were cured by vacuum bagging technique before testing in order to achieve the highest quality specimens. All the tests presented in this work are conducted on 100mm^2 squared size specimens, by using a standard 12.7mm steel hemisphere indentor. In this work multiple indentation and impact tests were conducted both at the initial test site and also away from the initial test site to determine the extent of damage zone.

The most important conclusions and findings drawn from the experimental results are as follows. From the low velocity multiple impacts, indentation testing, fractography, residual testing and dynamic analysis it can be concluded that through-thickness auxetic laminates are found to be better than the positive Poisson's ratio laminates, even though they were tested 20mm away from the vicinity of the initial test site. Their confined damage area can prevent the structure from catastrophic failure because the damage is more concentrated at the test site and is easy to repair due to the smaller damage area. A preliminary study into the high velocity impact on the through-thickness laminates and the low velocity impacts on the in-plane laminates was also carried out in order to study their impact response. Here, auxetic and the positive Poisson's ratio laminates show almost similar damage response to the high velocity impacts. However, auxetic in-plane laminates were found to have better resistant to an impact event as compared to the positive Poisson's ratio specimens.

ACKNOWLEDGEMENT

During course of completion the project objectives, many people assisted me and offered their support. I would like to express my sincere appreciation to my supervisors, Prof. Tahir Shah and Prof. Kim Alderson who helped me with their moral support, useful time and expertise in auxetic and polymeric materials. They guided me in right directions in spite of their busy schedules. I would also extend my appreciation to my second supervisor Prof. Andrew Alderson who helped me with his expertise and useful discussions which contributed to the solution of some of my problems in the project. This list would be incomplete if I do not thank my lab support staff, A. Zarie and all, for making cheerful working environment. I would like to express my gratitude to University of Bolton for providing me studentship to work on this project.

I have no words to express the gratitude and love I owe to my parents, brothers and sisters. I express my thanks to my wife, Aisha and our son Musa, for their moral support, and getting over all difficulties with me. I think this achievement is a small return for their constant support. Last but not least I would like to thank all my friends who have helped me directly or indirectly to complete this project with a sense of satisfaction.

LIST OF FIGURES

LIST OF TABLES

GLOSSARY

Angle-ply	Lamination method using plies of opposing fibre direction.
Anisotropic	Having different mechanical properties in different directions.
Coupon	Test Specimen used to obtain laminate mechanical properties.
Cure-cycle	Specific combination of pressure, vacuum and temperature to bond the layers of pre-preg.
CV	Coefficient of Variation
Debond	Area where two laminae have not bonded or are separated.
De-bulk	Consolidation of a few laminated plies with vacuum to ensure minimal voids and a quality bond.
Delamination	Form of damage, separation of adjacent laminae.
Fracture Toughness	Resistance of a material to crack growth.
Indentation Resistance	Resistance of a material's surface to the penetration of an object.
Interlaminar	Between the layers of a laminate (thickness direction).
Intralaminar	Across the layers of a laminate (transverse direction).
Isotropic	Having the same mechanical properties in all directions.
Laminate	Cumulative layers of pre-preg bonded together.
Orthotropic	Having the same properties in orthogonal directions.
Pre-preg	Long strand of fibres, impregnated with Resin, rolled onto a reel.
Release Agent	Spray or fabric that prevents bonding of the laminate resin to mould surfaces.
Stacking Sequence	Specific arrangement of oriented plies to give required mechanical properties in a laminate.

Void	An air pocket or gap within the lay-up that can be detrimental to mechanical properties.

Acronyms and abbreviations

a	longitudinal extension
2a	diameter of indentor
b	longitudinal extension
K	Bulk Modulus
E_{ijkl}	Constitutive tensor
E	Young's Modulus
G	Shear Modulus
G_I	Mode I Interlaminar Fracture Toughness
G_{IC}	Critical Mode I Interlaminar Fracture Toughness
H	Hardness
K	Stiffness
k_I	Plane strain Fracture Toughness
k_{IC}	Critical stress intensity factor
L	Applied axial Load
N	Negative auxetic specimen
P	Positive specimen (conventional composite)
t	thickness
ν	Poisson's ratio
σ	Stress
σ_c	ultimate stress

σ_L longitudinal stress

ε strain

ε_c ultimate strain

ε_L longitudinal strain

[....] Denote a sequence of ply orientation

[....]$_S$ The subscript's' indicates symmetry

[....]$_T$ The subscript 'T' sometimes indicates total laminate lay up

$|\mathbf{C}|$ Laminate Stiffness Matrix

$|\mathbf{S}|$ Laminate Compliance Matrix

x, y, z Global coordinate system of laminate

i, j, k, l Tensor notation counting 1 to 3

Subscripts used:

1. Longitudinal Direction or parallel to the fibre direction (also '**x**')
2. Transverse Direction/In-plane perpendicular to fibre (also '**y**')
3. Normal to the plane of ply or Through-Thickness Direction/out-of-plane (also '**z**')

CONTENTS

2 INTRODUCTION

One of the main complications to extensive use of composite materials is their susceptibility to impact damage. At low velocity impact (LVI) there is a penetration resistance due to high strain energy because strain energy is associated with deformation, delamination and matrix cracking. The low velocity impact event is accomplished with a wide contact area and is of more interest due to the tendency to produce internal damage with limited exterior visibility. The outer surface of the composite structure, however may not exhibit cracks and imperceptible levels of permanent damage[1].

The term 'composite' defines a combination of high strength and modulus continuous fibres bonded together in an organic matrix material. The degree of anisotropy can be controlled by altering the orientation of the continuous fibres within a composite to achieve the high load bearing capability in the loading direction. Therefore, the ability to tailor the degree of anisotropy offers an additional benefit and hence the directional mechanical properties are achieved in finished component. However, there is a new class of materials which have emerged over the last few decades which also offer exciting advantages over conventional materials.

This class of material was named **auxetics** by Evans[2] which have a negative Poisson's ratio[3] and comes from the Greek word *auxetos* meaning 'that which

may be increased'. The name arises from the fact that a material with a negative Poisson's ratio, increases in dimension in both the load and transverse directions on applying a tensile load. Auxetic materials have been known over 100 years with few applications. This type of material can be found in natural occurring substances i.e. some rock such as α-cristobalite and minerals, even animal such as the skin covering a cow's teats. A variety of such materials has been fabricated to date, including polymeric and metallic foams, microporous polymers and honeycomb structures. Therefore, studying these non-conventional materials is very interesting for original research and for future applications, particularly in medical such as dental floss, drug release ligament, bandages etc, in aerospace such as vanes for gas turbine engine, sound and vibration absorber etc and defense industries[3] [4] such as knee pads, protective clothing, helmet etc.

The work presented in this study is an attempt to bridge the gap of understanding between the multiple impact events in laminate stacking sequences with negative through-thickness and in-plane Poisson's ratio. Specimens are made with different stacking sequences to match the modulus value and tested over a range from the indentor nose region to the direction of damage and opposite to the direction of damage with the same indentor and support conditions. It is known that carbon fibre composites exhibit similar impact resistance and subsequent damage mechanism upon multiple impact events[5]. In this context the auxetic composite offers a significantly different mechanism, when studied together with the conventional carbon composites. Therefore, the knowledge and response of the impact event under the indentor nose and in the vicinity of the nose region

is an essential step in understanding the impact resistance away from the indentor nose region upon multiple impacts.

Previous, work has investigated the effect of the through-thickness Poisson's ratio on the fracture toughness and indentation resistance[6] of angle ply laminates under the indentor nose region only. The results so far have been encouraging with enhancements observed for axuetic laminates when re-tested away from the indentor nose region.

1.1 Thesis Objectives

The main aim of this project is to investigate the post impact behaviour of the auxetic carbon fibre composite materials. The proposal here is that auxetic laminates will show very much less damage and so retain their properties away from the indentor nose region, being easier to repair. In particular, the following objectives were examined for the first time and in detail:

- To conduct a pilot study on laminate configurations to identify the matched modulus of the auxetic and conventional configurations and their production for this work
- To perform a study into post quasi-static indentation of carbon composites away from the indentor nose region to evaluate and compare the response.

- To experimentally investigate the energy absorption capability of auxetic composites at failure and post failure in comparison with a positive Poisson's ratio but matched modulus.
- To examine the effect of low velocity impact damage away from the indentor nose in auxetic and matched modulus carbon fibre composite laminates.
- To conduct a preliminary study into high velocity impact damage behaviour of through-thickness auxetic and conventional laminates
- To use analytical dynamic analysis to investigate the low velocity impact response of auxetic and matched modulus laminates.
- To evaluate the residual properties of the laminates to find energy absorption capability.
- To perform the detailed micrography analysis of quasi-static and low velocity tests to examine the damage.

1.2 Structure of the Thesis

The main focus of this research work was to develop and investigate the auxetic in-plane and through-thickness carbon epoxy composites in order to provide a detailed understanding and comparison with conventional composites. In this work the post impact behaviour of the laminates was studied, not only under the nose but also in the vicinity of the indentor nose region to evaluate the effects of damage created because these are the candidate materials for primary structural components of aerospace industry.

The report of this research work is divided in to 7 chapters.

Chapter 1 contains the background and motivation of this work, the defined problem that has been dealt with, and the objectives of the thesis. This part is concluded with the scope of the work.

Chapter 2 describes; the auxetic composites, manufacturing, vacuum bagging, impact and indentation behaviour of carbon laminates, damage mechanism and the literature review on these specific technologies and materials.

Chapter 3 details on the introduction to materials, manufacturing methods, test equipment and methods used to characterise the resulting materials.

Chapter 4 presents the general results for all the experimental work carried out on the auxetic laminates and to compare them with the conventional laminates. It includes, characterization of the material using low velocity impact test (Instron Dyntaup® Model 9250HV Drop Tower Impact Tester), quasi-static indentation test (DARTEC Universal Hydraulic Indentation Testing Machine), damage analysis (Olympus SZ30-series zoom stereo microscope) and residual strength (ASTM D7137/ D7137M-05). The novelty of this chapter is the comprehensive study of the low velocity impact, post impact behavior under and away from the indentor nose region. A preliminary study

into high velocity impact on through-thickness laminates and low velocity impacts into in-plane lamintes was also launched to study their response on failure. This chapter presents all the results but detailed analysis of these results has been given in discussion chapter.

Chapter 5 describes the analytical dynamic analysis of the low velocity impact data including the results achieved in indentation tests. Detailed analysis in comparison with the other tests has been given in discussion chapter.

Chapter 6 examines all the experimental results, findings and observations made in this work in the form of discussion.

Chapter 7 introduces the overall conclusions that summaries the significance and novelty of the presented work with some important topics addressed for further investigation and development.

2 LITERATURE REVIEW

This chapter firstly sets out the definitions required when dealing with unidirectional carbon composite materials and then describes the elastic properties and Poisson's ratios in such bodies. A review of the literature follows, covering work done on the definition of the bounds on Poisson's ratio values in laminated fibre reinforced materials and how these bounds have been verified against the experimental data over the years. Then follows a review of the literature that deals with the work done to examine the behaviour of both the in-plane and through-thickness negative Poisson's ratios and how the occurrence and effects of negative Poisson's ratios have been modelled and measured.

2.1 Composite Materials

The development of advanced fibres in the late 1950s started a race to produce fibre reinforced composites [7], [8], [9]. Composite materials have great advantages, including light weight, improved fatigue life and corrosion resistance along with specific layups for optimum strength and stiffness and low assembly cost due to fewer parts for the final structure [10]. The specific strength (strength/density) and specific modulus (modulus/density) of high strength carbon fibres are higher than those of other competitor materials (see Figure 2-1). This explains the strength-to-weight ratio resulting in fuel savings, better performance and greater load bearing capability. Many important primary structural parts [11] have been manufactured from carbon fibre

reinforced composites. During the last two decades, the enhancement in computing power has made possible a great advancement in the selection of the structural materials and application of carbon fibre reinforced composites have been extended to complex [12] geometries including primary load transferring components.

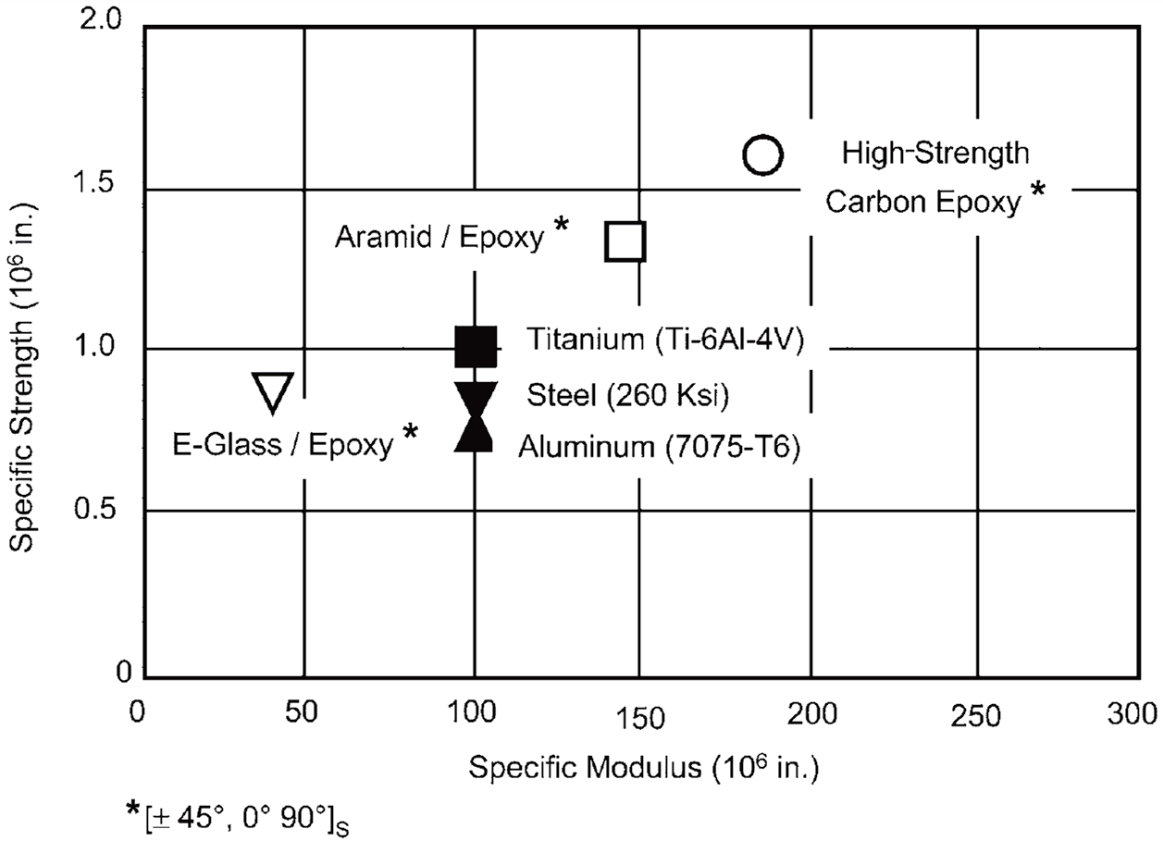

Figure 2-1 **Comparison of specific strength and modulus of high strength composites and some aerospace alloys**[10]

In recent years' composites have successfully replaced conventional materials in commercial structural assemblies. The most weight concerned, the aerospace [13] sector, is using composites to build structures like aircraft nose-cones, tails[14] or fuselages. Composite materials are excessively used in the primary structures and in the airframe of Boeing 787 compared with any

previous Boeing commercial airplane[15]. It should be noted that composites are not as efficient in carrying compression loads but are excellent at handling tension. Lowering the overall airplane weight, moving to a composite primary structure promises to reduce both the scheduled and non-routine maintenance burden on the airlines[15]. All small and large commercial aircrafts heavily rely on composites to decrease weight and increase fuel performance, the most significant example being the 50 percent composite airframe, the new Boeing 787 (see Figure 2-2) and A350 Airbus. In future all Airbus and Boeing aircrafts will use large amounts of high-performance composites [16], [14].

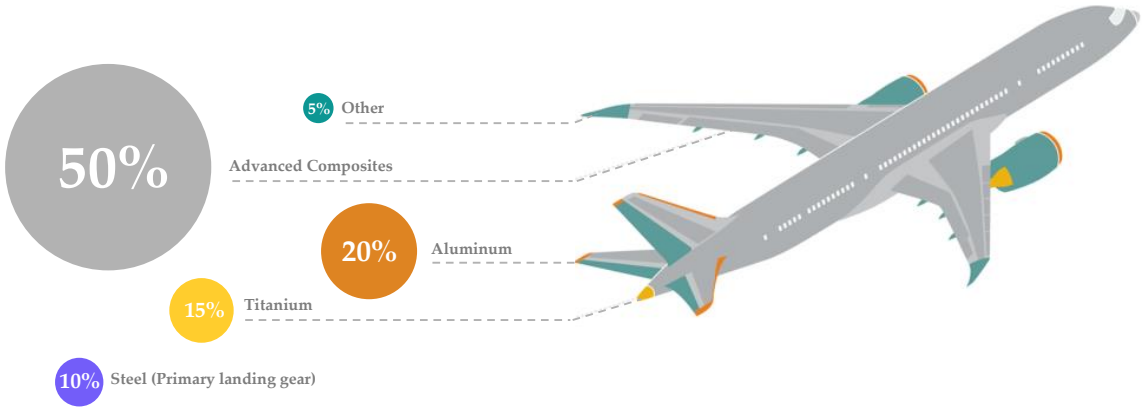

Figure 2-2 **Boeing 787 Dreamliner commercial airplane Source: The Boeing company**

2.2 Classification of Terms

Unidirectional fibre composites are promising materials, where high strength, stiffness, extraordinary durability and low weight are required. This behaviour contrasts with a metal or materials with randomly distributed grains. There are several terms which require definition; bulk materials such as metals and polymers are usually treated as isotropic materials while

composites are treated as anisotripic materials. Unidirectional composites can be used to predict the behaviour of continuous fibre multi-directional angle ply laminates. If the ply (see Figure 2-3) is loaded parallel to the fibres (0^o i.e 'x' direction), the modulus of elasticity E_{11} approaches that of the fibers. If the ply is loaded normal to the fibres in the 90^o i.e 'y' direction, the modulus E_{22} is much lower, approaching that of the relatively less stiff matrix. Since $E_{11} >> E_{22}$ and the moduli vary with the direction ($E_{0^o} \neq E_{45^o} \neq E_{90^o} \neq E$) within the material, the material is anisotropic, however the material is isotropic if the properties ($E_{0^o} = E_{45^o} = E_{90^o}$) are independent of direction within the material.

Composites are considered a subcategory of anisotropic materials that are classified as orthotropic. These materials show different properties in three mutually perpendicular directions. They have three mutually perpendicular axes of symmetry, and a load applied parallel to these axes produces only normal strains. However, if loads are not applied parallel to these axes, they produce both normal and shear strains. Therefore, orthotropic mechanical properties are a function of orientation.

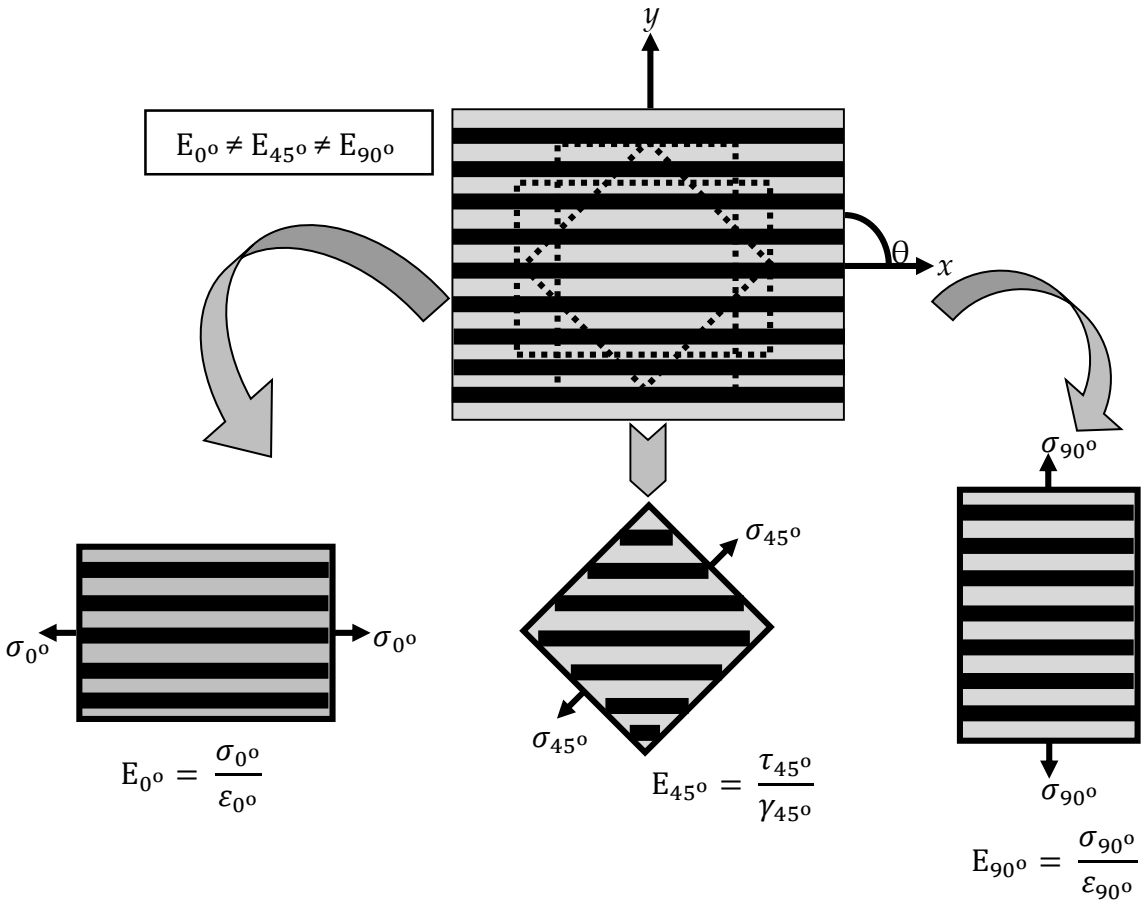

Figure 2-3 Element of anisotropic unidirectional ply under stress

2.3 Restriction on Poisson's ratio

It is well known that Poisson's ratio (named after the French mathematician, Simeon Dennis Poisson 21 June 1787-25 April 1840) [3], [17] is defined by the ratio of the transverse contraction strain ($\boldsymbol{\epsilon_2}$) to the longitudinal extension strain in ($\boldsymbol{\epsilon_1}$) a simple tension condition [18], [19].

$$\boldsymbol{\nu} = -\frac{\boldsymbol{\epsilon_2}}{\boldsymbol{\epsilon_1}} \qquad \textbf{Equation 2-1}$$

Since most engineering materials become thinner in cross section when stretched, (see Figure 2-4) Poisson's ratio in this situation is positive. The reason is that the inter-atomic bonds realign with deformation. However, some materials or structures contract in the transverse direction under uniaxial compression, or expand laterally when stretched, (see Figure 2-4). These materials or structures are said to have negative Poisson's ratio or to be auxetic.

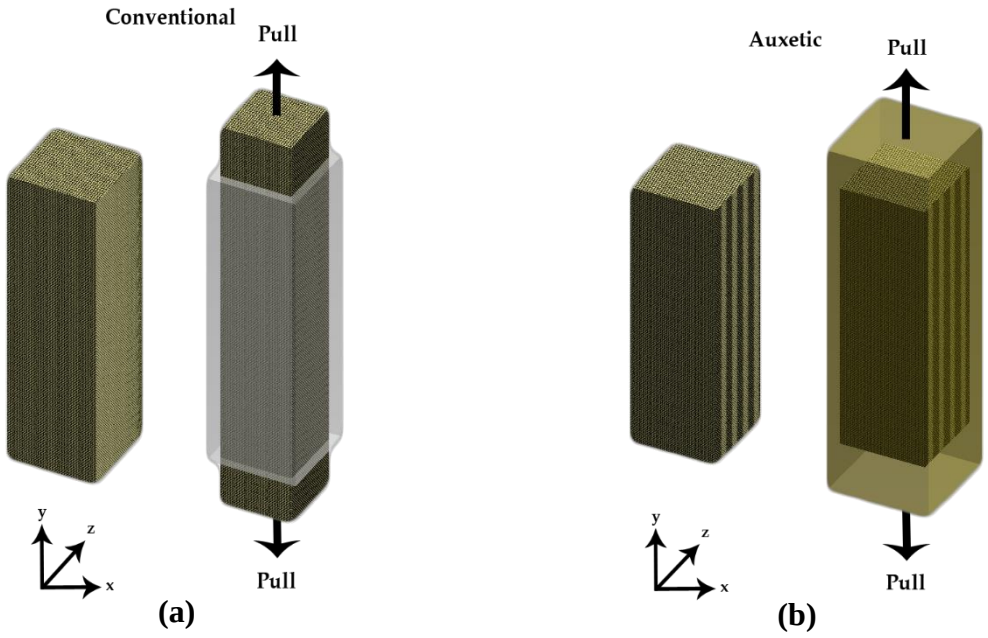

Figure 2-4 **(a) Deformation with positive Poisson's ratio**
(b) Deformation with negative Poisson's ratio with stretched

This behaviour does not contradict the classical theory of elasticity: based on the thermodynamic considerations of strain energy, the Poisson's ratios of isotropic materials can not only take negative values, but can have a range of negative values twice that of positive ones [18]. That is, the Poisson's ratio is bounded by two theoretical limits: it must be greater than -1, and less than or equal to 0.5, i.e.,

$$-\mathbf{1} < \nu \leq 0.5 \qquad \textbf{Equation 2-2}$$

The upper bound of the Poisson's ratio corresponds to rubber-like materials with an infinite bulk modulus [20], while the lower bound stands for an infinite shear modulus. In the case of isotropic elasticity, mechanical behaviour is described by any couple of parameters among these: Young's modulus E, Poisson's ratio ν, the bulk modulus K and Lamé's coefficients λ and G (also referred to as the shear modulus). Material stability requires the tensor of elastic moduli to be positive definite, resulting in a positive Young's modulus E and a Poisson's ratio ν ranging from −1, for unshearable materials, and 0.5 for incompressible or rubber like materials. Although as noted above materials naturally present a positive Poisson's ratio, negative Poisson's ratio materials, or auxetic [21], have been engineered since the mid-1980s with the pioneering works of [20], [22]–[24]. This new class of materials has been drawing more and more attention since then [25]–[29] due to their potential applications [3].

Auxetic materials show a unique characteristic [30]–[35] and exhibit higher resistance to shear strain. Shear resistance is mainly significant in structural applications [36]–[38] such as sheets or beams in buildings, cars and aircraft. According to continuum mechanics, most materials resist a change in volume as determined by the bulk modulus K more than they resist a change in shape, as determined by the shear modulus G. This aspect can be qualitatively

described by the relations [39], [40] between the shear (or rigidity) modulus G, the Young's modulus E, the bulk modulus KB (the inverse of the compressibility) and Poisson's ratio (ν). For isotropic material, the relations are [41], [42].

$$\mathbf{G} = \frac{\mathbf{E}}{\mathbf{2(1+\nu)}} \qquad \textbf{Equation 2-3}$$

and

$$\mathbf{K} = \frac{\mathbf{E}}{\mathbf{3(1-2\nu)}} \qquad \textbf{Equation 2-4}$$

Combining Equation 2-3and Equation 2-4 the following relation is obtained

$$\frac{\mathbf{(1+\nu)}}{\mathbf{(1-2\nu)}} = \frac{\mathbf{3K}}{\mathbf{2G}} \qquad \textbf{Equation 2-5}$$

A graphical representation of this relationship is shown in Figure 2-5. For conventional structural engineering materials, the value of K is typically larger than the value of G, which can be given;

$$\frac{\mathbf{(1+\nu)}}{\mathbf{(1-2\nu)}} \geq \frac{\mathbf{3}}{\mathbf{2}} \qquad \textbf{Equation 2-6}$$

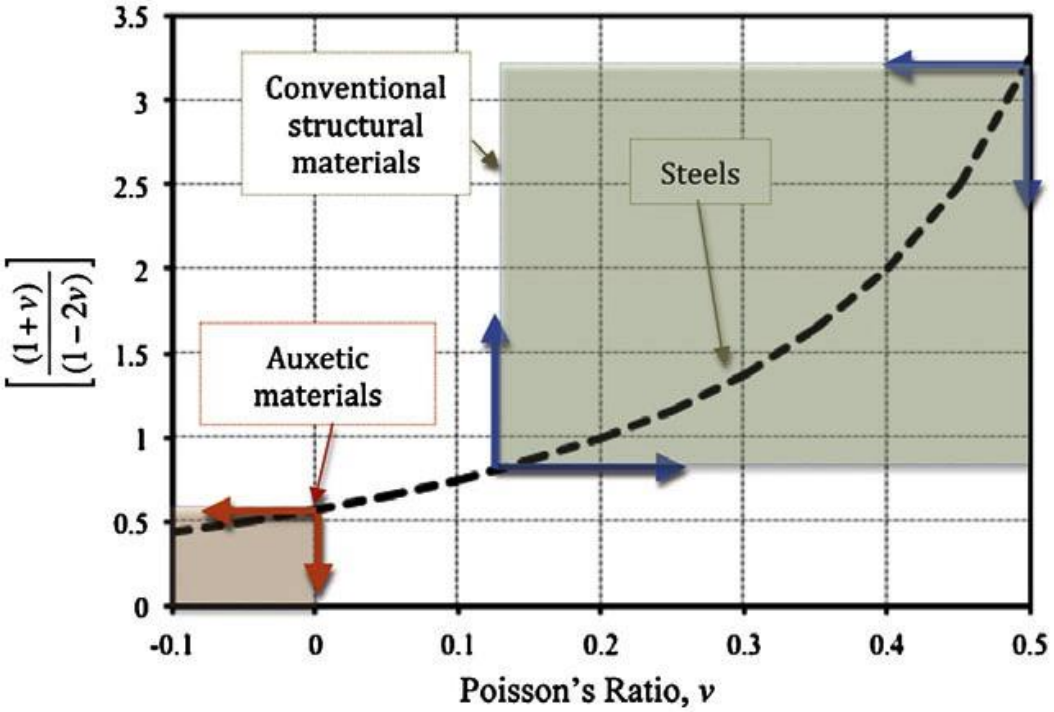

Figure 2-5 Relationship between Poisson's ratio and the value of $\frac{(1+\nu)}{(1-2\nu)}$ for conventional structural materials [42]

This restricts a conventional structural material to have its Poisson's ratio to be $\nu \geq \frac{1}{8}$. For a Poisson's ratio to be an auxetic $\nu \leq 0$, the value of the bulk modulus must be much less than the shear modulus, K << G. Meanwhile, Equation 2-5 can also be expressed as:

$$\mathbf{2G(1+\nu)} = \mathrm{K}\mathbf{(1-2\nu)} \qquad \textbf{Equation 2-7}$$

or

$$\boldsymbol{\nu} = \frac{\mathbf{(3K-2G)}}{\mathbf{2G+6K)}} \qquad \textbf{Equation 2-8}$$

For $\nu \rightarrow -1$, the shear modulus G tends towards $+\infty$. This relationship holds only for isotropic materials or transversely isotropic materials when the in-plane shear modulus is considered.

Considering other properties based on the classic elasticity theory[43], the indentation resistance or hardness of an isotropic material is inversely proportional to $(1- \nu^2)$, that is:

$$\mathbf{H} \propto \left[\frac{\mathbf{E}}{(\mathbf{1}-\boldsymbol{\nu}^{\mathbf{2}})}\right]^{\boldsymbol{\gamma}} \qquad \textbf{Equation 2-9}$$

Where H is hardness, and γ is a constant and is $\gamma = 1$ stands for uniform pressure distribution and $\gamma = 2/3$ [44] is Hertzian indentation.

If ν reaches -1, the hardness approaches infinite. Hardness has been studied for many of the synthetic auxetic materials produced to date and enhancements have been observed through materials as diverse as polymeric and metallic foams [45]; [46] carbon fibre composite laminates [47] and microporous polymers [35]. Furthermore, the hardness of the auxetic microporous ultrahigh molecular weight polyethylene (UHMWPE) was enhanced up to a factor of 3 over conventional UHMWPE [35], [48]. At lower loads (e.g., 10 ~ 100N), the indentation test revealed that the hardness was enhanced [49], [50] up to a factor of 8 if the Poisson's ratio was varied from approximately 0 to -0.8 [48], [26].

Negative Poisson's ratio can also result in enhanced toughness [51]. If one now considers the growth of a penny-shaped crack within an isotropic elastic brittle material under plane-strain conditions, the fracture toughness K_c is related to Poisson's ratio [52]. The mode I (opening) fracture stress of a structure from a pre-existing flaw is proportional to

$$K_c = \sqrt{\frac{2E\gamma}{1-\nu^2}} \qquad \textbf{Equation 2-10}$$

with γ the surface energy, and E is the Young's modulus. Thus, a material with a Poisson ratio of −0.3 would exhibit fracture toughness similar to those of typical metallic materials. With Poisson's ratio close to −1 and the same Young's modulus and surface energy, the material is expected to become very tough. This particular property was investigated by Choi and Lakes [53] for the case of auxetic copper foams.

Finally, if one considers the deflection of an isotropic elastic plate subject to a prescribed curvature along direction 1, the associated curvature along direction 2 is due to the Poisson effect, thus yielding [43]:

$$R_2 = -\frac{R_1}{\nu} \qquad \textbf{Equation 2-11}$$

with R_1 and R_2 the radii of curvature of the plate respectively along directions 1 and 2.

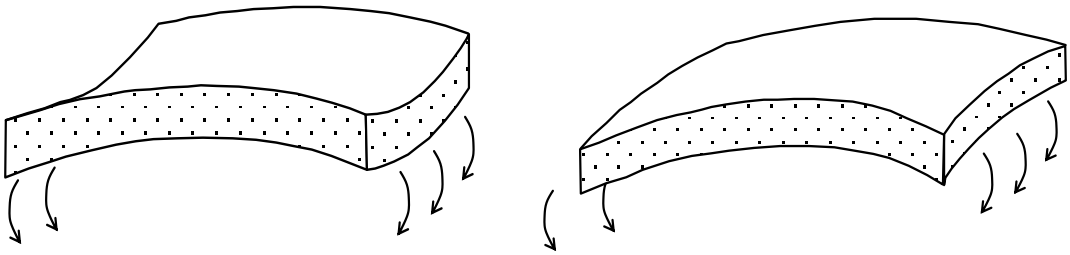

Anticlastic
(Saddle shape)
Curvature in
Conventional plate

(a)

Synclastic
(Dome shape)
Curvature in auxetic plate

(b)

Figure 2-6 (a) Anticlastic and (b) Synclastic double curvature

For conventional materials, this yields anticlastic (saddle-shaped) curvature (see Figure 2-6), whereas for auxetic materials, it yields synclastic (dome-shaped) curvature. This enables one to manufacture curved sandwich panels without core buckling. The synclastic curvature property was studied by Evans [36].

2.4 Elasticity in Anisotropic Composite Materials

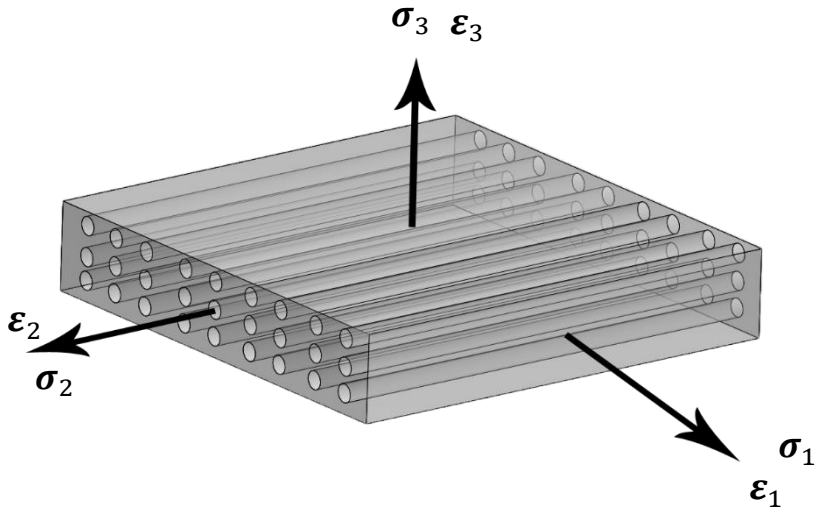

Figure 2-7 Notation for three dimensional stresses and strains

Consider a cube of linearly elastic and isotropic material under stresses in all directions (see Figure 2-7). The constitutive behaviour (Hooke's Law) i.e the material law which relates states of stress to states of strain is defined by;

$$\begin{bmatrix} \varepsilon_1 \\ \varepsilon_2 \\ \varepsilon_3 \\ \varepsilon_4 \\ \varepsilon_5 \\ \varepsilon_6 \end{bmatrix} = \begin{bmatrix} 1/E & -\nu/E & -\nu/E & 0 & 0 & 0 \\ -\nu/E & 1/E & -\nu/E & 0 & 0 & 0 \\ -\nu/E & -\nu/E & 1/E & 0 & 0 & 0 \\ 0 & 0 & 0 & 1/G & 0 & 0 \\ 0 & 0 & 0 & 0 & 1/G & 0 \\ 0 & 0 & 0 & 0 & 0 & 1/G \end{bmatrix} \begin{bmatrix} \sigma_1 \\ \sigma_2 \\ \sigma_3 \\ \sigma_4 \\ \sigma_5 \\ \sigma_6 \end{bmatrix} \quad \textbf{Equation 2-12}$$

Where the terms 1/E and 1/G relate applied stress to strain of the same type and with the same suffices and -ν/E terms relate stresses to strains in other directions. Equation 2-12 above is called the compliance matrix of an isotropic material. Hook's law can also be written in stiffness form that is equal to the inverse of the compliance matrix. For convenience, the following contracted notations are used;

Standard notation - σ_{11} σ_{22} σ_{33} τ_{31} τ_{23} τ_{12}

Contracted notation - σ_1 σ_2 σ_3 σ_4 σ_5 σ_6

Similar notations apply to strains.

A composite laminate comprising multiple layers of fibres in different directions under an applied load exhibits anisotropic behaviour in that stresses σ_1, σ_2 and σ_3 and their corresponding strains ε_1, ε_2 and ε_3 will all differ. Since in composites it is necessary to relate any stresses, σ_{ij} to any strains, ε_{kl}, and then

four suffices for physical stiffnesses are required. An essential ingredient in describing a material behaviour is the relation between strain ε and stress σ;

$$\sigma_{ij} = \boldsymbol{E_{ijkl}}\varepsilon_{kl} \qquad \textbf{Equation 2-13}$$

where $\boldsymbol{E_{ijkl}}$ is the constitutive tensor, and latin index notation counts from 1 to 3

In typical failure analysis of a unidirectional composite, the transversely isotropic material description is generally sufficient but within the post-failure degradation process the lamina begins to perform purely orthotropically if not absolutely anisotropically[54]. An orthotropic formulation of Hooke's law, which generalises the terms Young's Modulus, Shear Modulus and Poisson's ratio, can be written in terms of the compliance matrix:

$$\begin{bmatrix}\varepsilon_1\\ \varepsilon_2\\ \varepsilon_3\\ \varepsilon_4\\ \varepsilon_5\\ \varepsilon_6\end{bmatrix} = \begin{bmatrix} 1/E_1 & -(\nu_{21}/E_2) & -(\nu_{31}/E_3) & 0 & 0 & 0\\ -(\nu_{12}/E_1) & 1/E_2 & -(\nu_{32}/E_3) & 0 & 0 & 0\\ -(\nu_{13}/E_1) & -(\nu_{23}/E_2) & 1/E_3 & 0 & 0 & 0\\ 0 & 0 & 0 & (1/G_{23}) & 0 & 0\\ 0 & 0 & 0 & 0 & (1/G_{31}) & 0\\ 0 & 0 & 0 & 0 & 0 & (1/G_{12})\end{bmatrix}\begin{bmatrix}\sigma_1\\ \sigma_2\\ \sigma_3\\ \sigma_4\\ \sigma_5\\ \sigma_6\end{bmatrix} \qquad \textbf{Equation 2-14}$$

The Poisson's ratio is not symmetric in its indices since symmetry of the compliance leads to relations such as

$$\frac{\nu_{12}}{E_1} = \frac{\nu_{21}}{E_2}, \frac{\nu_{23}}{E_2} = \frac{\nu_{32}}{E_3}, \frac{\nu_{31}}{E_3} = \frac{\nu_{13}}{E_1} \qquad \textbf{Equation 2-15}$$

The stiffness matrix for orthotropic materials, found from the inverse of the compliance matrix, is given;

$$[S]=\begin{bmatrix} (1-\nu_{23}\nu_{32})/E_2E_3\Delta & (\nu_{12}+\nu_{13}\nu_{32})/E_2E_3\Delta & (\nu_{13}+\nu_{12}\nu_{23})/E_2E_3\Delta & 0 & 0 & 0 \\ (\nu_{21}+\nu_{23}\nu_{31})E_1E_3\Delta & (1-\nu_{13}\nu_{31})/E_1E_3\Delta & (\nu_{23}+\nu_{21}\nu_{13})/E_1E_3\Delta & 0 & 0 & 0 \\ (\nu_{31}+\nu_{21}\nu_{32})/E_1E_2\Delta & (\nu_{32}+\nu_{12}\nu_{31})/E_1E_2\Delta & (1-\nu_{12}\nu_{21})E_1E_2\Delta & 0 & 0 & 0 \\ 0 & 0 & 0 & G_4 & 0 & 0 \\ 0 & 0 & 0 & 0 & G_5 & 0 \\ 0 & 0 & 0 & 0 & 0 & G_6 \end{bmatrix}$$ **Equation 2-16**

where,

$$\Delta = \frac{\mathbf{1}-\nu_{12}\nu_{21}-\nu_{23}\nu_{32}-\nu_{31}\nu_{13}-\mathbf{2}\nu_{12}\nu_{23}\nu_{31}}{\mathbf{E_1E_2E_3}}$$ Equation 2-17

2.5 Negative In-plane Poisson's ratio ν_{12} Laminates

Tsai and Hahn [55], Donoghue [56] and Evans [57] and many authors[58]–[61] found negative in-plane Poisson's ratio, ν_{12} value in angle ply laminates. Donoghue [56] modelled the variation of ν_{12} with laminate off-axis angle for a range [±θ]s. He reported the negative in-plane Poisson's ratio occurs between off-axis angles 35° to 50°. The maximum value was found for θ =25° with a value of – 0.245 at an off-axis loading angle of 40°. The magnitude of the Poisson's ratio is significantly reduced for lower fibre orientations, where θ lies in the range 10°-15°. These variations in the in-plane Poisson's ratio value of simple symmetrical laminates are illustrated more clearly in Figure 2-8 below.

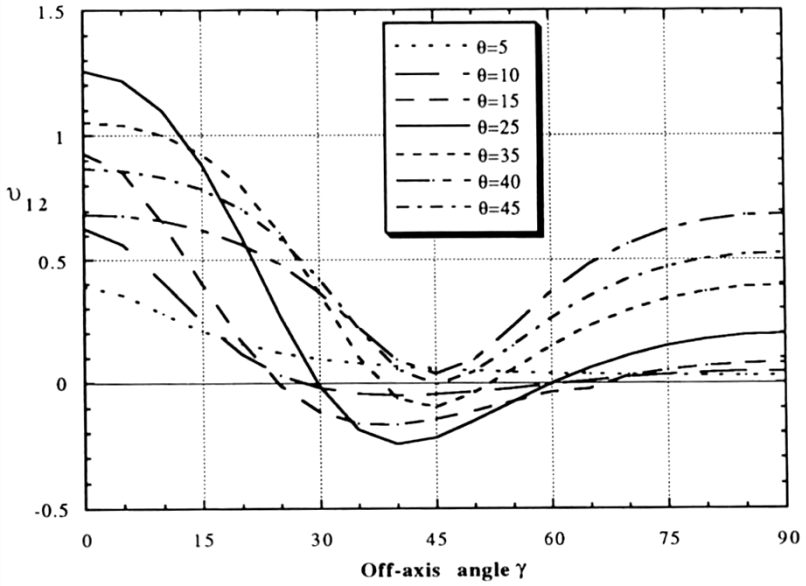

Figure 2-8 **In-plane Poisson's ratio for various angle ply laminates** [56]

Tsai and Hahn demonstrated ν_{12} reaches a minimum negative value at the off-axis angle –40 and specimen anisotropy is indicated by the steep descent in value between 15° and 30°.

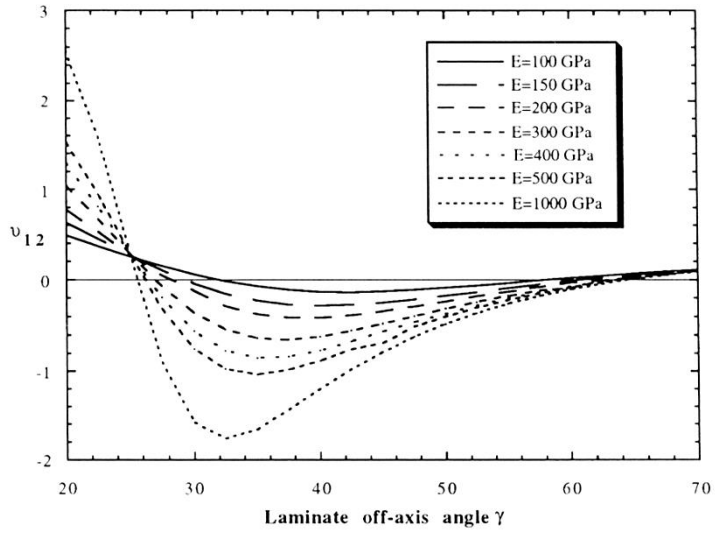

Figure 2-9 **Variation of in-plane Poisson's ratio laminate and tensile modulus**[56]

Donoghue also developed a model by varying the anisotropy of individual lamina layers used in $[\pm\theta]_s$ combinations. He reported that laminates with

higher tensile properties show much larger negative Poisson's ratio values (see Figure 2-9). The variation of Shear Modulus G with off-axis angle was studied in Donoghue's work and he described G as highly sensitive to the specimen anisotropy with both the in-plane Poisson's ratio and Shear Modulus G values being strongly affected by small changes in specimen anisotropy and fibre orientation, hence accurate prediction and measurement of either depends on the other.

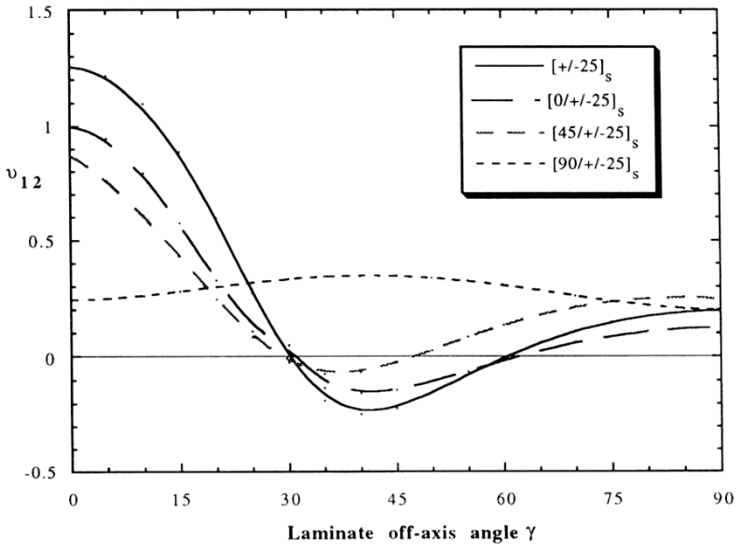

Figure 2-10 Effect of laminate anisotropy on the value of in-plane Poisson's ratio ν_{12}[56]

Reducing the anisotropy of laminates was also assessed in his work [56] to better understand which laminate configurations exhibit auxeticity (see Figure 2-10). It was found that including 0° plies in the laminate stacking sequence reduced the overall anisotropy which reduced the negative Poisson's ratio value and also that adding 45° layers into the laminate reduced the laminate anisotropy further.

Miki and Mirotsu [58] evaluated the behaviour of the Poisson's ratio in fibre laminate composites using laminate theory and a non-linear programming technique. They reported the minimum value of ν_{12}=-0.369 occurs in an unbalanced bi-directional laminate made up with 14.09° and 62.0° angle plies with 68% being made up of the 14.09° plies. They concluded that it is the shear deformation which yields the unusual values.

H Yeh and Zhang [59], [60] analysed the mechanisms and basic conditions for a negative Poisson's ratio in composite materials. They explained the presence of a small negative Poisson's ratio ν_{12}=–0.05 in $[20/70]_s$ glass fabric reinforced modified epoxy which was close to the theoretical estimation.

The above studies explain that the in-plane Poisson's ratio depends not only on the ply orientations and the degree of anisotropy within the laminate but also on the degree of anisotropy within the unidirectional lamina layers. The ratio is also a function of the orientation of the loading direction and off-axis angle, relative to the principal fibre axis.

2.6 Negative Through-Thickness Poisson's ratios ν_{13} Laminates

Tsai & Hahn [55], Herakovich [22], Bjeletich [62], Harkatie[63], Coenen [64] and several other researchers [22], [50], [56], [65]–[67] have studied the presence of a negative through-thickness Poisson's ratio in angle ply laminates either experimentally, analytically or by finite element method.

Through-thickness negative Poisson's ratio values of up to ν_{13} = -0.746 were produced over certain orientation angles for Kevlar and carbon reinforcements [68]. Hadi Harkati and co-researchers [63] reported the minimum value of the negative Poisson's ratio for different values of $[\pm\theta_2]_s$ using Kevlar, glass and carbon fibre angle ply laminates.

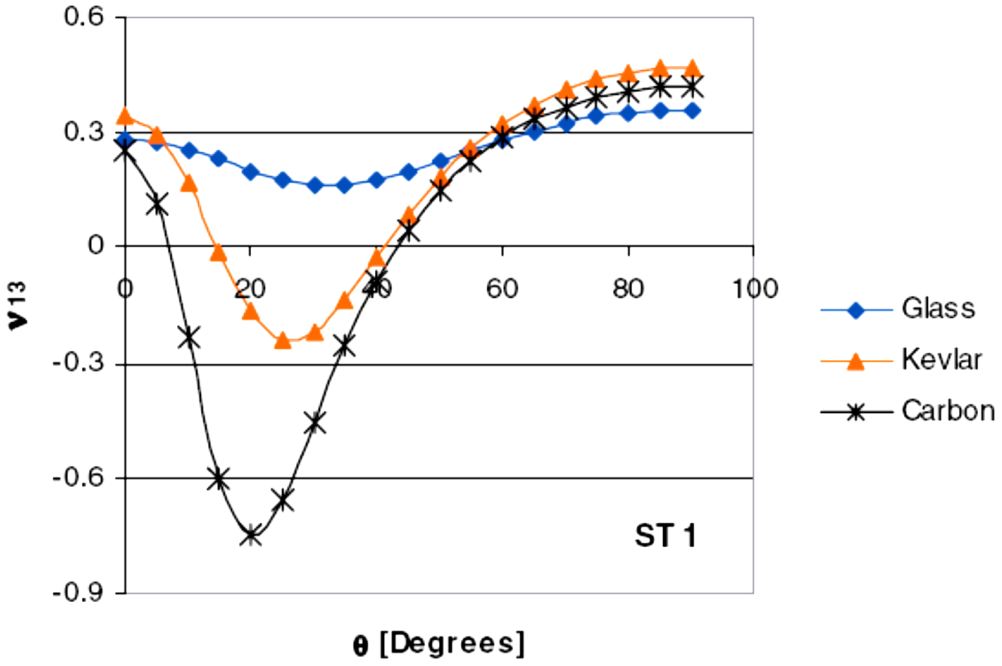

Figure 2-11 Influence of the orientation on reinforcement type for laminates[63]

They also modelled $[\pm\theta_2]_s$ auxetic behaviour in the through-thickness direction using FORTRAN 90 program (see Figure 2-11).

Herakovich [22] modelled laminates with negative ν_{13} values using two-dimensional laminate theory and three-dimensional constitutive equations. It was shown that ν_{13} (see Figure 2-12) varies radically [22] with fibre orientation.

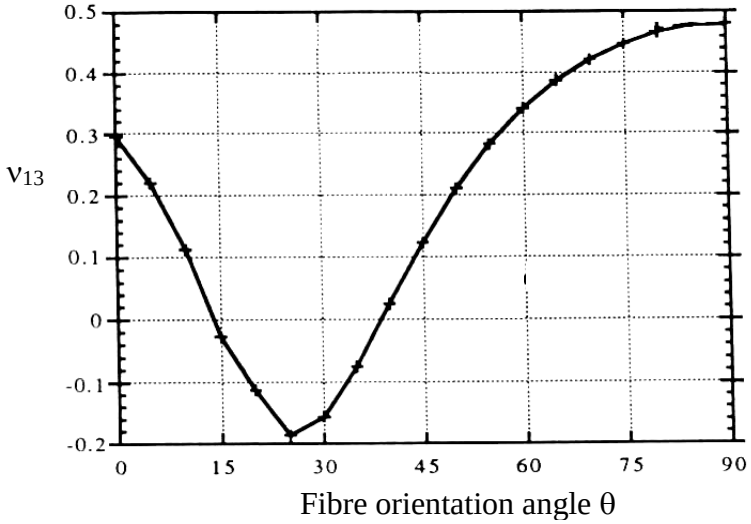

Figure 2-12 Variation of ν_{13} with bisector angle, $[\pm\theta]_s$ laminate

Herakovich [22] showed that negative through-thickness Poisson's ratio values are possible for a fibre orientation angle θ, range of 15°-40° and in simple symmetrical laminates are due to a high degree of normal-shear coupling and the constraining influence of adjacent layers. There are a wide range of laminates which can be tailored to have this effect. However, the percentage of 0° layers decreases the maximum negative Poisson's ratios and the orientation angles over which they occur.

Sun and Li [69] carried out a numerical investigation for through-thickness Poisson's ratios for $[\pm\theta]_s$ combinations for a range of fibre orientation angles of 0°-90° following Herakovich's work. The negative through-thickness Poisson's ratio in symmetrical angle-ply laminates was found to be in agreement with Lempriere's criteria [70].

Al-Khalil & Soden [71] calculated the three dimensional effective elastic constants for filament wound glass, Kevlar and carbon epoxy filament wound

tubes including the effective elastic constants in the through-thickness direction. It was reported that the through-thickness Poisson's ratio varied greatly with winding angle between the angles ±30° and ±60° but relatively little outside this range. The values reported in some cases corresponded with remarkably high in-plane Poisson's ratios i.e. larger than unity again in agreement with Lempriere's [70] findings that negative values and values greater than one are possible in orthotropic layered materials.

Herakovich's findings was confirmed by Donoghue [56], he reported that at the 0° loading direction the $[\pm 30]_s$ laminate has ν_{13}=-0.156 and ν_{12}=1.24 for the AS4/3501 material he used, and also that the values for in-plane Poisson's ratio do not fall below 1.0 until an off-axis loading angle of approximately 16°.

Donoghue [56] examined the variation of mechanical properties of the $[\pm 30]_s$ laminate. When the shear modulus and both longitudinal and transverse moduli of the unidirectional layers are varied, the variation of ν_{13} with increasing pre-preg E_1 is shown in Figure 2-13. It was found that as E_1 is increased the shear modulus and in-plane Poisson's ratio increase, the through-thickness Poisson's ratio decreases and becomes more negative, whilst the transverse modulus is virtually unaffected.

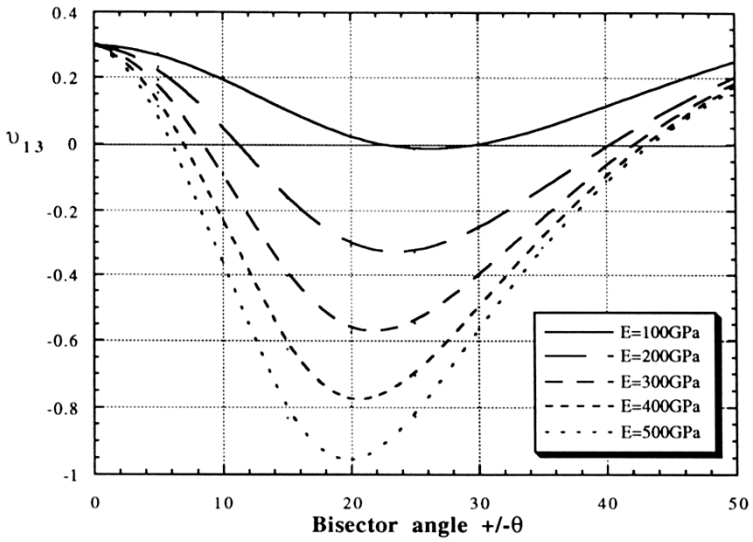

Figure 2-13 Effect of increasing pre-preg anisotropy on the magnitude of ν_{13}

The values for both in-plane and through-thickness Poisson's ratios in the $[\pm 30]_s$ laminate were shown to be quite strongly affected by the value of shear modulus in the ply material. It was noted that the lower the value of G_{12} in the UD ply the greater the negative value of ν_{13} will be in the laminate. It was also mentioned by Miki and Mirotsu[58] who reported remarkable experimental shear deformations of laminates with zero and negative Poisson's ratios under uni-axial loading.

Non-contact strain measurement can be performed using video extensometer [72] for the measurement and hence verification of Poisson's ratio in the laminates. This technique can also verify the presence of negative Poisson's ratio both in through-thickness and in-plane specimens. The software of this equipment calculates the average value of the ten thickness measurements and the output results are in the form of load versus displacement in a similar way as calculated for all other tensile tests. These results can be cross verified by

conducting tests on specimens having strain gauges therefore allow actual contact strain measurements.

2.7 Auxetics

Love described in his book published in 1944, a natural auxetic material [73], which was quite controversial [74], although existence of materials with either negative or zero Poisson's ratio may have been known more than two centuries [75] ago. Natural auxetic materials include: cancellous bones, cow teat skin, living cat skin, some natural minerals such as a-Cristobalite (SiO_2), pyrolytic graphite, single crystals i.e pyrite (FeS_2), and some types of zeolites such as siliceous zeolite MFI-Silicalites[49], [76]–[79]. The documented evidence of a synthetic auxetic material was large-scale cellular structures in the form of two-dimensional silicone rubber or aluminium honeycombs deforming by flexure of the ribs [3] studied by Gibson and Ashby [80], [81]. Negative Poisson's ratio polyurethane foam with re-entrant structure were first developed by Lakes in 1987 [20], [82]. This polymeric foam had a Poisson's ratio of -0.7.

In his work, the term ''auxetic'' was not used by Lakes to describe these materials. This terminology came 4 years later, in 1991, and was coined by Evans [3]. The word is derived from the Greek word auxetos, which means ''that which tends to increase''. The term is then applied to the work on the

microporous polymers such as polyethylene with negative Poisson's ratio [2], [30][83] [84].

2.7.1 Potential Applications of Auxetics

Auxetic materials offer a unique dimension for achieving unusual and enhanced mechanical performance. Table 2-1 summarizes the potential applications from various research works [3], [82], [85]–[99]

Table 2-1 Summary of the potential applications of the auxetic materials

Field	(Existing and potential) Application
Aerospace	Vanes for gas turbine engine, thermal protection, aircraft nose-cones, wing panel, sounds and vibration absorber, rivet
Automotive	Bumper, cushion, thermal protection, sounds and vibration absorber parts , fastener
Biomedical	Bandage, wound pressure pad, dental floss, artificial skin, drug release ligament anchors. Surgical implants (similar to that of bone characteristics), Mattress for hospital beds to protect patients from bedsores
Military (defence)	Protective clothing, body armour, helmet, bullet proof vest, knee pad, glove
Sensors/ actuators	Hydrophone, piezoelectric devices, various sensors
Textile Industry	Fibres, functional fabric, colour-change straps or fabrics, threads

2.8 Failure in Laminates

Failure in composite materials, as in most materials, is primarily due to flaws. These internal flaws are voids generated during processing [100], [101].

2.8.1 Strength of Composites

In case of composites, like other properties, it would be reasonable to predict that the strength of composites is described by the rule of mixtures where Young's modulus, E, has been substituted with tensile strength;

$$\boldsymbol{\sigma_{comp} = \sigma_m(1 - V_f) + \sigma_f V_f} \qquad \textbf{Equation 2-18}$$

Here $\boldsymbol{V}$ is the volume and this would only be valid when both the fibre and matrix have the same strain to failure, which is not possible. Therefore, Equation 2-18 is insufficient in evaluating the strength of a unidirectional fibre composite[102].

Aveston and co-researchers presented a model based on load transfer between the matrix and fibre [103]. The strain to failure of the relatively ductile matrix for many cases is significantly higher than that of the relatively brittle fibre. The load is transferred to the matrix on failure of the fibres. The matrix and therefore the composite will fail, if the stress in the matrix at the point the fibres fail, σ'_{mu} is sufficiently high. This is represented in Equation 2-19 [103].

$$\sigma_{fu}V_f + \sigma'_{mu} > \sigma_{mu}(1 - V_f) \quad \textbf{Equation 2-19}$$

Composite laminate theory has been used in a variety of ways to predict failure. Tuttle [104] summarizes various failure criterion including Tsai-Hill and Tsai-Wu [104]. Hill expanded the von Mises criterion in 1950's for the yielding and subsequent failure of orthotropic metals. Tsai then tailored Hill's method for composites [102], [105]. A simplified edition of the Tsai-Hill failure criterion is given by the inequality

$$\frac{(\sigma_{11})^2}{(\sigma_{11}^{fT})^2} + \frac{(\sigma_{22})^2}{(\sigma_{22}^{yT})^2} + \frac{(\tau_{12})^2}{(\tau_{12}^{y})^2} - \frac{\sigma_{11}\sigma_{22}}{(\sigma_{11}^{fT})^2} < 1 \quad \textbf{Equation 2-20}$$

where failure of a transversely isotropic i.e. isotropic in the *x-y* plane, will not occur when Equation 2-20 is satisfied. The superscript T refers to tension, composites act in a different way in tension and compression, also the superscripts f and y refer to failure and yield respectively. Tsai and Wu later presented a failure criterion based on the composite laminate theory that predicts failure mathematically as a matrix [106]. They also said that, failure will not occur if inequality Equation 2-21 is met for plane stress in the x-y plane.

$$X_1\sigma_{11} + X_2\sigma_{22} + X_{11}\sigma_{11}^2 + X_{22}\sigma_{22}^2 + X_{66}\tau_{12}^2 + 2X_{12}\sigma_{11}\sigma_{22} < 1 \quad \textbf{Equation 2-21}$$

The constant coefficients (X_1, X_2 ....) are based on the ultimate failure and yield strengths of the material in different directions; consequently, they are calculated using the ultimate tensile and compressive strengths in various directions. A number of terms dropped to zero for the plane stress as described in Equation 2-21 which is a general case. The failure criterion for pure tension, i.e. the load applied in the σ_{11} direction, is further reduced to give Equation 2-22;

$$\boldsymbol{X_1\sigma_{11}^{fT} + X_{11}(\sigma_{11}^{fT})^2 = 1} \qquad \textbf{Equation 2-22}$$

2.9 Types of Damage in Laminated Composites

2.9.1 Micro Damage

The initiation of failure of any material commences on the micro-mechanical level. The manufacturing process of the fibre matrix composite induces micro-damage at lamina scale. Considerable residual stresses may exist in the matrix after the curing [107] due to the difference in coefficients of thermal expansion between the fibre and matrix and due to the matrix shrinking during polymerisation. Such stresses may cause flaws [54] in the form of microscopic matrix cracks and local fibre-matrix debonding (see Figure 2-14b). Any applied stress may lead to rapid growth of these micro-defects in the structure. Microscopic hackles are generated in the matrix under the applied shear loading (see Figure 2-14a). Due to an applied load parallel to the fibre direction,

the early fracture of individual fibres causes failure in the adjacent matrix due to the locally concentrated load (see Figure 2-14c). These micro-defects can be found by studying the stiffness [108] or its acoustic emission [109]. These micro-defects influence the material's stiffness and its strength.

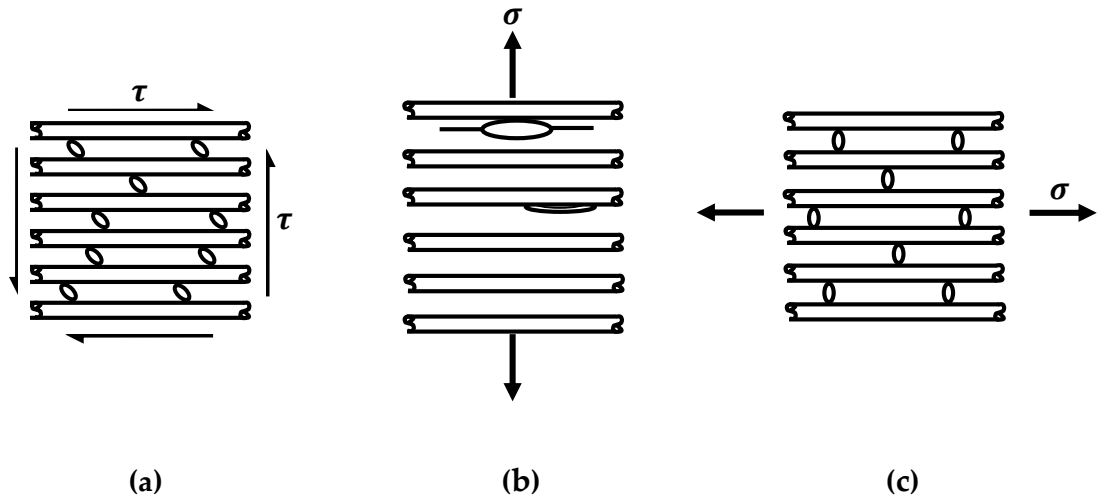

Figure 2-14 **Different form of micro-defects in unidirectional lamina (a) Hackles due to shear load (b) matrix cracks and local fibre-matrix debonding due to fibre perpendicular tension, and (c) local matrix failure due to fibre parallel tension.**

2.9.2 Fibre and Inter Fibre Damage

In fibre matrix composites two macroscopic types of failure occur at lamina level which are fibre fracture and inter-fibre fracture.

The fibre fracture mode defines the load case, where the entire lamina abruptly separates in fibre parallel direction. The lamina behaves totally differently in this direction whether subjected to tension or compression. The tension load applied to the fibre parallel direction leads to the separation on a fibre perpendicular fracture plane. The load bearing capacity in this direction is strongly dominated by the fibres. Similarly, micro-damage in the matrix due

to any additional applied load perpendicular to the fibre[110], [111] or shear [112] does not affect the load bearing capacity in the fibre direction. However, the load bearing capacity in fibre direction is greatly influenced by the load applied to the fibre perpendicular direction due to the varying lateral contraction behaviour of the fibres and the matrix.

The compressive load applied in the fibre parallel direction, the creation of a fibre fracture strongly depends on the material system, i.e. the interaction between fibres and matrix. The load applied in compression, tension or shear to the fibre perpendicular direction, failure of the lamina will ultimately occur by an inter fibre fracture. This term defines a macroscopic crack running through the matrix material or along fibre-matrix boundaries through an entire lamina.

2.9.3 Interlaminar Fracture

Delamination of a laminated composite occurs due to the separation of two or more laminae. This type of failure may be due to inter-laminar stresses i.e. through-thickness tension, in-plane or through-thickness shear. Delamination and inter-fibre fracture interact with each other and delamination initiates at the point where a macroscopic inter-fibre crack meets the interface between two laminae.

Delamination is unique as a mode of failure to the laminated fibre reinforced composites [113]. Ply delamination can occur in any of the individual modes or as a mixed-mode failure. Interlaminar cracking due to the anisotropic interaction of the layers is a primary cause which occurs due to stresses in the x-y plane parallel to the fibre direction. Matrix cracking can induce a separation of the layers, if a normal tensile stress is applied. Moreover factors such as free edges, surface scratches, local defects and machining defects create stress risers where a local delamination is possible [113].

Matrix microcracking, matrix splitting, fibre debonding and fibre breakage also play a vital role in delamination. The entanglement of the fibre tows due to resin flow between the matrix resin and the fibre bundles creates fibre bridging and can restructure the effect that porosity induces on the bulk properties [114].

2.10 Impact of Composite Plates

This portion of the literature review offers an introduction to impact behaviour of angle ply laminates and reasons for better understanding of this phenomenon and also explains likely failure mechanisms.

The failure of an angle ply composite is more complicated than that of a single plate, due to the stacking sequence of various layers with different orientations and properties [115]. Therefore, damage may occur in some plies in the form

of local failure before it fails completely. In many applications the first failure of any layer is not tolerable because it degrades the strength and stiffness of the whole structure [116].

The manner in which composite materials respond to impact loading and the way in which the kinetic energy of the projectile is dissipated is very different from that of metals. Metals absorb a large amount of energy due to their ductile nature and impact damage is not regarded a serious threat in metallic structures [117]. For low and intermediate incident energies, metals absorb energy through elastic and plastic deformation. The metals may deform plastically at their yield stress before work hardening and it is easy to predict them using fracture mechanics principles [118].

In many composites, due to the brittle nature of the constituents, the ability to undergo plastic deformation is extremely limited. Energy is instead absorbed through the creation of large areas of fracture with corresponding reductions in strength and stiffness. However, a well-known issue with angle ply laminates is their poor resistance to accidental impact by foreign objects [119]. The impact itself may take many forms, such as a low velocity impact by a large mass, travelling a few metres per second or a high velocity impact by a small mass travelling hundreds of metres per second. The former could occur for example as a dropped tool during manufacture and this is simulated using a falling weight or swinging pendulum test method, the latter is simulated

using a ballistic launcher such as a gas gun which replicates the impact of small flying particles of debris. In these two extremes the response of the component is likely to be very different [120]. Under low velocity impact conditions, where the contact zone between the target and projectile is relatively large, the whole structure responds, thus allowing absorption of kinetic energy at points well away from the point of impact. High velocity impact loading by a small projectile tends to induce a more localised form of target response resulting in the dissipation of energy over a comparatively small region of the component [121].

Swanson and Christoforou [122], [123] have developed a procedure for establishing the limits of the quasi-static approximation for the calculation of the impact response of structures. There are many other quadratic failure criteria that exist for composite plates [35], [124]. The most common used ones are Tsai-Hill, Hoffman, Hencky-Von Mises and Tsai-Wu criteria. Hill predicted an extension of the von Mises yield criterion for anisotropic materials having equal value of strengths both in tension and compression. For a three dimensional stress state Hill's criterion is given by

$$F\left(\sigma_x - \sigma_y\right)^2 + G(\sigma_x - \sigma_z)^2 + H(\sigma_z - \sigma_x)^2 + L\left(\sigma_{yz}\right)^2 + M(\sigma_{xz})^2 + N\left(\sigma_{xy}\right)^2 < 1 \qquad \textbf{Equation 2-23}$$

Composite materials experience much larger strain depending on the magnitude of the impact and strain rates. Therefore, composite materials must be evaluated at the expected strain rates of their intended application. A critical assessment of the damage mechanism and extent of damage is required to evaluate the type of damage and structural degradation and to propose the repair procedures. The type of damage and the extent of degradation are significantly influenced by the nature of the impact response. However, it not simple to identify the parameters that determine the type of the impact response [122].

2.11 Low Velocity Impact

If the contact duration of the penetrating object is longer than the time period of the lowest mode of vibration of the structure, the phenomenon is regarded as a low velocity impact event. This is in context with intermediate velocity (10-50m/s) [121], high/ballistic (small mass) velocity (50-1000m/s) [125], and hyper velocity (>2-5km/s) regimes. In this work low velocity impact is studied which results usually from situations arising from production, hailstones, hurricane, tornado debris, foreign object debris on roads and runways, dropped tools during maintenance, and this occurs specifically velocities below 10m/s [121], [126]–[129]. Composites are especially prone to internal defects caused by low velocity impact. In many cases, damage is not evident on the surface but it can significantly propagate through the laminates,

forming a complex network of delaminations and matrix cracks (see Figure 2-15) as an internal damage.

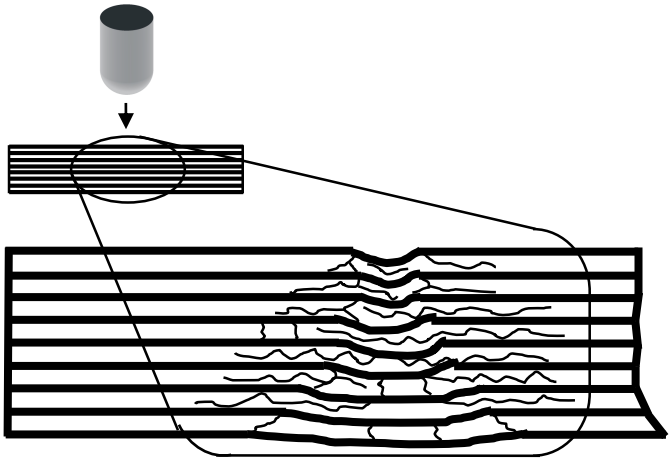

Figure 2-15 Delaminations and matrix cracking in a thick laminate due to impact damage[10]

Depending on the significant of the damage, it can reduce the structural integrity, residual strength and service life therefore increasing the risk of unexpected fatigue failure [130], [131].

The damage tolerance is considered typically a resin dominating property. Therefore, the right choice of a toughened resin can considerably improve the resistance to impact damage [10].

By contrast in the case of high velocity impact the maximum amount of damage is caused at incident energies that are sufficient to cause penetration. The impactor penetrates the laminate relatively cleanly, losing little energy, causing little cracking away from the hole and resulting in smaller reductions in strength with more damage on the back of the specimen.

2.11.1 Multiple Low Velocity Impacts

In practical situation, it is more likely that multiple low-velocity impact events happen because of the situations arising from production i.e hailstones, hurricane, tornado debris, foreign object debris on roads and runways, dropped tools during maintenance [132] than the single impact. If the damage locations are in close proximity, this can raise the subject of more serious interaction.

In spite of this, few studies have focused multiple low velocity impact damage. Paul et al. [133], Malekzadeh et al. [132] and Galea [134] have analysed multiple low velocity impacts in different scenarios and concluded that significant interaction does exist between multiple impacts on the same structure. The target composite material may attain micro-stresses after the initial impact and micro-damage, arising in a pre-stress and/or pre-damage state. A decrease in the stiffness and an increase of the contact duration was observed in response of multiple impacts [135]–[137] and indentation developed gradually at the impact location. Damage growth was observed to increase linearly due to stiffness degradation with multiple impacts for the unidirectional angle ply and cross ply laminates

Recently, Appleby-Thomas et al. [138] addressed the effect of multiple ice projectile impacts on woven and unidirectional carbon fibre composite square

plates and they established a range of damage types. Multiple low velocity impacts on auxetic structures have never been assessed but this study set out to study the effect of multiple impacts in auxetic through-thickness direction carbon fibre composites.

2.12 Modes of Failure in Low Velocity Impact

As discussed, above unlike in metals where damage is initiated on the front or impact surface, in composite materials a complex formation of damage occurs and is quite often undetectable on the surface. Impact damage instead consists of a combination of internal failures including matrix cracking, delamination between adjacent plies and failure of the fibres. In this way the impact energy is absorbed through these internal damage mechanisms and the resulting plastic deformation can severely reduce the strength or stiffness of the structure with little or no visible sign of damage.

Low velocity impact damage of fibre reinforced epoxy composites has been investigated both analytically and experimentally. In many studies, the damage created by a single energy level has been experimentally investigated in through-thickness direction for composites [139]. However, the damage appears more severe in low velocity impact due to enough interaction time between target and impactor that generates stresses over wider area. A significant amount of residual stresses may also exist in a structure after curing

due to matrix shrinking during polymerization and due to a difference in coefficient of thermal expansion [140], [12]. These stresses may induce flaws in the form of local defects. Any applied further load can cause abrupt growth of these micro-defects regarding dimension and quantity [141].

The impact damage resulting from low velocity impact is potentially considered the most dangerous to angle ply laminates because it is undetectable [126], [121]. The damage is evident itself in many states [126], and numerous investigations have considered the delaminations are more responsible for reduction in residual properties of the composite and stiffness [142], [143]. Furthermore, experimental evidence signify that matrix cracks disseminate abruptly and over long distances [144], [145]. Angle ply laminates follow numerous modes of failure due to their heterogeneous and anisotropic nature.

2.12.1 Matrix Cracking and De-bonding

They appear parallel to the fibres due to tension, compression or shear. Richardson and Wisheart [146] predicted matrix cracking, in low velocity impact, as the first type of damage between fibres and matrix. Depending on the crack site in a laminate, matrix cracks may occur due to different reasons[147]. They may be initiated by high transverse shear stresses, or flexural stresses. Transverse shear stresses are related to the contact force and contact area [148]. Due to the high transverse shear stresses induced by contact

edges of the impactor, some cracks may appear as inclined (see Figure 2-16) in the upper and middle plies. High tensile bending stresses that are prevailing due to the flexure deformation of the laminate may induce some cracks on the back face and are typically vertical bending cracks.

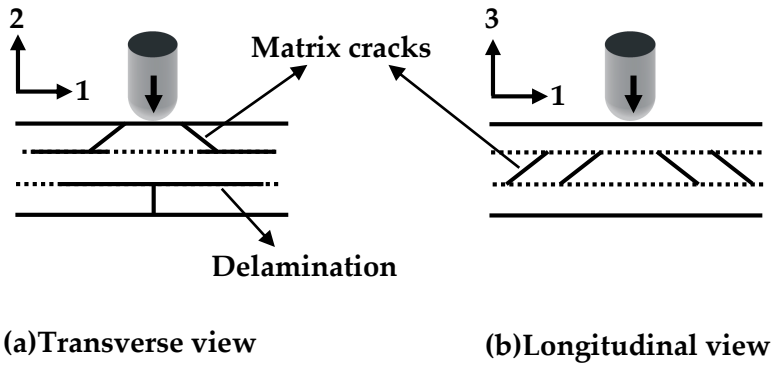

Figure 2-16 Schematic demage mechanism in an impacted composite plate[130]

The growth of damage usually appears through matrix cracking followed by delamination growth and ultimately fibre failure [149], [150]. In general, matrix cracks and delaminations are related to each other and this is the reason that matrix cracks divert into delaminations once the cracks reach to the adjacent plies with a different fibre direction.

Therefore, due to strong interaction, the two types of damage do not appear independently. Richardson and Wisheart predicted that "Delamination only occurs in the presence of a matrix crack." [146].

2.12.2 Delamination

A delamination is a separation of plies that initiates and develops in the presence of a matrix crack. Delaminations increase in size and run in the resin

concentrated location specifically between plies of different fibre orientation [146], [151], [152]. Delaminations do not always grow precisely, but can propagate adjacent to the boundary. Delamination is launched primarily as a mode I fracture (although mixed mode fracture can also happen) because of high through-thickness normal stresses originated by the occurrence of the matrix cracks and high interlaminar shear stresses along the interface [153]–[155]. These are induced by the bending stiffness mismatch between neighbouring angle plies of various orientations. Some authors have predicted a bending mismatch coefficient between two adjacent angle plies [156]. The greater the mismatch, the greater is the delamination area [153], [154]. Material properties, stacking sequence and laminate thickness have a great influence on the mismatch.

The delaminations are usually peanut shaped with the major axis parallel with the fibre orientation (see Figure 2-16) of the layer below the interface [157], [158]. Delamination growth is considered to be the most energy consuming damage mechanism and therefore defines the influencing damage process during an impact event [157]. The majority of the energy absorbed in the laminate during an impact event disseminates into delamination growth. The absorbed energy per unit area is found to be constant for delamination growth [121]. The delamination area can be described from the maximum impact force generated, and the interlaminar fracture toughness is subsistent of delamination size. A linear relationship exists between the peak force and

delamination area. The dominant failure mode of propagation is fracture Mode II [159], [160].

2.12.3 Fibre Failure

Fibre failure happens after matrix cracking and delamination during the damage process. This appears underneath the indentor because of the locally high stresses, and indentation effects (mainly governed by shear forces), and on the non-impacted face because of high bending stresses. Fibre failure is the main governing failure mode in tension loading and the residual strength is primarily influenced by the extent of fibre failure during impact. Usually, the distribution of fibre failure through-thickness is more or less uniform for all laminates and the extension in the width direction is quite narrow. Fractographic analysis of impact studies predicts that the fibre failure is confined under the point of impact [161]. Fibre failure is a precursor to catastrophic penetration. The energy required for fibre failure due to lower interface flexure is given by [162].

$$E = \frac{\sigma^2 wtL}{18E_f} \qquad \textbf{Equation 2-24}$$

where σ = flexural strength, E_f = flexural modulus, w = width, L = unsupported length and t = specimen thickness.

2.12.4 Penetration

Penetration is a macroscopic mode of failure and happens when the fibre failure achieves a significant level, letting the indentor completely penetrate the material. The impact energy penetration limit rises quickly with the thickness of the specimen. The key types of energy absorption in the process of laminate penetration are; shear-out, delamination and elastic flexure. Among all these mechanisms, shear-out mechanism is responsible for 50- 60% energy absorption based on the thickness of the plate. A number of possible parameters including tow size, fibre sizing, orientation, matrix type and interface have an influence on the penetration process [163]. A recommended analytical model of penetration to represent the energy absorbed is[164]:

$$E = \pi\gamma^2 td \qquad \textbf{Equation 2-25}$$

where γ = fracture energy, d = diameter of impactor, and t = plate thickness.

2.13 Equivalence of Quasi-static and Low Velocity Impacts

Many researchers have studied equivalence between quasi-static loading and low velocity impacts for composite laminates. The effect of loading rate was assessed quasi-statically [165], [166] to ascertain the origin of certain features of the impact force-histories as it was observed that the different resin systems each had distinct and reproducible features. The load displacement curves

were compared with the impact force curves. It was reported that the curves were practically identical to some extent. Both curves began on the same loading path, showed the initial unloading and reloading 'First Failure' point and both changed stiffness and load along the same path up to the maximum load. C-Scan also showed that the type and extent of the damage was virtually identical. In fact, it was reported that no features distinguished one from the other, the same was true for further investigations at different load levels. These results suggest that the extent of the damage was controlled by the applied force only and is independent of loading rate. The main features occurred in each system was investigated however it was noted that for different material systems the amounts of damage present at each stage will be different.

Sjobolom [56] also evaluated the equivalence of the impact force histories for low velocity impact and quasi-static indentation tests. Quasi-isotropic specimens of 48 plies were tested simply supported on a 123mm diameter ring. The correspondence of the two test methods was reported as reasonably good. The dynamic response obviously included vibrations. However, the main features of the failure process were clearly distinguishable. Thinner laminates with 16 angle plies were also researched and showed no difference between the quasi-static and low velocity impacts.

On examination of the failure of specimens under test, Sjobolom concluded that failure was completely driven by the strain compatibility of the different plies. The damage observed showed the same typical conical shape under the indentor, implying that the rate effects on failure behaviour are minor. In this way the damage created in the tests carried out as part of both the impact and quasi-static element of this work can be compared directly. Inertia forces in the early portion of the impact cause the vibrations. The amplitude of the vibrations depends on the velocity and mass of the plate and is therefore reduced. However, increasing the test velocity increases the amplitude of the vibrations; because of this more scatter is expected in results from a low velocity impact test.

Nevertheless, Wiggenraad and Ubels [131], Elber [166], Rilo and Ferreira [152] confirmed the equivalence between quasi-static loading and low velocity impacts and observed that, although quasi-isotropic laminates undergo higher loads than angle ply laminates, they present more rigorous damage. However, recent investigations into low velocity impact of auxetic carbon fibre laminates have shown improved energy absorption and residual property than that of the conventional carbon fibre laminates[167].

3 EXPERIMENTAL METHODS

This chapter describes the materials used for the preparation of both out of plane and in-plane carbon epoxy composite laminates and the experimental methods used throughout this project.

3.1 Laminate Materials

The manufacturing of laminates with negative Poisson's ratios depends on the stacking sequence and anisotropy of the individual ply material[66], [3]. It is important that each ply is highly anisotropic i.e. having much greater stiffness in one direction than in the other to produce the specific and peculiar interaction between adjacent plies, which creates the auxetic effect in the structure[50]. Unidirectional carbon fibres and also Kevlar fibres in an epoxy matrix represent the most suitable combination. The pre-preg material used in this work is supplied in the form of continuous unidirectional carbon fibres, 12k tow, set in an epoxy thermo set matrix on a paper backing. The material consists of IM7carbon fibres and 8552 Epoxy resin [168]. These fibres are some of the stiffest available and the epoxy is a tough high performance resin suitable for high strength applications[169], making this fibre and matrix combination a highly anisotropic individual ply material and therefore suitable for this application.

3.2 Laminates Design & Fabrication

Sufficient pre-preg layers were cut out with the fibres oriented in the required directions as tabulated in and shown in Figure 3-1 for each stacking sequence.

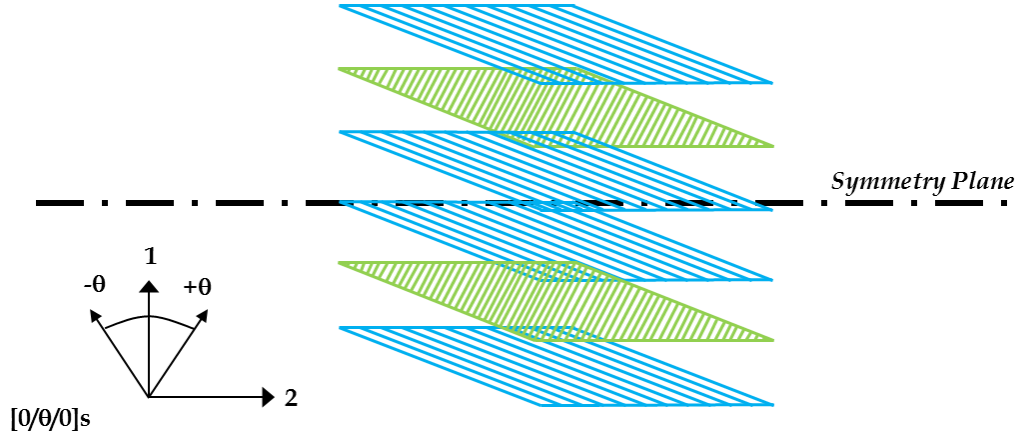

Figure 3-1 Symmetric angle-ply lay-up

Lamination was performed in a dust free environment on grease free surfaces and extreme care was taken to avoid contamination of each lamina surface during the fabrication process as this could seriously affect the quality and performance of the composite. Any obstruction in the path of the fibres will also destroy the uniform distribution of fibres and cause a disturbance within the structure which will be amplified with each successive layer.

For this work a pair of through-thickness and a pair of in-plane Poisson's ratios as listed in Table 3-1 are studied. These pairs are further referred to as negative and positive Poisson's ratios specimens. These specimen configurations have been designed and tested in previous work [56], [167], [170] and are given below in Table 3-1.

Table 3-1 Configuration and predicted Poisson's ratio values[56], [167], [171], [50]

		Predicted AS4/ 3501 values			
		Out of Plane			
Sample	**Lay-ups**	ν_{13}	ν_{31}	ν_{23}	ν_{32}
Auxetic (Na)	[±30]s	-0.156	-0.030	0.341	0.274
Positive (Pa)	[35/-20/25/40/-85/40/25/-45/35/-15/25/40]s	0.187	0.036	0.342	0.131
		In-Plane			
		ν_{12}		ν_{21}	
Auxetic (Nb)	[0/15/75/15]s	-0.134		-0.058	
Positive (Pb)	[0/-70/10/25]s	0.446		0.198	

3.3 Vacuum Bagging

Laminates were stacked in accordance with the required sequence with each successive ply placed directly on top of the other ply. Special care was taken to remove air bubbles between the adjoining layers. Gentle finger pressure was used to smooth out each layer ensuring good contact is made. This improves the quality of the finished laminate by reducing the void content in the specimen and extra care should be taken at this stage.

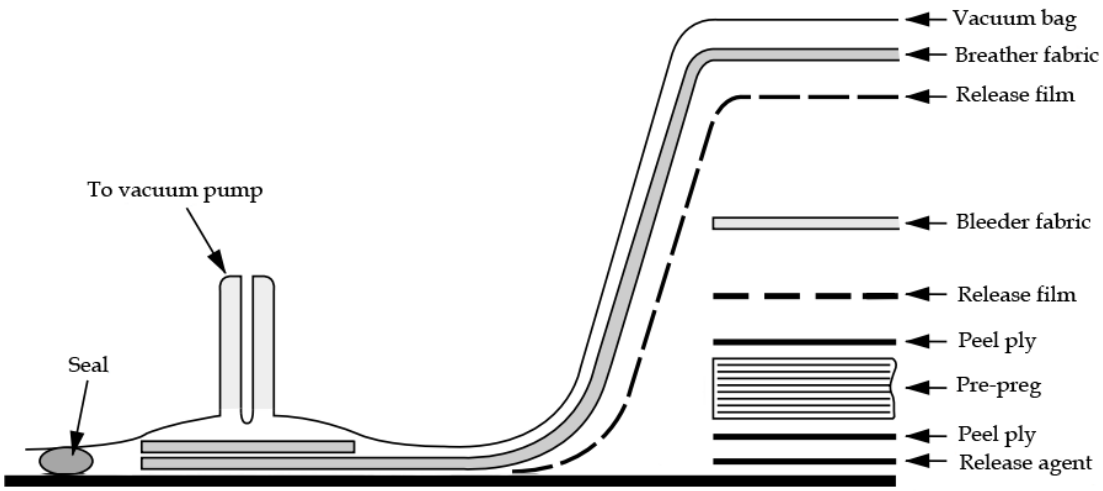

Figure 3-2 Vacuum bag configuration

The Vacuum bag was prepared according to the schematic description as shown above in Figure 3-2 for each specimen before placing it in the vacuum oven using a smooth flat base-plate to cure the unconsolidated specimens. Sufficient thickness (approx 10mm) of the metal plate was required to avoid warp under heat and pressure during the curing procedure. It is recommended that the surface finish of the plate should be of good quality to avoid undesirable patterns or marks on the surface of the consolidated specimens. Once lamination was complete, a top metal plate was placed carefully on the top of the unconsolidated pre-preg. Both the base and top plates were required covering by a PTFE peel ply and a release agent to aid the removal of the specimens after curing. After the top plate, it was necessary to put a layer of breather fabric to allow the air to be evacuated efficiently from the lay-up during the curing cycle. A vacuum valve attachment was necessary to allow even application of the pressure over the entire system.

Once the whole system i.e. plates, breather material, peel ply, bleed fabric and vacuum valve were ready; everything was made airtight using a high temperature nylon bagging film. Vacuum sealant was applied at the edges of the base plate to ensure no gaps or creases exist between the metal and the sticky black tape. The assembly is shown in above Figure 3-2.

3.4 Curing Cycle

The Vacuum bag assembly was placed in an oven to follow a set of strict conditions[168] for final curing of the specimens as shown in Figure 3-3. This vacuum oven had an air circulation fan for uniform heating and cooling.

Figure 3-3 Vacuum oven

A vacuum pressure of 0.8 bar was applied to each laminate stack prior to heating. The complete consolidation stage was achieved by curing the lay-up giving a series of ramps (2-3°C/min) and dwells of the various temperatures as shown in the schematic diagram Figure 3-4.

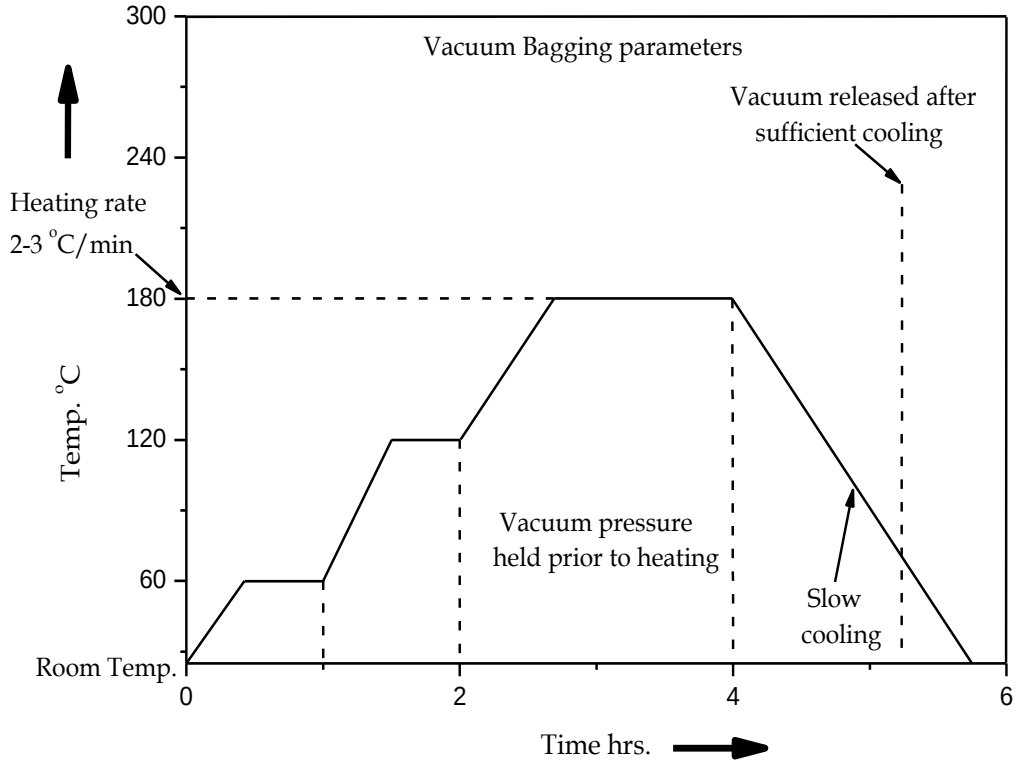

Figure 3-4 Pre-Preg Recommended Cure Cycle

This was monitored carefully at thirty minutes intervals to ensure when the lay-up reached the holding temperature of 180°C and the system was maintained at this temperature for 120 minutes. The oven and contents were then cooled slowly, until the temperature reached room temperature before removing the vacuum pressure and opening the bag.

3.5 Determination of Laminate Properties

3.5.1 Tensile Properties

Mechanical properties such as the ultimate tensile strength, tensile strain, tensile modulus and Poisson's ratio of engineering materials are commonly determined by simple mechanical tests[169], [172]. An Instron 3369 tensile testing machine as shown in Figure 3-5 with 50kN load cell and a crosshead speed of 2mm/min was used to perform and measure the mechanical properties. The specimens were prepared in accordance with the aerospace industry standard[173] with carbon fibre epoxy end tabs to facilitate gripping of the specimen during the test. It was required that the 250mm x 25mm specimens fail within the gauge length between the end tabs.

Figure 3-5 Instron® 3369 tensile testing machine

3.6 Specimen Configuration

In this work, as mentioned previously in, both the through-thickness and the in-plane Poisson's ratio specimens were prepared for detailed investigation. Each laminate measured 300x300mm^2 and had 24 layers. After preparation, the thickness of the specimens was precisely measured to 4.7mm from all the sides before starting further tests. These plates were further cut down after consolidation to 9 equal sized specimens of each 100x100mm^2, which were required for the testing procedures. All auxetic composite specimens were classified as 'N' (negative Poisson's ratio) and all conventional composite specimens were marked as 'P' (positive Poisson's ratio).

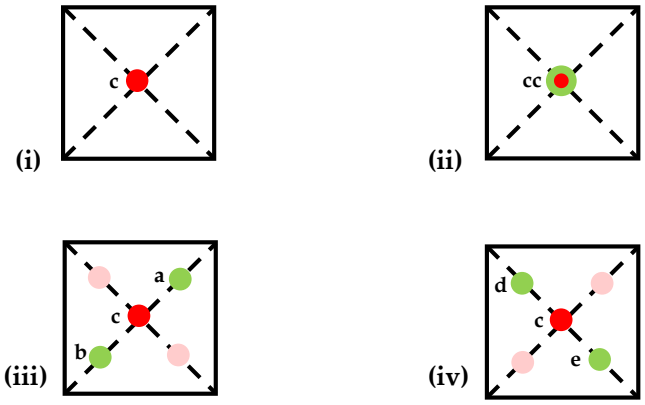

Figure 3-6 **Test site markers (i) "c" Centre (ii) "cc" Re-testing at centre (iii) "a or b" Damage direction (iv) "d or e" Perpendicular to damage direction**

In this project a detailed analysis was proposed for studying behaviour in the vicinity of the indentor site. It was therefore necessary to mark each test site of the specimen with clear and understandable notation for discussing their features. A series of schematic diagrams are shown in Figure 3-6. In these

diagrams; "c" represents test site at centre, "cc" represents a re-tested site at centre, "a or b" represent test sites along the direction of damage and "d or e" represent test sites perpendicular to the direction of damage.

3.7 The Indentor & Its Configuration

Quasi-static indentation and low velocity impact (LVI) tests were conducted using a standard penetrative steel hemisphere indentor of 12.7mm diameter as shown in Figure 3-7.

Figure 3-7 Hemispherical steel indentor

The indentor exerts its penetrative force, as shown in Figure 3-8, onto the surface of the simply supported specimens directly under the centre for the first stage of test. A subset of each configuration was then re-tested using the same procedure according to the test sites illustrated in Figure 3-8

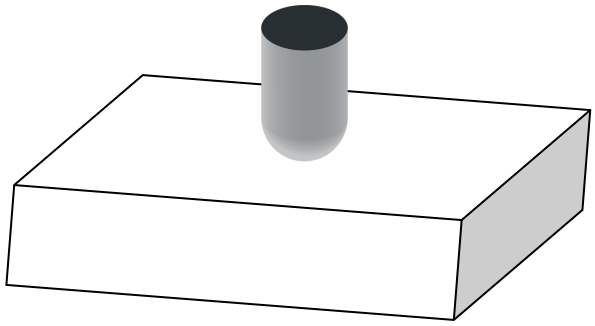

Figure 3-8 Impact and Indentation configuration

3.8 Quasi-Static Indentation Resistance

In previous work[56],[174], [64], indentation was performed only at the centre i.e at one location using indentors of different sizes to assess the response of auxetic specimens. In the work presented here, the main focus is the post indentation response in the vicinity of the indentation site.

To investigate in more depth for both through thickness and in-plane behaviour of all the configurations, each initial test was carried out to catastrophic failure to capture both the elastic effect and the next stage in the failure process utilizing a full investigation into damage resistance. An example of the plots generated by indentation testing is given in Figure 3-9. The slope of the initial linear portion and ultimate failure linear portion of each graph was calculated to give an intimation of the though-thickness and in-plane stiffness of each specimen. The next stage was to extract more illustrative results from the graphs, such as values for energy absorbed to the first and subsequent failure point and the load and displacement values.

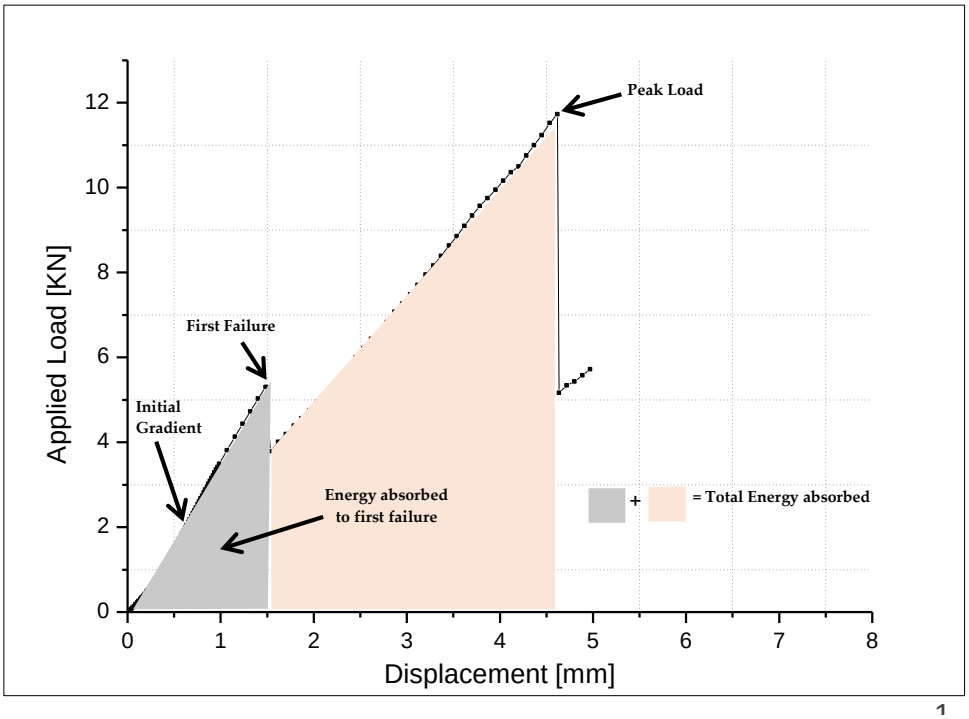

Figure 3-9 Gradients from Initial and Ultimate Energy Absorption Calculation

3.8.1 Test Procedure

The indentation tests[47], [174] were carried out as shown below in Figure 3-10 using a crosshead speed of 2mm/min to a depth of 5mm, which was enough for full failure. These tests were repeated on at least three specimens for each configuration at the centre c and also in the vicinity at 20 mm away from the initial test site i.e a, b, d and e. All test specimens were placed on a 50mm internal diameter test fixture. This circular base plate was taken from the impact rig to ensure the same support conditions for both test types.

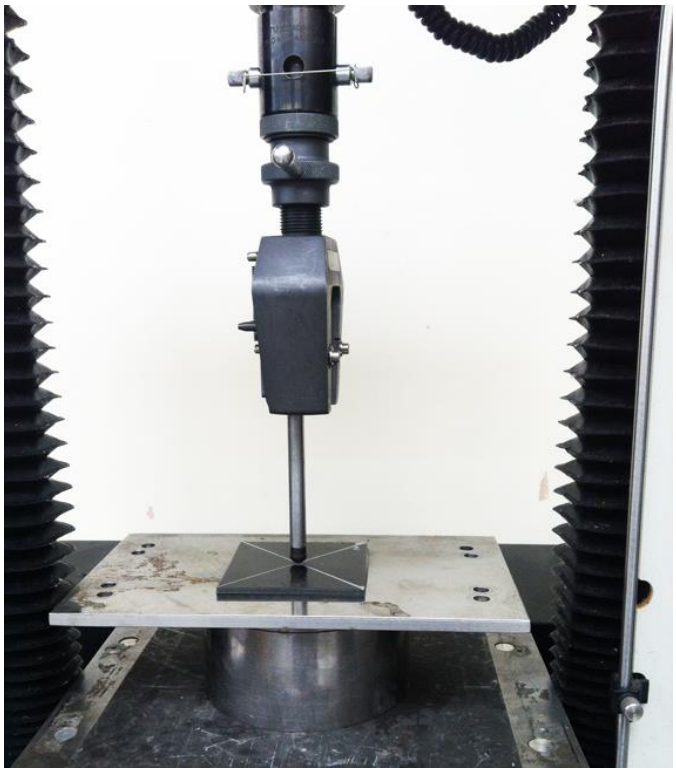

Figure 3-10 DARTEC Universal Hydraulic Indentation Testing Machine

In this investigation no clamping was applied to any specimens during the indentation tests. Load displacement data was recorded throughout the test with the help of the software of the machine.

All the specimens of the first stage were re-loaded as illustrated in Figure 3-6, well into the elastic failure region to reveal the surrounding area of the initial test site of the each specimen for detailed study. The re-indentation was allowed both at centre and away from the centre at pre determined locations. It was decided after initial investigation to focus on the surrounding area of 20mm radius away from the indentor nose for each specimen. Load-displacement was also recorded throughout this cycle and plotted for the analysis of out of plan and in-plane specimens.

3.9 Low Velocity Impact (LVI) Damage

The main focus of this test is to ascertain the impact damage behaviour of the auxetic laminates. Low velocity impact test is simulated by a variety of drop weight machines. For this work, a low velocity impact (LVI) testing facility was employed which consists of a guided instrumented drop weight. However, the Instron impact tester, as shown in Figure 3-11, was instrumented with a model 8902-01 15.6kN tup, 12.7mm (½") hemispherical tup insert (indentor), and Impulse™ data acquisition and analysis system (DAS). The ASTM standard method[175] was used for each specimen to take as a reference to fix some of the governing parameters.

Figure 3-11 Instron Dyntaup® Model 9250HV Drop Tower Impact Tester

This instrument is restricted to a maximum impact velocity of 14.0 m/s and maximum drop mass of 14.5kg. In this work, the falling mass was kept constant at 4.8kg, and the drop-height was changed to reproduce the required amount of energy striking the specimen. The machine was also fitted with a catch mechanism to allow only single bounces on the specimen. The pneumatic manifold attached to the rebound brakes exerts pressure to prevent the drop weight and tup assembly from contact with the specimen again. An accelerometer and a strain gauged load cell were attached to the data acquisition system (DAS) to record the data throughout the test event.

3.9.1 Test Procedure

To investigate the auxetic behaviour of the laminates, impact tests were designed based on the findings of the indentation tests. At least four coupons were tested for each laminate configuration for accuracy of the data obtained.

The support conditions, indentor size and the base plate (50mm internal diameter), were set to follow the indentation test configuration. The data obtained from the impact tests was plotted as force-time histories and also load-displacement curves.

3.10 High Velocity Impact (HVI) Damage

It is important to match the experimental setup as close as possible to the original "real life" situation, provided that it leads to reliable results. In this context, the closest match is a gas gun facility[176]. The gas gun facilities utilize pressurized gas to accelerate a projectile to achieve the high velocity impact condition. High velocity impact damage of the through-thickness specimens, produced within this project were measured by a high strain impact rig set up of the University of Southampton. Design of the rig meets the following parameters and specifications:

- High speed low mass projectile (or impacting element);
- The impacting element must have a simple geometry;
- Specimen must be completely supported at the far end of the horizontal rig set up;
- Energy transmitted through the specimen (output) must be recorded;
- The rig was set up to allow the load to be applied horizontally only;
- Impacting (input) energy must be recorded.

A 9mm diameter ball bearing was selected as the impacting element; a tube was used as the delivery method. Spring, hydraulic and pneumatic systems were compared at the design stage as methods to move the ball bearing from rest to impacting velocity. A compressed air system was selected because of the convenience of a compressed air supply within the laboratory, repeatability of test conditions and cost of components required.

It was decided to use a shock accelerometer to measure the transmitted energy (output) received on the rear of the sample and compare this to the impacting energy (input) from the ball, measured with light gates. A 50 cm long block was placed behind the impacted samples and the accelerometer was attached to the end of this block. The effect of a sharply applied, localized disturbance in a medium soon transmits or 'spreads' to other parts of the medium, i.e. when the ball strikes the front side of the sample, various waves will propagate through that specimen. As these waves meet free surfaces they reflect, cluttering the original waveform with repeating information. The long block was used to reduce the reflection interval, thus allowing a 'cleaner' signal to be recorded.

Figure 3-12 High velocity impact testing rig

This horizontal rig was designed in-house at University of Southampton and built by Safire Design Engineers Ltd in Southampton. A photograph of the rig

is shown in Figure 3-12, and a simple schematic is presented in Figure 3-13. The high velocity impact rig has the following key features:

- 9 mm ball bearings;
- Smooth bore barrel;
- Compressed air system;
- Electrical and measurement system;
- Specimen holder and block.

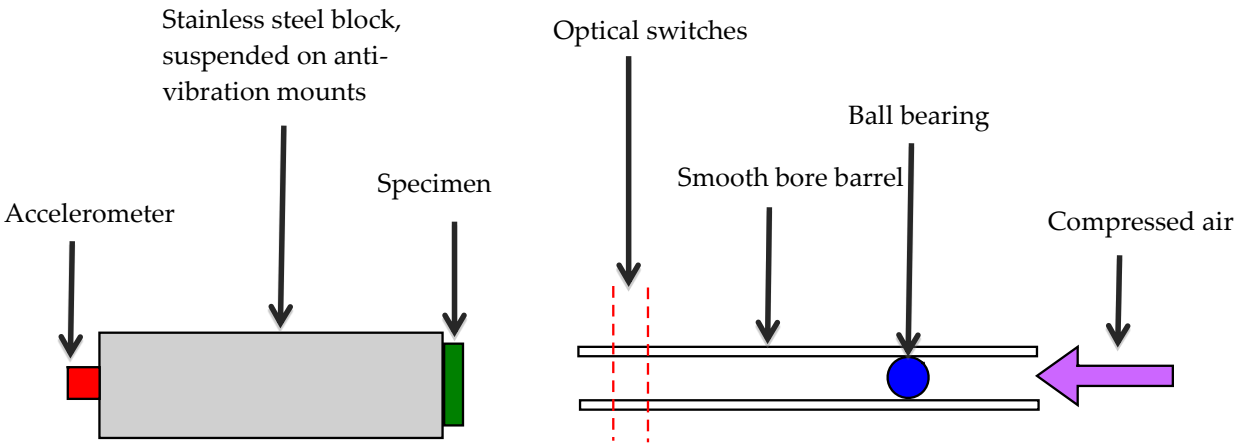

Figure 3-13 Schematic of high velocity impact rig

The accelerometer produces readings of shock and can be used to calculate energy during a certain part of the impact event. The light gates produce a reading of barrel velocity. All other testing parameters are listed below;

Specimens	**24-ply**	**Unit**
Variable		
Ball bearing	AISI 52100 G10	
Ball mass	0.002978	kg
Accelerometer	50000	g

Gain	x10	
Video sample rate	150110.000	Fps
Video exposure	6.300	μs

The input energy for high velocity impact was maintained by monitoring the air pressure in the gas gun and a pressure of 60psi was enough to give 93m/s impact velocity.

3.11 Damage Analysis

Fractographic analysis was performed on all the fractured specimens to identify the damage mechanisms. This is a simple way of ascertaining the true extent and the form of damage present in a composite laminate after testing such indentation or impact. In this work, each specimen was sectioned along the 0^o of the test site direction when there were more than one test sites away from the centre. There was only one different case, where specimens were re-tested at centre only and sectioned along the 0^o along the direction of fibre failure. A diamond coated rotary cutter was used for this purpose and care was taken during cleaning and drying the specimen edge to preserve the damage zone and to avoid the loss of the prevailing features on the edge.

Once the specimens were clean and dry, an Olympus SZ30-series zoom stereo microscope was used for the inspection of damaged specimens. The set–up is shown in Figure 3-14, and it includes a microscope, an Olympus 4040 Camera

and LCD. This microscope series has a working magnification range of 9X to 120X, zoom range of 0.09X to 4X, and working distance of 110mm. During this research work a magnification of 10X was used for the fractrographic analysis.

Figure 3-14 Damage inspection set-up apparatus

Fractographs of the damage area were analysed and compared directly across the test sites and types to describe their overall extent and depth along with the number, size and severity of the damage delaminations.

3.12 Residual Strength

This is another damage technique to evaluate the residual strength by compression after an impact event (CAI) of the material. In order to measure

the residual strength of the low velocity impact tested specimens, the ASTM test method for measuring the residual strength is employed as a reference, i.e., ASTM D7137/ D7137M-05 [177]. This method is linked to the standard ASTM D7136/D7136M-05 [175] for drop-weight impact test method. This technique depends on the amount of damage present in the specimen; as it is only applicable to the scenario with barely visible impact damage. i.e not to those subjected to full failure level. In this work auxetic specimen with in-plane Poisson's ratio can be analysed using this technique. Specimens were re-loaded quasi-statically[177], where the loading nose was applied at the centre using the parameters and test conditions discussed previously. In response of the residual tests, peak load achieved for each specimen is recorded and compared across the different specimen types.

This simple form of test provides valuable information about damage tolerance of the different specimen types and conclusions can be drawn due to the effect of this type of damage on the performance of each specimen.

4 EXPERIMENTAL RESULTS

This chapter contains the results obtained throughout this project, starting with the properties of the materials used for laminate manufacturing. Mechanical properties of the specimen are also given in this chapter. Results are presented for quasi-static indentation tests; conducted at the centre, away from the centre in the damage and opposite to the damage direction. All these tests were conducted using a standard penetrative steel hemisphere indentor of 12.7mm diameter as shown in Figure 3-7.

Results for these quasi-static tests are presented in terms of Load displacement and Energy absorbed to 'first failure' and Load, displacement and Energy absorbed to maximum load with other interesting features of the Load displacement curves highlighted. Typical examples are provided here for indentation at the centre and away from centre, both in the damage direction and opposite to the damage direction.

The chapter then presents the results of the low velocity impact (LVI) investigation for the through-thickness specimens. Impact tests have been carried out at three different impact sites with the standard 12.7mm steel hemispherical indentor. Based on the quasi-static indentation behaviour, it was decided to concentrate on indentation at the centre and 20mm away from the indentation centre for the impact investigation. The results are reported in

terms of the maximum load and displacement, duration of the impact event and total energy absorbed, again with any interesting features duly noted. The typical force time histories for each impact site are presented for comparison purposes.

This chapter then reports on the quasi-static indentation and low velocity impact behaviour along with the residual strength of the in-plane auxetic specimens. The quasi-static indentation tests were carried out to full damage load and the low velocity impact tests have been carried out at three different energy levels using the same indentor and support conditions. Results for the quasi-static tests are presented in terms of Load, Displacement and Energy absorbed to 'first failure' and Load displacement and Energy absorbed to maximum load for full specimen damage. The results for the impact tests are reported in terms of load displacement, duration of the impact event and total energy absorbed with any interesting features duly noted. The typical load displacement behaviour for each impact level is presented for comparison purpose. Residual testing was also performed for each impact level and the results of the residual loading work are presented and the secondary load displacement curves compared to those for non impacted specimens. This chapter also describes a preliminary investigation into the high velocity impact (HVI) response of the through-thickness auxetic specimens. The results are tabulated to present the impact velocity, rebound velocity, input energy and rebound energy of each specimen with their other characteristics.

The chapter finishes with damage analysis with the internal damage revealed by fractography being described for each specimen type. The relevance of these experimental findings is discussed in the Discussion Chapter – 6.

4.1 Determination of Laminate Properties

4.1.1 Pre-preg Properties

Tensile coupons were used to perform tensile tests with the three different stacking sequences in order to obtain the properties of the lamina materials used in this work; four coupons per stacking sequence were tested for each material and the values are given in Table 4-1

Table 4-1 Tensile Properties at Room Temperature (25° C) for IM7/8552

Property	Symbol	Carbon	Units
Ultimate Tensile Strength	σ_{ult1}	1248	MPa
Longitudinal Tensile Modulus	E_1	150	GPa
Major Poisson's ratio	ν_{12}	0.33	-
Transverse Tensile Strength	σ_{ult2}	20	MPa
Transverse Tensile Modulus	E_2	7	GPa
Shear Strength	G	122	MPa
Shear Modulus	G_{12}	6	GPa
Volume Fraction	V_f	63	%

4.1.2 Stacking Sequence Tensile Properties

Tensile tests were also carried out to measure the elastic constants of each of the four laminate configurations under investigation. The results are tabulated below in, Table 4-2.

Table 4-2 Measured Stacking Sequence Tensile Properties

Nomenclature	Specimen Configuration	Elastic Modulus (GPa)	Poisson's ratio (ν_{12})	Max Load (kN)
N_a	$[\pm 30]_S$	49.6	1.5	34
P_a	$[35/-20/25/40/-85/40/25/-45/35/-15/25/40]_S$	49.8	0.6	32
N_b	$[0/15/75/15]_S$	64.8	-0.14	29
P_b	$[0/-70/10/25]_S$	61.7	0.47	28

Experimentally obtained values for the elastic constants are compared to those obtained using classical laminate theory as described in Section 2.4, the results are shown in Table 4-3.

Table 4-3 Comparison of Predicted and Measured Stacking Sequence Properties

Property	N_a		P_a		N_b		P_b	
	Exp	CLT	Exp	CLT	Exp	CLT	Exp	CLT
Elastic Modulus (GPa)	49.6	51	49.8	53	64.8	63.4	61.7	60.2
Poisson's ratio (ν_{12})	1.5	1.4	0.6	0.56	-0.14	-0.134	0.47	0.466

Exp Experimentally obtained values
CLT Classical Laminate Theory

As can be seen in the tables above, reasonable agreement was obtained between the experimentally obtained and predicted values of stacking sequence elastic properties.

4.2 Quasi-Static Indentation Resistance of Through-Thickness specimens

Quasi-static indentation tests were accomplished by indenting a 12.7mm hemispherical penetrative object to evaluate the performance of the auxetic

composites. Tests were carried out on four specimens of each configuration to provide the reproducibility and reliable experimental results. The specimens were loaded at a rate of 2mm/min in all tests and the loading nose was applied in three different sets of sequences; at the centre, at 20mm away from the centre in the damage direction and also 20mm away from the centre opposite to the damage direction. All specimens were tested to an indentation depth of 5mm in order to achieve a full spectrum of load displacement behaviour until failure. This identification helps in distinguishing all the features of the failure process.

The load displacement data of each recorded test is plotted for single and multiple indents, indented at the centre compared to those indented 20mm away in the vicinity of indentor nose region. Experimental results are also tabulated in terms of initial gradient, load, displacement and energy absorbed to first failure and load, displacement and energy absorbed to peak load.

4.2.1 Quasi-Static Indentation at Centre

Typical load displacement plots for each specimen type for indentation at centre are presented below in Figure 4-1. The measured values are presented in the tables (see Table 4-4 and Table 4-5) in terms of initial gradient, load, displacement and energy absorbed to first failure and load displacement and energy absorbed to peak load. These values are in the form of an average value from the four sets of results obtained, with appropriate errors in the table.

Table 4-4 Experimental First Failure Values, indentation at centre

Specimen Type	Displacement (mm)	Load (kN)	Energy Absorbed (J)	Initial Gradient (kN/mm)
P_a	1.16	4.51	2.55	3.98
CV	0.043	0.004	0.008	0.007
N_a	1.48	5.30	3.84	3.77
CV	0.014	0.047	0.010	0.013

Table 4-5 Experimental Peak Load Values, indentation at centre

Specimen Type	Displacement (mm)	Load (kN)	Energy Absorbed (J)
P_a	4.24	9.86	23.11
CV	0.007	0.002	0.001
N_a	4.62	11.73	27.62
CV	0.009	0.003	0.001

The auxetic specimen shows a higher average first failure load of 5.3kN compared to the positive Poisson's ratio specimen, which undergoes first failure at 4.51kN.

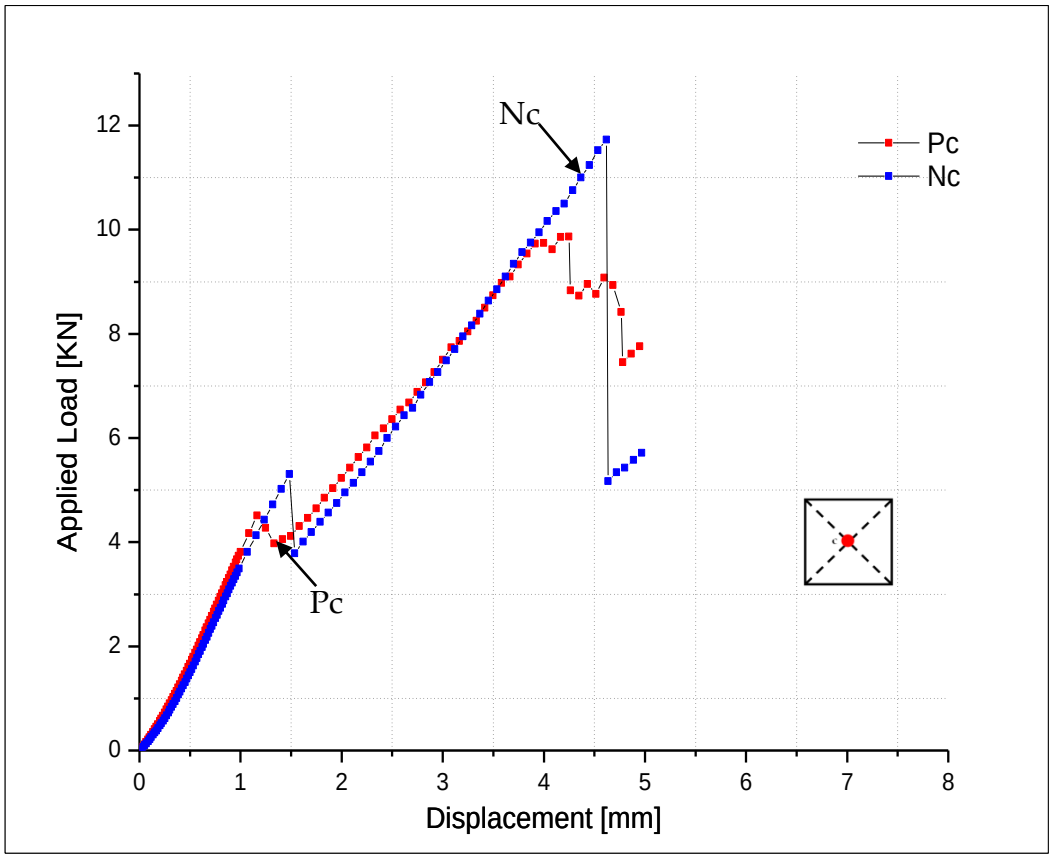

Figure 4-1 Load Displacement Curves, Indentation Centre

Similarly, the displacement value on the curve for the first damage point is 19% higher for the auxetic specimen as compared to the positive Poisson's ratio specimen.

It can be observed form the graph and the values presented in Table 4-5 that the auxetic specimens achieve higher peak load before final failure. i.e. 11.73kN which is 16% higher as compared to the peak load of 9.86kN for the positive Poisson's ratio specimen. The values for the energy absorption are also calculated.

4.2.2 Quasi-Static Indentation and Re-Indent at Centre

To evaluate the performance of all the configurations, square specimens were loaded and re-loaded at the centre. In both the cases the specimens were loaded at a rate of 2mm/min to an indentation depth of 5mm to an applied load, which achieved full damage. The load displacement curves for re-indentations are significantly different from those of the initial indentation. During re-indentation at the centre, there is no first failure point. However, the curves show a maximum load before failure and typical load displacement curves are shown for each specimen type in Figure 4-2.

Table 4-6 Experimental Peak Load Values of Indentation and Re-Indent at Centre

Specimen Type	Displacement (mm)		Load (kN)		Energy Absorbed (J)	
	C	CC	C	CC	C	CC
P_a	4.24	3.83	9.86	7.76	23.11	12.05
CV	0.007	0.008	0.002	0.004	0.001	0.003
N_a	4.62	4.41	11.73	10.90	27.62	19.24
CV	0.009	0.018	0.003	0.042	0.001	0.009

Values for load displacement to peak load and final gradient (see Table 4-6) were obtained. Energy absorption values during the failure process are also calculated from the load displacement data using a simple integration technique.

The initial indentation event reflects similar behaviour as described in section 4.2.1 but the re-indentation event does not show a first failure point as damage has been initiated. However, in auxetic specimen the peak load during the test occurred at much higher level of displacement, 4.41mm compared to 3.83mm in positive specimen types.

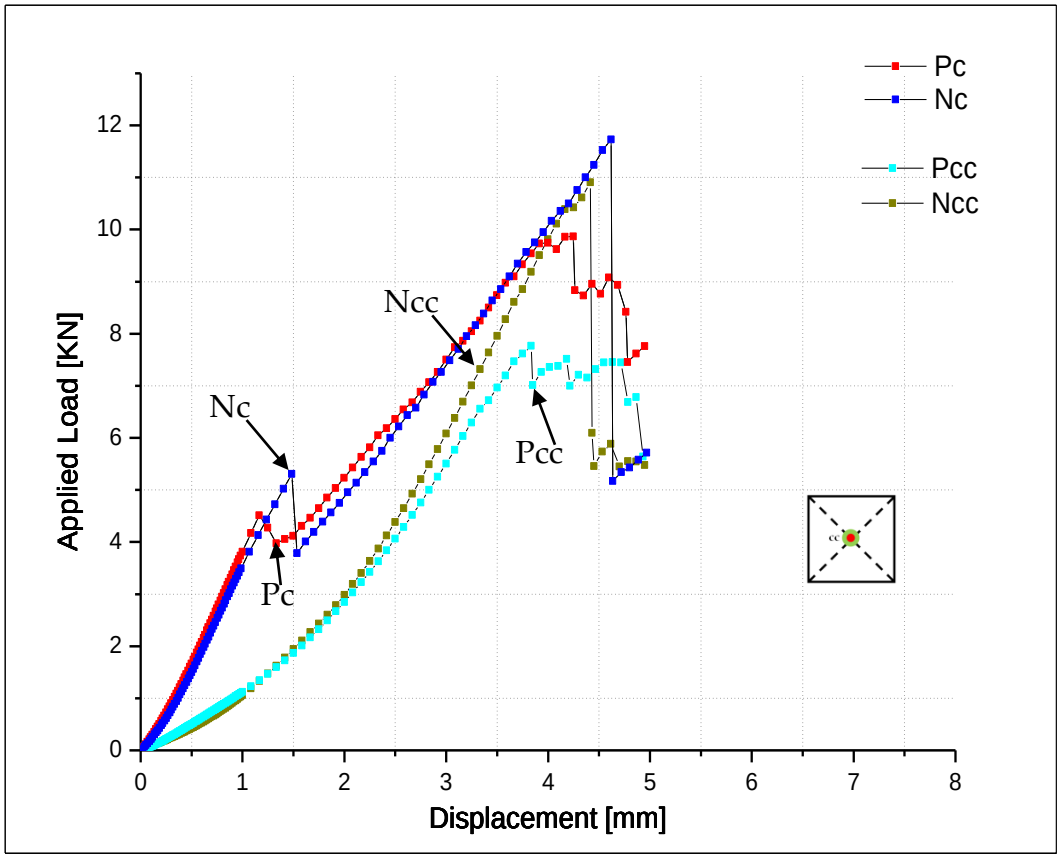

Figure 4-2 Load Displacement Curves, Indentation and Re-indent at Centre

The residual peak load for the auxetic specimens was 10.9kN compared with 7.76kN for the positive Poisson's ratio specimen and the enhancement observed was 28%. This suggests that the auxetic specimens required higher loads to cause damage and therefore were more resistant to the re-indentation event. The values for energy absorbed at this stage of the failure process agree

with the auxetic enhancements observed thus far i.e. 19J for auxetic and 12J for positive specimen.

4.2.3 Quasi-Static Re-Indentations along the direction of damage

Tests were carried out 20mm away from the centre of the initial indentation at sites "a" and "b" along the damage direction to the full specimen damage load (see Figure 4-3). The loading nose was applied at a crosshead speed of 2mm/min to a penetration depth of 5mm. In this way the damage process for each material type could be evaluated and the major features of the load displacement curve identified. Typical load displacement curves for each specimen type are shown in Figure 4-3.

Table 4-7 Experimental First Failure Values, damaged direction

Sp. Type	Displacement (mm)			Load (kN)			Energy Absorbed (J)			Initial Gradient (kN/mm)		
	a	b	c	a	b	c	a	b	c	a	b	c
P_a	-	-	1.16	-	-	4.51	-	-	2.55	-	-	3.98
CV	-	-	0.04	-	-	.004	-	-	0.008	-	-	.007
N_a	2.16	2.11	1.48	3.82	3.85	5.30	2.83	2.95	3.84	2.32	2.39	3.77
CV	0.007	0.14	.014	0.01	0.01	.046	0.01	0.11	.010	0.02	0.01	.013

The values from the plots are presented in the tables (see Table 4-7 and Table 4-8) in terms of initial gradient, load, displacement and energy absorbed to first failure and load displacement and energy absorbed to peak load. These

are the average values from the four sets of results obtained, with appropriate errors.

As can be seen from Table 4-7, the load displacement curves of the auxetic specimen clearly show the first failure point compared to the curves of positive Poisson's ratio specimens. The curves at "a" and "b" for positive Poisson's ratio specimens indicate the presence of delaminations in the specimen prior to the indentation event in the vicinity of the indentor nose region and due to this reason these curves display no first failure point after re-indentation.

Table 4-8 Experimental Peak Load Values, the damaged direction

Specimen Type	Displacement (mm)			Load (kN)			Energy Absorbed (J)		
	a	b	c	a	b	c	a	b	c
P_a	4.6	3.83	4.24	7.01	6.65	9.86	12.94	10.80	23.11
CV	0.05	0.10	.007	.031	.007	.002	.017	.049	.001
N_a	5.00	5.53	4.62	8.98	9.33	11.73	18.38	23.65	27.62
CV	.015	.009	.009	.009	.004	.003	.011	.024	.001

The latter part of the failure process under this form of loading shows a clear enhancement for both auxetic curves in terms of the peak load value and the energy absorbed to this point. The peak load values for auxetic specimen occur at 8.98kN and 9.86kN (see Table 4-8) respectively for curves "a" and "b" with an enhancement of approximately 21% compared to the positive specimen where peak load values for curves "a" and "b" occur at 7.01kN and 6.65kN. During indentation away from the initial indentation point, auxetic specimens

responded as undamaged at both sites 20mm away from centre and show similar peak load values to the initial indentation test. There is a distinct difference in the load displacement curves observed in the auxetic specimen.

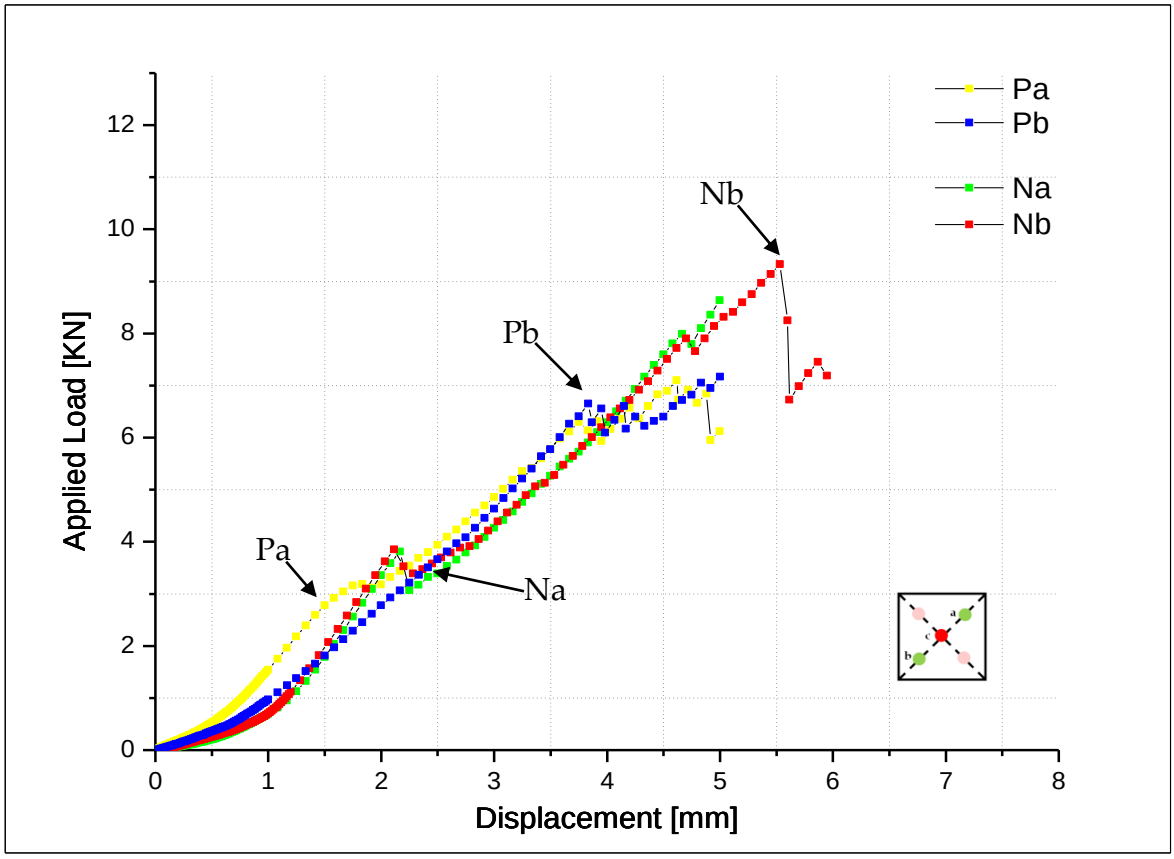

Figure 4-3 Indentation away from the centre along the direction of damage

Similarly, the energy absorption values at this failure stage again show an auxetic enhancement and the energy absorbed for auxetic and positive Poisson's ratio specimens are 18.38J, 12.94J at site "a" and 23.65J, 10.80J at site "b", respectively.

4.2.4 Quasi-Static Re-Indentation perpendicular to the direction of damage

To evaluate the performance of auxetic laminates in the vicinity of the indentor nose region, tests were also carried out perpendicular to the damage direction. The sites "d" and "e" were marked 20mm away at both sides of the centre indentation region. Tests were carried out on four pre- indented specimens of each configuration the indentation tests were performed using the same parameters as mentioned in the above failure process to give an indication of the load displacement behaviour of each material type to total specimen failure at both test sites. Typical load displacement curves are presented for each specimen type in Figure 4-4.

Table 4-9 Experimental First Failure Values, opposite to the damaged direction

Sp. Type	Displacement (mm)			Load (kN)			Energy Absorbed (J)			Initial Gradient (kN/mm)		
	d	e	c	d	e	c	d	e	c	d	e	c
P_a	1.41	1.33	1.16	3.47	2.68	4.51	2.51	1.72	2.55	2.49	2.08	3.98
CV	.044	.058	0.04	.110	.037	.004	.021	.055	.008	.031	.068	.007
N_a	1.8	1.91	1.48	4.56	3.55	5.30	3.67	2.50	3.84	2.42	2.15	3.77
CV	.080	.026	.014	.014	.024	.046	.024	.062	.010	.026	.028	.013

The results are tabulated in terms of initial gradient, load, displacement and energy absorbed to first failure and load, displacement and energy absorbed to peak load Table 4-9 and Table 4-10 present an average value from four sets of experimental data for each specimen type with the coefficient of variation.

Table 4-10 Experimental Peak Load Values, opposite to the damaged direction

Specimen Type	Displacement (mm)			Load (kN)			Energy Absorbed (J)		
	d	e	c	d	e	c	d	e	c
P_a	4.5	4.53	4.24	8.9	8.41	9.86	19.43	17.96	23.11
CV	.033	.045	.007	.067	.013	.002	.037	.062	.001
N_a	4.9	4.9	4.62	9.7	10.60	11.73	22.03	23.28	27.62
CV	.124	.045	.009	.059	.075	.003	.033	.025	.001

The values presented in the above tables and the graph (see Figure 4-4) show significant features after testing perpendicular to the damage direction. First failure of auxetic specimen at site "d" occurs at a displacement and energy value of 1.8mm and 3.67J compared to 21.6%, which is much higher displacement value of positive Poisson's ratio specimen. Indentation behaviour of first failure point at site "e" for the auxetic specimen shows a 30% increase in displacement value compared to the positive Poisson's ratio specimen. Load at initial failure point is also significant for the auxetic specimens with an increase of 24% which is attained at 4.56kN load compared to 3.47kN load of the positive Poisson's ratio specimen.

Similarly, the peak load of the auxetic specimen was found to be 8% higher at site "d" compared to 8.9kN load of the positive Poisson's ratio specimen. However, at site "e" the auxetic specimen appears to have a 20% increase in the peak load and attains value of 10.6kN load compared to the positive Poisson's ratio specimen.

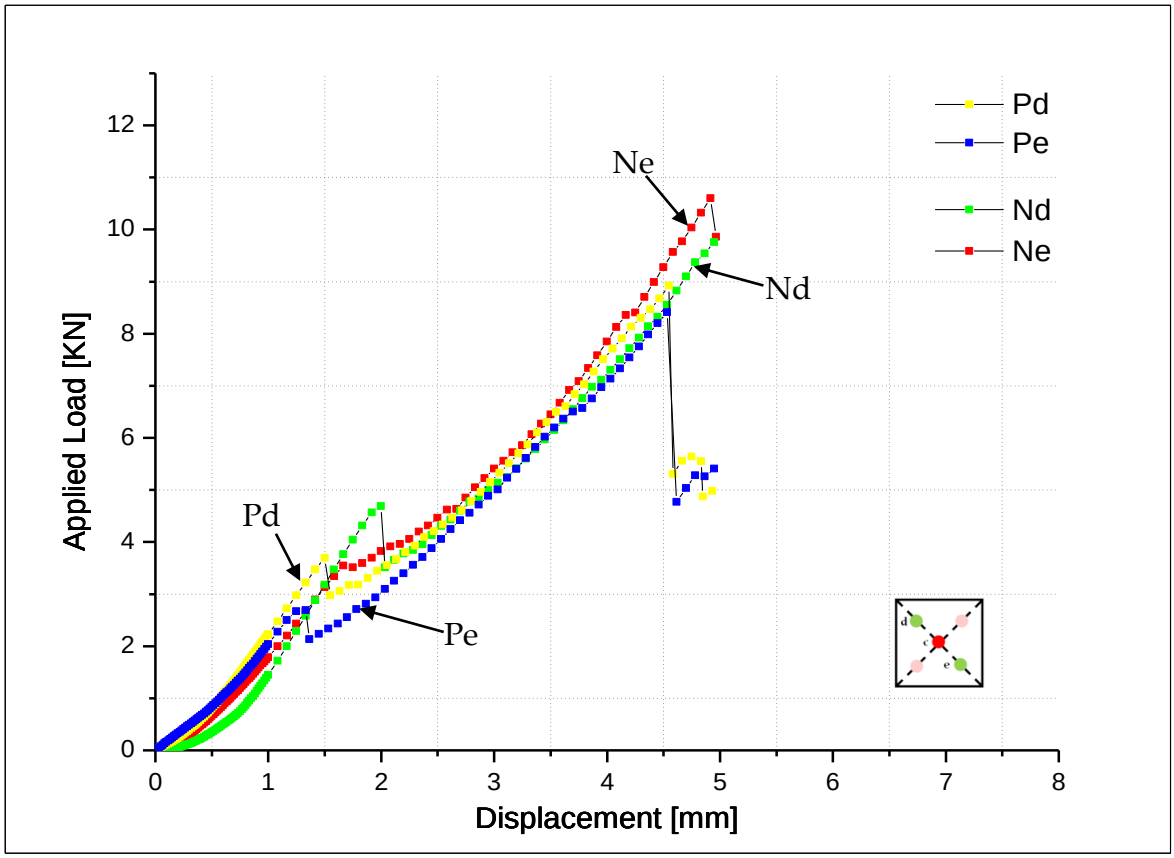

Figure 4-4 **Indentation away from the centre, opposite side along the direction of damage**

The auxetic specimens show a clear enhancement in the energy absorption at both sites "d" and "e" with energy values of 22.03J and 23.28J compared to the positive Poisson's ratio specimen energy values of 19.43J and 17.96J, respectively.

4.3 Low Velocity Impact Resistance (LVI) of Through-Thickness Specimens

As already described in the previous Chapter –3, a low velocity impact (LVI) investigation has been conducted using a drop-weight impact machine to follow the same experimental set up as for the quasi-static indentation tests. These tests were carried out at constant velocity to achieve full damage in the specimens and the impact height was monitored to achieve a constant velocity of 3.5m/sec. All other corresponding test parameters are listed below;

Indentor:	12.7mm (hemispherical)
Drop weight:	4.82 kg
Drop height:	0.6 m
Impact Energy:	29 Joules

The results for each data set of impact tests are presented as Force-Time Histories.

4.3.1 Impact at Centre

The initial low velocity impact investigation was performed on square specimen of each configuration to study the impact behaviour at full specimen damage. All the test parameters were set up according to the above described specifications to allow impact at the centre of each specimen. Load deflection

plots are significantly different for the auxetic specimens. Load deflection curves will be discussed in more detail in Discussion Chapter – 6 but these curves (see Figure 4-5) are plotted here to show the interesting features of each specimen. Certain values are directly taken from the plots to represent different parts of the failure process of each specimen, such as deflection, energy absorbed, peak load and gradient. The results presented in Table 4-11 are the average values form the four sets of results obtained, with the coefficient of variation (CV).

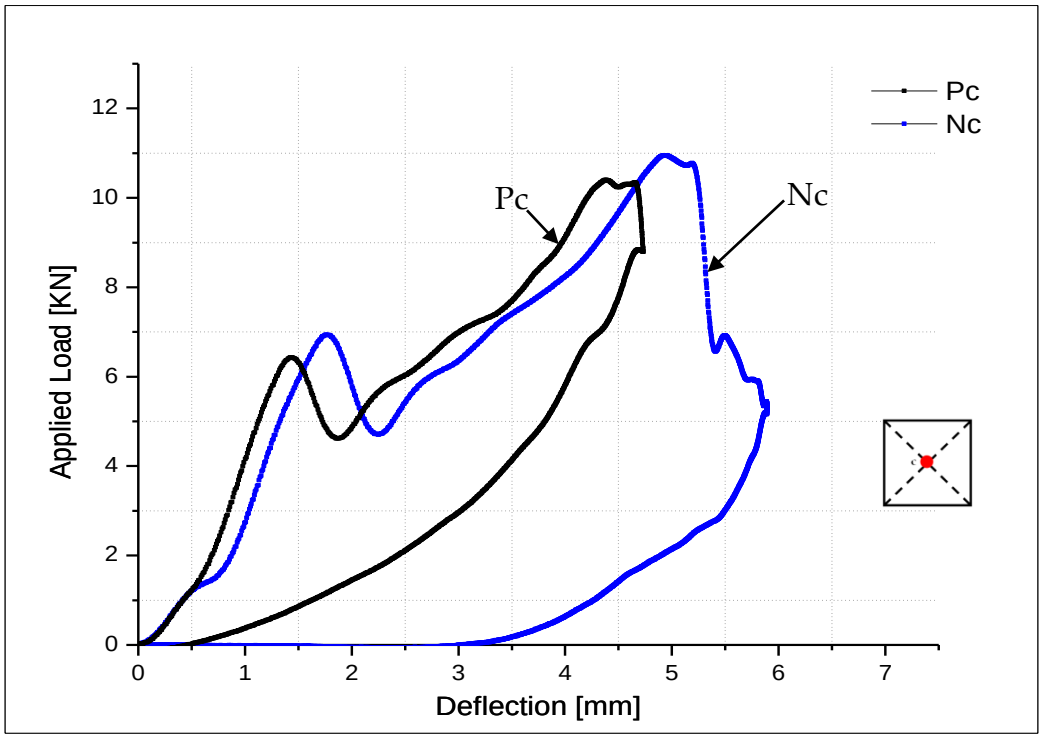

Figure 4-5 Force Time Histories, Impact at centre

It is interesting to note that at the first failure point the auxetic specimen shows higher average initial load of 6.98kN (see Table 4-11) for delamination compared to the 6.32kN load of the Positive Poisson's ratio specimen. The

energy absorption value at this point is also observed to be higher for the auxetic specimen.

Table 4-11 Experimental First Failure Values, Impact at centre

Specimen Type	Deflection (mm)	Load (kN)	Energy Absorbed (J)	Gradient (kN/mm)
P_a	1.43	6.32	3.69	6.18
CV	0.052	0.119	0.104	0.133
N_a	1.78	6.98	4.15	5.48
CV	0.075	0.066	0.051	0.057

As can be seen from the above plot and the values presented in the Table 4-12 below, the auxetic specimens also achieve significantly higher peak loads. The maximum load before failure in the auxetic specimens is 11.01kN and that is higher compared to the positive Poisson's ratio specimen.

Table 4-12 Experimental Peak Load Values, Impact at centre

Specimen Type	Max Deflection (mm)	Max Load (kN)	Energy Absorbed (J)
P_a	4.36	10.32	24.10
CV	0.034	0.038	0.014
N_a	4.94	11.01	25.62
CV	0.029	0.008	0.013

The energy absorption values at this point follow the same trend as observed in case of quasi-static indentation away from centre in the damage direction with the auxetic specimens showing higher values compared with the positive Poisson's ratio specimens.

4.3.2 Re-Impact at Centre

Specimens of each configuration were impacted and the re-impacted at the centre to achieve the full failure. The drop height was maintained to achieve the energy required for full damage and data were acquired for further analysis. Load deflection curves were plotted (see Figure 4-6) in order to find the interesting features of the re-impact event.

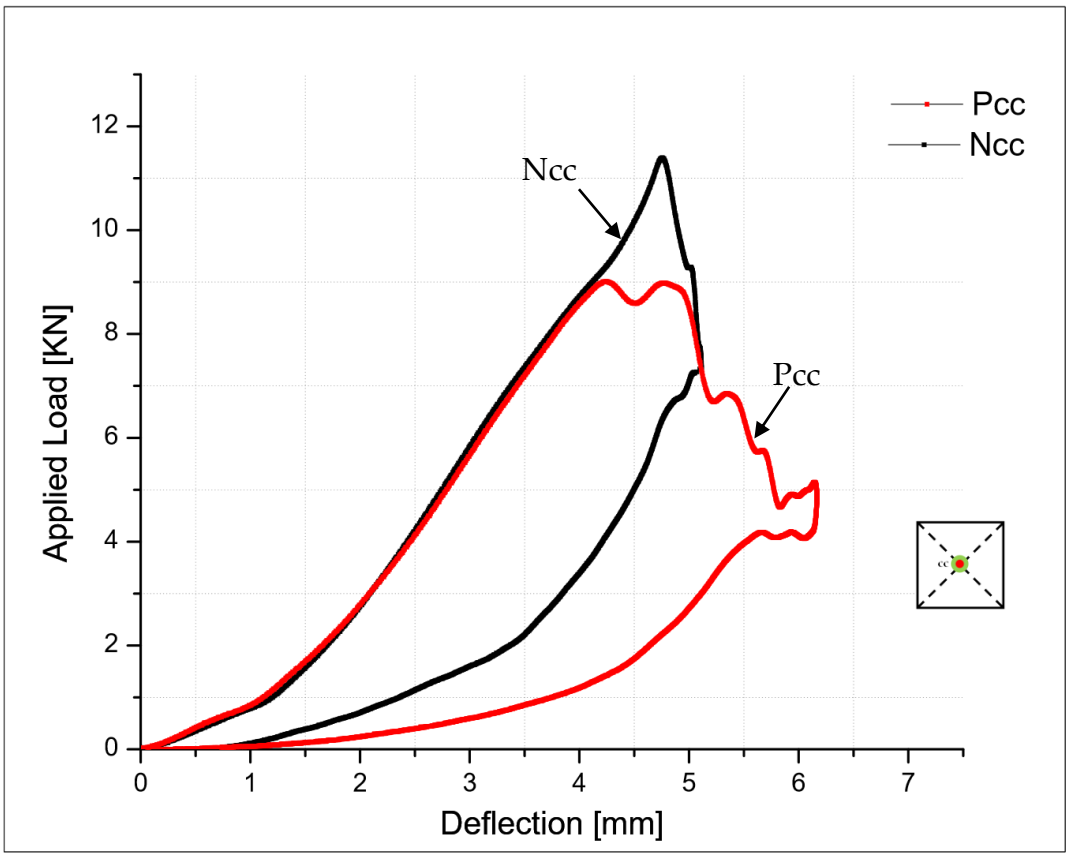

Figure 4-6 Force Time Histories, Impact and Re-Impact at Centre

Load, deflection and absorbed energy of the impact event were recorded in Table 4-13. Simple integration technique was used to calculate the energy absorption values from the plots.

The load, deflection curves are significantly different for the re-impact event than those of the initial impact event. The first failure point and change in the gradient disappear in the re-impacted specimen.

Table 4-13 Experimental Peak Load Values, Impact and Re-impact at centre

Specimen Type	Max Deflection (mm)		Max Load (kN)		Energy Absorbed (J)	
	C	CC	C	CC	C	CC
P_a	4.36	4.41	10.32	10.13	24.10	16.6
CV	0.034	0.049	0.038	0.104	0.014	0.020
N_a	4.94	5.09	11.01	12.65	25.62	15.47
CV	0.029	0.022	0.008	0.037	0.013	0.027

The re-impact event shows entirely a unique trend for both the specimens with no sign of the first failure point on the curve, (see Figure 4-6), and this is because the damage has already been initiated in the initial impact event.

4.3.3 Re-Impacts along the damage direction

To evaluate the performance of the auxetic specimens, tests were carried out 20mm away at sites "a" and "b" from the centre of initial impact site along the damage direction. Test parameters were controlled to allow 29J impact energy for each material type to achieve full damage and the major features were identified on the plots (see Figure 4-7).

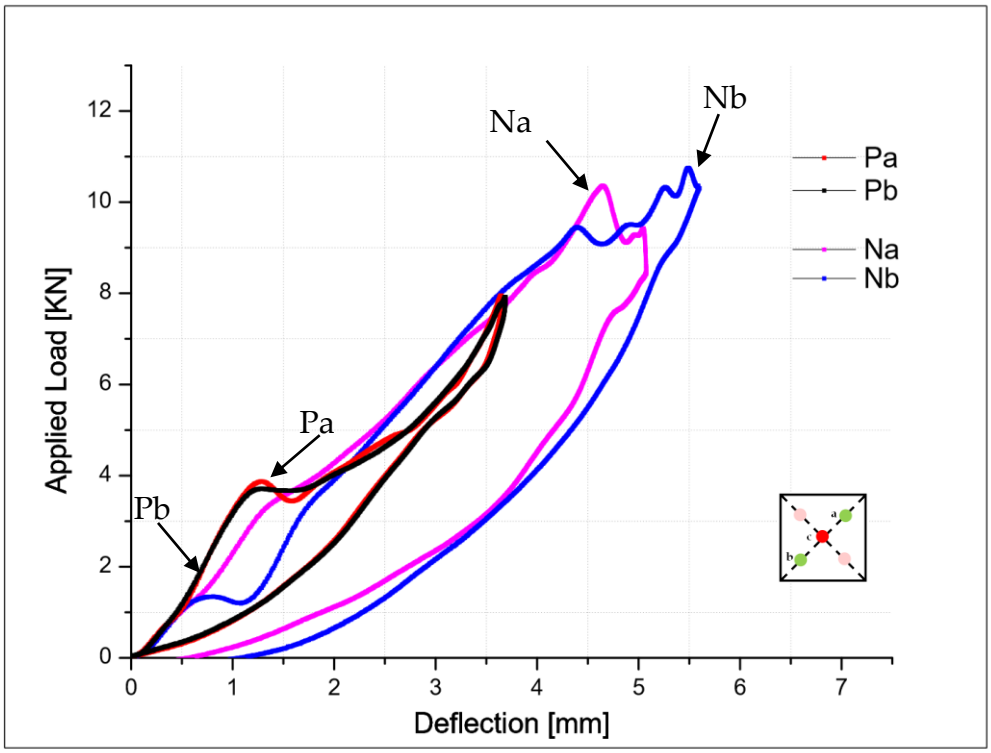

Figure 4-7 Load Deflection Plots, Impact at damaged direction

Table 4-14 Experimental First Failure Values, damage direction

Sp. Type	Deflection (mm)			Load (kN)			Energy Absorbed (J)			Gradient (kN/mm)		
	a	b	c	a	b	c	a	b	c	a	b	c
P_a	1.27	1.26	1.43	3.70	3.86	6.32	2.08	2.15	3.69	4.20	3.71	6.18
CV	.061	.094	.052	.025	.016	.119	.029	.024	0.104	.034	.178	.133
N_a	1.51	1.86	1.78	3.54	3.35	6.98	2.11	2.17	4.15	1.96	1.98	5.48
CV	.051	.058	.075	.010	.056	.066	.031	.049	0.051	.229	.154	.057

The values from the plots are presented in Table 4-14 and Table 4-15 in terms of gradient, load, deflection and energy absorbed to the first failure and load, deflection and energy absorbed to peak load of the full event.

The values listed in the table are the average values from four sets of tests with appropriate errors.

Table 4-15 Experimental Peak Load Values, along the direction of the damage

Sp. Type	Max Deflection (mm)			Max Load (kN)			Energy Absorbed (J)		
	a	b	c	a	b	c	a	b	c
P_a	3.72	3.68	4.36	7.96	7.94	10.32	13.76	13.79	24.10
CV	.063	.058	.034	.091	.087	0.038	.064	.068	0.014
N_a	4.98	5.88	4.94	10.47	10.8	11.01	25.37	27.26	25.62
CV	.127	.053	.029	.074	.070	0.008	.043	.034	0.013

The plots for the auxetic specimens indicate a clear enhancement in terms of energy absorption and peak load values. The values for energy absorption are also observed to be approximately 46.8% higher for the auxetic specimen compared to the positive Poisson's ratio specimens. This trend in the properties will be examined in detail in the Discussion chapter.

4.3.4 Re-Impacting perpendicular to the damage direction

Tests were also carried out 20mm away at sites "d" and "e" from the centre of initial impact site perpendicular to the damage direction. Low velocity impact test parameters were set accordingly so that the damage process of each specimen type could be evaluated and the major features of the plots identified. Typical curves for each specimen type are plotted in Figure 4-8. The extracted

data in Table 4-16 represents the load, deflection, energy absorbed and gradient of the impact event to peak load.

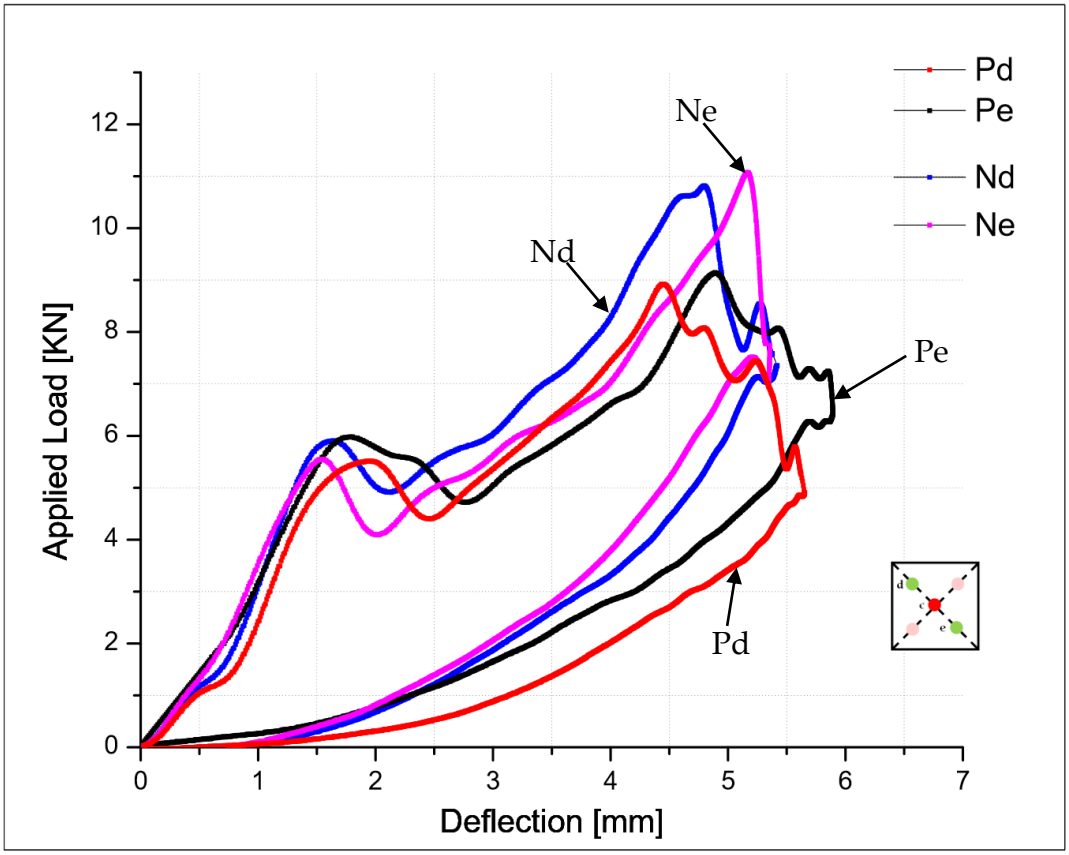

Figure 4-8 **Load Deflection Plots, Impact opposite side along the direction of damage**

These are the average values from the four sets of results, with appropriate errors. The peak load values of the auxetic specimens presented in the table are slightly higher correspond with the values of 11.10kN and 11.01kN at sites "d" and "e" respectively compared to the positive Poisson's ratio type specimens. The energy absorption values at these sites are also significantly higher than the positive Poisson's ratio specimens and are found to be approximately 20% higher for the auxetic specimens.

Table 4-16 Experimental Peak Load Values, opposite to the direction of damage

Sp. Type	Max Deflection (mm)			Max Load (kN)			Energy Absorbed (J)			Gradient (kN/mm)		
	d	**e**	**c**	**d**	**e**	**c**	**d**	**e**	**c**	**d**	**e**	**c**
P_a	4.46	4.62	4.36	8.93	9.09	10.32	20.81	20.56	24.10	6.10	5.97	6.18
CV	.041	.035	.034	.059	.082	0.038	.034	.090	0.014	.054	.150	0.133
N_a	4.89	5.16	4.94	10.8	11.10	11.01	24.26	25.92	25.62	5.23	5.15	5.48
CV	.026	.059	.029	.091	.038	0.008	.046	.053	0.013	.093	0.112	0.057

Gradient is also an interesting characteristic to predict the material's response, with lower value of an impact event indicating higher resistance to penetration [178]. Auxetic specimens are found tougher than the positive type specimens and hence they are more resistant to penetration of a foreign object.

4.4 Quasi-Static Indentation of In-plane Specimens

Quasi-static Indentation tests were performed on all in-plane specimens to evaluate their behaviour in response to an indentation event. The specimens were loaded at a rate of 2mm/min with a penetration object of 12.7mm to an indentation depth of 5mm to achieve full specimen damage. The data was recorded throughout the test and typical load displacement plots for each specimen types are presented below (see Figure 4-9). The values extrapolated are presented in Table 4-17 in terms of load, displacement and energy absorption. A simple integration technique was used to calculate the energy

absorbed. As in previous tests, these are the average values from four sets of tests, with coefficient of variation.

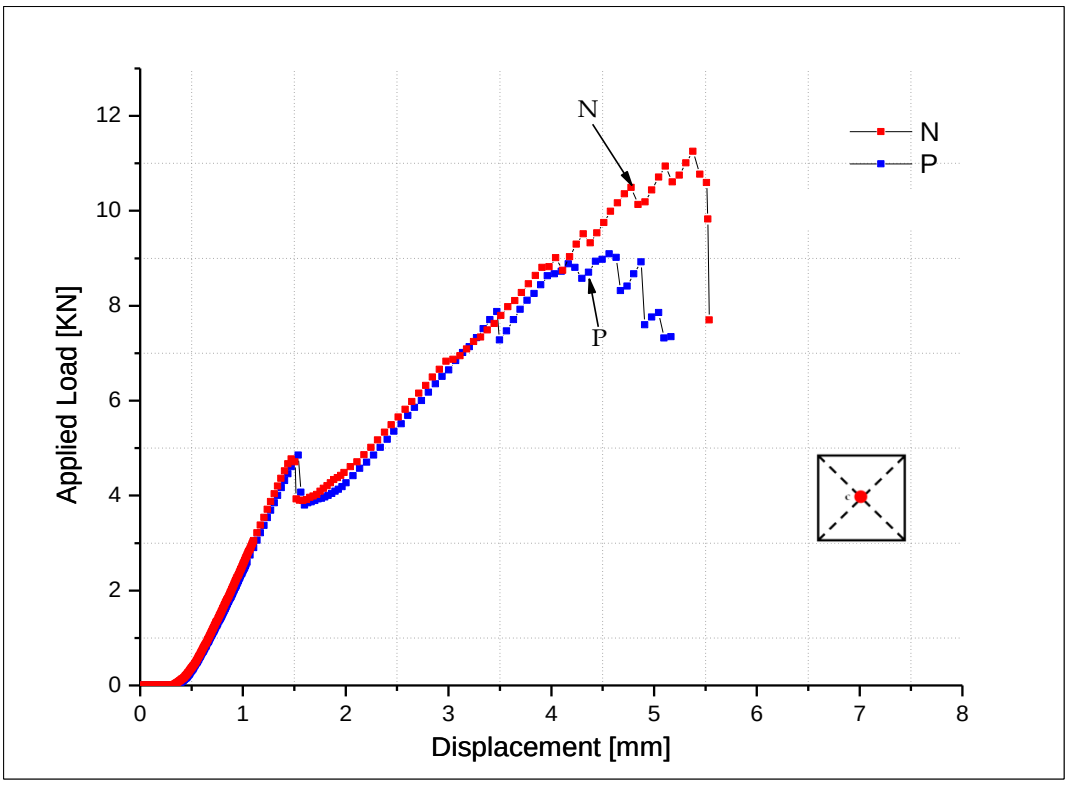

Figure 4-9 Load Displacement Indentation Curves at full damage load

The values presented in the table show significantly different trends for the auxetic and positive Poisson's ratio specimens. Such type of failure in auxetic in-plane specimens occurs at a displacement value of 5.37mm that is 15% higher compared to the positive Poisson's ratio specimen. A clear auxetic enhancement is also evident for the energy absorbed with a 27% increase.

Table 4-17 Experimental Peak Load Values, Indentation at full damage load

Specimen Type	Displacement (mm)	Load (kN)	Energy Absorbed (J)	Gradient (kN/mm)
P_b	4.56	9.09	23.15	3.06
CV	0.170	0.0879	0.057	0.223
N_b	5.37	11.25	31.82	3.95
CV	0.0821	0.0443	0.042	0.188

Similarly, peak load value for the auxetic specimens is much higher and failure occurs at 11.25kN that is 19% higher compared to the positive specimen types and this will be examined in detail in the discussion chapter later.

4.5 Low Velocity Impact Resistance of In-plane Specimens

Low velocity impact tests have been carried out using the same experimental setup as for the quasi-static indentation tests. In this work a fixed weight (4.3741kg) Instron Dyntaup Model 9250HV Drop Tower Impact Tester was used. Also both the in-plane indentation and impact tests were performed using a 12.7mm indentor as loading object. For detailed impact investigation three impact levels were chosen to replicate the different stages of the failure process as revealed by quasi-static loading.

4.5.1 Impact level 1

Drop height: 0.0659m

Impact Energy: 3.15Joules

Impact velocity: 1.137m/sec

Thickness: 4.7mm

Experimental results are plotted for both types of specimens. At the first energy level under impact loading, before the onset of damage,

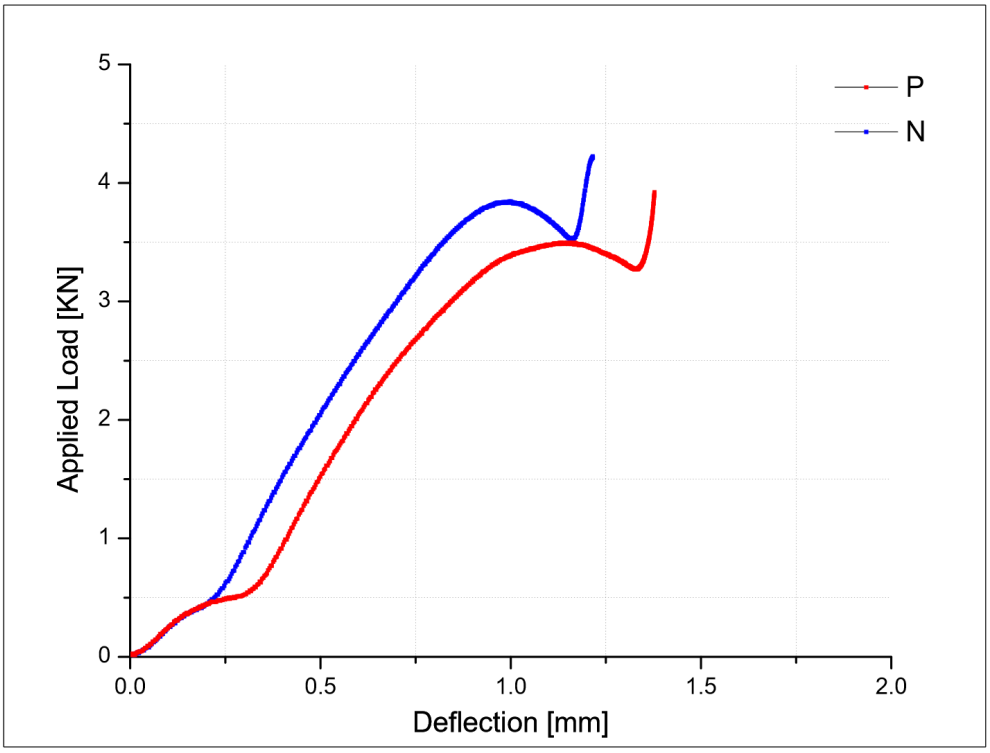

Figure 4-10 Load Deflection Plots, Impact Level 1

The auxetic specimens sustain slightly higher peak load values than the positive Poisson's ratio specimen, as shown in load deflection plots (see Figure 4-10). A summary of the values obtained is provided in Table 4-18 below.

Table 4-18 Experimental Failure Values, Impact level 1

Specimen Type	Deflection (mm)	Load (kN)	Energy Absorbed (J)
P_b	1.12	3.47	2.01
CV	0.507	0.133	0.300
N_b	1.05	3.85	1.97
CV	0.190	0.104	0.342

4.5.2 Impact level 2

Drop height: 0.2532m

Impact Energy: 12.1Joules

Impact velocity: 2.228m/sec

Thickness: 4.7mm

At this impact energy level the first failure point of the laminate failure process has been isolated and is the only notable feature on quasi-static load displacement curve. This is very useful, as it has allowed load, deflection and energy absorption values to be compared across the specimen types and with the values observed under quasi-static testing. It also provides an idea of the amount of energy that each specimen can absorb before the onset of failure enabling the damage threshold for each specimen to be identified.

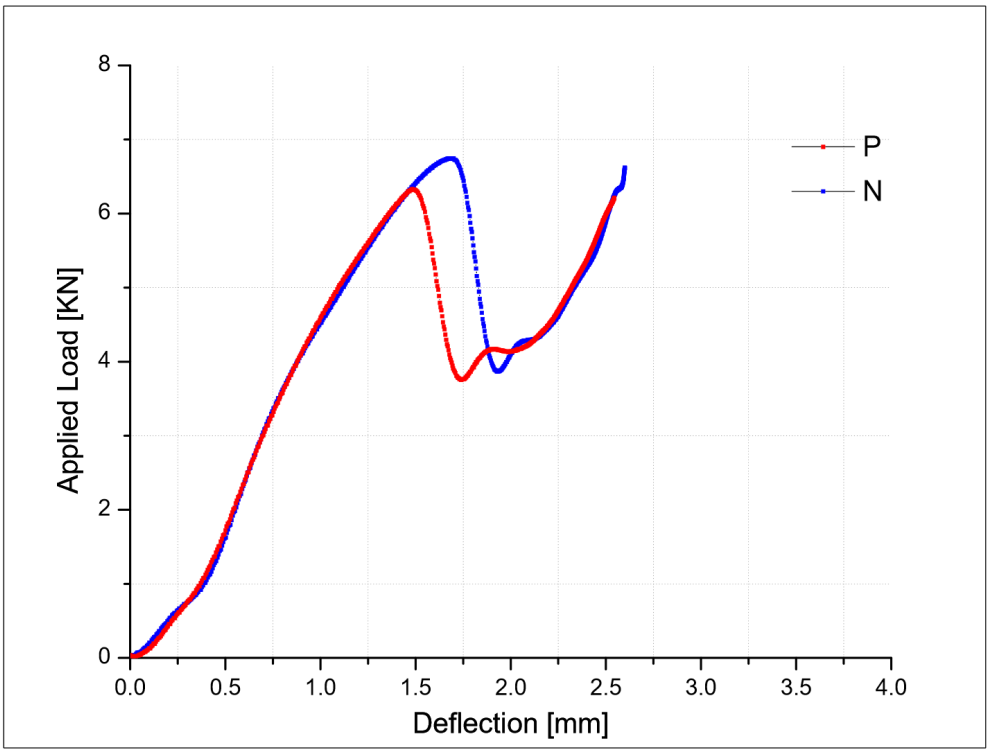

Figure 4-11 Load Deflection Plots, Impact Level 2

The load deflection plots in Figure 4-11, observed for the auxetic and positive Poisson's ratio specimens show, almost similar trends before the failure point in curves for the both specimens However the failure point appears to be a different event. In the Auxetic specimen, the calculated value of the gradient is lower as listed in table Table 4-19.

Table 4-19 Experimental Peak Load Values, Impact level 2

Specimen Type	Deflection (mm)	Load (kN)	Energy Absorbed (J)	Gradient (kN/mm)
P_b	1.50	6.34	4.73	4.67
CV	0.315	0.037	0.172	0.174
N_b	1.70	6.67	6.12	3.79
CV	0.259	0.032	0.079	0.135

It is interesting to note that the maximum deflection values are almost same across the specimen types but the amount of energy absorbed during this impact event is observed higher in the auxetic specimens.

4.5.3 Impact level 3

Drop height: 0.658m

Impact Energy: 31.4Joules

Impact velocity: 3.589m/sec

Again at this impact energy, the curves are very similar to each other in terms of the first failure point and peak loads for the auxetic and positive Poisson's ratio specimens as shown in Table 4-20.

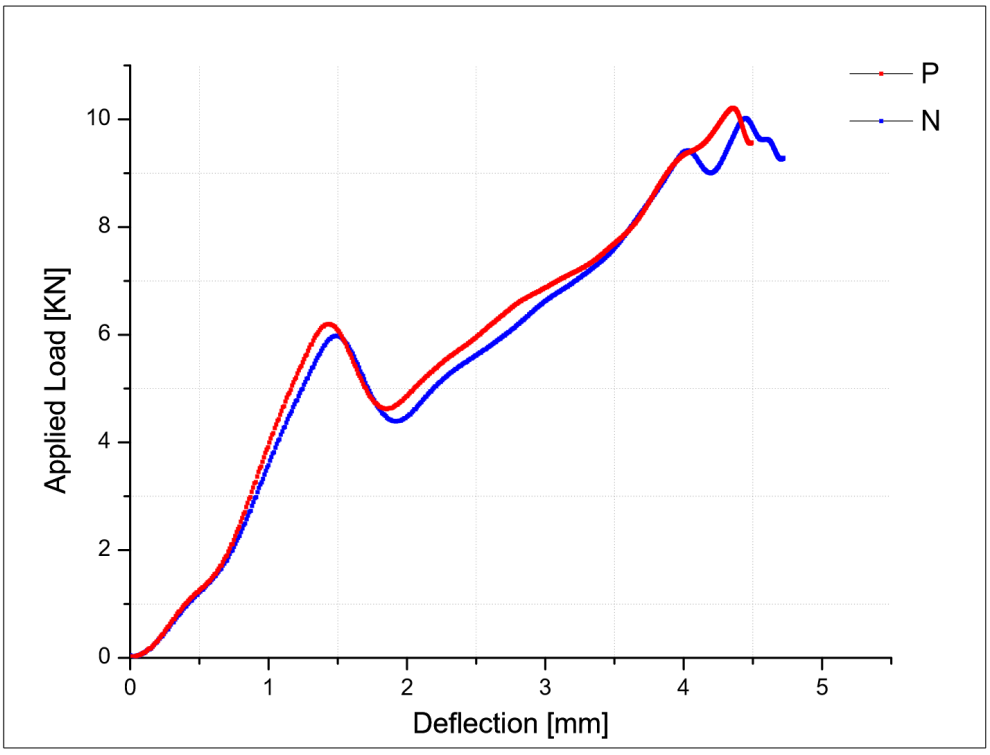

Figure 4-12 Load Deflection Plots, Impact Level 3

Table 4-20 Experimental First Failure Values, Impact level 3

Specimen Type	Deflection (mm)	Load (kN)	Energy Absorbed (J)	Gradient (kN/mm)
P_b	1.43	6.21	3.83	6.75
CV	0.181	0.074	0.195	0.071
N_b	1.50	6.54	3.91	5.90
CV	0.160	0.097	0.104	0.130

The maximum load and energy absorbed in the auxetic and positive Poisson's ratio specimens is shown in Table 4-21.

Table 4-21 Experimental Peak Load Values, Impact level 3

Specimen Type	Deflection (mm)	Load (kN)	Energy Absorbed (J)
P_b	4.36	10.24	23.72
CV	0.157	0.052	0.028
N_b	4.45	10.04	23.98
CV	0.123	0.078	0.019

4.6 Residual Testing of In-plane Specimens

Impact specimens; as described in Chapter 3 "Experimental Methods", have been reloaded quasi-statically using the same indentor and test parameters as for both the impact test and for the indentation tests carried out on specimens with a negative in-plane Poisson's ratio. A "residual" load, displacement plot is obtained from which load displacement and absorbed energy values at

different stages of the failure process are recorded in the same way as previously discussed. These residual values can then be compared with average values (see Table 4-22 and Table 4-23) of the original quasi-static investigation so that the amount of damage and resulting loss in load carrying capability in the specimen after the different impact events can be assessed.

Table 4-22 Experimental First Failure Values, Indentation at full damage load

Specimen Type	Displacement (mm)	Load (kN)	Energy Absorbed (J)	Gradient (kN/mm)
P_b	1.53	4.90	1.62	1.56
CV	0.309	0.087	0.274	0.207
N_b	1.46	4.76	2.63	1.48
CV	0.252	0.081	0.131	0.223

This is a very simple and effective way of comparing the amount of damage present in different types of the specimens. It gives a clear insight into the damage in each specimen when cross referenced with fractographic analysis.

Table 4-23 Experimental Peak Load Values, Indentation at full damage load

Specimen Type	Displacement (mm)	Load (kN)	Energy Absorbed (J)
P_b	4.56	9.09	23.15
CV	0.114	0.036	0.031
N_b	5.37	11.25	31.82
CV	0.051	0.057	0.038

Residual tests have been carried out for energy levels one, two and three and results are presented in terms of "residual" load displacement plots. The values from these plots are tabulated which are the average from two specimens tested at each energy level.

4.6.1 Low velocity impact level 1

The load displacement plot (see Figure 4-13) for the indentation after impact of 3.15 Joules specimens shows the similar trends to the quasi-static indentation plot (see Figure 4-9), that reveals a first failure point and then continues with a reduced gradient to a peak load value. This gives a clear indication that for impact level one, first failure had not occurred, and is confirmed by the impact force histories, which show no evidence of damage event, and the damage analysis revealed no visible damage. Hence it can be concluded that 3.15 Joules is indeed below the damage threshold for all the tested specimens. The values from the plots are tabulated in Table 4-24 and Table 4-25 in terms of load, displacement and energy absorption to first failure and peak load point.

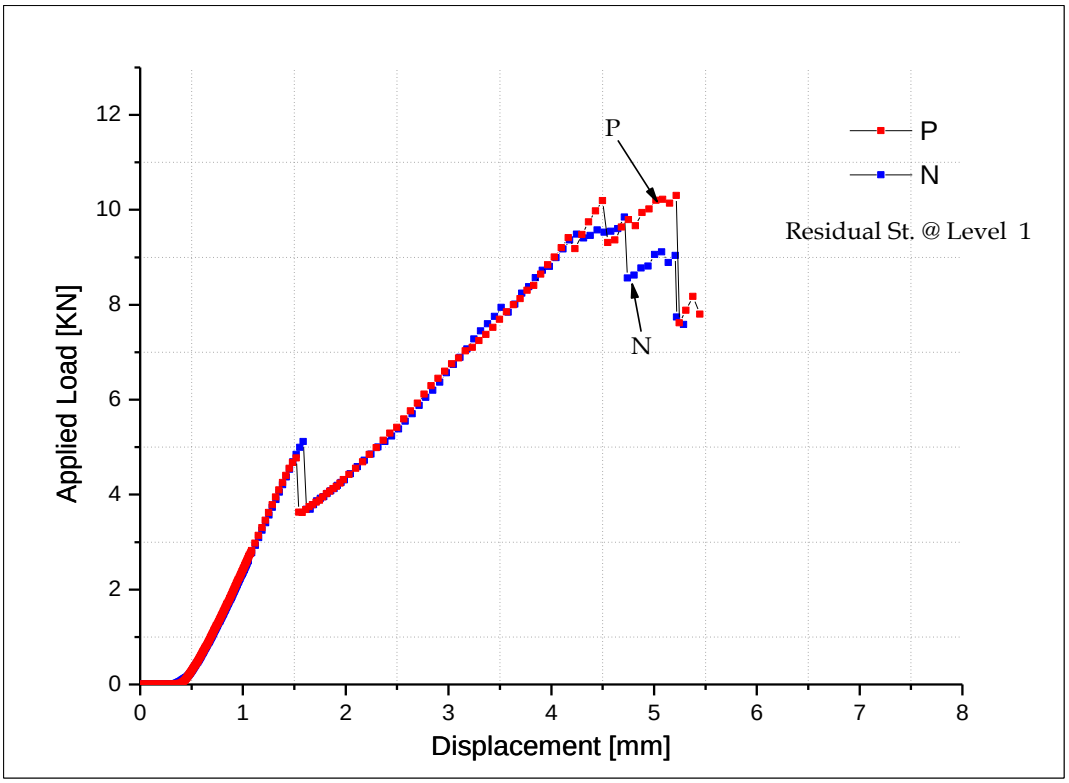

Figure 4-13 Residual Load Displacement plot, Impact level 1 specimen

At the first failure point, the auxetic specimens achieved a load of 5.11kN, compared to 4.70kN for positive Poisson's ratio specimens as shown in Table 4-24.

Table 4-24 Experimental First Failure Values Impact level 1 – Residual loading

Specimen Type	Displacement (mm)	Load (kN)	Energy Absorbed (J)
P_b	1.49	4.70	2.62
CV	0.364	0.125	0.225
N_b	1.58	5.11	2.98
CV	0.279	0.084	0.189

In terms of peak load and general behaviour after first failure, similar trends are observed as for the original quasi-static tests. However, in this case the peak load value is lower for the auxetic specimens.

Table 4-25 Experimental Peak Load Values Impact level 1 – Residual loading

Specimen Type	Displacement (mm)	Load (kN)	Energy Absorbed (J)
P_b	4.98	10.19	22.52
CV	0.185	0.052	0.040
N_b	4.71	9.87	20.74
CV	0.114	0.056	0.029

4.6.2 Low velocity impact level 2

The impact event for these specimens occurred at 12.1J and residual testing can assess the behaviour and the effect of failure event for each specimen type. There is no evidence of the first failure (see Figure 4-14) after residual testing of impact level two specimens. The load displacement plot for the auxetic specimen exhibits lower performance compared to the positive Poisson's ratio specimen. This suggested the expected trend for auxetic specimens after initial impact event due to the presence of more localized damage area under the indentor nose region. The reduction in load carrying capability as shown in Figure 4-14 of the auxetic specimen is 7% as compared to the positive Poisson's ratio specimens. This trend is also observed for energy absorption, which is more severe and, the difference of value is 29%.

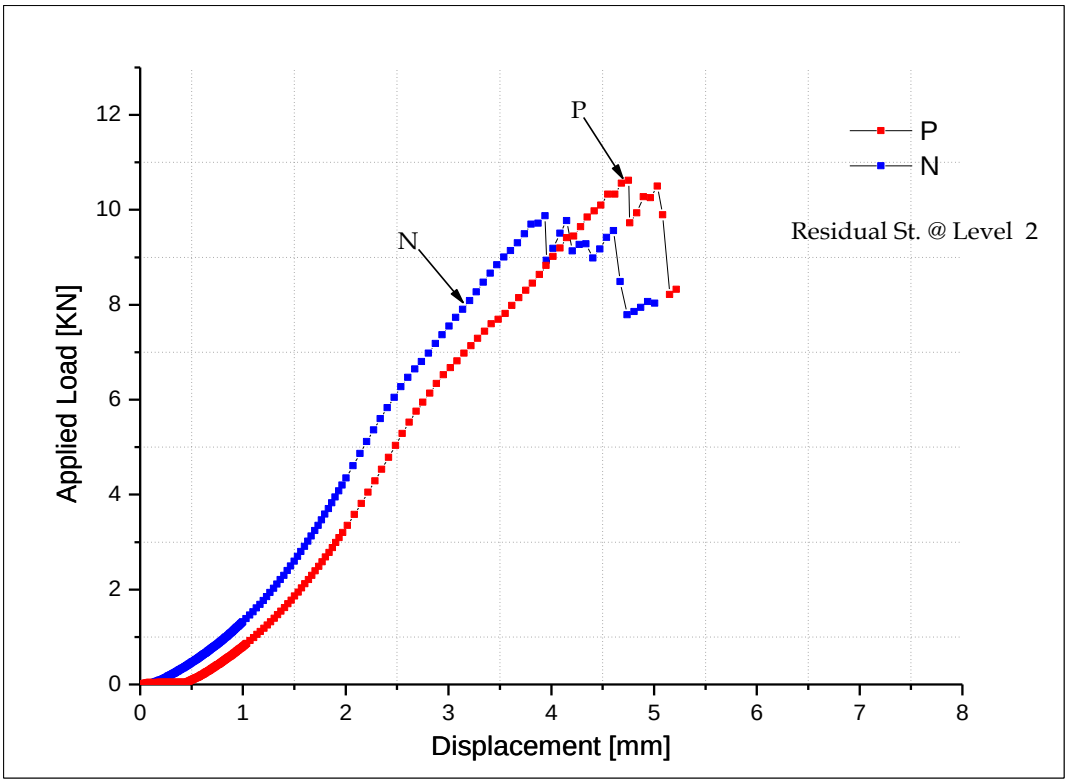

Figure 4-14 Residual Load Displacement plot, Impact level 2 specimen

The only conclusion at this stage that can be drawn; is that this event appears more severe for the auxetic specimen but occurs at higher levels of load and energy to create the damage in the positive Poisson's ratio specimens. Further conclusions will be deduced after analysing the impact level three and also when a complete insight of the damage observed for all specimens, under all test conditions, are fully dealt with in the "Discussion Chapter 6".

Table 4-26 Experimental Peak Load Values Impact level 2 – Residual loading

Specimen Type	Displacement (mm)	Load (kN)	Energy Absorbed (J)
P_b	4.75	10.62	22.67
CV	0.142	0.044	0.044
N_b	3.98	9.87	17.57
CV	0.168	0.060	0.037

4.6.3 Low velocity impact level 3

The residual load displacement plot for the impact level "3" specimens is shown in Figure 4-15. The gradient of the auxetic specimen is not very low here in this case. Again this suggests that the first failure event was more severe for the auxetic specimen and as such the residual strength of the specimen after this point is lower.

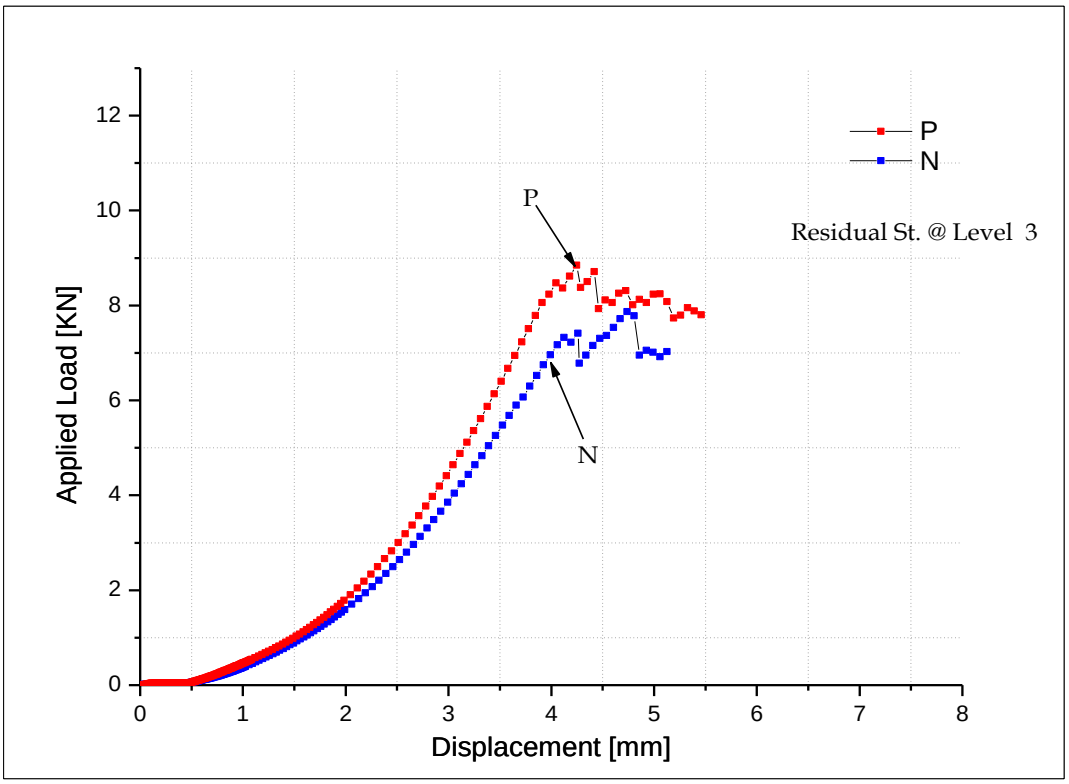

Figure 4-15 Residual Load Displacement plot, Impact level 3 specimen

It is evident from the peak load of the residual tests on the impacted specimens that the positive Poisson's ratio specimens still show slightly better residual load carrying capability as shown in Table 4-27.

Table 4-27 Experimental Peak Load Values Impact level 3 – Residual loading

Specimen Type	Displacement (mm)	Load (kN)	Energy Absorbed (J)
P_b	4.24	8.84	16.71
CV	0.168	0.111	0.035
N_b	4.73	7.86	14.52
CV	0.198	0.081	0.057

4.7 High Velocity Impact Resistance (HVI) of Through-thickness Specimens

A preliminary investigation into high velocity impact (HVI) failure has been conducted using a gas gun operated by compressed air to allow a 9mm diameter steel ball to strike the surface of a 30mm^2 specimen.

These tests were conducted at two different energy levels to measure the response of through-thickness auxetic and positive Poisson's ratio specimens. Impact velocity and impact energy were measured during the tests to compare across the specimen types.

Input Energy 12 (J)

Air pressure 60psi

Table 4-28 Experimental Values of High Impact velocity, 90m/sec

Specimen type	units	P_a		N_a	
		Measured values	CV	Measured values	CV
Light gate Delta time (0.02m)	μs	216.00	0.027	215.90	0.015
Impact velocity (light gates)	m/s	93.00	0.038	92.66	0.028
VideoEDR	μs	2.80	0.094	3.0	0.033
Video measured impact velocity	m/s	90.00	0.035	90.40	0.016
Video measured rebound velocity	m/s	22.00	0.096	24.30	0.042
Input energy (light gate)*	J	12.70	0.032	12.78	0.031
Input energy (video)	J	12.10	0.029	12.16	0.015
Rebound energy (video)	J	0.72	0.119	0.88	0.073
Loss of energy from ball (video-video)	J	11.43	0.022	11.79	0.056
Loss of energy from ball (light gates-video)	J	11.25	0.028	11.91	0.036

At least three specimens were tested for each case and the average values obtained are listed with appropriate errors in Table 4-28 and Table 4-29.

The values listed in Table 4-28 show slightly higher values of rebound velocity for the auxetic specimens when impacted at approximate 12J energy. This behaviour is also evident from loss of energy from the ball itself and the auxetic specimens show slightly higher values for the loss of energy compared to the positive Poisson' ratio specimen.

Input Energy 19 (J)

Air pressure 90psi

Table 4-29 Experimental Values of High Impact velocity, 109m/sec

Specimen type	units	P_a		N_a	
		Measured values	CV	Measured values	CV
Light gate Delta time (0.02m)	μs	180.63	0.020	175.50	0.024
Impact velocity (light gates)	m/s	110.84	0.013	114.08	0.018
VideoEDR	μs	3.0	0.033	3.0	0.080
Video measured impact velocity	m/s	109.53	0.019	109.63	0.023
Video measured rebound velocity	m/s	30.86	0.049	31.91	0.082
Input energy (light gate)*	J	18.312	0.057	19.39	0.041
Input energy (video)	J	17.86	0.071	17.89	0.066
Rebound energy (video)	J	1.45	0.104	1.52	0.179
Loss of energy from ball (video-video)	J	16.57	0.102	16.37	0.103
Loss of energy from ball (light gates-video)	J	16.86	0.119	17.67	0.064

To evaluate the high velocity impact performance of the auxetic and positive Poisson's ratio specimens, tests were also conducted at 19J energy. Again, here three specimens of each configuration were tested with the same test conditions as described above and data were recorded throughout the test and as shown in Table 4-29. The rebound velocity was observed to be 3% higher in the auxetic specimens as compared to the positive Poisson's ratio specimens. In high velocity impact, the bounce back phenomena of the steel ball, after striking to an auxetic specimen shows a higher energy loss as compared to the positive Poisson's ratio specimen. This energy loss is observed 4% higher than in the case of striking with positive Poisson's ratio specimen. High velocity impact response was observed almost similar for both the auxetic and positive Poisson's ratio specimen. This will be described in detail in "Discussion Chapter 6" with reference to the previous work and the published literature.

4.8 Damage Analysis

All the through-thickness specimens were tested at the centre and a subset of these specimens was then re-tested at the same site. These specimens were sectioned along the 0^o principal material axes e.g. (see Figure 4-16) through the centre of the test site for inspection with an optical microscope. A third group of the specimens was tested at the centre of a square specimen and then re-tested both sides along the damage direction. These specimens were sectioned along the damaged direction for inspection with an optical microscope as shown Figure 4-20. A final group was tested at the centre and then re-tested both sides opposite to the damaged direction. These specimens were then sectioned as shown in (see Figure 4-22) for inspection by an optical microscope. This method of inspection allows delaminations and other types of damage to be identified through-thickness of each specimen and the extent of damage was measured from the fractographs. All the in-plane auxetic and positive Poisson's ratio specimens were also sectioned for detailed analysis of the damage profile after impact and residual strength measurement. Lastly, fractograpic analysis was conducted on through-thickness specimens after high velocity impact tests to measure the extent of damage.

4.9 Fractographic analysis of Quasi-static Indentation Testing

The results of the fractographic analysis are presented for the quasi-static indentation tests together with a brief summary of the findings for each different test.

4.9.1 Through-thickness specimens

4.9.1.1 Indentation at Centre

Figure 4-16 Fractography of positive specimen; Indentation at Centre

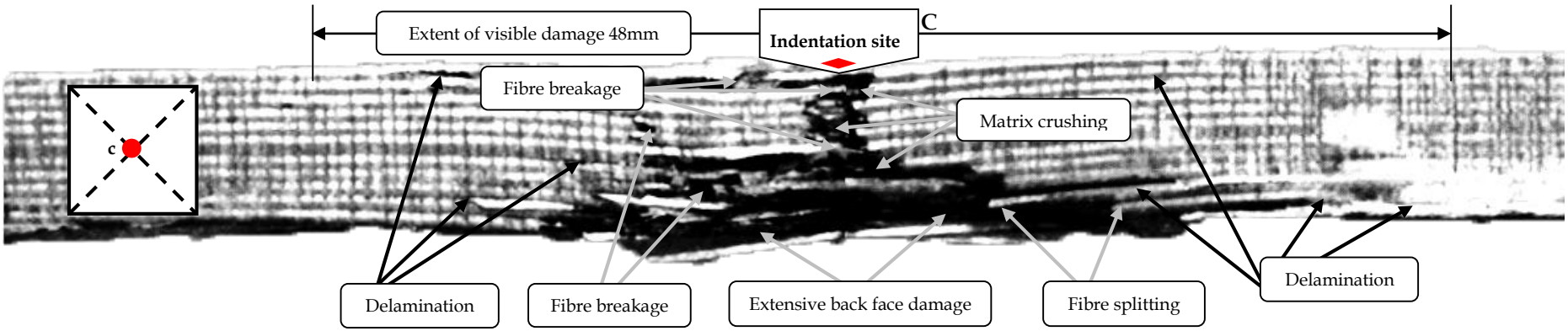

Summary of Damage

Sectioning of this indented specimen reveals an irregular type of damage progression through the specimen thickness, characterized initially by fibre breakage and severe matrix crushing. This is followed by a region of fibre breakage through the thickness and by a much more severe and scattered region of breakage and delamination. In this way the damage region does widen significantly towards the back face of the laminate, where there is a considerable amount of damage.

Figure 4-17 Fractography of auxetic specimen; Indentation at Centre

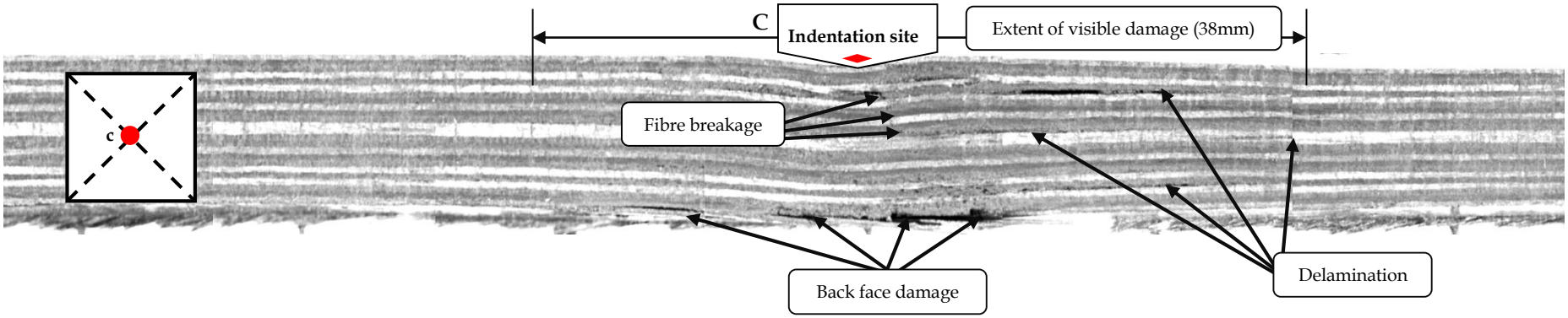

Summary of Damage

This indented specimen reveals a systematic progression of damage through the thickness and severity increases slightly towards the back face of the laminate. Through the laminate thickness, there are a few discernible delaminations. The progressive fibre breakage characterises the damage directly under the indentor nose resulting in back surface failure accompanied by very localised delaminations.

4.9.1.2 Re-Indentation at Centre

Figure 4-18 Fractography of positive specimen; Indentation and Re-Indentation at Centre

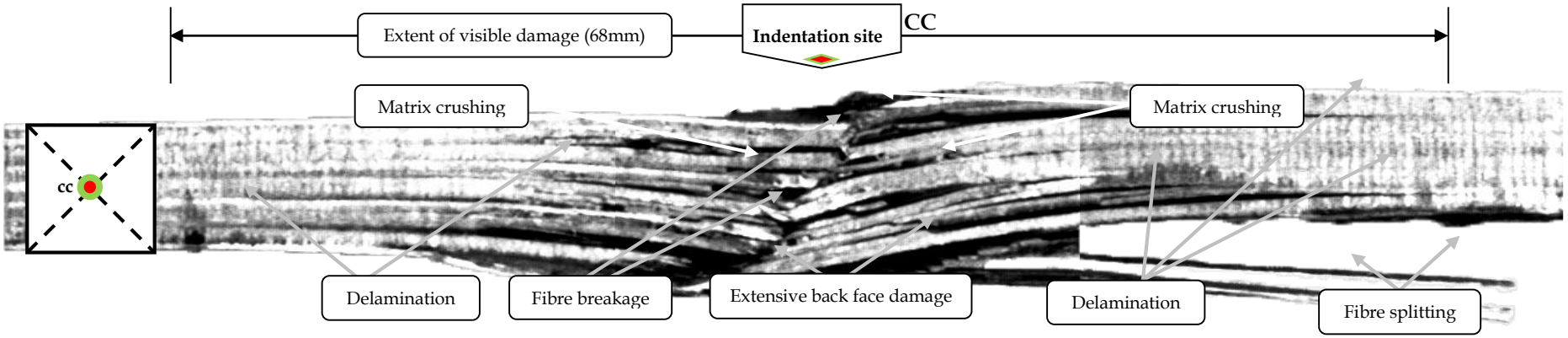

Summary of Damage

Fractographic analysis of Re-indented positive Poisson's ratio specimen reveals more severe damage through the specimen thickness. The damage is mainly composed of matrix crushing under the indentor nose with fibre breakage and many large delaminations through the thickness. Delamination becomes wider towards the back face, accompanied by fibre splitting and matrix crushing. Here, damage through the thickness takes the form of a very wide inverted pine tree, being almost as wide at the top as the bottom.

Figure 4-19 Fractography of auxetic specimen; Indentation and Re-Indentation at Centre

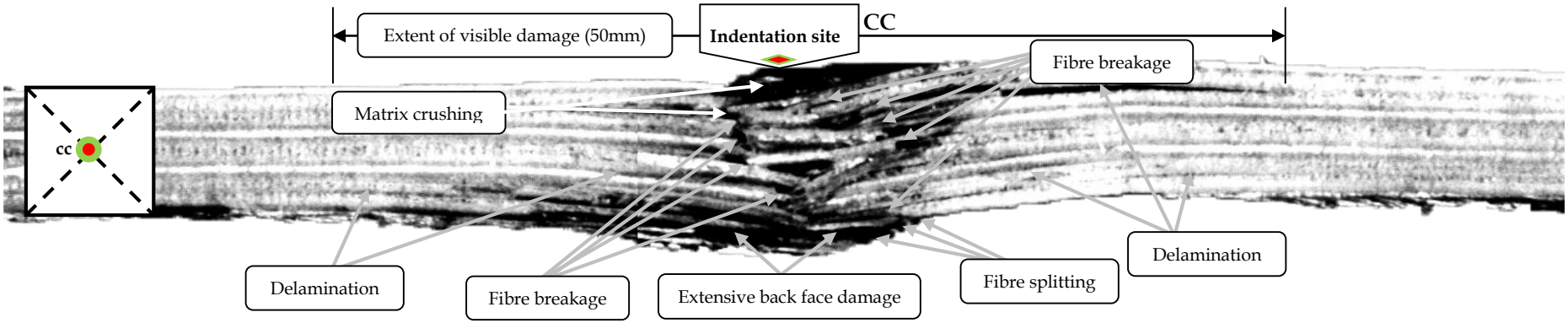

Summary of Damage

Sectioning of this auxetic specimen reveals a considerable localized amount of damage under the indentor nose. This damage shows severe fibre breakage leading to back surface failure, accompanied by a few delaminations and fibre splitting. Delaminations are not as widely spaced below the mid-plane of the specimen. However, the progression of the damage through the specimen thickness is much more localised and directly under the indentor nose, in this way creating a much narrower inverted pine tree.

4.9.1.3 Indentation along the damage direction

Figure 4-20 Fractography of positive specimen; Indentation along the damage direction

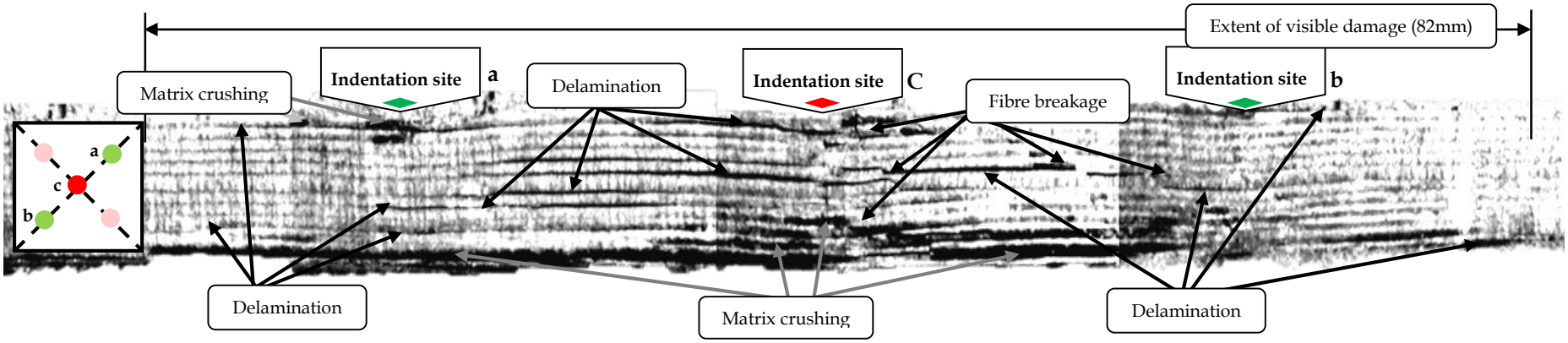

Summary of Damage

Fractographic analysis of the sectioned positive Poisson's ratio specimen reveals a disordered type of damage through the specimen thickness. Damage at site "c" is initiated by matrix crushing and fibre breakage; followed by large delaminations, which spread and widen to the back surface of the specimen. The damage at sites "a" and "b" due to Re-indentation is mainly characterised by fibre crushing and delaminations unlike the specimen shown in Figure 4-20.

Figure 4-21 Fractography of auxetic specimen; Indentation along the damage direction

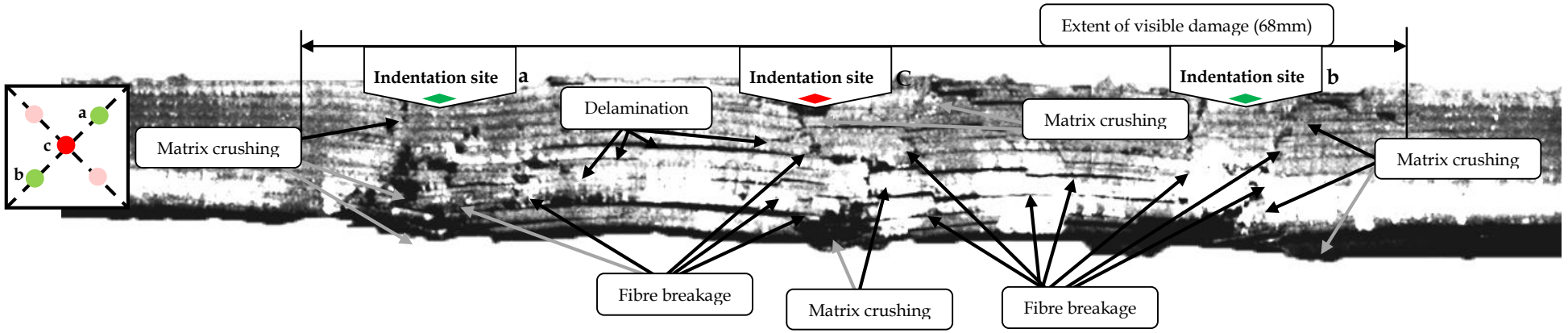

Summary of Damage

Indentation testing of the negative Poisson's ratio specimen reveals a systematic damage progression mechanism. This damage is initiated by matrix crushing at each site with extensive fibre breakage, which moves downward towards the back face of the specimen. The severity of the damage is obvious under each indentation site. Uniformly distributed delaminations are found on both sides in the vicinity of site "c", which are characterized by fibre breakage. No obvious delamination was found in the outer region of indentation sites "a" and "b"

4.9.1.4 Indentation opposite to the damage direction

Figure 4-22 Fractography of positive specimen; Indentation opposite to the damage direction

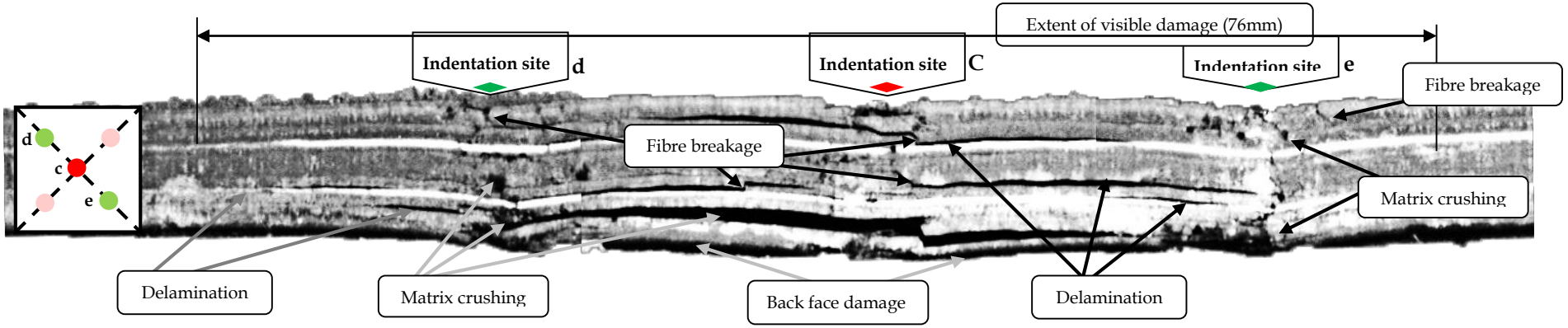

Summary of Damage

The indentation testing fractograph of the sectioned specimen reveals a randomly distributed damage pattern. This damage is characterized by matrix crushing with a considerable amount of delamination and a randomly distributed small amount of fibre breakage. Delaminations run through the indentation sites "d" and "e" and also move downward throughout the specimen thickness.

Figure 4-23 Fractography of auxetic specimen; Indentation opposite to the damage direction

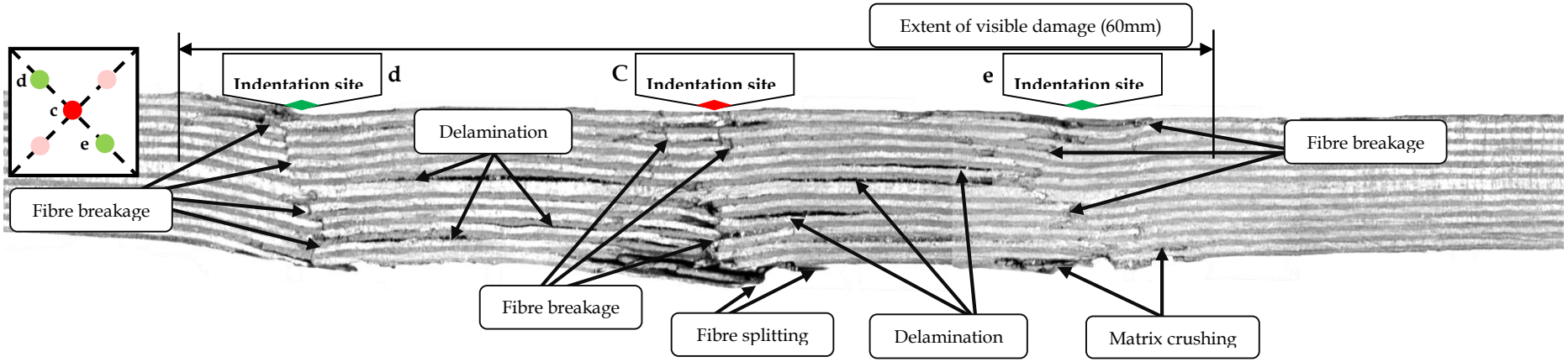

Summary of Damage

The sectioned auxetic indented specimen reveals uniformly distributed damage. This damage is composed of matrix crushing followed by fibre breakage, which is uniformly distributed through the thickness of the specimen. The damage is more severe below the mid-plane under the indentation sites. Few delaminations are also found, which are restricted to between the damage sites "d" and "e"

A detailed insight into the above tests is shown in graphical representation for each type of specimens. The extent of damage measured both in the through-thickness auxetic and the positive Poisson's ratio specimens are shown in Figure 4-24.

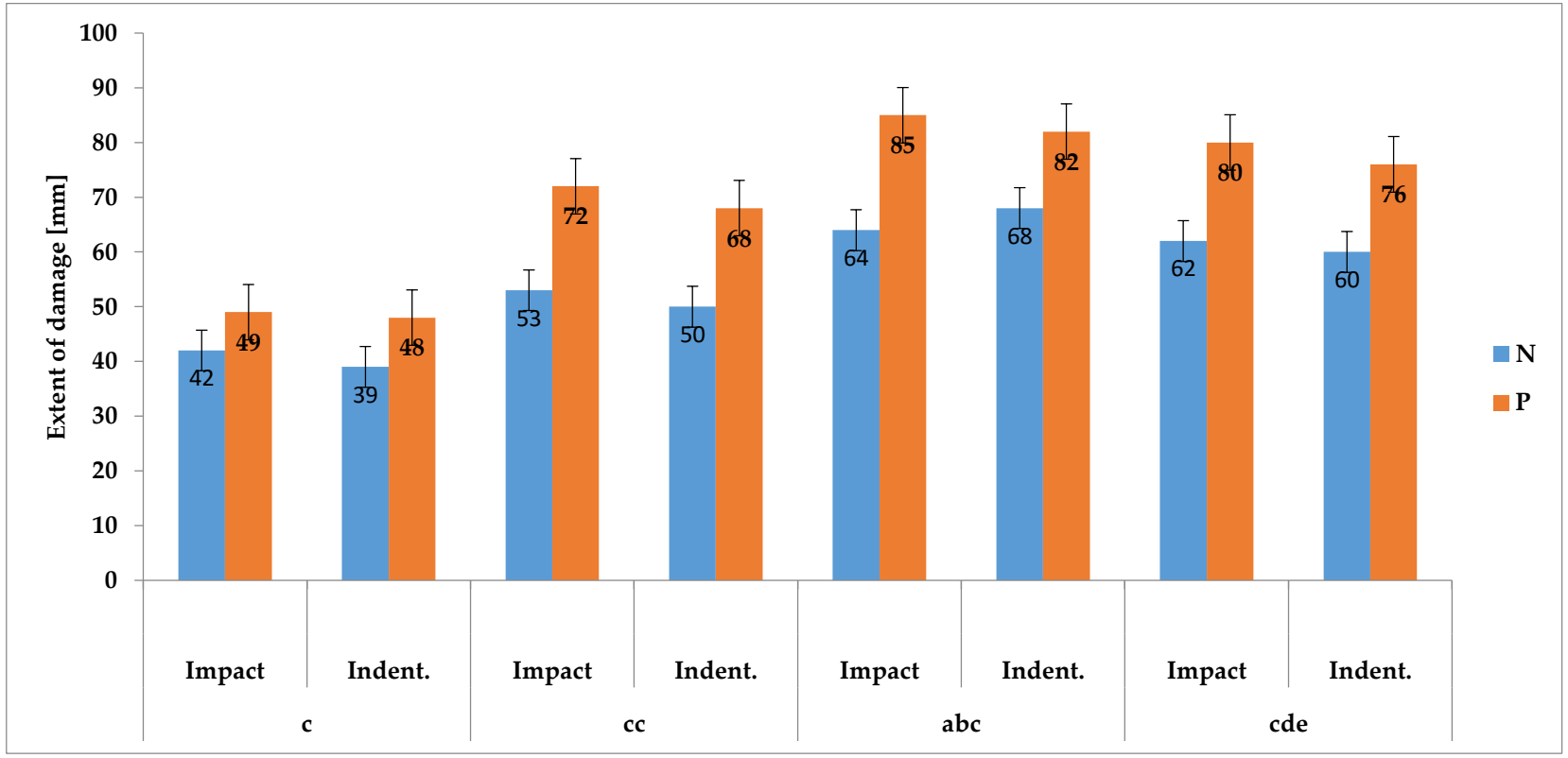

Figure 4-24 **Extent of damage [mm] in auxetic and positive Poisson's ratio specimens**

Similarly, results are also presented in Figure 4-25 as absorbed energy in comparison with the extent of damage for both the auxetic and positive Poisson's ratio specimens. It is obvious from the graph that the auxetic specimens tend to absorb more energy with less amount of extent of damage compared to the positive Poisson's ratio specimens.

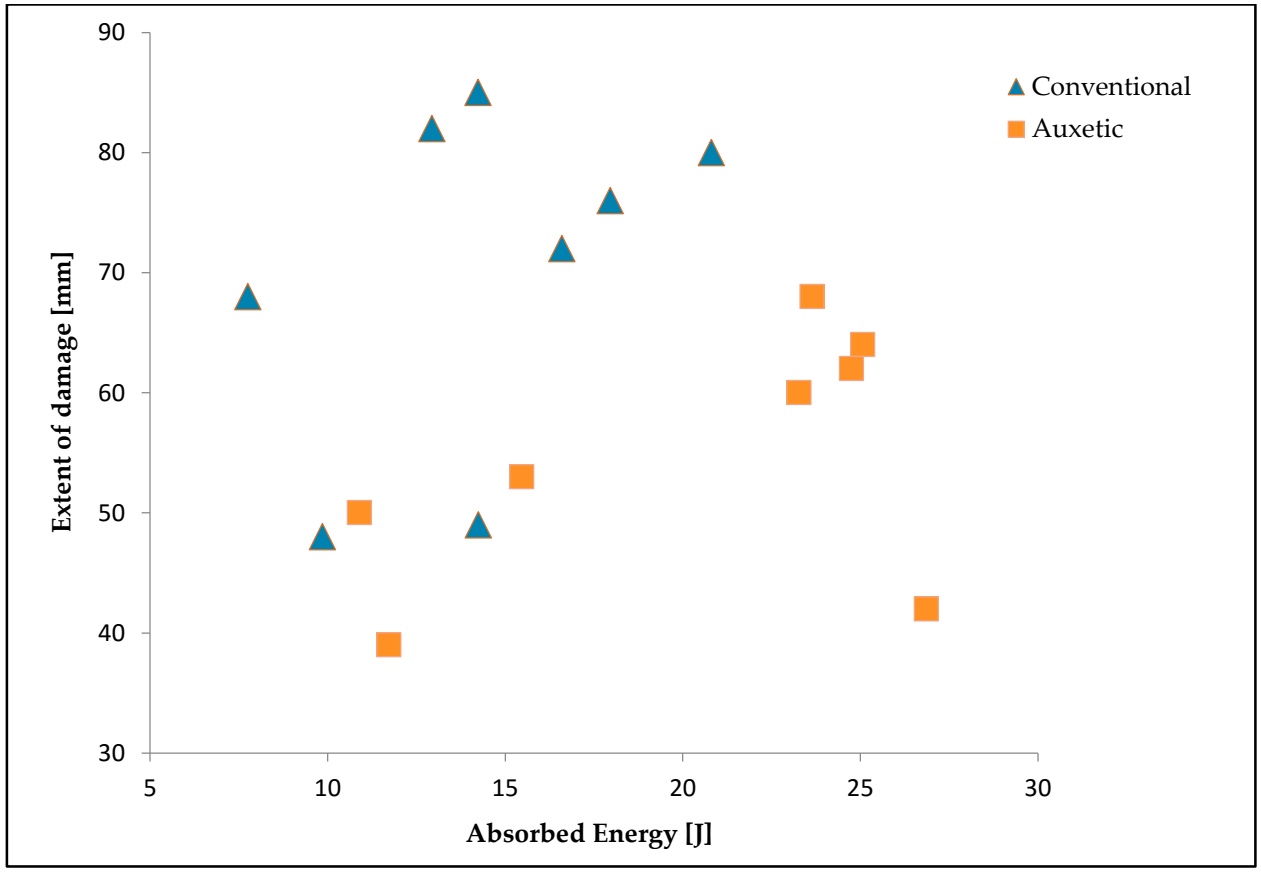

Figure 4-25 Extent of damage vs absorbed energy

4.9.2 In-plane specimens

All the In-plane specimens were sectioned after indentation to full damage load and investigation was carried out to study the indentation response of the auxetic specimens. A brief summary of each sectioned specimen is given below;

Figure 4-26 Positive In-plane specimen after full damage load

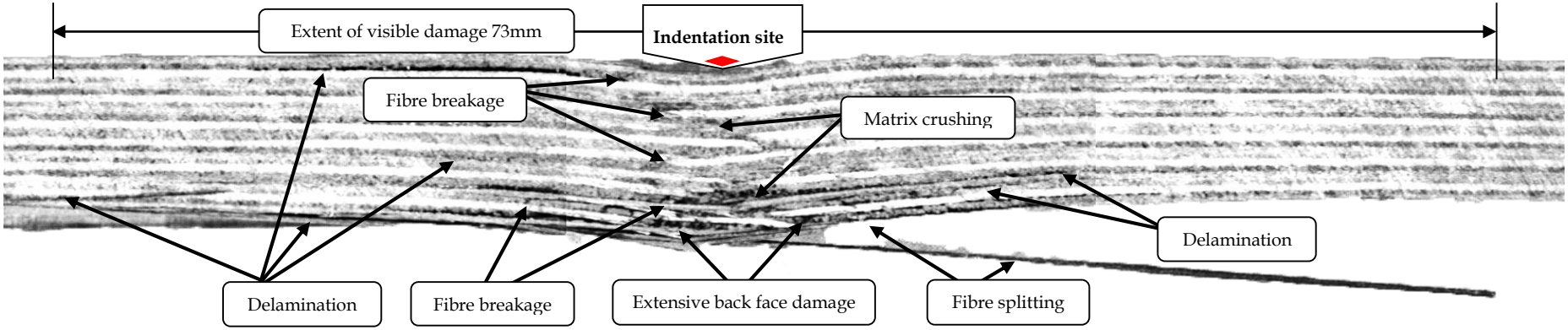

Fractographic analysis of this indented specimen reveals a randomly distributed damage pattern. The damage is characterized by matrix crushing with a considerable amount of delamination and small amount of randomly distributed fibre breakage. Delaminations run across the specimen and increase in number towards the back face of the specimen.

Figure 4-27 Auxetic In-plane specimen after full damage load

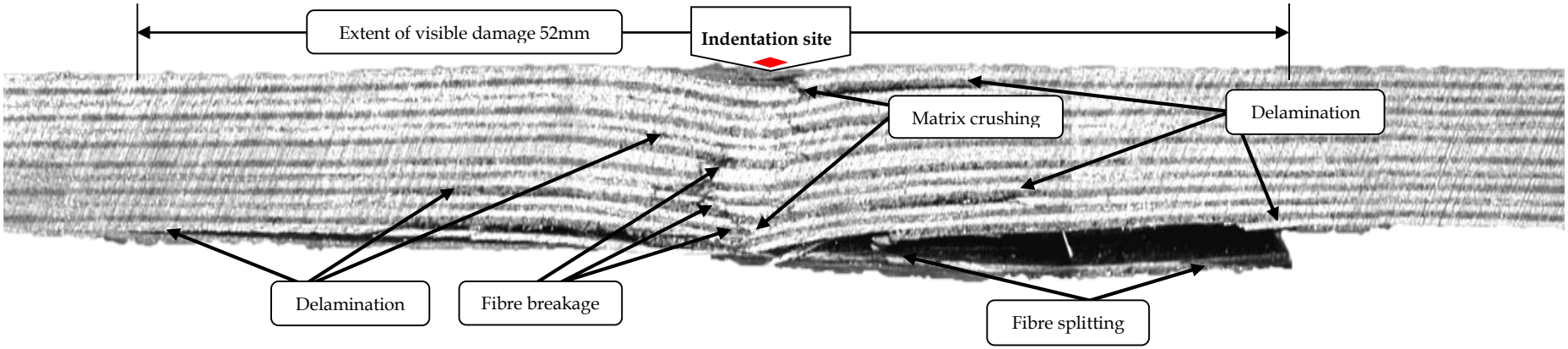

Sectioning of the indented specimen shows quite orderly progression of damage from top to bottom of the laminate. There is a slight increase in the severity towards the back face of the laminate. Delaminations are more uniformly distributed throughout the specimen. The damage is characterised by progressive fibre breakage under the indentor nose resulting in back face failure accompanied by few large dalaminations at the back surface of the laminate

4.10 Fractographic analysis of Low Velocity Impact testing (LVI)

4.10.1 Through-thickness specimens

4.10.1.1 Impact at Centre

Figure 4-28 Fractography of positive specimen; Impact at Centre

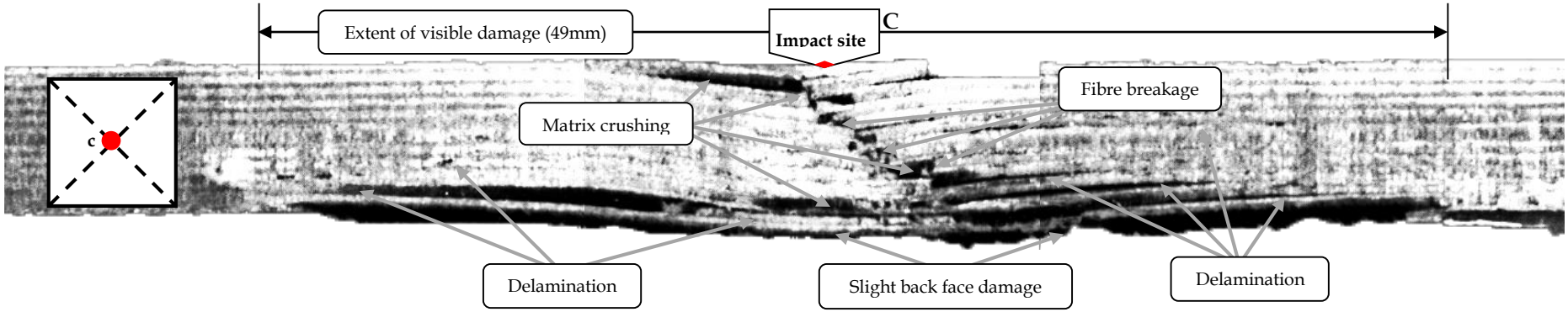

Summary of Damage

The damage revealed by fractographic analysis for this positive Poisson's ratio specimen shows an array of different types of damage through the thickness direction, initiated by severe matrix crushing and fibre breakage. Fibre failure follows throughout the specimen and becomes much more severe and dispersed with a considerable amount of large delaminations towards the back face region.

Figure 4-29 Fractography of auxetic specimen; Impact at Centre

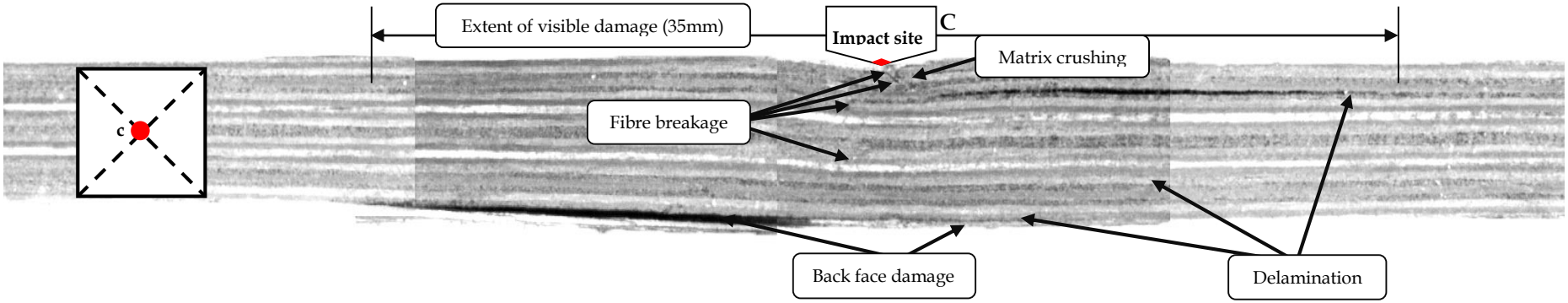

Summary of Damage

The damage revealed by fractographic analysis for this auxetic specimen shows a considerable amount of damage under the indentor nose. This damage is similar to that of the indented auxetic specimen; matrix crushing directly under the impact site, followed by fibre breakage leading to back surface failure, accompanied by small delaminations.

4.10.1.2 Re-Impact at Centre

Figure 4-30 Fractography of positive specimen; Impact and Re-Impact at Centre

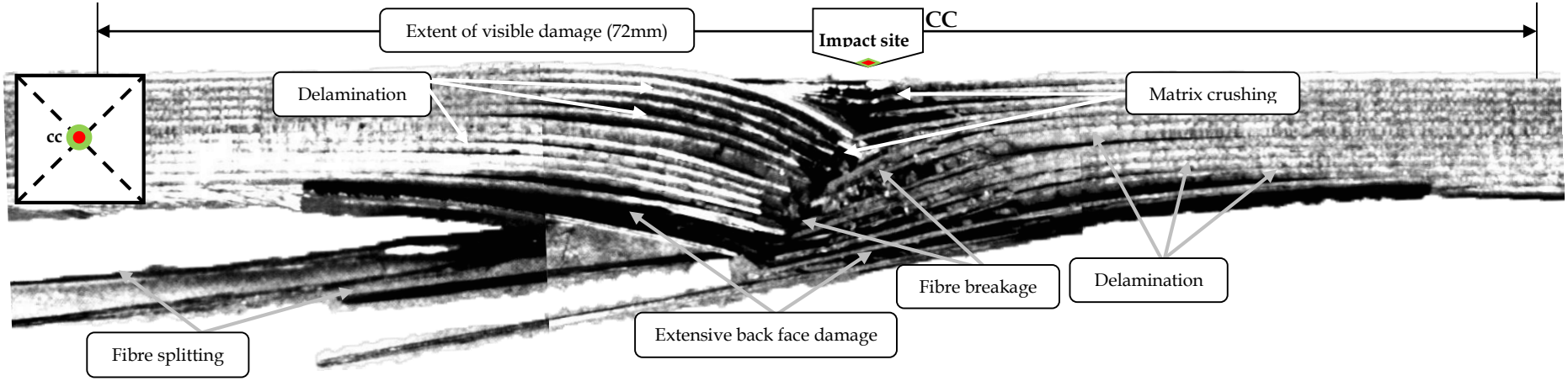

Summary of Damage

The impacted and re-impacted at the centre specimen reveals extensive damage through the specimen thickness. This damage is similar to the indented and re-indented specimen (see Figure 4-30) and is characterised by a series of delaminations followed by severe matrix crushing under the indentor nose and fibre breakage. Delaminations widen towards the back surface with more matrix crushing and fibre splitting. Here the damage through the thickness takes the form of a very wide inverted pine tree, being almost as wide at the top as the bottom.

Figure 4-31 Fractography of auxetic specimen; Impact and Re-Impact at Centre

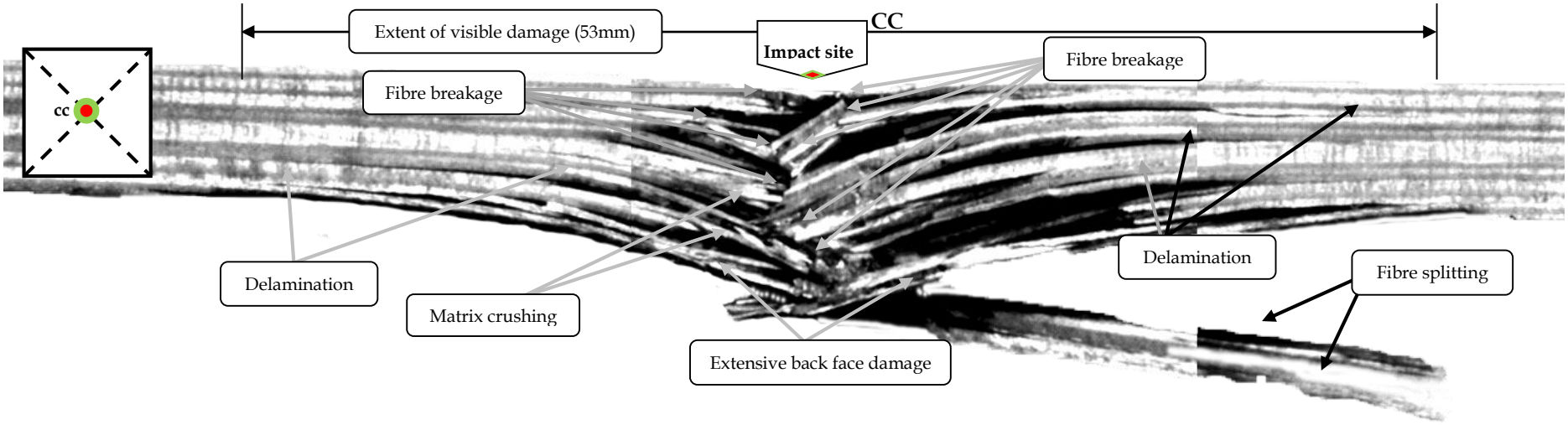

Summary of Damage

Fractographic analysis of the re-impacted auxetic specimen revealed a systematic progression of damage under the indentor nose. This damage resembles the indented specimen (see Figure 4-31). The damage is characterized by severe fibre breakage and matrix crushing leading to back face failure, accompanied by delaminations and fibre splitting. Progression of the damage through the thickness results in a much narrower inverted pine tree compared with the positive specimen.

4.10.1.3 Impact along the damage direction

Figure 4-32 Fractography of positive specimen; Impact along the damage direction

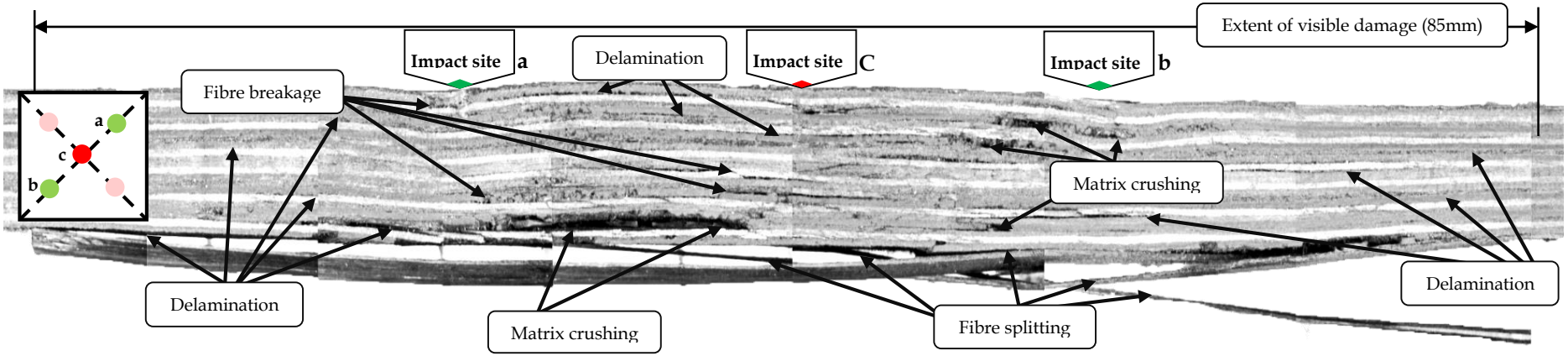

Summary of Damage

Sectioning of the impacted specimen reveals an irregular type of damage, which is characterised by fibre breakage and a small amount of matrix crushing, followed by large delaminations through the thickness of the specimen. Delaminations become more severe and widen after the mid-plane with fibre splitting out at the back surface of the specimen. Again the sites "a" and "b" are mainly characterised by delaminations and fibre crushing.

Figure 4-33 Fractography of auxetic specimen; Impact along the damage direction

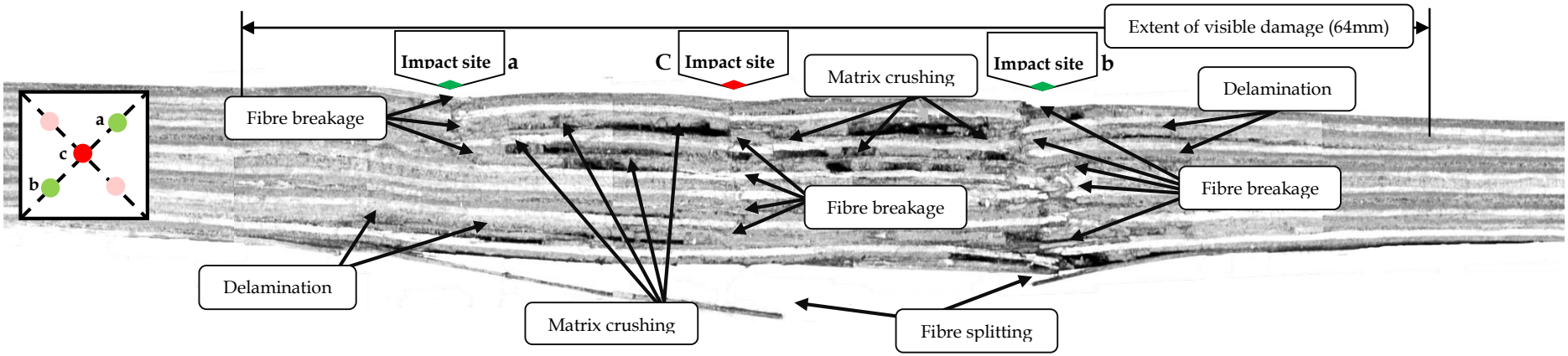

Summary of Damage

Low velocity impact (LVI) testing of the auxetic specimen reveals more concentrated damage under the indentor nose. This damage at each site is initiated by fibre breakage, followed by the matrix crushing through the specimen thickness. Above the mid-plane of the specimen and between the damage site "a" and "b", more delaminations are found with fibre crushing. These delaminations are not as long as those found in the specimen shown in Summary of Damage

Sectioning of the impacted specimen reveals an irregular type of damage, which is characterised by fibre breakage and a small amount of matrix crushing, followed by large delaminations through the thickness of the specimen. Delaminations

become more severe and widen after the mid-plane with fibre splitting out at the back surface of the specimen. Again the sites "a" and "b" are mainly characterised by delaminations and fibre crushing.

Figure 4-33. Also a small amount of fibres splitting out of the back face of the specimen is seen.

4.10.1.4 Impact opposite side of the damage direction

Figure 4-34 Fractography of positive specimen; Impact opposite to the damage direction

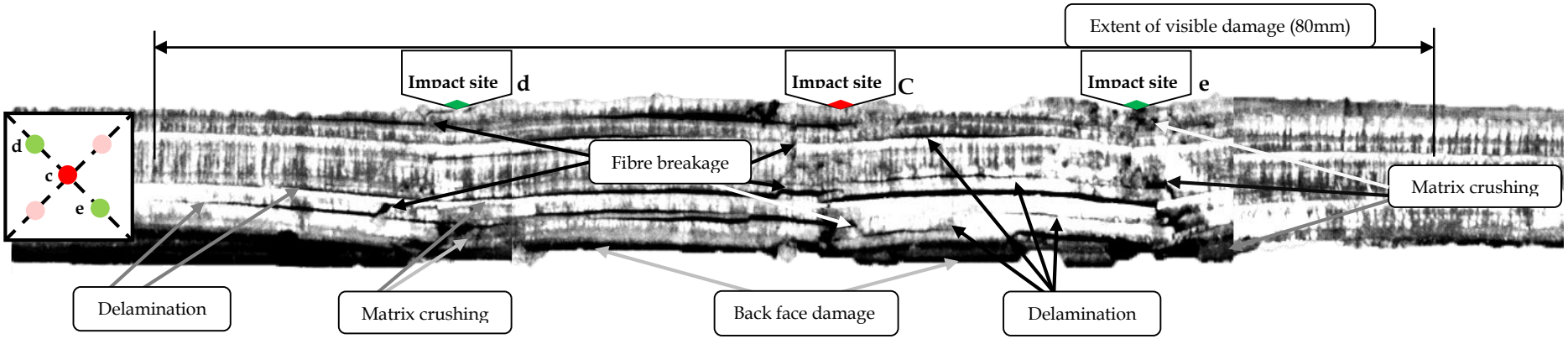

Summary of Damage

Fractographic analysis of low velocity impact (LVI) tested positive Poisson's ratio specimen reveals an array of different types of damage. This damage is similar to the indented specimen (see Figure 4-34), which is initiated by matrix crushing under

the indentor nose. These delaminations are wider towards the back surface of the specimen and also run away from the indentation sites "d" and "e".

Figure 4-35 Fractography of auxetic specimen; Impact opposite to the damage direction

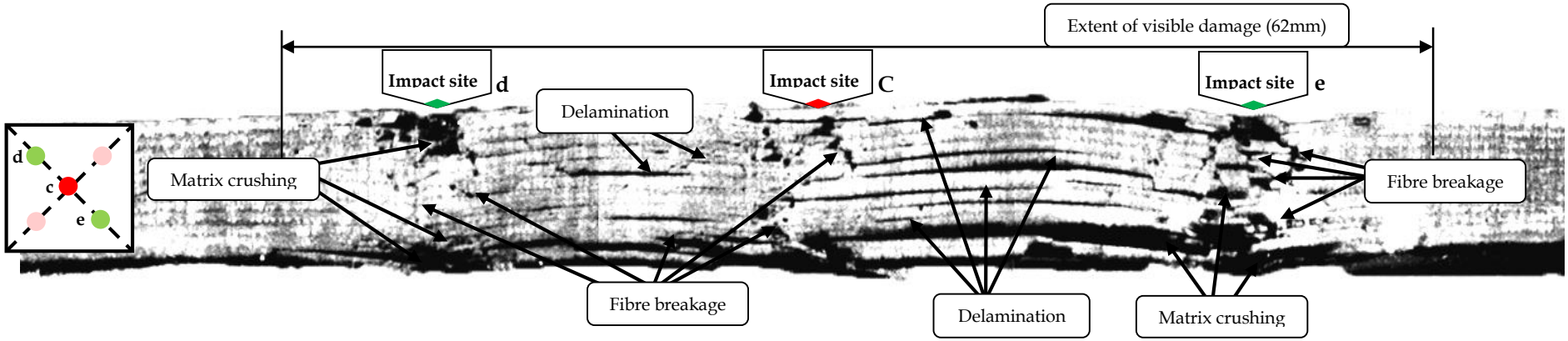

Summary of Damage

Fractographic analysis of low velocity impact (LVI) testing of the negative Poisson's ratio specimen reveals systematic damage through the specimen thickness. This damage is characterized by matrix crushing with fibre breakage, which is

similar to the indented specimen (see Figure 4-35). Delaminations are also found between the damage sites "d" and "e".

Severe damage is only found under the indentor nose and includes severe matrix crushing.

4.11. Low velocity Impact (LVI) and Residual Testing of In-plane specimens

4.11.1. Impact level 1

Figure 4-36 Positive In-plane specimen after; Impact level 1 – Residual loading

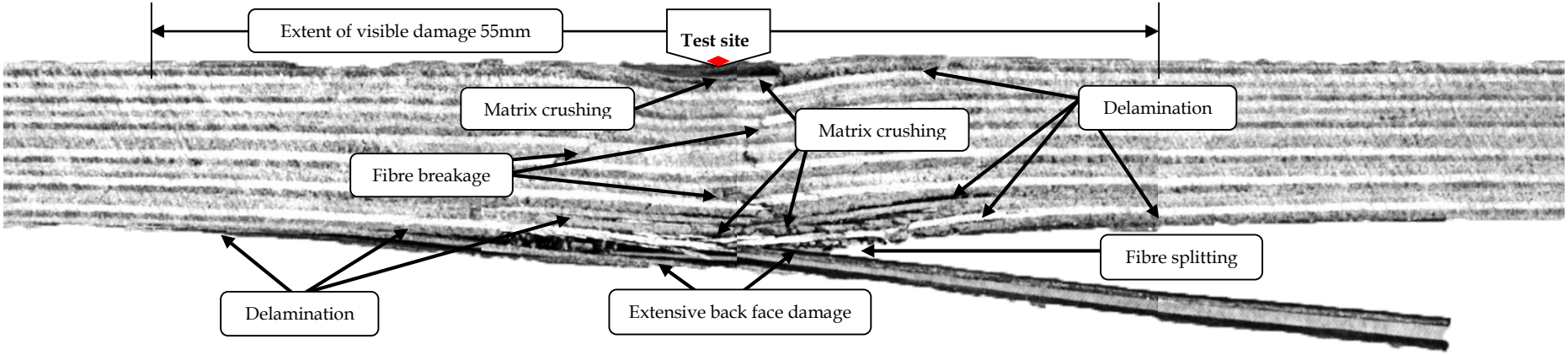

Sectioning of this specimen, indented with 12.7mm indentor, shows that there is no effect of the force applied for level 1 residual testing. All the damage present in the specimen is due to the previous impact event and this damage appears in the upper half of the specimen thickness and is characterised by the formation of few shear cracks joining of two delaminations. However these delaminations are relatively large and appear more towards the back face of the laminate.

Figure 4-37 Auxetic In-plane specimen after; Impact level 1 – Residual loading

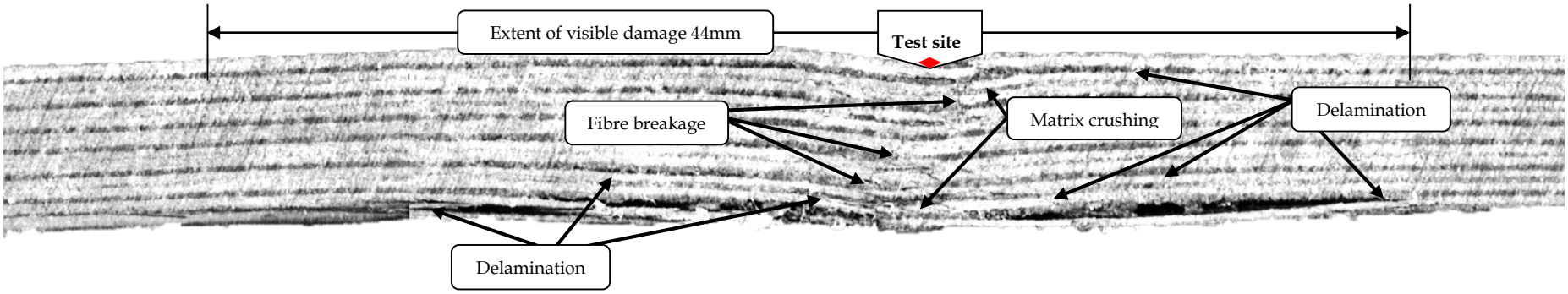

Fractographic analysis of auxetic specimen after impact level 1 and residual loading reveals similar trend as was found in the positive Poisson's ratio specimen after impact level 1. Here delaminations are relatively smaller than the positive Poisson's ratio specimens and fibre breakage is also evident at the back face of the laminate.

4.11.2. Impact level 2

Figure 4-38 Positive In-plane specimen after; Impact level 2 – Residual loading

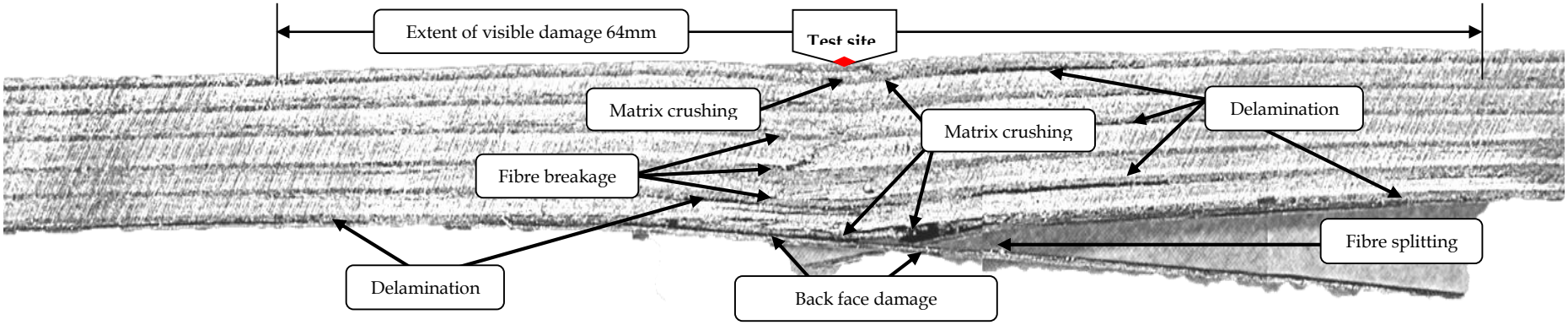

Fractographic analysis of the sectioned specimen shows a disordered type of damage through the specimen thickness. The damage is initiated by matrix crushing and fibre breakage under the indentor nose; followed by delaminations which spread

and widen to the back surface of the specimen. Fibre breakage and fibre splitting is more severe at the back face of the specimen.

Figure 4-39 Auxetic In-plane specimen after; Impact level 2 – Residual loading

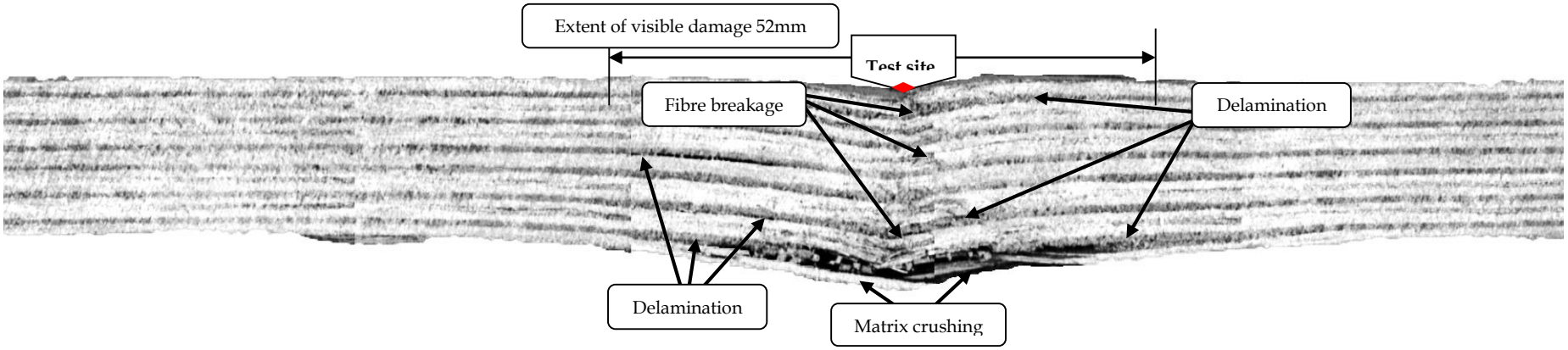

Sectioning of this specimen reveals a uniformly distributed damage pattern through the specimen thickness. The damage is characterised by fibre breakage and matrix crushing at the back face of the laminate. However, delaminations are relatively smaller than the above specimens and appear more uniformly throughout the laminate.

4.11.3. Impact level 3

Figure 4-40 Positive In-plane specimen after; Impact level 3 – Residual loading

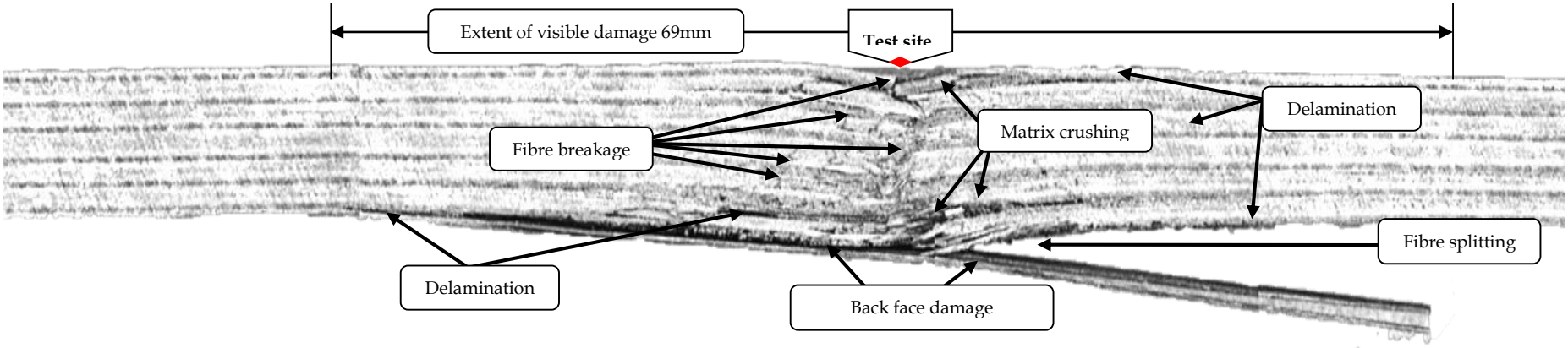

Fractograph of the residual testing sectioned specimen reveals severe matrix crushing under the indentor nose and at the back face of the specimen. A large number of randomly distributed shear cracks are observed followed by the delaminations. The failure of the laminate occurs with fibre splitting and crushing at the back face of the laminate.

Figure 4-41 Auxetic In-plane specimen after; Impact level 3 – Residual loading

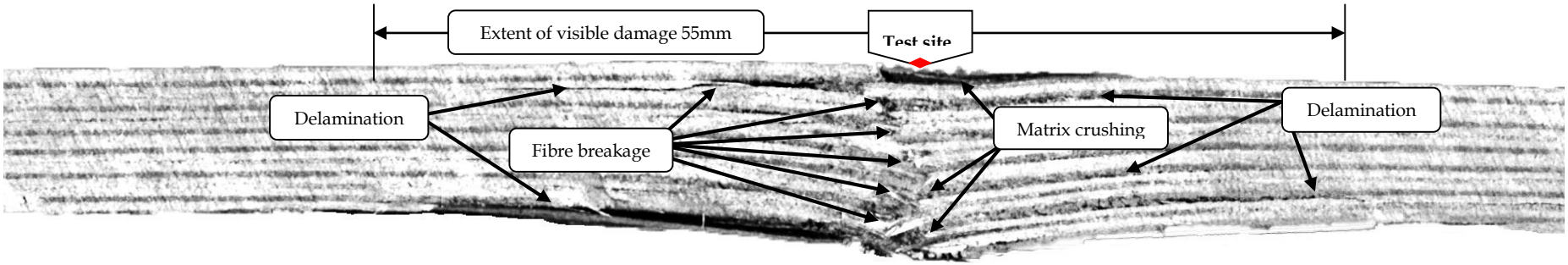

The sectioned auxetic specimen reveals uniformly distributed damage. This damage is composed of maxtrix crushing followed by severe fibre breakage which is uniformly distributed through the thickness of the specimen. The damage is more severe below the mid-plane under the indentation site. A number of small delaminations are also found, which are present through the laminate.

4.12. Fractograpy of High velocity Impact (HVI) Damage of Through-thickness Specimens

High velocity impact specimens were sectioned for detailed insight of the impact response.

Fractographic analysis of the specimens (see Figure 4-42a & Figure 4-42b) tested at 90m/sec velocity reveals matrix crushing only at the point of contact between the steel ball and laminate. The sectioned surfaces of both the auxetic and the positive Poisson's ratio specimens do not reveal delamination or fibre breakage away from the initial matrix crushing zone. There is not much difference between their extents of damage and damage profile at this velocity.

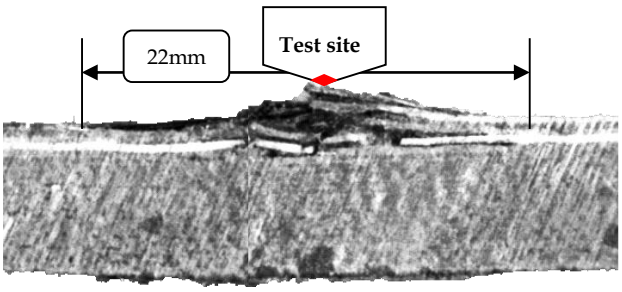

(a) Fractograph Pa (HVI) @ 90m/s

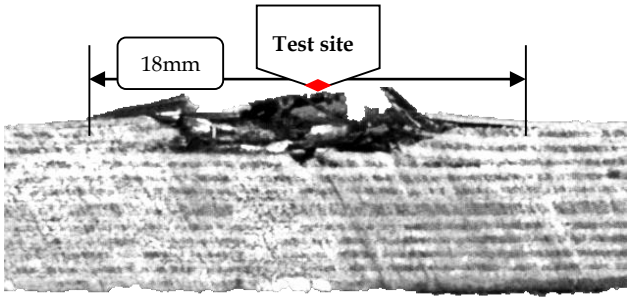

(b) Fractograph Na (HVI) @ 90m/s

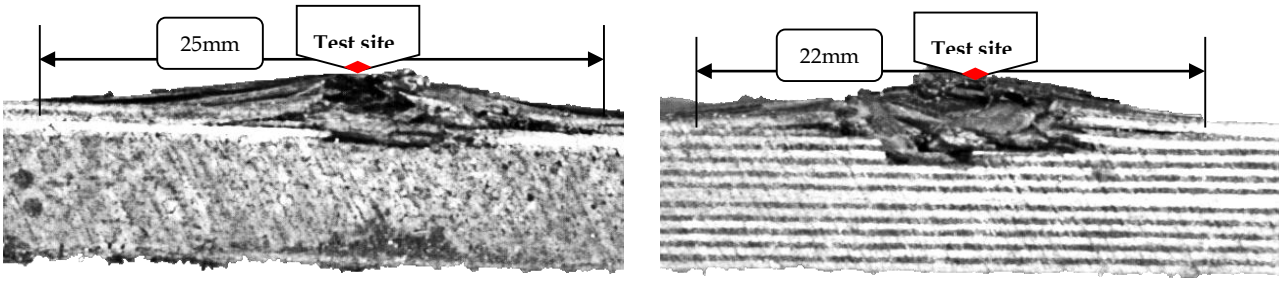

(c) Fractograph Pa (HVI) @ 110m/s **(d) Fractograph Na (HVI) @ 110m/s**

Figure 4-42 Damage of Auxetic and positive Poisson's ratio through-thickness specimens

High velocity impact tests were also conducted at 110m/sec in order to study the damage morphology of the auxetic and positive specimens. Fractographs of the auxetic and positive Poisson's ratio specimens as shown in Figure 4-42c and Figure 4-42d and they both appear to be slightly different in terms of the extent of damage. There is no evidence of delamination and fibre breakage in any part of the sample. Severe matrix crushing is apparent at the contact point of the ball. This suggests that there is no marked difference in impact response for both the auxetic and the positive specimens at high velocity impact.

5 DYNAMIC ANALYSIS

5.1 Analytical Dynamic Analysis

This chapter describes a brief review of the method and detailed procedure for dynamic analysis using mass spring modelling.

As discussed in Chapter – 4 previously, impact tests have been performed at different sites on each specimen away from the indentor nose using the same parameters i.e. support condition, impact mass and set up. Specimens were allowed to impact to full damage corresponding to the quasi-static indentation load displacement curves. The impactor and the specimen may be modelled as a mass spring system due to the nature of the impact tests conducted[179], [180].

The mass vibrates if it is slightly displaced from its rest position and released; this is the simplest form and represents a single degree of freedom, as shown in Figure 5-1, fastened to a spring and constrained to parallel movement to the spring. Studies show that the displacement of the mass from its rest position is a sinusoidal function of time; and such sinusoidal vibrations are called "Simple Harmonic Vibrations".

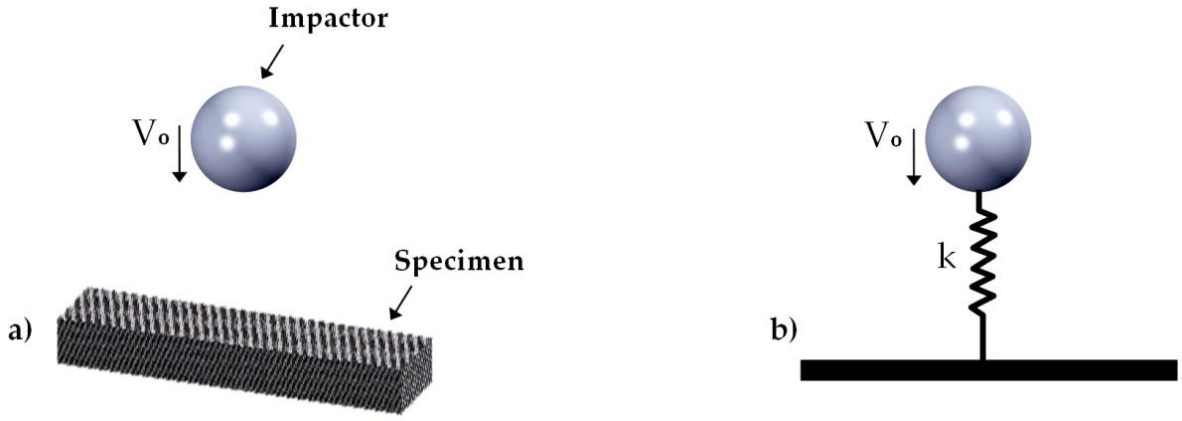

Figure 5-1 a) Impact event, b) Simple mass spring system

The only physical restrictions placed on the equation for the motion of a simple oscillator are that the restoring force is directly proportional to the displacement (Hooke's law), the mass be constant, and there be no losses to attenuate the motion. These restrictions lead to simple harmonic motion and the frequency of the vibrations become independent of amplitude. A number of authors [179]–[181] successfully used this method for carbon epoxy composite plates[121], [182], glass epoxy composite panels[183], [184] and filament wound pipes[185]. The specimen is considered a mass less spring impacted by a mass 'm' in this simple model. For this approximation, the contact force history of the specimen, $\mathbf{F}_A$, at any time **t** is given by[186];

$$F_A = V_o\sqrt{(mk)}.\sin(\omega t) \qquad \text{Equation 5-1}$$

Here; V_o is impact velocity, k is specimen stiffness constant and t is time elapsed and $\omega = \sqrt{\left(\frac{k}{m}\right)}$ defines undamped natural frequency.

The contact force history is a sine pulse and predicts that the contact force increases linearly with the velocity of projectile. It also increases with the square root of mass and of the stiffness. The support conditions or the size of the specimen have no bearing on the above equation. Such variables can be taken into account by using a non-linear i.e (changes with applied load) specimen stiffness 'k' which is obtained from quasi-static indentation tests of the simply supported specimens[186]. Comparing the predicted and experimentally determined values of the maximum force and impact duration demonstrates the accuracy of this method. The accuracy of such a model was enhanced by Christoforou et al.[187] allowing the value of estimated 'k' to vary along the slope of the quasi-static indentation force displacement curve[188] as shown below in Figure 5-2.

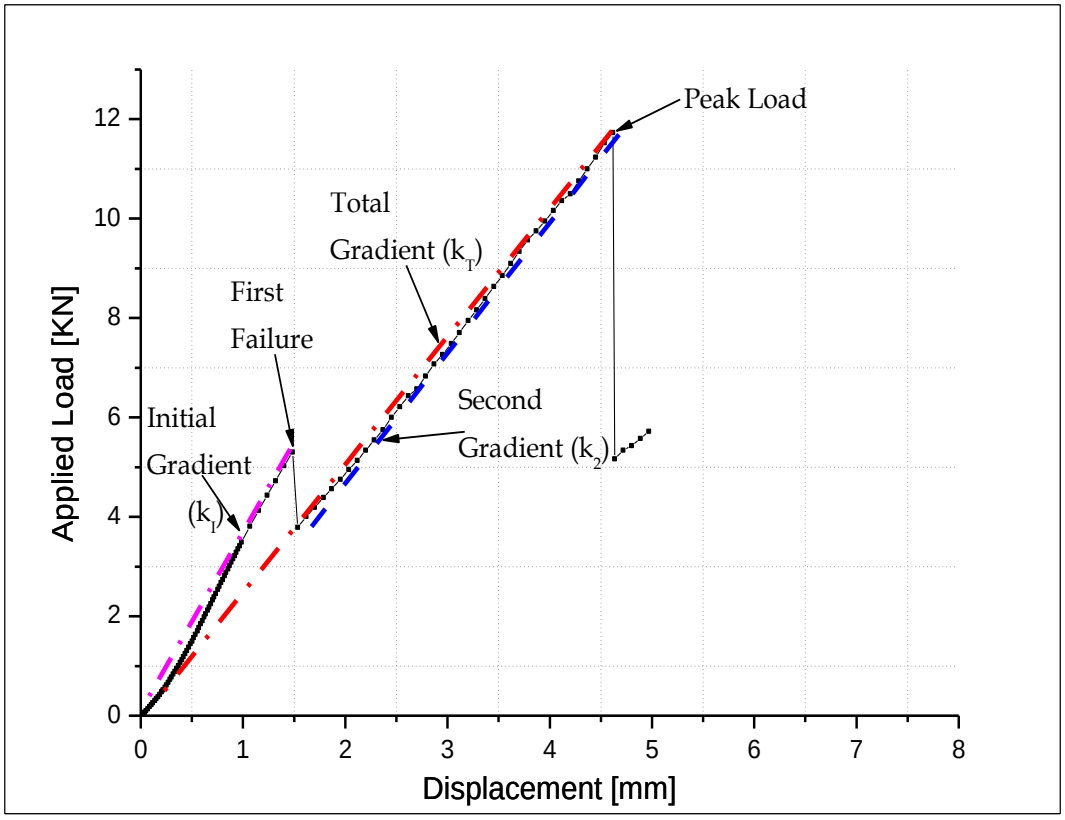

Figure 5-2 Schematic representation of the gradients used

Tangents to the curve at different load values are obtained. A non-linear approximation is obtained by inputting this new value in the equation at the point corresponding to the appropriate force value.

5.2 Gradient Methods

Three methods for calculating the stiffness constant 'k' are used in this work. The first method is the total gradient from the quasi-static indentation force displacement curve of each specimen i.e from the origin of the curve to the peak load under test as shown above in schematic diagram Figure 5-2.

This gradient gives an approximation of the stiffness of the specimen throughout the loading range until failure of the specimen and will be considered as Method-One 'kт'. Another approximation to the transient load time behaviour of the specimen is achieved by using the gradient of the initial portion of the quasi-static load displacement curve until the first failure and this is considered as Method-Two 'kı'. These very simple methods of estimation are found to be reasonably accurate, which are demonstrated in the following section of the results in this chapter. The methods described above are also considered linear approximation. Finally, there is a Method Three '(kI & k2); which is the gradient of the initial portion of the quasi-static indentation curve and slightly reduced gradient of the next portion of the curve to produce a varying stiffness constant.

5.2.1 Results

As discussed in section 5.1 of this chapter, in order to investigate the transient load deformation behaviour of the specimens and to assess the energy absorbed during the impact event, a simple mass spring models have been used in this study. This is accomplished by calculating and plotting a theoretical force time history with the actual trace for each specimen. Once losses have been incorporated such as friction, heat, noise creation and experimental errors, the divergence in each case provides an estimation of the energy absorbed during the development of the damage. A comprehensive description is given in 'Discussion'

Chapter – 6 combined with the findings of these results of damage analysis for the through-thickness specimens.

5.2.2 Linear Approximation

All the plots for the linear approximation have been achieved from the total overall gradient (k_T) of the quasi-static load and the initial gradient (k_I) of the quasi-static load displacement curves. The results from these plots are presented as experimental vs predicted loads in Table 5-1 and actual vs predicted times in Table 5-2.

Table 5-1 Comparison of actual vs predicted load – k_I, and k_T

Specimen Type		Impact Velocity 'V_o' (m/s)	k (x10^6 N/m)		Max Load (kN)		
					Actual	Predicted	
			k_I	k_T		Method-2	Method-1
N_a	Nc	3.46	3.77	2.42	10.82	14.75	11.90
	Ncc	3.46	-	2.43	12.79	-	11.92
	Na	3.46	2.32	1.86	10.43	11.57	10.38
	Nb	3.46	2.39	1.84	9.10	11.78	10.38
	Nd	3.46	2.42	2.16	9.73	11.84	10.64
	Ne	3.46	2.15	2.04	11.10	11.14	10.90
P_a	Pc	3.46	3.98	2.37	8.04	15.25	11.58
	Pcc	3.46	-	1.98	9.01	-	10.71
	Pa	3.46	1.87	1.71	7.03	10.44	9.90
	Pb	3.46	-	1.69	8.13	-	9.98
	Pd	3.46	2.49	1.86	8.89	11.99	10.44
	Pe	3.46	2.08	1.74	9.14	10.99	10.08

Table 5-2 Comparison of actual vs predicted duration – k_I, and k_T

Specimen Type		Impact Velocity 'Vo' (m/s)	k (x10⁶ N/m)		Duration (ms)		
					Actual	Predicted	
			k_I	K_T		Method-2	Method-1
Na	Nc	3.46	3.77	2.42	4.72	3.55	4.44
	Ncc	3.46	-	2.43	5.31	-	4.44
	Na	3.46	2.32	1.86	5.42	4.51	5.05
	Nb	3.46	2.39	1.84	5.49	4.50	4.96
	Nd	3.46	2.42	2.16	5.92	4.44	5.12
	Ne	3.46	2.15	2.04	5.87	4.79	4.93
Pa	Pc	3.46	3.98	2.37	4.63	3.48	4.49
	Pcc	3.46	-	1.98	7.00	-	6.28
	Pa	3.46	1.87	1.71	6.5	5.02	5.32
	Pb	3.46	-	1.69	7.06	-	5.50
	Pd	3.46	2.49	1.86	6.61	4.38	5.08
	Pe	3.46	2.08	1.74	6.47	4.93	5.35

The predicted behaviours for each specimen is also plotted as a composite graph against actual impact force histories. This gives a good insight into the linear approximations of 'Method one' and 'Method Two'.

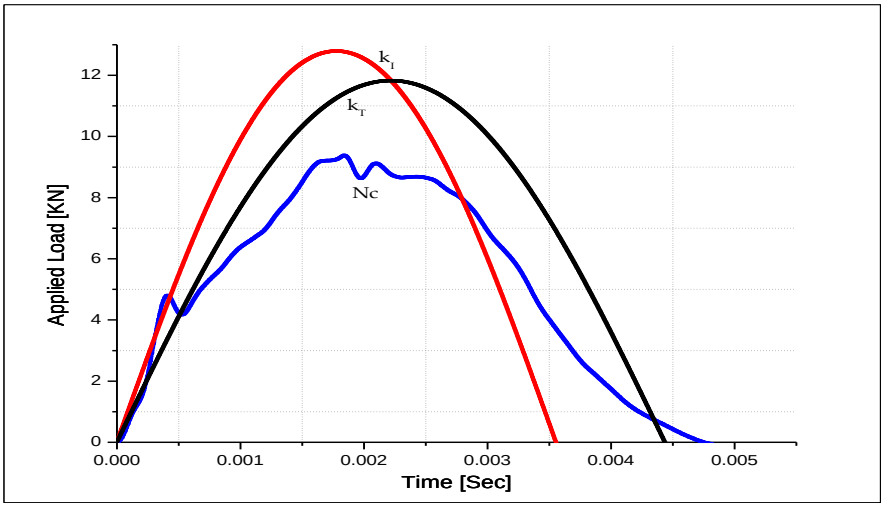

Figure 5-3 Experimental (blue) vs predicted (black & red) for Nc – k_I and k_T

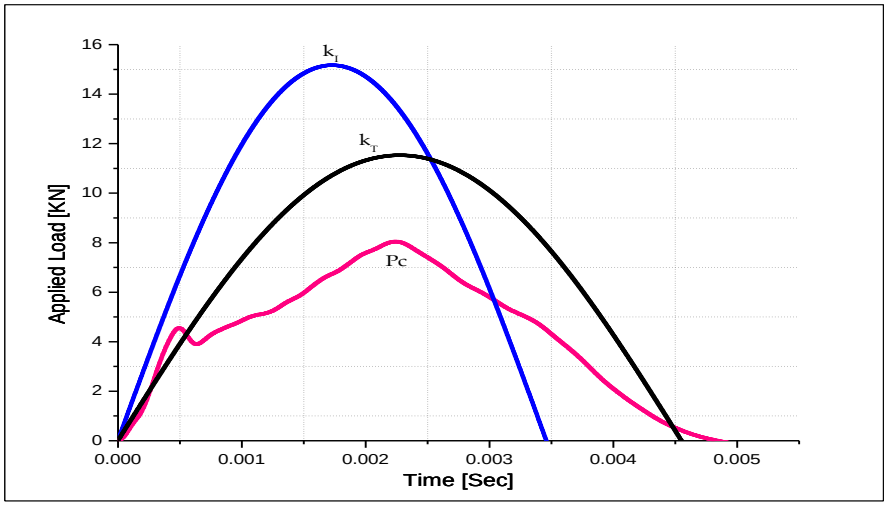

Figure 5-4 Experimental (pink) vs predicted (black & blue) for Pc – k_I and k_T

In case of method one (k_T), the difference in maximum load for the auxetic specimen Nc (see Figure 5-3) is only 1.08kN compared to 3.74kN for the positive Poisson's ratio specimen Pc (see Figure 5-4) both impacted at the centre. This method also shows good agreement for impact duration. Similarly, method two (k_I) repeats the same trend but appears with higher difference in the maximum load and impact duration for both the auxetic and the positive Poisson's ratio specimens.

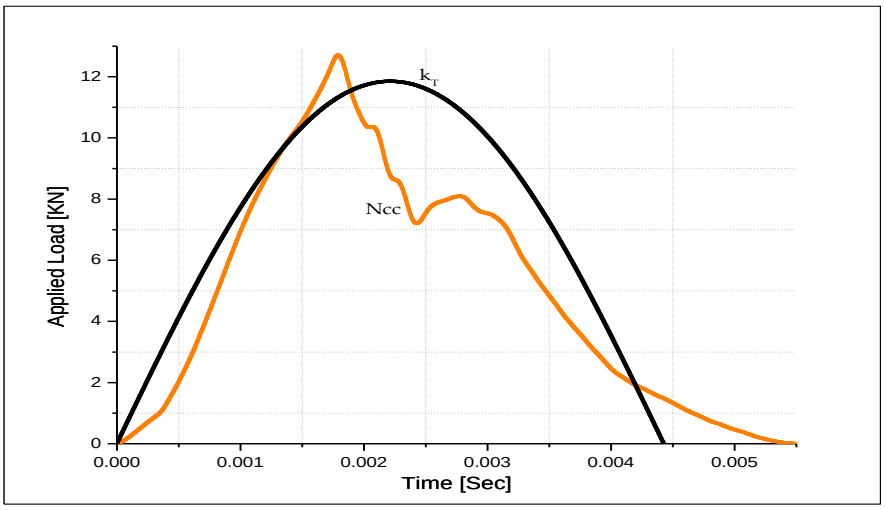

Figure 5-5 Experimental (orange) vs predicted (black) for Ncc – k_T

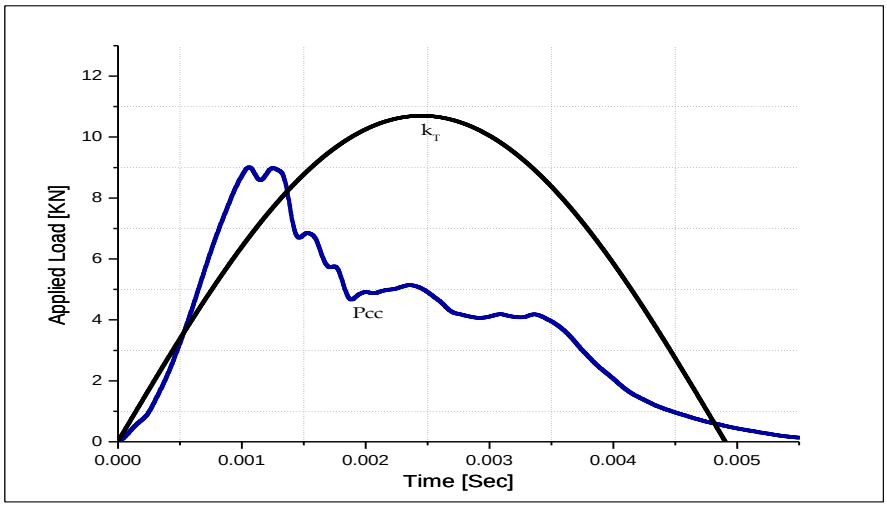

Figure 5-6 Experimental (blue) vs predicted (black) for Pcc – k_T

When both the auxetic and positive Poisson's ratio pre-impacted specimens were re-impacted at the centre, they show only a single peak before failure. In this scenario it was possible to use one method "k_T" only to predict the behaviour of both the specimens. The difference in maximum load to the predicted load for the auxetic specimen Ncc is 0.87kN as shown in Figure 5-5 and is 1.7kN for the positive Poisson's ratio Pcc as shown in Figure 5-6. Similarly the difference in the

impact duration for the auxetic specimen Ncc is 0.87ms as opposed to 0.72ms for the positive Poisson's ratio specimen Pcc.

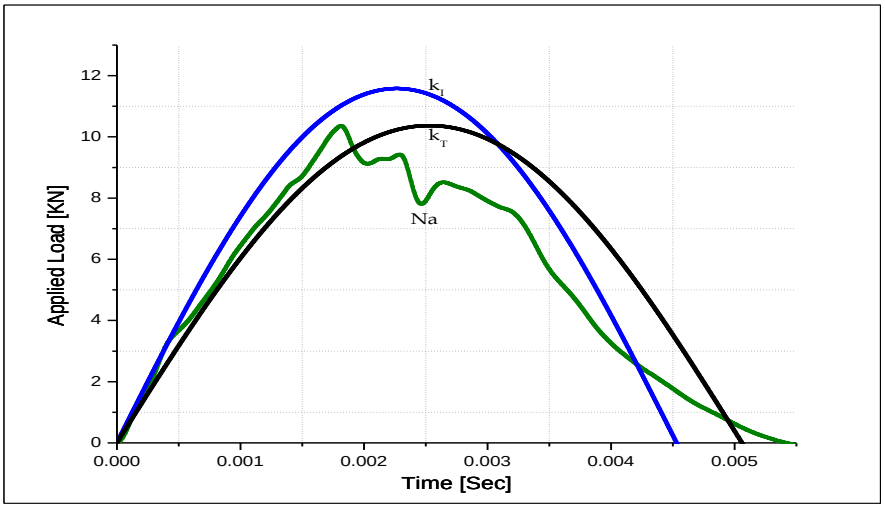

Figure 5-7 Experimental (green) vs predicted (black & blue) for Na – k_I and k_T

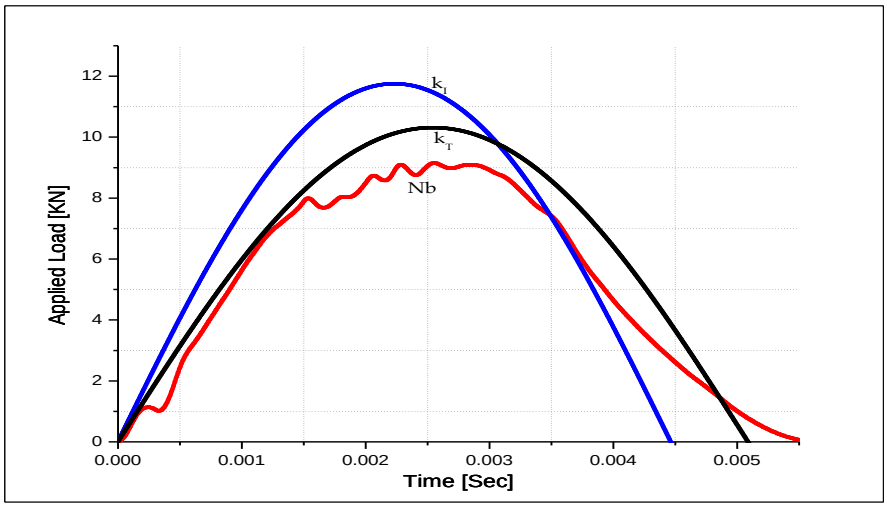

Figure 5-8 Experimental (red) vs predicted (black & blue) for Nb – k_I and k_T

However, when the specimens are tested 20mm away both along and opposite to the damage direction, from the centre of the initial impact site the overall prediction is found to be in good agreement for the auxetic specimens. This behaviour is under predicted for the positive Poisson's ratio specimens. In the

auxetic specimens the stiffness value taken from the quasi-static results provides a closer estimation of the low velocity impact response. However, this does not take into account the amount of damage caused, hence the discrepancy in maximum load and the impact duration, which are both underestimated. The overall stiffness parameters k_T and k_I are higher for the auxetic specimens than the positive Poisson's ratio specimen due to the enhanced performance under quasi-static load.

Again, method one predicts more close results for, auxetic Na and Nb specimens when they are re-tested 20mm away from the initial impact site in the direction of damage. The auxetic specimens show less difference in the maximum load, which is 0.5kN and 1.28kN for Na (see Figure 5-7), and Nb (see Figure 5-8) respectively compared to the positive Poisson's ratio specimens, where the difference is 2.87kN and 3.41kN for Pa (see Figure 5-9), and Pb (see Figure 5-10), respectively.

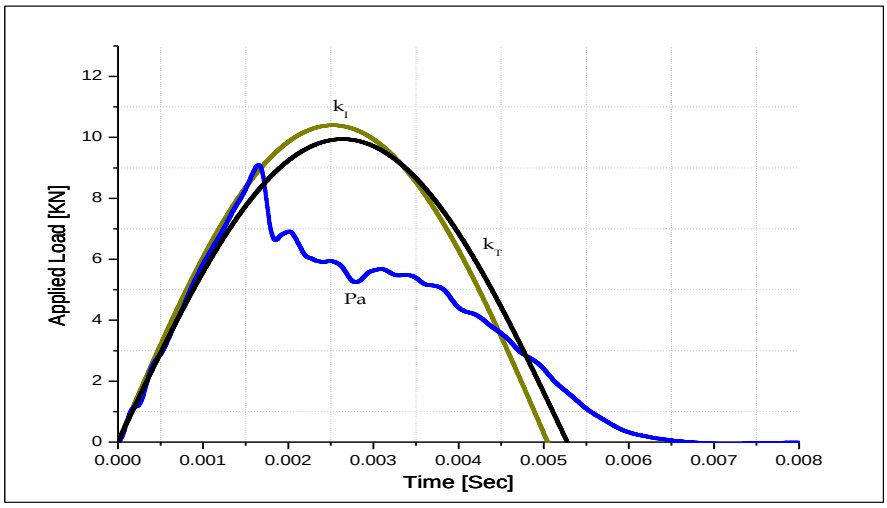

Figure 5-9 Experimental (blue) vs predicted (black & dark yellow) for Pa – k_I and k_T

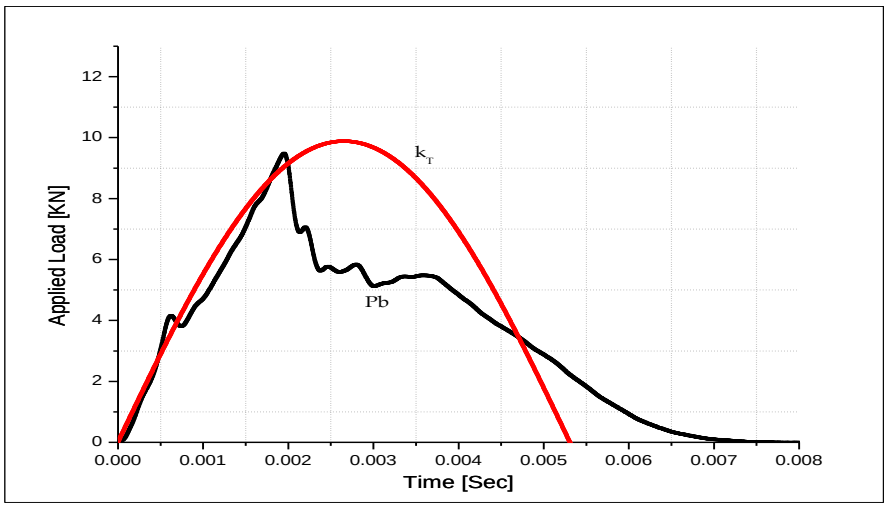

Figure 5-10 Experimental (black) vs predicted (red) for Pb – k_T

The trend in stiffness constant value (see Table 5-1) shows, method one is less accurate for Pa and Pb and also the difference in the impact duration deviates to a large value from the actual impact duration. The difference in the impact duration for the auxetic specimen is 0.37ms and 0.53ms respectively for Na and Nb compared to 1.18ms and 1.56ms, respectively for the positive Poisson's ratio

specimen Pa and Pb. Method two replicates the same trend as found in method one for the auxetic specimens, however, here this occurs at higher values of impact duration, and maximum load for Na and Nb type specimens.

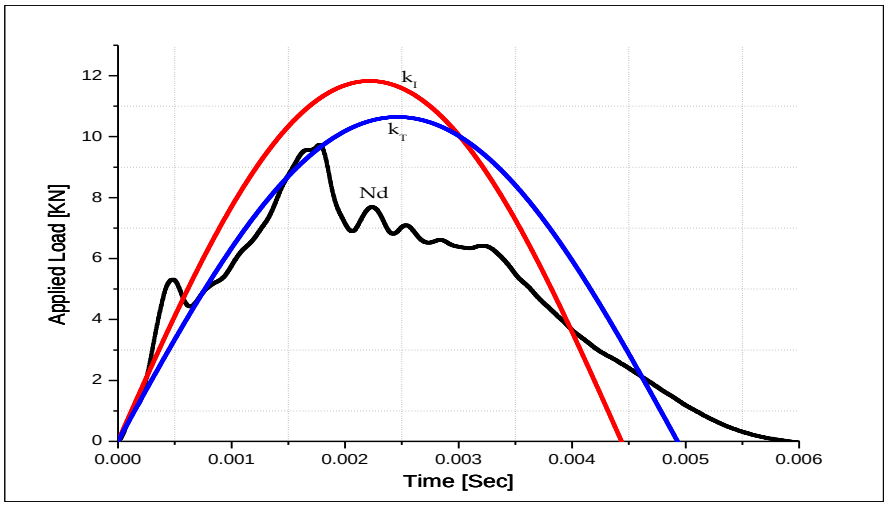

Figure 5-11 Experimental (blac) vs predicted (red & blue) for Nd – k_I and k_T

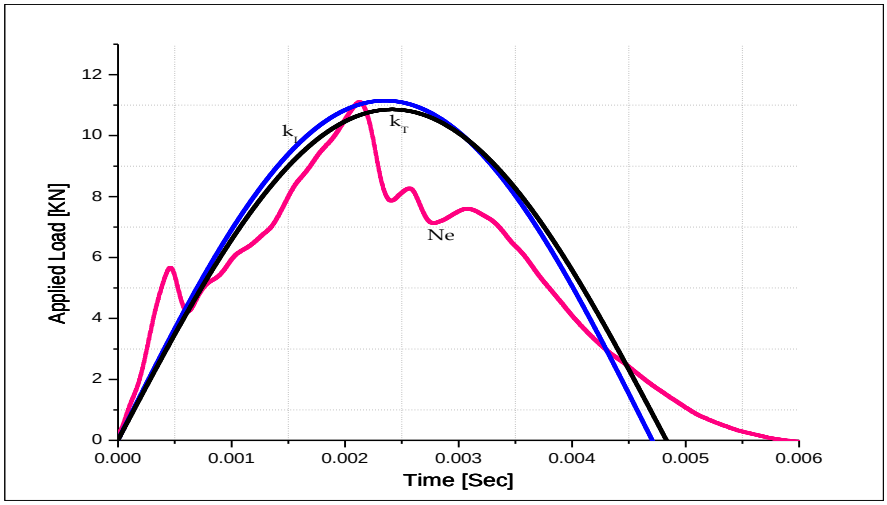

Figure 5-12 Experimental (pink) vs predicted (black & blue) for Ne – k_I and k_T

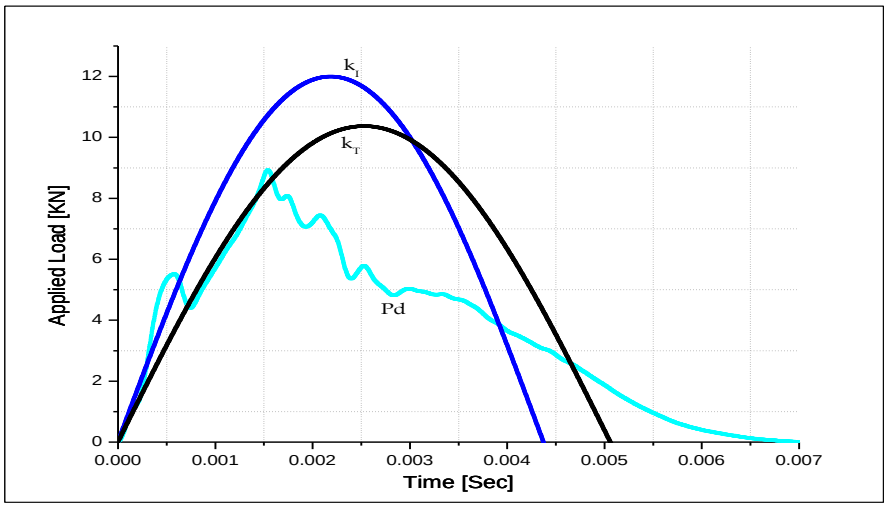

Figure 5-13 Experimental (cyan) vs predicted (black & blue) for Pd – k_I and k_T

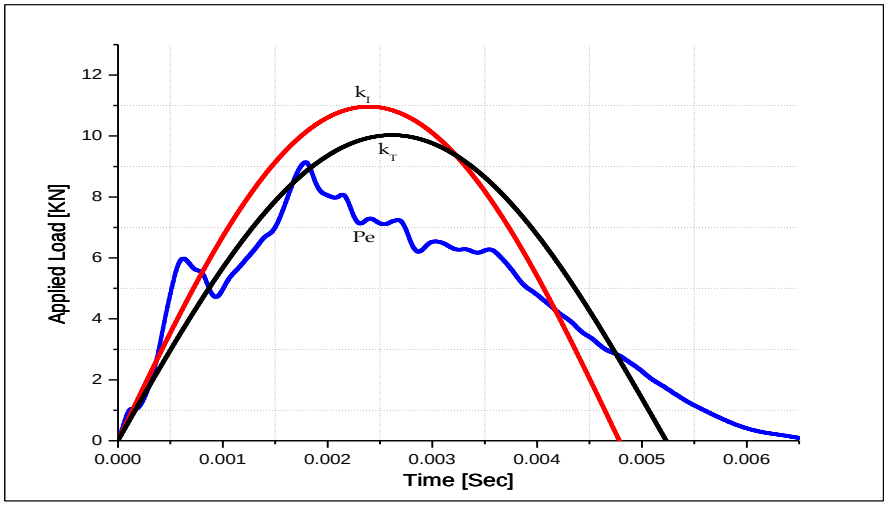

Figure 5-14 Experimental (blue) vs predicted (black & red) for Pe – k_I and k_T

The re-test of the both the auxetic and the positive Poisson's ratio specimens (see Figure 5-11 to Figure 5-14), 20mm away opposite to the damage direction from the centre impact site, showed a similar trend as was observed in the above specimens. In case of method one, the difference in maximum load for Nd and Ne is merely 0.91kN and 0.2kN, respectively, which is higher in case of Pd and Pe and both show a difference in maximum load of 1.55kN and 0.94kN, respectively. Similarly, the differences in impact duration for the auxetic specimen are Nd

0.8ms and Ne0.94, respectively opposed to Pd 1.53ms and Pe 1.12ms, respectively for positive Poisson's ratio specimens.

5.2.3 Non-Linear Approximation

In the case of the non-linear value of specimen stiffness constant, two gradients are used; the initial gradient taken from the linear portion of the curve followed by the gradient of the next portion of the graph. There are no predicted results for the impact tests of Ncc and Pcc, as there is no damage present in these specimen i.e. first failure has not occurred upon retesting at the centre so it was not possible to change the k value used in the approximation, as the load value does not reach the appropriate value.

Table 5-3 Comparison of actual vs predicted results – method three

Specimen Type		Impact Velocity 'V_o' (m/s)	k (x10^6 N/m)		Max Load (kN)		Duration (ms)	
			k_1	k_2	Actual	Predicted	Actual	Predicted
N_a	Nc	3.46	3.77	2.58	10.84	12.20	4.48	4.30
	Ncc	3.46	-		-	-	-	-
	Na	3.46	2.32	2.06	10.41	10.95	5.06	4.80
	Nb	3.46	2.39	1.90	9.13	10.47	5.20	5.00
	Nd	3.46	2.42	1.96	9.76	10.64	5.45	4.93
	Ne	3.46	2.15	2.26	11.14	11.42	5.37	4.58
P_a	Pc	3.46	3.40	2.30	8.07	11.52	4.63	4.55
	Pcc	3.46	-		-	-	-	-
	Pa	3.46	1.87	1.74	8.05	10.02	5.18	5.23
	Pb	3.46	-		-	-	-	-
	Pd	3.46	2.49	2.06	8.97	10.90	6.23	4.80
	Pe	3.46	2.08	2.01	9.14	10.77	6.47	4.86

All the experimental results for this method are presented in Table 5-3 below. The initial portion of the graphs (see Figure 5-15 to Figure 5-23) after an impact event are identical to that already observed in Method Two and as such will not be considered further here. The most interesting portion of the graphs is the point where the gradient is reduced i.e. the portion after first failure point. This portion of the graph truly compares the response of the single and multiple impacts at centre or away from the centre of the initial impact event.

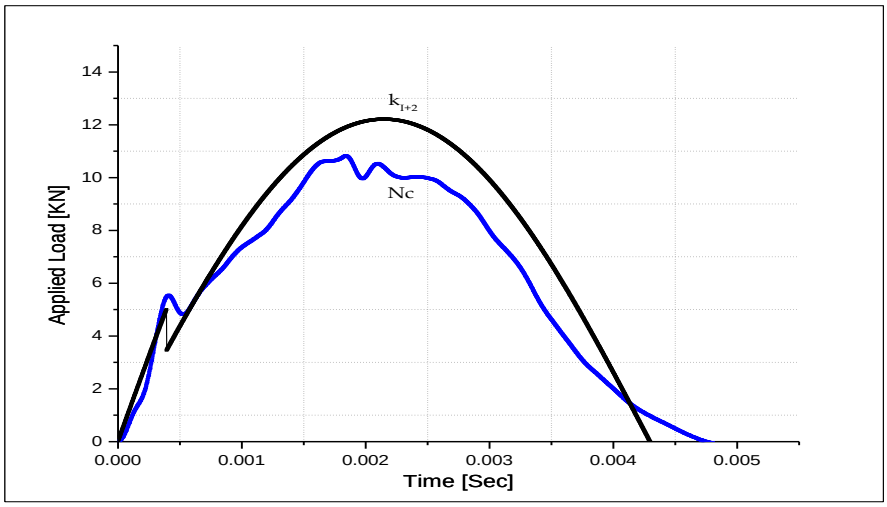

Figure 5-15 Experimental (blue) vs predicted (black) for Nc – Method Three

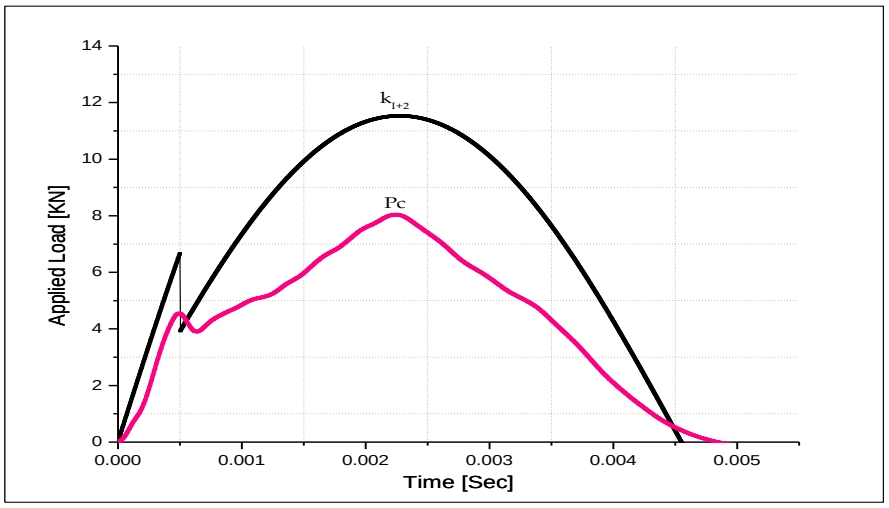

Figure 5-16 Experimental (pink) vs predicted (black) for Pc – Method Three

This method gives more precised curve for prediction of the auxetic specimens as compared to the positive Poisson's ratio specimens. This is obvious due to the small difference in maximum load between actual and predicted load curve that is 1.36kN for Nc as shown above in Figure 5-15 and Figure 5-16.

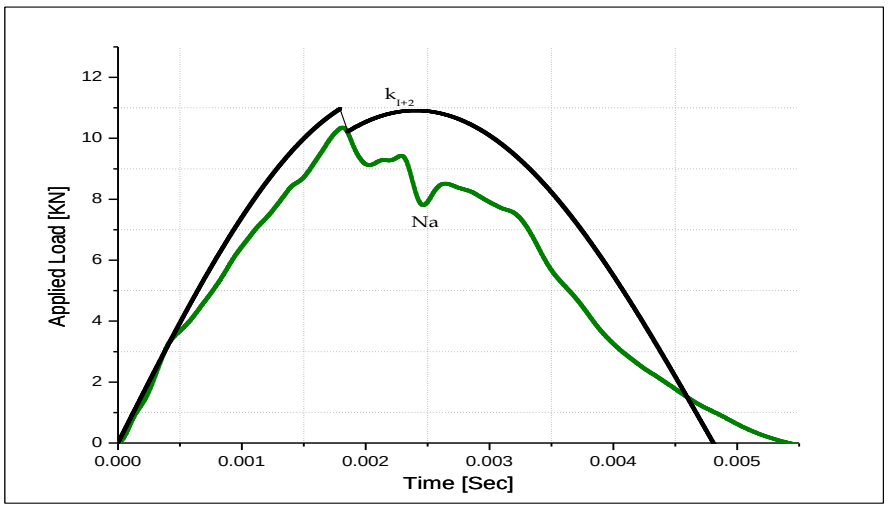

Figure 5-17 Experimental (green) vs predicted (black) for Na – Method Three

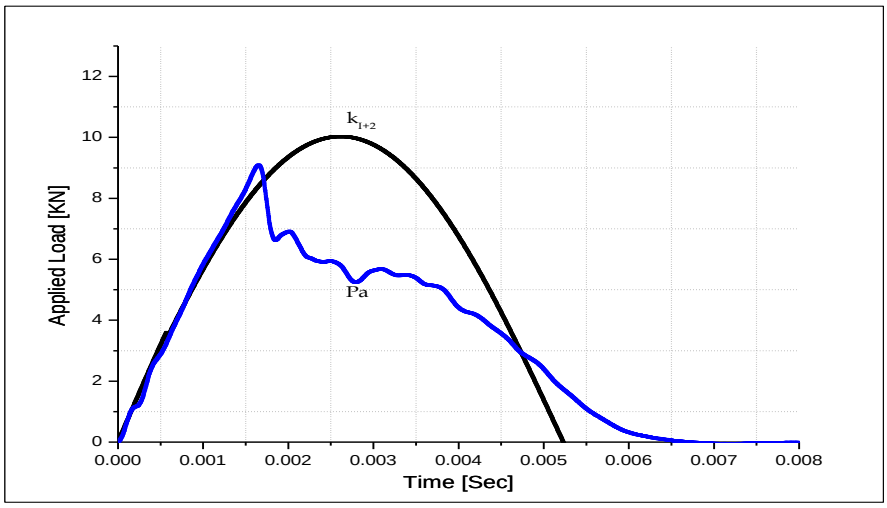

Figure 5-18 Experimental (blue) vs predicted (black) for Pa – Method Three

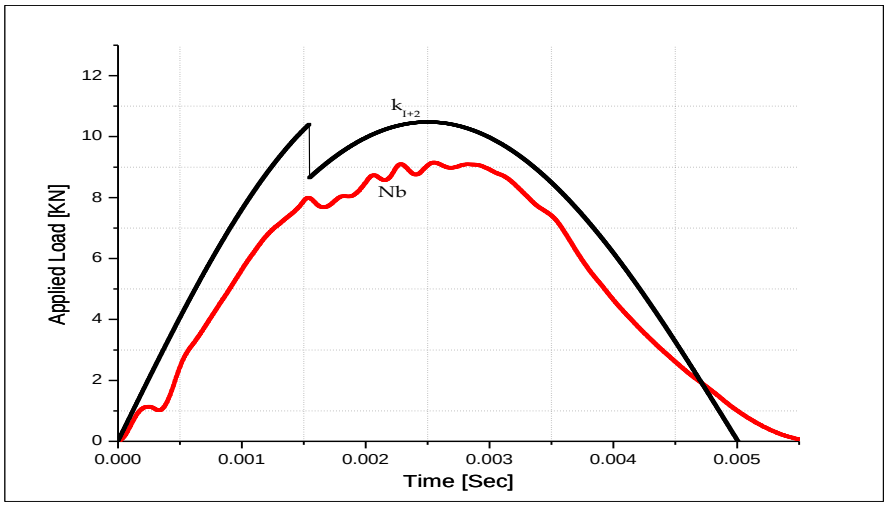

Figure 5-19 Experimental (red) vs predicted (black) for Nb – Method Three

All the predicted curves as shown in Figure 5-17 -Figure 5-19 were also plotted for the specimens tested 20mm away in the damage direction to assess the overall behaviour of the specimens. Here, the auxetic specimens show a closer estimation to the actual load over predicted loads when compared with positive Poisson' ratio specimens. This also confirms the presence of large delaminations observed in the positive Poisson's ratio specimens.

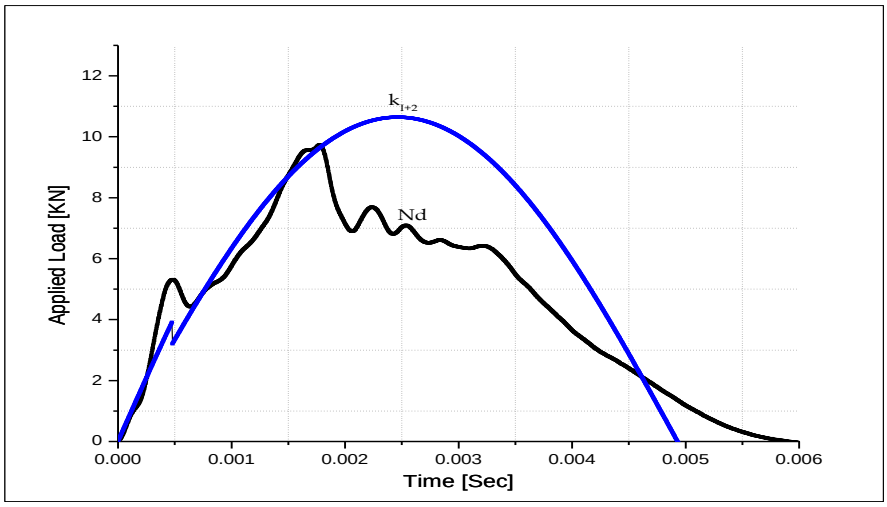

Figure 5-20 Experimental (black) vs predicted (blue) for Nd – Method Three

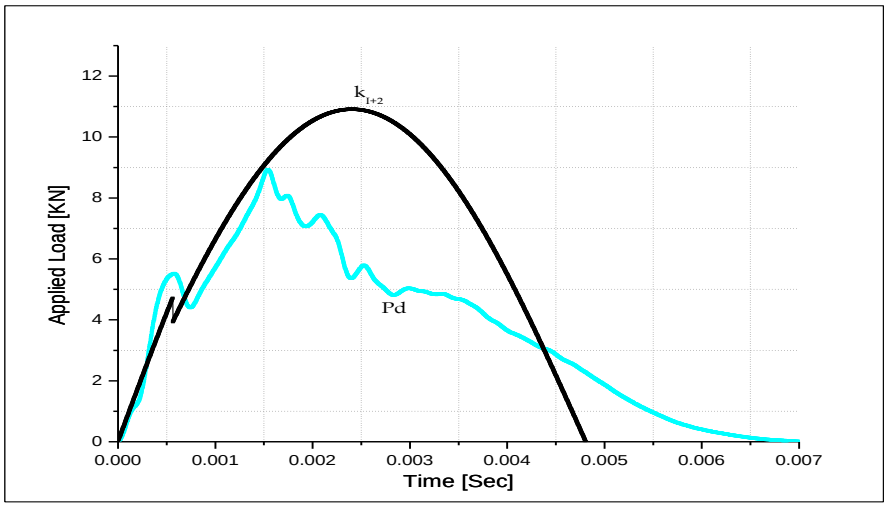

Figure 5-21 Experimental (cyan) vs predicted (black) for Pd – Method Three

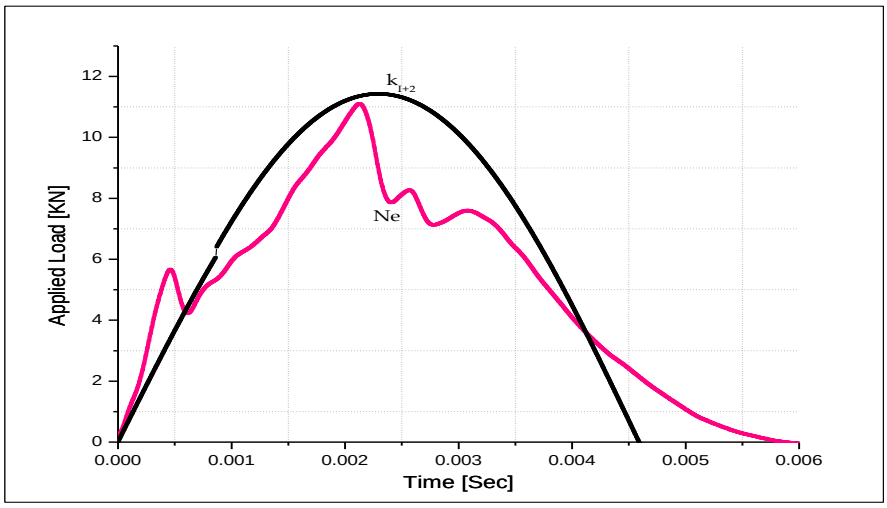

Figure 5-22 Experimental (pink) vs predicted (black) for Ne – Method Three

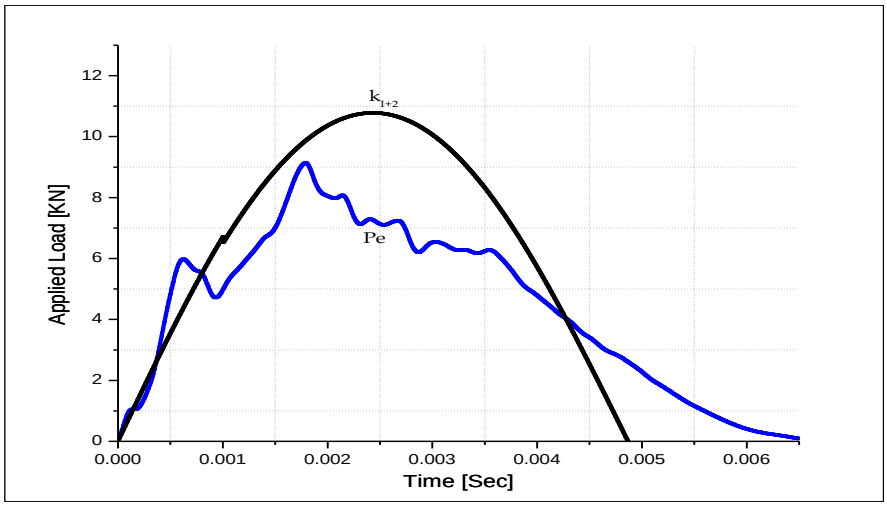

Figure 5-23 Experimental (blue) vs predicted (black) for Pe – Method Three

Similarly, the predicted curves were also superimposed on the actual test curves for the specimens tested 20mm away opposite to the damage direction, as shown in Figure 5-20- Figure 5-23. The trend in the stiffness constant and the peak load is less accurate for the positive Poisson's ratio specimens compared to the axuetic specimens. The difference in the peak load for the auxetic specimen is only 0.88kN and 0.28, respectively for Nd and Ne specimens. However, this difference is

slightly higher for the positive Poisson's ratio specimens, which are 1.93kN and 1.63kN, respective for Pd and Pe. In the positive Poisson's ratio specimens the prediction of the first failure point continues to be very close to the actual and the gradient after this point is similar but does deviates sooner due to the spread of the damage away from the initial impact site.

6 DISCUSSION

6.1 Manufacturing of Auxetic Composite Laminates

All the stacking sequences used in the present work have previously been shown to have specific values of through-thickness and the in-plane Poisson's ratio to allow comparisons to be carried out of the effect of the sign and size of this ratio on the impact resistance and hardness of the laminate[56], [64], [63]. The pre-preg material has already been used for through thickness[64] Poisson's ratio and the properties of the laminates have been predicted for the same stacking sequences but for the in-plane Poisson's ratio properties have been calculated[63] through modelling work only. Many authors have described the fact that higher the anisotropy of the lamina material, greater the possibility of a negative Poisson's ratio.

In order to proceed with detailed analysis on the laminates it has been vital to verify the properties of the laminates made and tested to confirm the auxeticity of the $[\pm 30]_s$ and $[0/15/75/15]_s$ laminate in particular. The objective has been accomplished in a number of ways. Firstly, the properties of the lamina material were obtained experimentally through simple tensile testing and Classical Laminate Theory (CLT) was then used to obtain laminate properties for all the stacking sequences used. The conclusions from each of these measurement

techniques and the importance of the findings for this investigation and to the previous work by other authors will be discussed below.

6.1.1 Determination of Lamina Properties

The tensile tests were carried out in order to obtain experimental values of the elastic constants as given in Table 6-1 for IM7/8552 material used in this work and these values were compared to the values obtained in previous work by V. L. Coenen[64] using the same technique.

Table 6-1 Elastic constants of Lamina, previous work[64] **& current work**

Property	**IM7/8552**	
	Previous	Current
E_1 (GPa)	145	150
E_2 (GPa)	8	7
G_{12} (GPa)	6	6
ν_{12}	0.31	0.33
ν_{21}	0.02	0.02

This is obvious from the modulus $\mathbf{E_1}$ in the 1-direction of the lamina material is higher for the pre-preg used in the present study, also the modulus $\mathbf{E_2}$ in the 2-direction is lower. This provides a pre-preg material with considerably greater anisotropy, suitable for investigations of this type into the effect of a negative

Poisson's ratio on mechanical performance. The effect of negative Poisson's ratio on the mechanical performance can be investigated if a pre-preg material has considerably greater anisotropy. This is obvious from longitudinal Poisson's ratio 0.33, which has a strong effect on the predicted values of Poisson's ratio for the $[\pm 30]_s$ and $[0/15/75/15]_s$ lamina. Donoghue[56] predicted the value for $[\pm 30]_s$ as shown in the Figure 6-1.

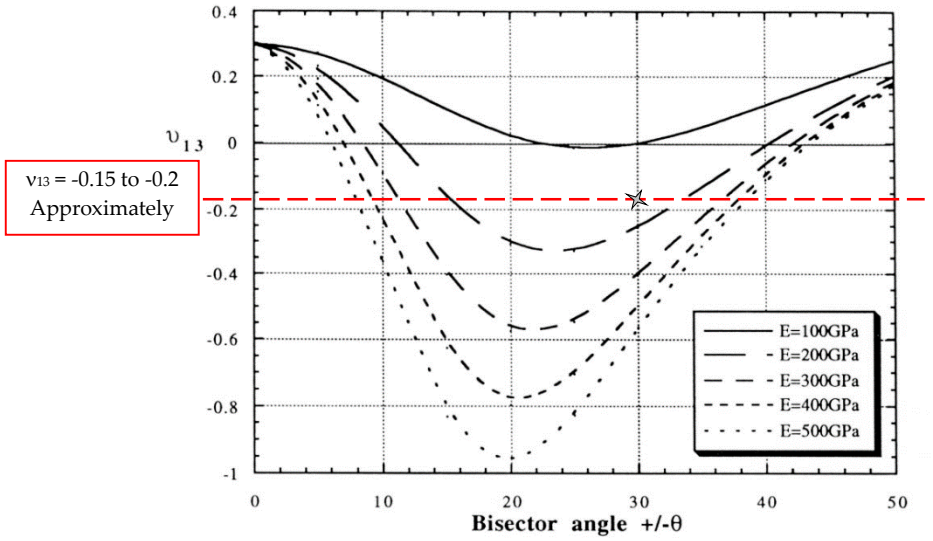

Figure 6-1 [± θ]s Variation of ν_{13}, with Bisector Angle & Increasing Lamina E_1 [56]

The extrapolated value from the above plot, as shown in Figure 6-1 for a lamina material with the longitudinal modulus value E_1 = 150GPa as is the case for the pre-preg material used in this work, gives an approximate value for υ_{13} for the $[\pm 30]_s$ laminate of between -0.15 and -0.2. Donoghue reported a value of -0.156,

and as such, according to theory, the value for IM7/8552 should be higher than this and could be nearer to -0.2 because of the value of E_1.

A similar graph for a range of laminar material moduli has been plotted for the variation of υ_{12} with bisector, angle as shown in Figure 6-2. Classical Laminate Theory and IM7/8552 lamina properties have been used to obtain this plot. The curve for the condition E_1=150GPa shows an approximate value of 1.6 for υ_{12} of $[\pm 30]_s$ laminate.

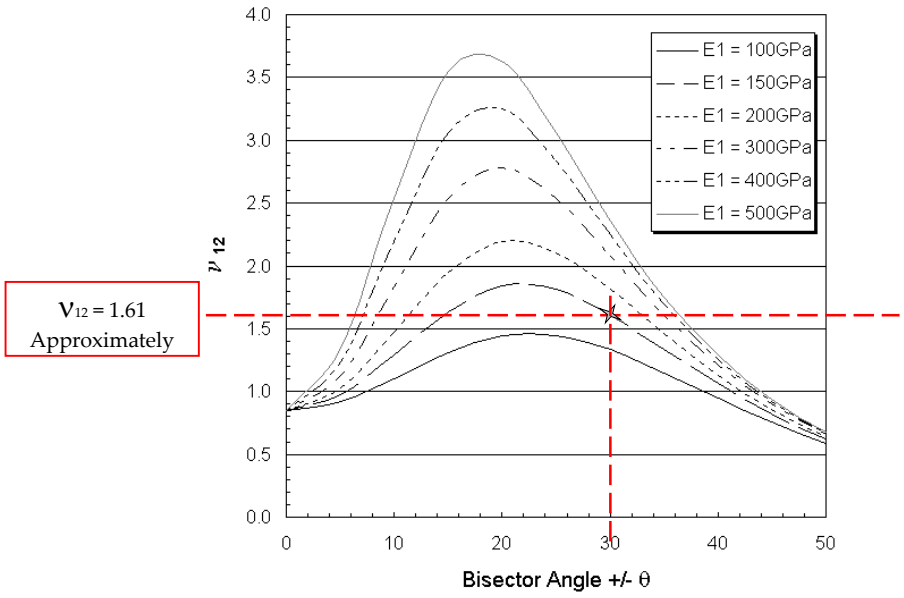

Figure 6-2 Variation of ν_{12}, with Bisector Angle [± θ]s & Increasing Lamina E_1 [56]

Another simple prediction is carried out for IM7/8552 pre-preg with E_1=150GPa as shown in the plot
Figure 6-3, and this can be compared to the preceding predictions for υ_{12} and υ_{13} for a range of pre-preg E_1 values.

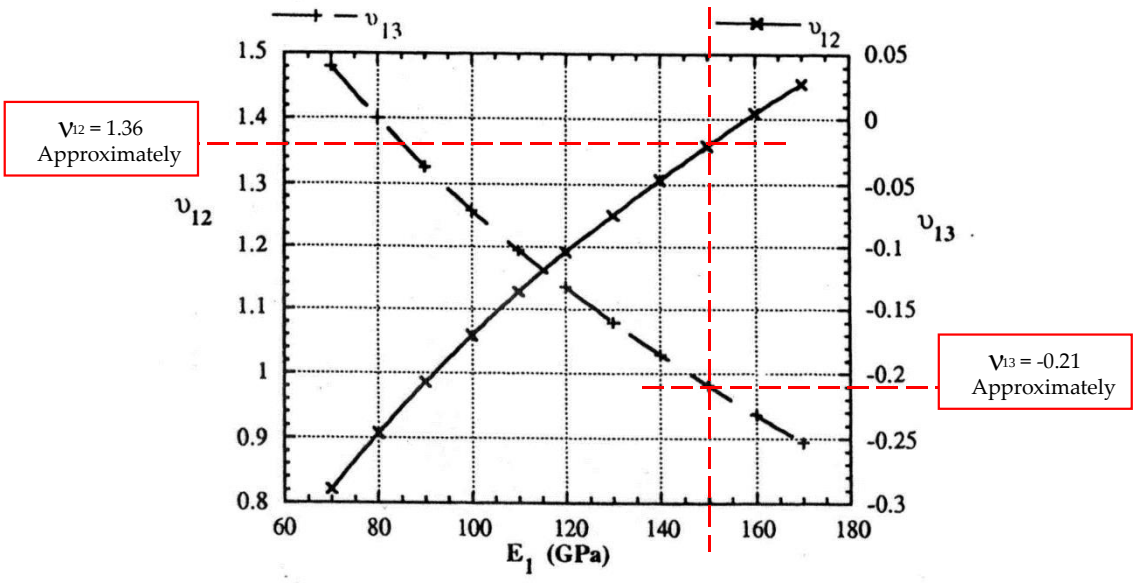

Figure 6-3 Variation in ν_{12}, & ν_{13} with Increasing Lamina E_1 [56], $[\pm 30]_s$ Laminate

The above plot as shown in

Figure 6-3, a simple predictions are achieved for IM7/8552 pre-preg material and this can be compared to previous predictions for a range of pre-preg E_1 values. The value predicted for υ_{13} is approximately –0.2 in both cases, though there is a disparity between the predicted value υ_{12}. The value obtained in the present work with the help of Classical Laminate Theory (CLT) is approximately 1.6 compared to the approximate value of 1.36 predicted by Donoghue [56].

Using the experimentally obtained lamina material properties, the elastic constants of the $[\pm 30]_s$ laminate were achieved by commercially available laminate analysis program, Classical Laminate Theory (CLT)[189]. The values calculated with the help of the commercially available analysis program, as shown in Table

6-2, are very close; the only distinction being the predicted value for the in-plane Poisson's ratio υ_{12}.

Table 6-2 Predicted Properties of [±30]s laminate, previous [56] & current work

	IM7/8552		AS4/3501 [38]	
	CLT	The laminator	Ultrasonic Immersion	Software Prediction
E_1 (GPa)	51	53	37	50
E_2 (GPa)	9	11	19	12
G_{12} (GPa)	27	30	19	26
ν_{12}	1.4	1.42	0.78	1.243

Certain presumptions are made as mentioned previously when using CLT, i.e. the laminate under consideration is of infinite size; as such no importance is given to edge effects. Edge effects are important to the performance and hence characteristics of a real laminate. In this way, the values achieved can only be considered as an approximation.

6.1.2 Determination of Laminate Properties

The discussion here will now look at the measured values, for the longitudinal Modulus E_1 and the in-plane Poisson's ratio υ_1. The values obtained are listed in Table 6-3.

Table 6-3 Measured Stacking Sequence Tensile Properties

Nomenclature	Specimen Configuration	Elastic Modulus (GPa)	Poisson's ratio (ν_{12})
N_a	$[\pm 30]_S$	49.6	1.5
P_a	$[35/-20/25/40/-85/40/25/-45/35/-15/25/40]_S$	49.8	0.6
N_b	$[0/15/75/15]_S$	64.8	-0.14
P_b	$[0/-70/10/25]_S$	61.7	0.47

These values are compared to the values achieved by CLT and also to the predicted values described by V. L. Coenen[167] and [63] for the laminates with the same stacking sequences manufactured using IM7/8552. The modulus values E_1 and the in-plane Poisson's ratio υ_{12} values are compared separately for more accuracy. Good agreement is observed in terms of the E_1 values for all specimens as shown in Table 6-4.

Table 6-4 E_1 (GPa); Predicted and Measured values using IM7/8552

Property	Sample	Specimen Configuration	EXP	CLT	PR
Through-thickness	N_a	$[\pm 30]_S$	49.6	51	43
	P_a	$[35/-20/25/40/-85/40/25/-45/35/-15/25/40]_S$	49.8	53	51
In-plane	N_b	$[0/15/75/15]_S$	64.8	63.4	-
	P_b	$[0/-70/10/25]_S$	61.7	60.2	-

Exp Experimentally obtained values
CLT Classical Laminate Theory
PR Measured in previous study by V. L. Coenen

The predicted values of V. L. Coenen are very close to the measured values, as expected due to the similar material used in the pre-preg manufacturing.

Similarly, the in-plane Poisson's ratio υ_{12} values are compared and to some extent these values exhibit better agreement; here the largest range in values is obvious for the through-thickness auxetic specimen as shown in Table 6-5. The greater positive value of the in-plane Poisson's ratio specimen suggests a highly anisotropic pre-preg and thus auxetic behaviour is present in the through-thickness direction.

Table 6-5 Predicted and Measured υ_{12} values using IM7/8552

Nomenclature	Specimen Configuration	EXP	CLT	PR
N_a	$[\pm 30]_S$	1.5	1.4	1.6
P_a	$[35/-20/25/40/-85/40/25/-45/35/-15/25/40]_S$	0.6	0.56	0.6
N_b	$[0/15/75/15]_S$	-0.14	-0.134	-
P_b	$[0/-70/10/25]_S$	0.47	0.466	-

Exp Experimentally obtained values
CLT Classical Laminate Theory
PR Measured in previous study by V. L. Coenen

This can be summarised here, the experimentally measured values obtained through the tensile testing, compare very well with the predicted values.

6.2 Quasi-static Indentation Resistance of Through-Thickness Specimens

Previous work by V.L. Coenen[56] investigated a range of indentors and loading rates for positive and auxetic through-thickness Poisson's ratio laminate stacking sequences. The purpose was to determine whether the improvements in indentation resistance ascertained in other auxetic materials are possible in auxetic composite laminates and the effect of the size and sign of the through-thickness Poisson's ratio. Here in this work, the focus was to assess whether the enhancements in indentation resistance are retained after the initial indentation event in the area away from the indentor nose region in both positive and auxetic laminate stacking sequences. Re-indentation was carried out under and away from the nose region for detailed analysis of each specimen and compared to the behaviour of the single indented specimens.

A series of tests were designed using a 12.7mm sized steel hemisphere indentor with a loading rate of 2mm/min to an indentation depth of 5mm to achieve the full spectrum of load displacement behaviour until failure[64]. All the specimens were placed on a 50mm internal diameter test fixture. The test sites, as discussed in previous Chapter -4 of section 4.2, were located at the centre and 20mm away in the vicinity of the initial indentation region of the 100x100mm^2 specimens. In this way, both quasi-static and low velocity impact testing has been conducted

using exactly the same test configuration, each of the tests will be discussed in turn, beginning with a comprehensive discussion of the conclusions from the quasi-static investigation.

The plots of the experimental data are discussed in detail in the following sections of this chapter. The first clearly distinguishable point on the plots is the 'first failure' point. This indicates the onset of damage within the laminate and is a good indication for any differentiating behaviour and can be the initial measurement of an auxetic enhancement. The region up to this failure point has been used to achieve the initial gradient (initial specimen stiffness value) and the value for energy absorption taken as the area under the graph to this point.

The second feature investigated was the region up to the peak load reached before failure during the test. This peak point has been compared in terms of the load value, the displacement and energy absorption. The final comparison between all the specimens is of the overall shape of the plot, specifically the performance after peak load i.e. is the load level continued for any considerable amount of time, and is there a sudden drop in load carrying capability after peak load or are there any other features not particularly noticed in the other specimens?

Comparisons of the features discussed above are reported in turn for simplicity, firstly across the indentation site under the indentor nose region for the first and second failure point and secondly the behaviour is compared across the specimens for indentation sites away from the indentor nose region. This last comparison enables the conclusions to be drawn concerning the effect of indentation under and away from the indentor nose region.

6.2.1 Indentation Behaviour under the Indentor Nose Region

It is important to understand each stage of the single indentation behaviour, under the indentor nose region before proceeding further for multiple indentations under and away from the initial indentation site. Particular examples of such plots for these specimens are given below for reference as shown in, Figure 6-4 and Figure 6-5.

6.2.1.1 Single Indentation & First Failure Point across the Specimens

Looking at the indentation response of the specimens under the indentor nose region in terms of the first failure point, there was a marked difference; a clear auxetic enhancement was observed, which occurred at a higher load value of

5.3kN than the positive Poisson's ratio specimen. The energy absorbed up to this failure point also appeared to be enhanced in the positive Poisson' ratio specimen.

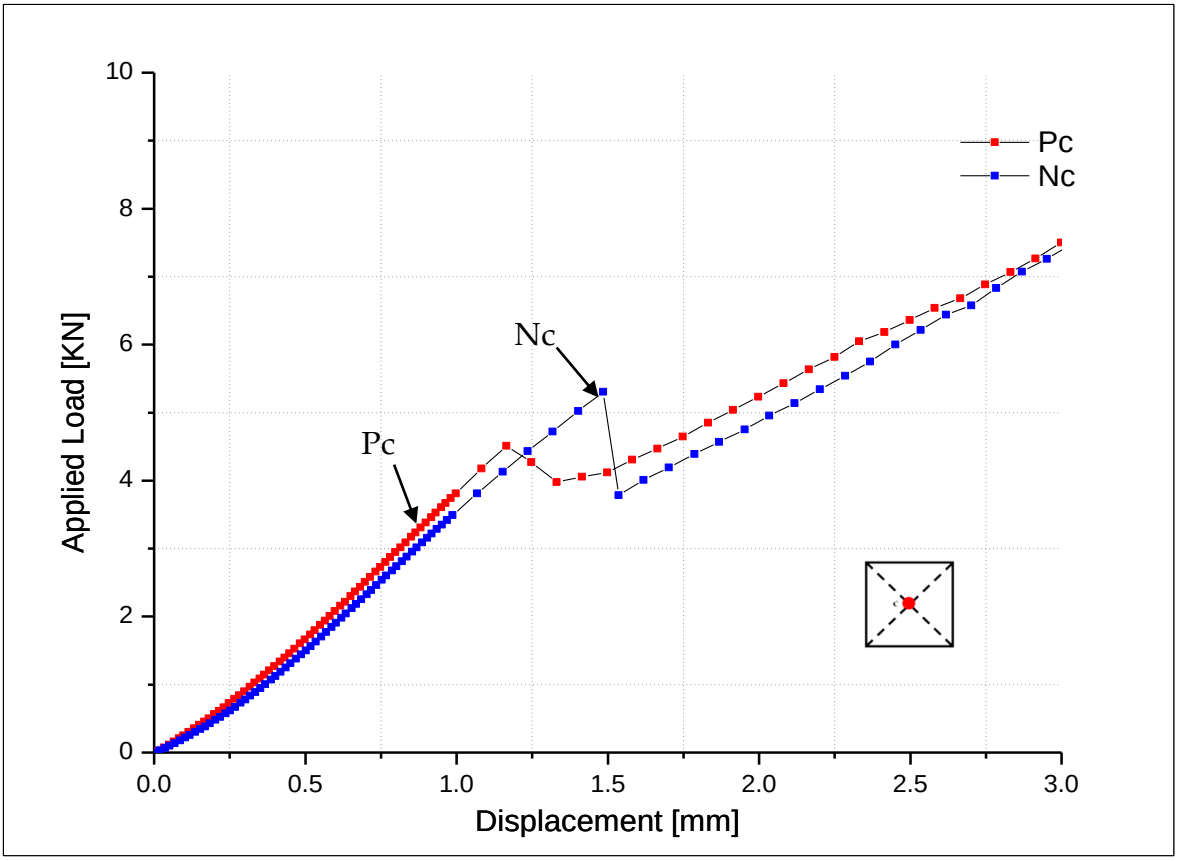

Figure 6-4 **Single Indentation at Centre; First Failure point on Load Displacement Curves**

It is interesting to note that the positive Poisson's ratio specimen has similar gradient to the auxetic specimen. This indicates that the response in terms of gradient/modulus is indicative of the pre-preg properties. It can be concluded here that the results achieved are truly evidence of an enhanced auxetic resistance to indentation.

6.2.1.2 Single Indentation & Second Failure Point across the Specimens

A detailed examination of the results revealed a clear enhancement, even well into the failure process. The peak load for the auxetic specimen was measured to be 11.73kN compared to the positive Poisson's ratio specimen which attained a value of 9.86kN at peak failure point, as shown in plot Figure 6-5.

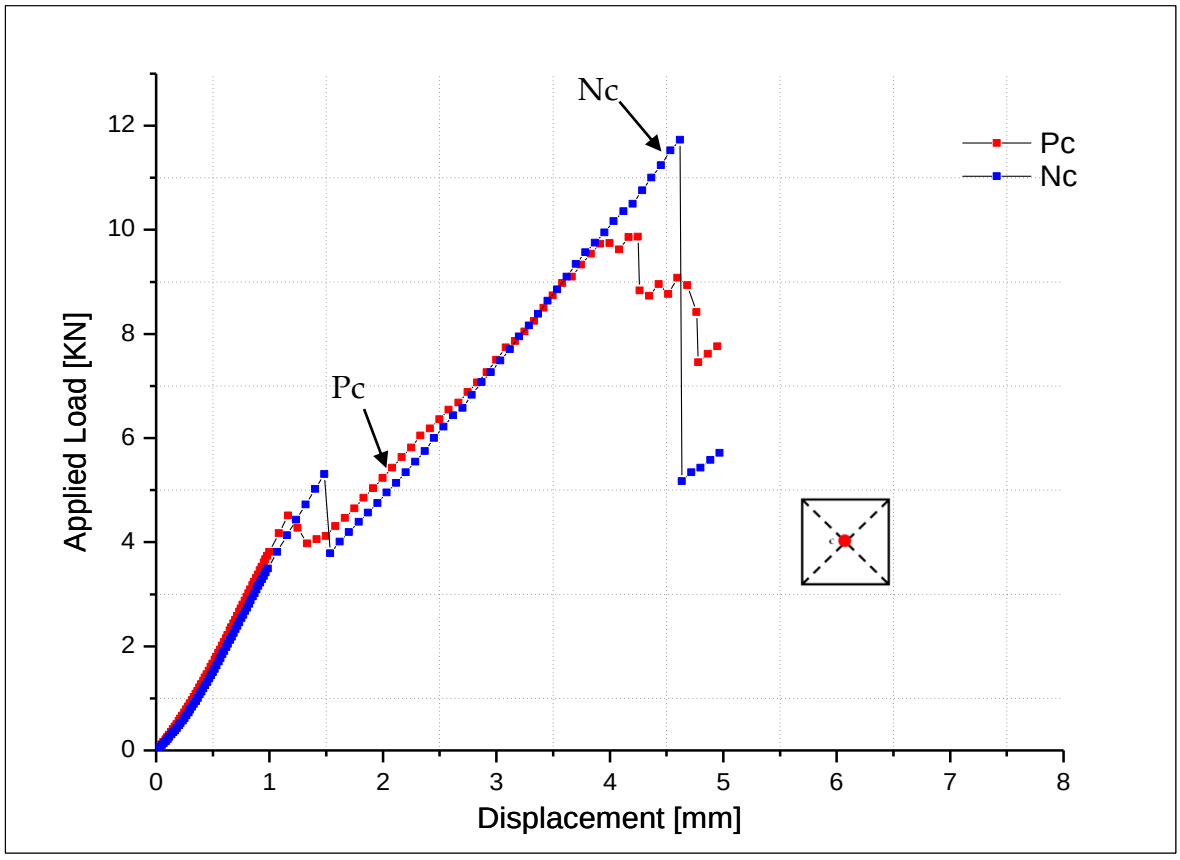

Figure 6-5 **Single Indentation at Centre; Second Failure point on Load Displacement Curves**

The peak point on curves proceeded in significantly different manner for both plots during the final load drop. This load drop was sustained longer for the

positive Poisson's ratio specimens compared to the auxetic specimens and showed catastrophic failure after this level. Hence, the results show that the auxetic specimens attain greater peak load and the energy absorbed is also considerably high. The confidence in making these statements about auxetic enhancement here is due to the consistency attained in the results thus far and the clear differences in the failure behaviour observed in the specimens. This auxetic enhancement is further studied upon re-testing these specimens at the same site or away from the initial indentation site.

6.2.1.3 Re-Indentation Across the Specimens

All the specimens of the previous stage were quasi-statically re-loaded to achieve the full damage. The re-indentation curves are shown in Figure 6-6 for both the auxetic and the positive Poisson's ratio specimens; these curves revealed an entirely different trend compared to the initial indentation stage. Here, in this failure process peak load is achieved without reaching first failure point and this occurs only if a complete delamination stage was attained previously.

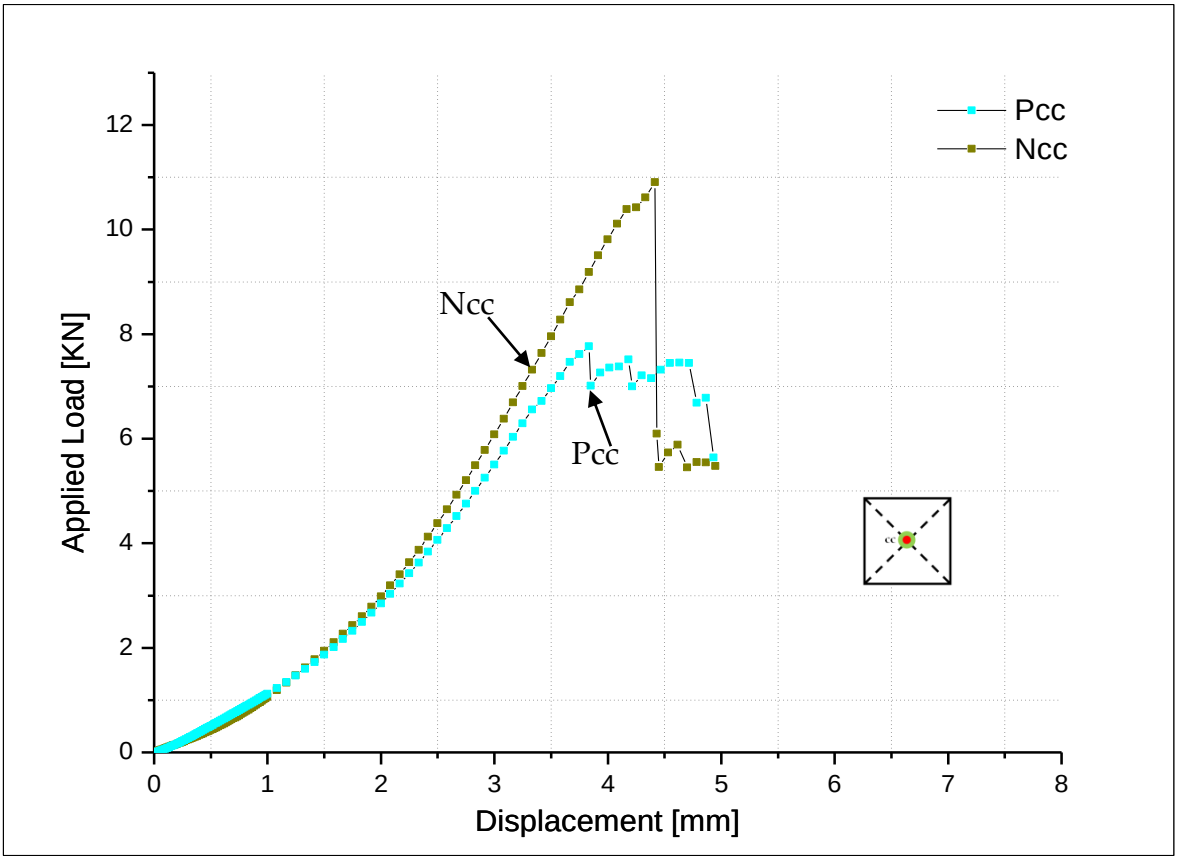

Figure 6-6 Re-Indentation at Centre and Load Displacement Curves

However, a clear enhancement is sustained in the auxetic specimens at peak load and this is also evident from the energy absorbed by the axuetic specimens which is 19J compared to the positive Poisson's ratio specimens, which absorbed 12J at this indentation event.

6.2.2 Re-Indentation Behaviour in the Damage Direction

This study was further proceeded, with the re-indentation in the vicinity of the indentor nose region of the previously centre indented specimens. This stage was accomplished by indenting each specimen, 20mm away both sides, along the 0^{o} (damage direction) of the initial indentation site as shown in Figure 6-7.

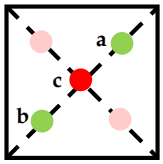

Figure 6-7 Test site markers "a and b" in the damage direction

6.2.2.1 Away from the Indentor Nose region In the Damage Direction site "a" (see Figure 6-8)

The resulting plots revealed that there is no sharp indication of first failure for positive Poisson's ratio specimens but it is much more pronounced for auxetic specimens as shown in Figure 6-8.

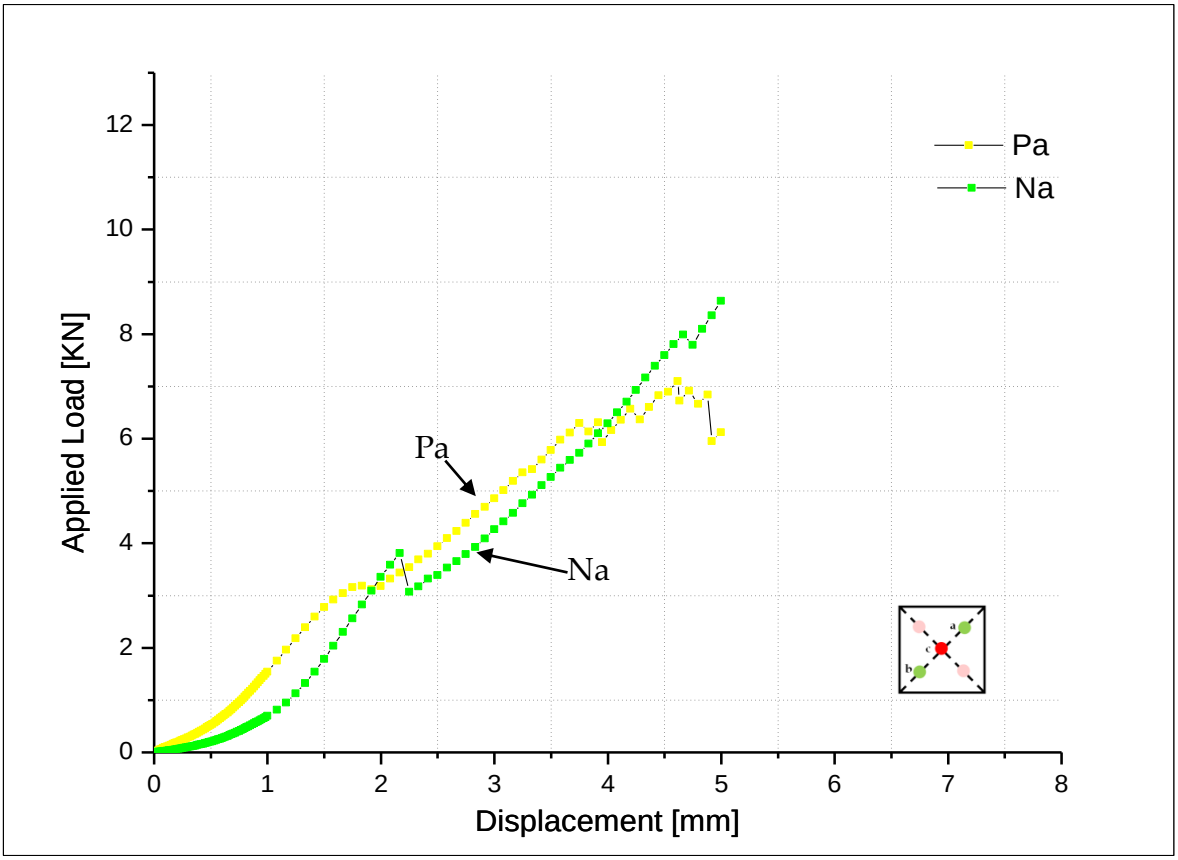

Figure 6-8 Load Displacement Curves; Indentation in the Damage direction 'a'

This is due to the presence of more developed delaminations in the positive Poisson's ratio specimen as shown in Figure 4-20,.prior to the indentation event in the vicinity of the indentor nose region and due to this reason these curves display reduced first failure point after re-indentation, as shown in results Chapter 4 section 4.9.1.3. However, the latter part of the failure process that the second failure or peak load remains unaffected after the initial indentation event in the vicinity of indentor nose region. It can be concluded here that the auxetic specimens tend to be quite unaffected away from the initial indentation site.

6.2.2.2 Away from the Indentor Nose region In the Damage Direction site "b"

The re-indentation at site "b" also revealed similar trends as discussed in the above case. There is no sharp indication of the first failure for the positive Poisson's ratio specimen but this failure is apparent for the auxetic specimens as shown in Figure 6-9.

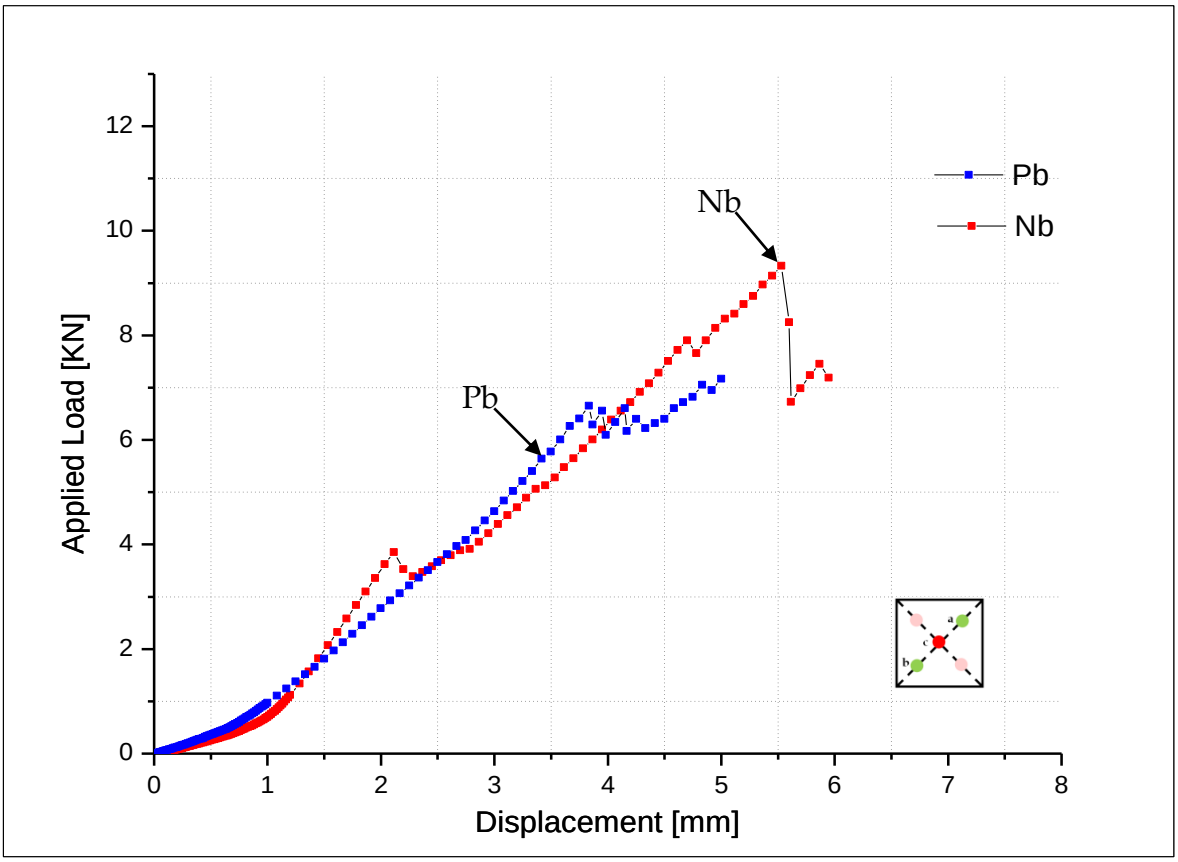

Figure 6-9 Load Displacement Curves; Indentation in the Damage direction 'b'

In the positive Poisson's ratio specimens, as shows in Chapter 4 section 4.9.1.3, delamination occurs during the initial indentation event, which spreads out far away from the indentor nose region. This is the reason that these curves show a

slight deviation for the first failure point upon re-indentation event. However, the latter part of the failure process under this form of loading, the auxetic specimens remains unaffected after the initial indentation event under the indentor nose region. Here, it may be concluded that the auxetic specimens tend to behave quite different compared to the positive Poisson's ratio specimens.

6.2.3 Re-Indentation Behaviour Opposite to the Damage Direction

The re-indentation in the vicinity of the indentor nose region of pre-indented specimens were carried out 20mm away at sites "d" and "e" along the 90° (opposite to the damage direction) of the initial indentation site as shown in Figure 6-10.

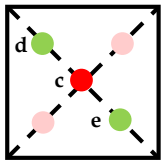

Figure 6-10 Test site markers "d and e" perpendicular to damage direction

6.2.3.1 Away from the Indentor Nose & Opposite to the Damage Direction site "d"

The resulted plots revealed that the auxetic specimens show higher first failure point and the peak load point compared to the positive Poisson's ratio specimens as shown in Figure 6-11.

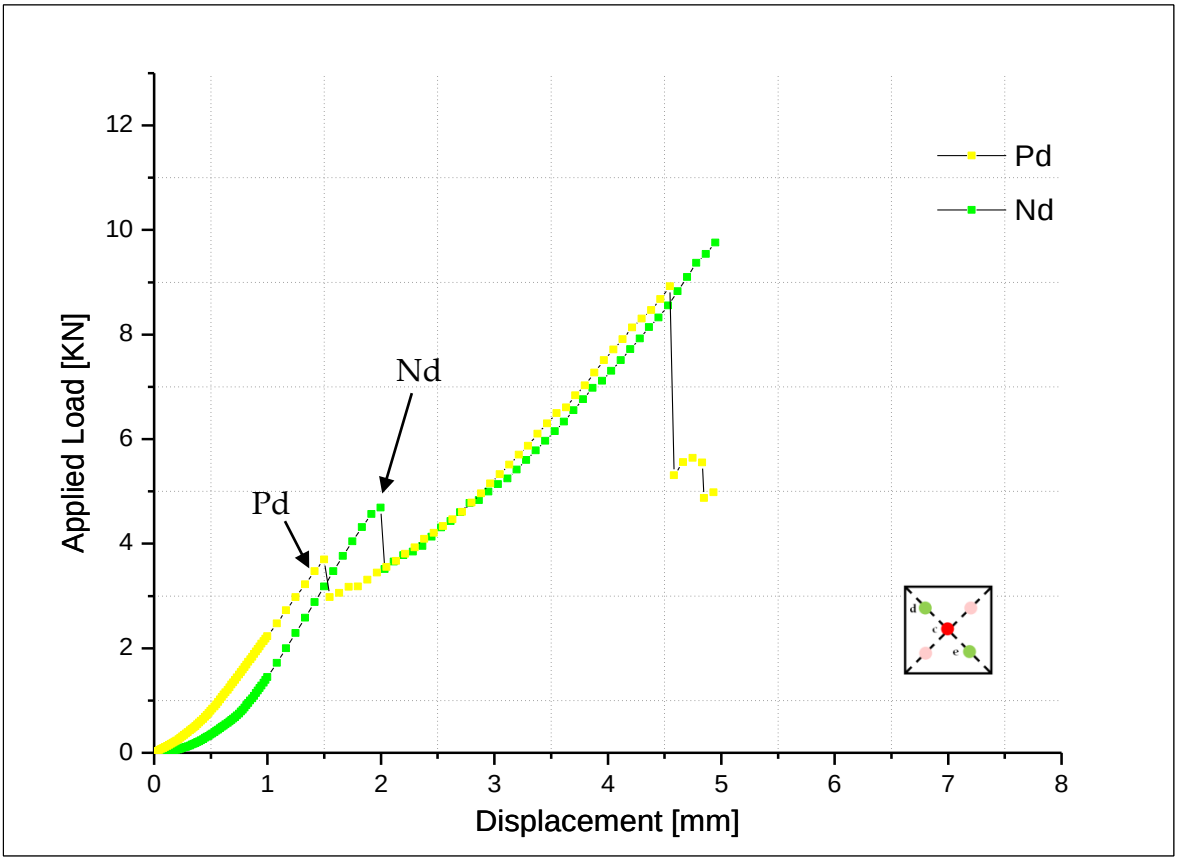

Figure 6-11 **Indentation Opposite to the Damage direction 'd' and Load Displacement Curves**

This is due to the reason that the damage area in the auxetic pre-indented specimens is confined and limited to the indentor nose region. Hence these curves show higher first failure point and peak load after re-indentation in the auxetic specimens compared to the positive Poisson's ratio specimens. Here, it can be observed from the re-indentation curves that the auxetic specimens remain unaffected upon re-indentation in the vicinity of the indentor nose region. Thus auxetic specimens possess better load bearing properties even after multiple indentation events.

6.2.3.2 Away from the Indentor Nose & Opposite to the Damage Direction site "e"

The re-indentation curves of site "e" show similar trend to that as discussed in above case. The first failure point and peak load point in auxetic specimens as shown in Figure 6-12, are both higher compared to the positive Poisson's ratio specimens.

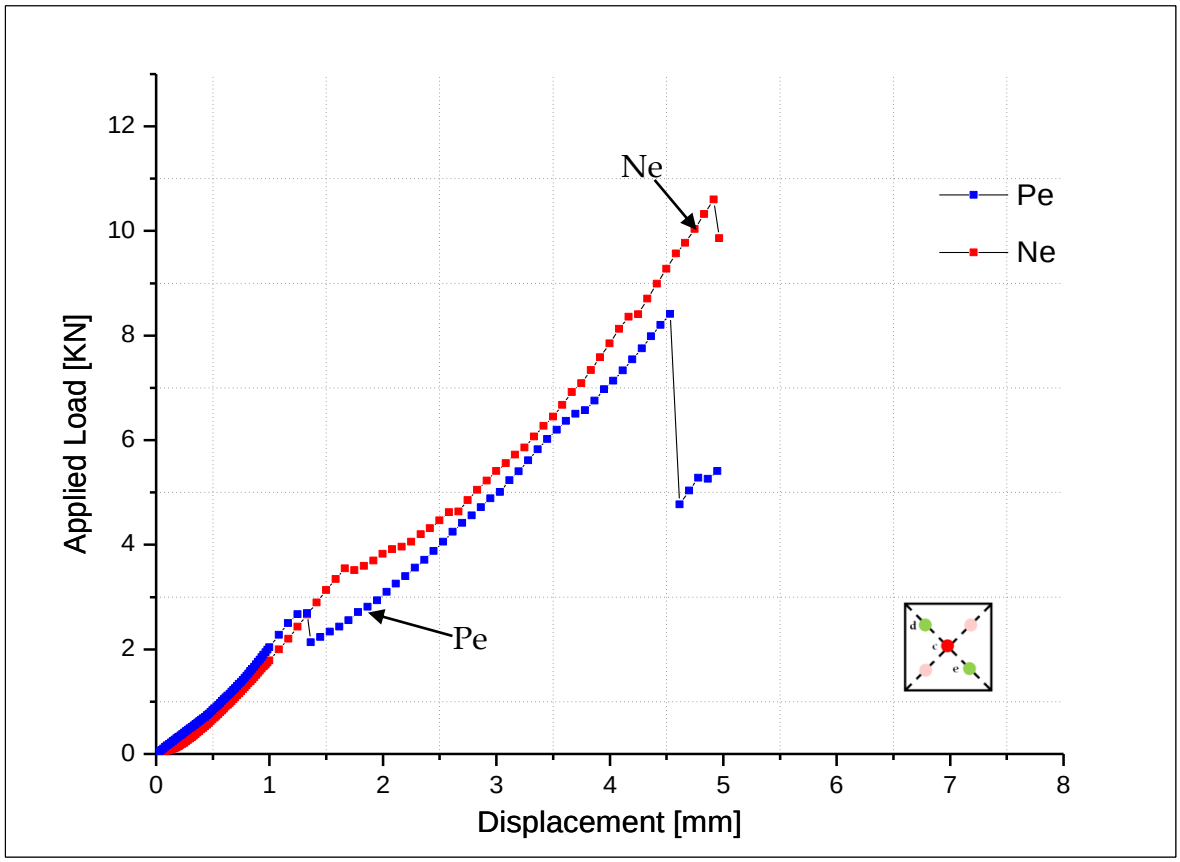

Figure 6-12 Indentation Opposite to the Damage direction 'e' and Load Displacement Curves

The damage area in the indented auxetic specimens is more concentrated in the vicinity of the indentor nose region due to the initial indentation event compared

to the positive Poisson's ratio specimens as show in results Chapter 4, section 4.9.1.4. This is clearly evident from the re-indentation curves of the auxetic specimens because they resist more before failure at first and second failure point and hence show higher load bearing capacity. It is obvious from the above plots that auxetic enhancement sustains even after initial indentation event compared to the positive Poisson's ratio specimens.

6.3 Low Velocity Impact of Through-Thickness specimens

The purpose of the low velocity impact (LVI) investigation was to determine whether the improvements in impact resistance ascertained in other auxetic materials are possible in auxetic composite laminates and the effect of the size and sign of the through-thickness Poisson's ratio. In this work the focus was to assess whether the impact resistance is retained after the initial indentation event in the area away from the impactor nose region in both the positive and the auxetic laminate stacking sequences. Re-impacts of the pre-impacted specimens were carried out under and away from the nose region for detailed analysis of each specimen and compared to the behaviour of the single impact event.

The test parameters comprise a 12.7mm sized steel hemisphere indentor for impact tests to achieve the full profile of impact energy until failure. All the

specimens were supported by 50mm internal diameter test fixture for the testing purpose. The test sites were located at the centre and 20mm away in the vicinity of the initial indentation region of the 100x100mm^2 specimens. These parameters are same as those used for the indentation tests.

All the features of the resulting plots are reported in turn for simplicity, firstly across the impact site under the impactor nose region for first and second failure point. The behaviour is also compared across the specimens for the impact site away from the impactor nose region. This last comparison enables the conclusions to be drawn concerning the effect of low velocity impact under and away from the impactor nose region. Auxetic specimens form a confined failure region under the indentor nose, as compared to the positive Poisson's ratio specimens upon multiple impact events, and thus sustain better load bearing capacity.

6.3.1 Impact Behaviour under the Nose Region

The first set of each type of specimens were allowed to impact at the centre of the 100x100mm^2 plate. Experimental data from the impact tests are in the form of a continuous recording of force and time. This data is plotted as force deflection curves and detailed features of these curves are discussed below.

6.3.1.1 Single Impact & Failure Points across the Specimens

Force deflection plots of the auxetic and the positive Poisson's ratio specimens could be described as showing similar trends as those observed during the quasi-static investigation. The positive Poisson's ratio specimens exhibit a small first failure event followed by a smooth transition up to peak load at which the load drops swiftly to the minimum point of the plot.

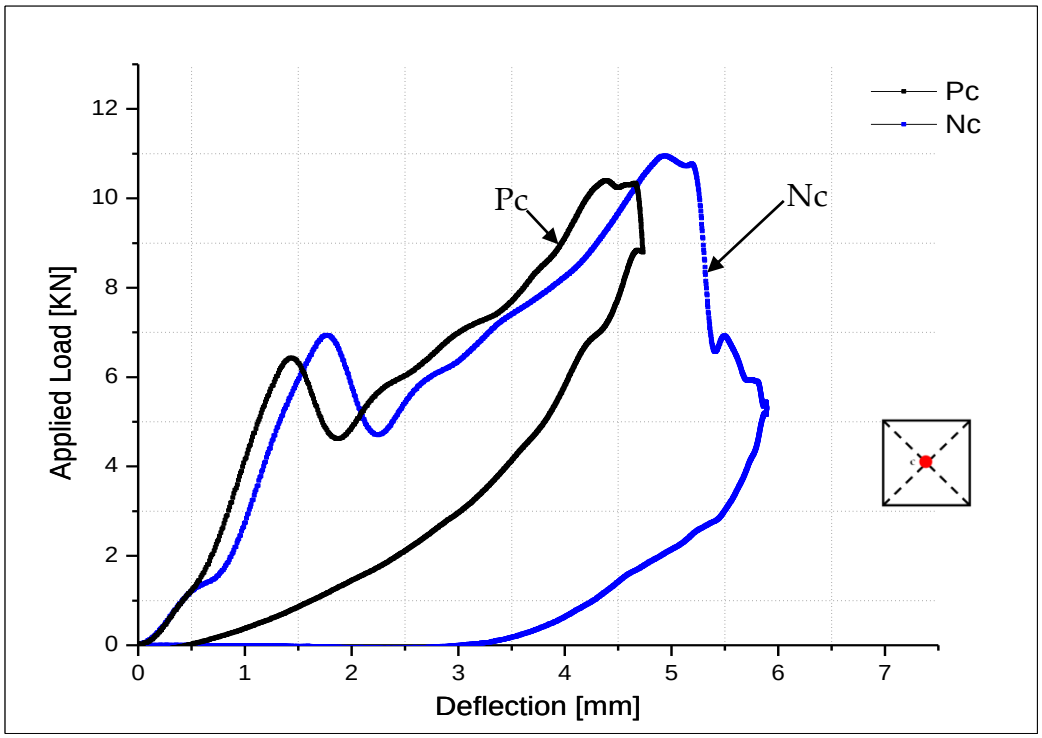

Figure 6-13 Single Impact at Centre and both Failure Points on Load Deflection Plots

The auxetic specimens show a higher first failure point, after which the curve again proceeds to another large peak load level than for the positive Poisson's ratio specimen. The peak load for auxetic specimen was 11.01kN compared to the

positive Poisson's ratio specimen that attained lower peak failure point as shown in Figure 6-13. These results are quite reproducible and a detailed examination of the results revealed the presence of auxetic behaviour even well into the failure process. The energy absorption values at this point follow the same trend as observed in case of quasi-static indentation away from centre in the damage direction with the auxetic specimens showing higher values compared with the positive Poisson's ratio specimens. The results of this impact phase are also compared with a matched modulus[190] of a quasi-isotropic laminate of the similar modulus and material, and have found good agreement between the both specimen.

6.3.1.2 Multiple Impacts across the specimens

All initially impacted specimens were subjected to re-impact tests under the same conditions at the same initial impact site in order to achieve full damage. The absence of first failure point clearly indicates the presence of delaminations in the specimens before the re-impact event started. The auxetic specimens are observed to fail at much higher peak load, as shown in Figure 6-14, to a value of 12.65kN that is higher compared to the positive Poisson's ratio type specimens. This suggests that auxetic specimens required higher load to cause failure and therefore they are more resistant to re-impact event. The auxetic specimens show

less resistance, as shown in Chapter 4 section 4.10.1.2, to failure and absorb more energy compared to the positive Poisson's ratio specimens.

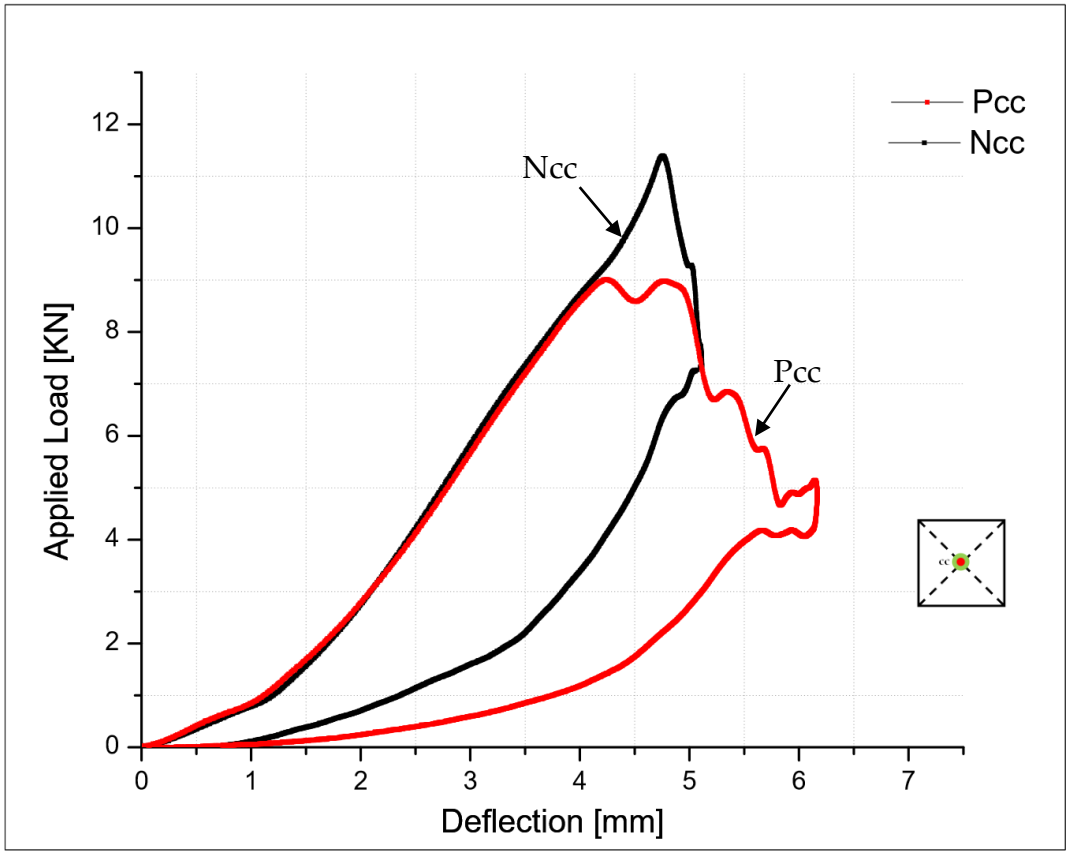

Figure 6-14 Re-Impact at Centre and Load Deflection Plots

As the peak load is achieved without reaching first failure point, this also indicates complete delamination has been achieved previously under the nose region during the initial indentation event.

6.3.2 Impact Behaviour in the Vicinity of the Nose Region

A group of specimens were re-impacted 20mm away on both sides of the initial site of impact event in the vicinity of the impactor nose region along the 0^{o} (damage direction) as mentioned above in Figure 6-7.

6.3.2.1 Away from the Impactor Nose region In the Damage Direction site "a"

The re-impact curves of both the auxetic and the positive Poisson's ratio specimens show dissimilar behaviour as illustrated in Figure 6-15.

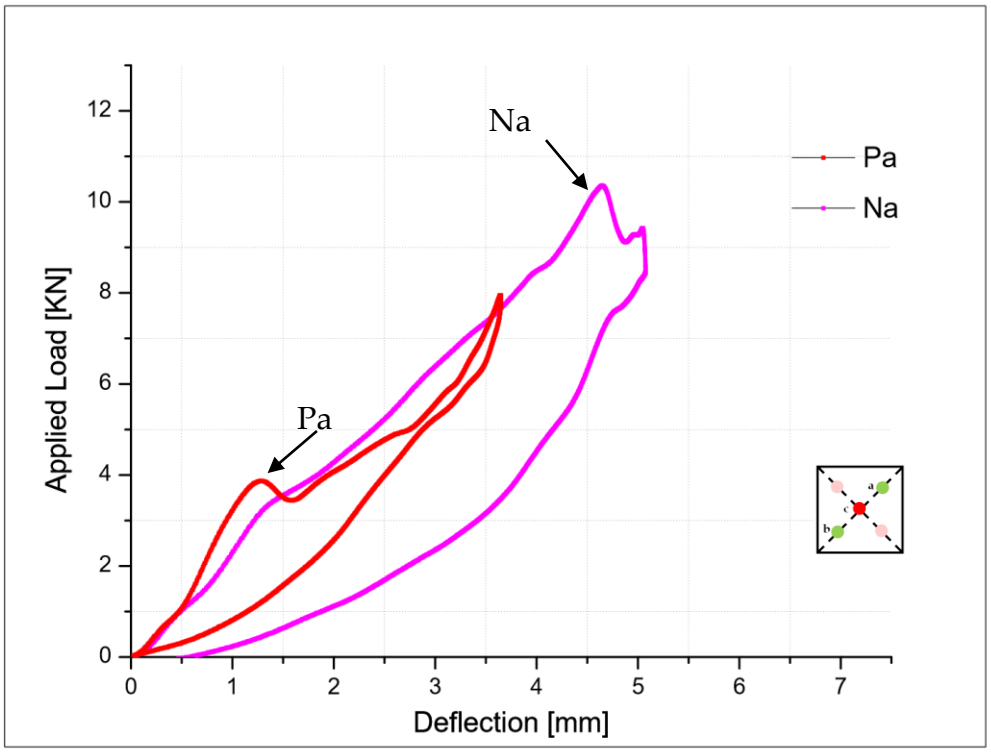

Figure 6-15 Load Deflection Plots; Impact at site 'a' in the Damage direction

The presence of delamination in the vicinity of the positive Poisson's ratio specimens does not allow these to absorb enough energy before failure as show previously (Chapter 4 section 4.10.1.3).

Although the auxetic specimens show more resistance to failure even after the initial indentation event in the vicinity of the indentor nose region and this indicates a clear enhancement in the energy absorption compared to the positive Poisson's ratio specimens. It appears that the auxetic specimens tend to be least affected away from the initial indentation site.

6.3.2.1 Away from the Impactor Nose region In the Damage Direction site "b"

The re-impact curves of site "b" of both the auxetic and the positive Poisson's ratio specimens revealed a unique trend, as shown in Figure 6-16, after the re-impact event. The auxetic specimens sustain loads longer before the final failure but the positive Poisson's ratio specimens abruptly lose their load bearing resistance.

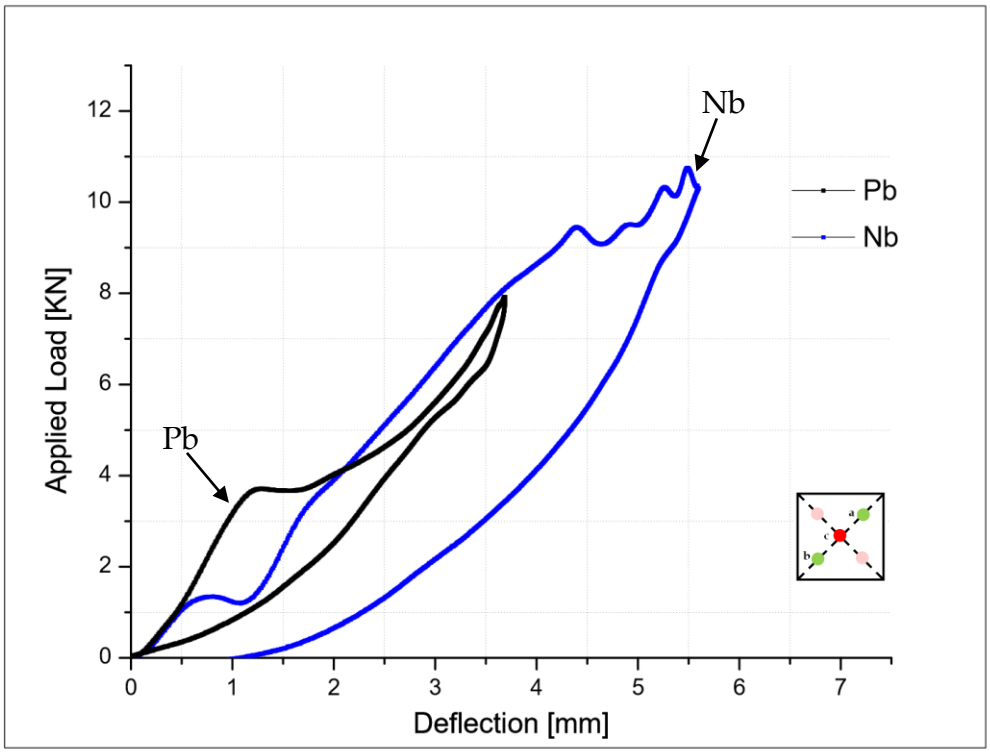

Figure 6-16 Load Deflection Plots; Impact at site 'b' in the Damage direction

The force deflection curve in the auxetic specimens shows many small uneven regions, revealing that the load is sustained for longer duration before the final failure but the curve for the positive Poisson's ratio specimen abruptly reduces to a minimum value after the peak load. The presence of delaminations under the impact region in the positive Poisson's ratio specimens leads to catastrophic behaviour as show in Chapter 4 section 4.10.1.3. This has been confirmed by testing a large number of specimens and therefore it can be concluded that the auxetic specimens remain the least affected away from the initial indentation site.

6.3.3 Re-Impact Behaviour Opposite to the Damage Direction

All the specimens were also re-tested 20mm away on both sides of the initial site of impact event in the vicinity of the impactor nose region along the 90° (opposite to the damage direction as shown above in Figure 3-6).

6.3.3.1 Away from the Impactor Nose & Opposite to the Damage Direction site "d"

The re-impact curves of site "d" show different behaviour for both the auxetic and the positive Poisson's ratio specimens. The auxetic specimens show higher peak load point compared to the positive Poisson's ratio specimens, as shown in Figure 6-17.

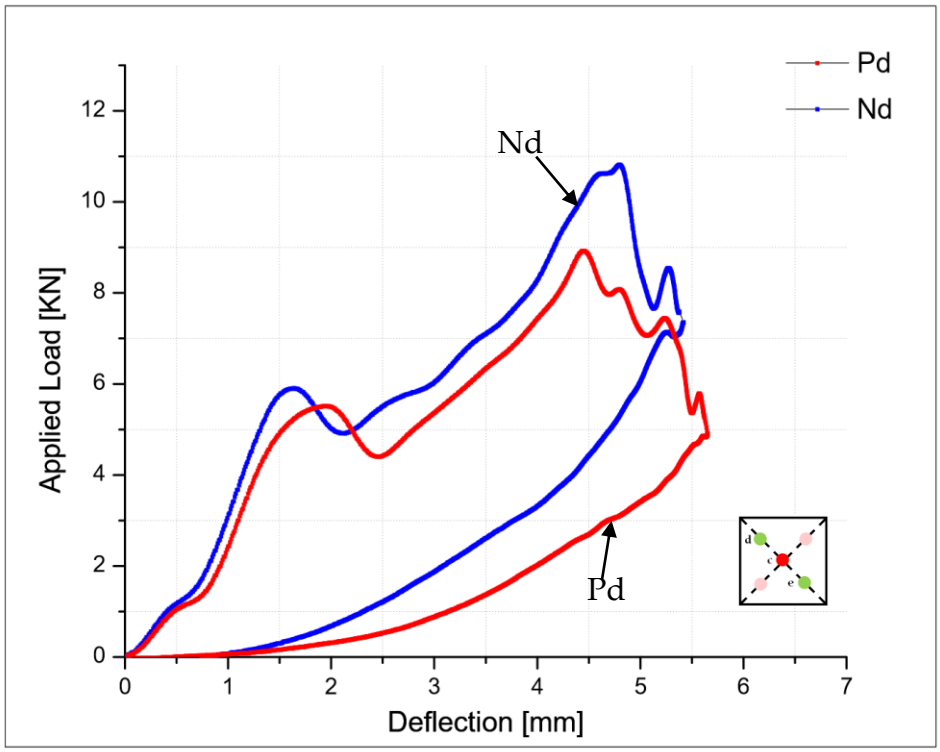

Figure 6-17 Load Deflection Plots; Impact at site 'd' Opposite to the Damage direction

The damage area produced during the initial impact event in the auxetic specimens seems more concentrated and limited to the impactor nose region compared to the positive Poisson's ratio specimens. It is quite evident from the re-impact curves of the auxetic specimens because they show little more resistance before the final failure point and hence show better load bearing capacity. This is obvious from the above plots that the auxetic behaviour sustains even after the initial impact event compared to the positive Poisson's ratio specimens.

6.3.3.2 Away from the Impactor Nose & Opposite to the Damage Direction site "e"

The re-impact tests were also carried out at site "e" for both type of specimens and they show unique trends as discussed in above case "d". The peak load point in auxetic specimens is found higher as shown in Figure 6-18 compared to the positive Poisson's ratio specimens. The auxetic specimens are found to have abrupt load drop compared to the positive type specimens.

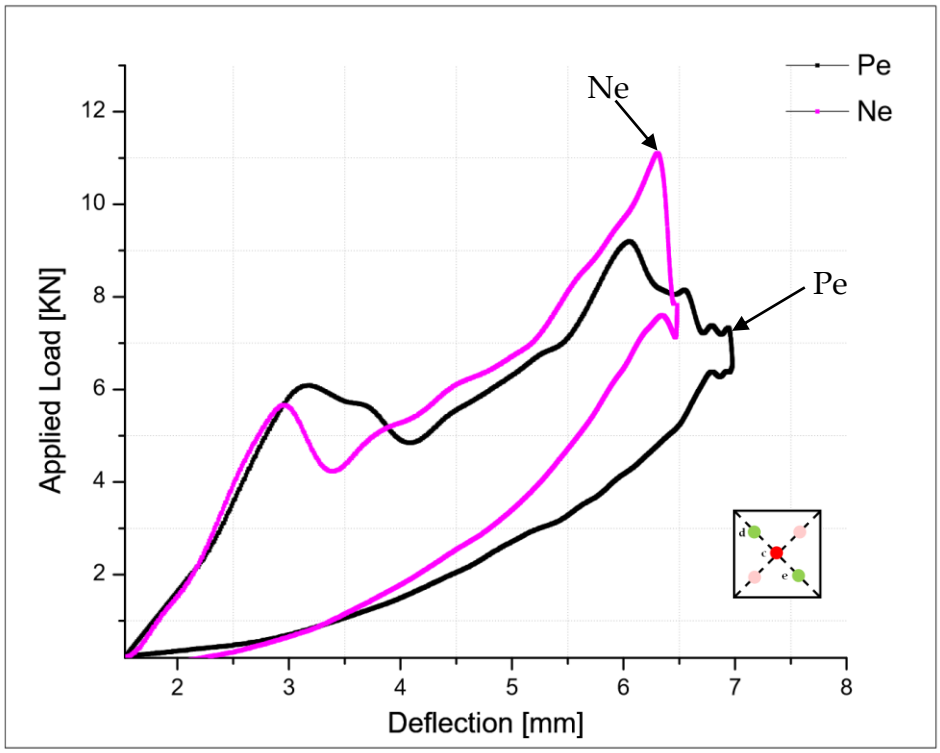

Figure 6-18 Load Deflection Plots; Impact at site 'e' Opposite to the Damage direction

It is clearly evident from the plots that the auxetic enhancement is still seen to be better even after the impact events compared to the positive Poisson's ratio specimens.

6.3.4 Dynamic Analysis of Through-Thickness Specimens

This is another interesting feature to evaluate the experimental data obtained throughout this work for the through-thickness specimens. Here, both linear and non-linear approximations were found in good agreement for the actual plots of the auxetic specimens. These plots offer a good prediction of auxetic behaviour;

both in terms of initial response, maximum load and to a lesser degree for the duration of the impact. It is obvious from the tabulated data, listed in Chapter 5 sections 5.2.2-5.2.3, that the overall approximation is always found closer for the auxetic specimens tested at either test location. This approximation of predicting behaviour is merely observed for the positive Poisson's ratio specimens and is only limited to the centre indentation of the specimens.

6.4 Quasi-static Indentation Resistance of In-plane specimens

In this investigation, quasi-static indentation tests were carried out on 100mm^2, simply supported specimens at a load rate of 2mm/min using 12.7mm sized steel hemisphere indentor to an indentation depth of 5mm, with a back support of 50mm hollow test fixture, to achieve the full spectrum of load displacement behaviour until failure. This has been confirmed by examining a large number of specimens and a good agreement of repeatability of these results was found in all the specimens. The curves of the in-plane specimens do not show distinct difference for the first failure point but a clear auxetic enhancement is observed in terms of the second failure, which occurred at a higher load (15%). The energy absorbed to this point of failure was also greatly enhanced (27%) over that recorded for the positive Poisson's ratio specimens.

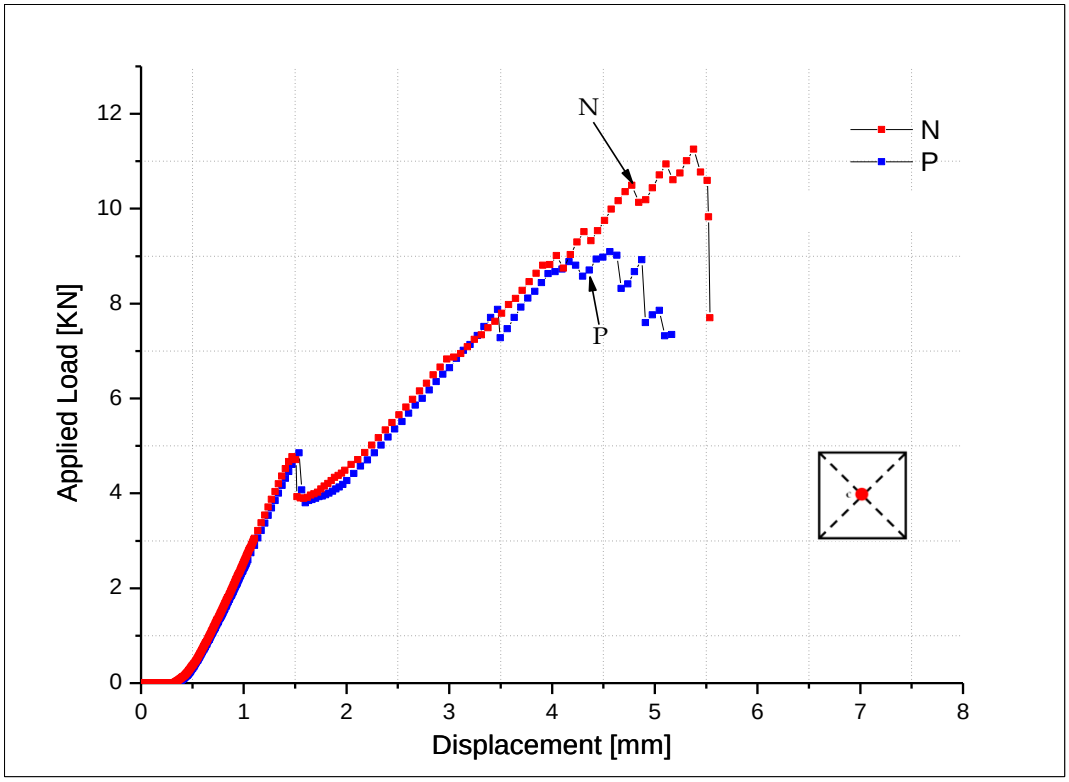

Figure 6-19 Load Displacement Indentation Curves at full damage load

It was concluded that, when all these factors are taken into account, the results obtained were good evidence of enhancement of auxetic resistance to indentation at the second failure point.

6.5 Low Velocity Impact Resistance of In-plane Specimens

In this section each type of specimens has also been tested and compared in terms of impact resistance by low velocity impacts, using a range of impact velocities and energies. All this impact work focuses on the 12.7mm sized indentor, as it has

already provided the most interesting results under the quasi-static loading condition.

This impact testing program was carefully designed to best examine the results achieved from the quasi-static tests. It was decided to impact all the specimens corresponding to the various stages of the failure process as observed during quasi-static loading. In this way, three impact energy levels were chosen corresponding to before the first failure, the region directly after the first failure and peak load of the quasi-static test at 5mm indentation depth.

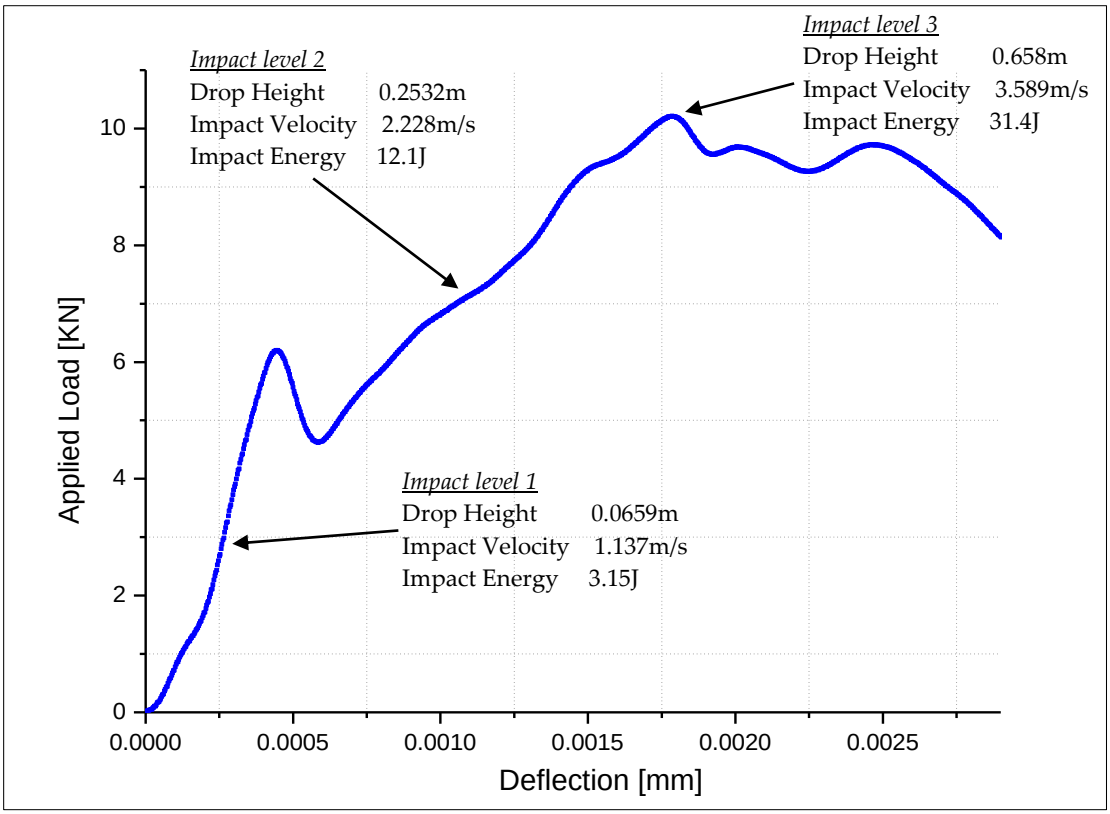

Figure 6-20 Load time stages replicate for the impact investigation

These points are marked clearly on the quasi-static load displacement plot in Figure 6-20, the corresponding impact velocities, energies and drop heights are also provided for the reference purpose.

The impact test results are in the form of force histories i.e. force versus time for the duration of the impact event. These plots provide points for direct comparison across the specimens, for example the maximum load and the duration of the event and these points have been directly compared across the specimen types.

Each test condition is compared in turn across the specimen types and then the way in which each specimen responds to increasing impact velocity is discussed in detail to assess what effect this has on the specimen behaviour.

6.5.1 Low Velocity Impact Level 1

This impact level was selected to reproduce the stage of the quasi-static load displacement curve up to the first failure point to observe the 'elastic' behaviour of the specimens. It was evident from the force deflection, for both types of the specimens tested, that no damage had occurred. This has been confirmed by fractography (section 4.5.1 of Chapter 4) and residual testing. However, it was interesting to assess the impact behaviour of each specimen type to find whether

there are any minor differences in the specimen response indicated by the impact durations or maximum load values.

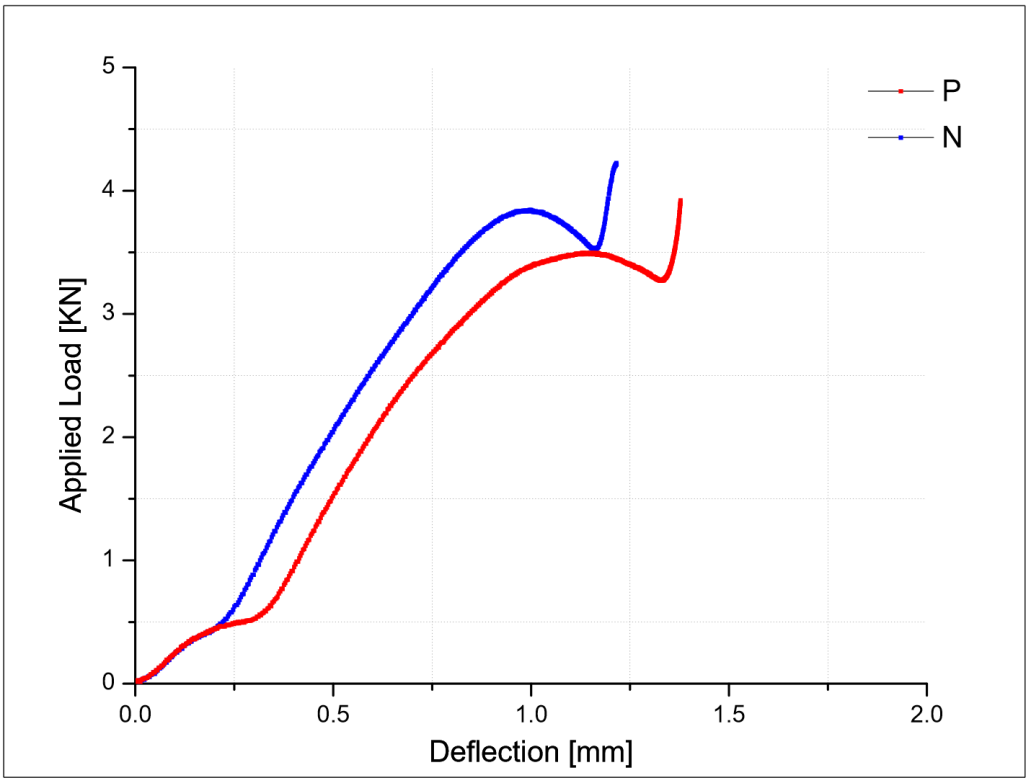

Figure 6-21 Force Deflection Plots, Impact Level 1

The maximum load achieved is slightly higher for the auxetic specimens as shown in Figure 6-21 and that is the only distinguishable difference between the curves. The values of the absorbed energy are closer to the positive Poisson's ratio specimens.

6.5.2 Low Velocity Impact Level 2

This impact level is an important step to successfully isolate the first failure point. The impact event is directly compared across the specimen types in the similar way as for the indentation test. The behaviour of the specimens after this impact event is also compared in order to assess the extent and size of the failure. In this case, a slight auxetic behaviour was observed even at the higher strain rate.

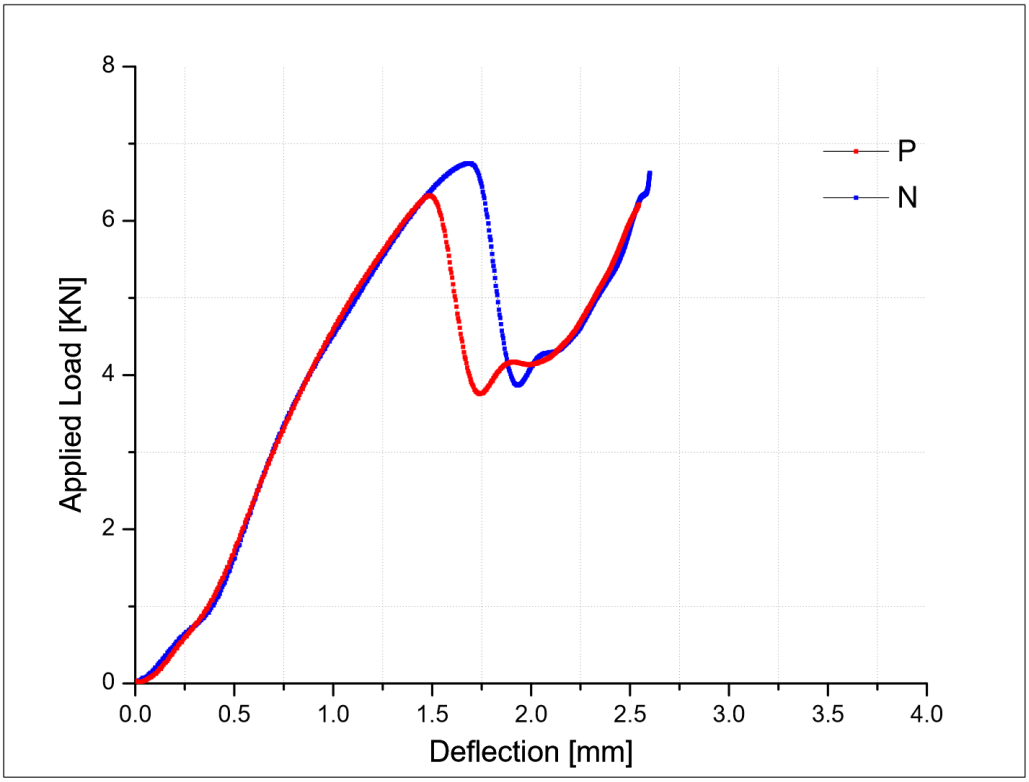

Figure 6-22 Force Deflection Plots, Impact Level 2

This event is obviously isolated and clear on the force deflection plots and appears at slightly higher loads for the auxetic specimens with small amount of energy absorbed to this point as shown in Figure 6-22.

However, the first failure load level is the only maximum load achieved during the impact event for the auxetic specimens compared to the positive Poisson's ratio specimens. Despite there being minor real differences in the values achieved from these tests, they do not appear to be distinct differences in the specimen behaviour.

6.5.3 Low Velocity Impact Level 3

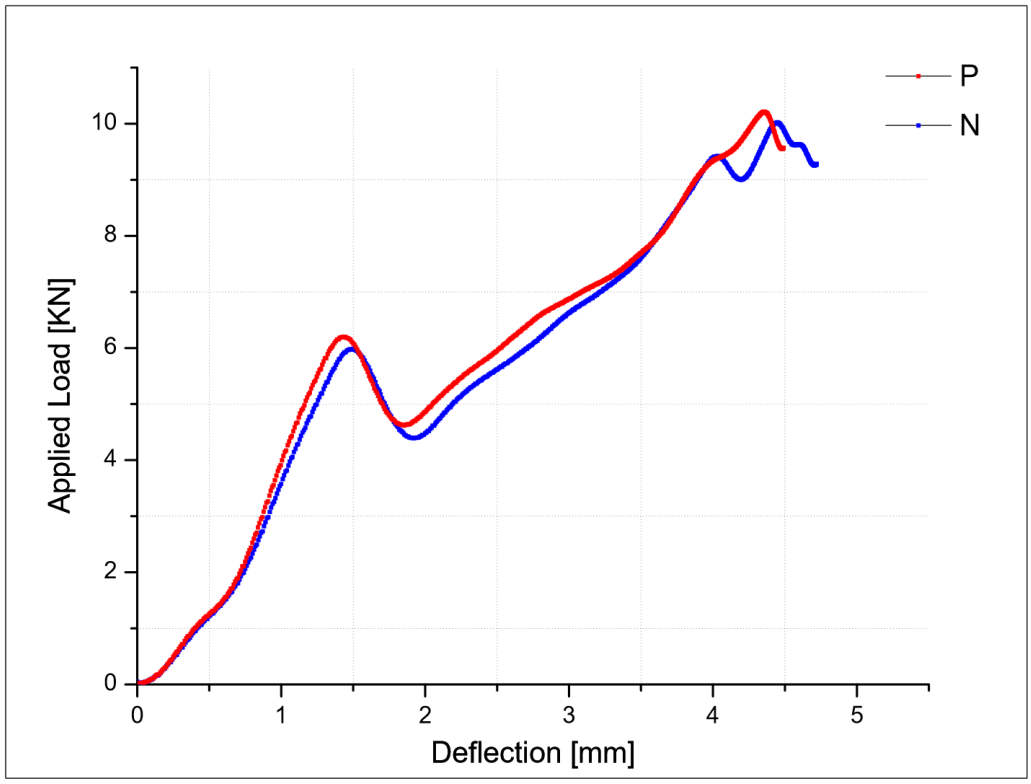

Figure 6-23 Force Deflection Plots, Impact Level 3

This was test designed to replicate the peak load that is reached in the indentation event; however, shapes of the curves are very similar here across the specimen types. Though the overall shape of the force histories offer identical response

within the specimens as shown in Figure 6-23, but the energy absorption values are slightly different.

The true reason behind this and the nature of the differences in the specimen behaviour will not be fully understood until residual strength; as discussed in section 6.6.3; of these specimens is evaluated.

6.6 Residual Testing of In-plane Specimens

This testing program has revealed very useful information and some interesting results. Here, all the low velocity impact test specimens of each level have been reloaded for quasi-static indentation tests to estimate the effect of the damage at various levels to assess the residual load carrying capability of the laminates.

6.6.1 Residual Testing of Impact Level 1

It was observed in response of the residual testing of low velocity impact level 1 that both types of specimens show an incomplete damage during the impact event because of the under loading condition, which is confirmed as shown in Chapter 4 section 4.11.1. This impact level, due to under loading condition, does not reveal any significant features to consider important.

6.6.2 Residual Testing of Impact Level 2

At this impact level under residual loading, it was surprising to find that the auxetic specimens, which had previously shown a clear enhancement under quasi-static indentation and low velocity impact testing, revealed the lowest performance here.

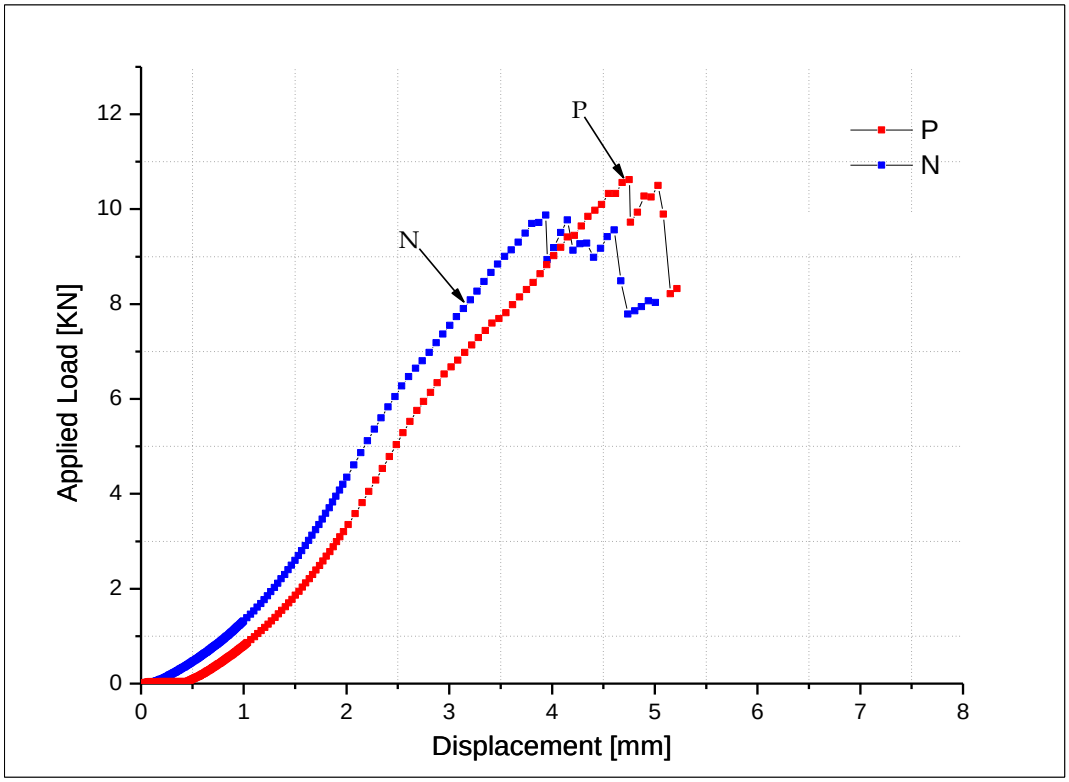

Figure 6-24 Residual Load Displacement plot, Impact level 2 specimen

The gradient for the positive Poisson's ratio specimen was observed to be higher compared to the gradient of the auxetic specimens at this impact level and the peak load was also found to be higher in the positive Poisson's ratio specimens as shown in Figure 6-24. The enhancements observed under quasi-static loading to this point were no longer evident for the auxetic specimen.

It is important to study the actual damage present in the specimens to obtain the true description for this poor performance after impact event in the auxetic specimens compared to the positive Poisson's ratio specimen. The fractographic analysis of the positive Poisson's ratio specimens revealed a greater number of delaminations with a small amount of back surface damage. The presence of such damage would definitely degrade the performance of the laminate under residual loading. The impact energy is dissipated in the creation of a number of large delaminations in the positive Poisson's ratio specimens, whereas it is clear that the auxetic specimen, with damage solely directed under the indentor nose region would show lower performance. The effect of the back face fracture combined with the highly localised damage provides an obvious explanation of this initially surprising result.

6.6.3 Residual Testing of Impact Level 3

The difference in residual strength of the specimens is still noticeable as the impact level is increased. In fact, the positive Poisson's ratio specimens show slightly higher gradient at impact level three compared to the auxetic specimens. In terms of both the gradient and the peak load, the positive Poisson's ratio specimen with higher modulus value has the higher trend towards residual

performance. Though the nature of the impact damage found in the positive Poisson's ratio specimens has thus far been characterised by several large delaminations and the impact energy has been utilised in the creation of the damage far away from the original impact site, thus providing greater residual strength when reloaded quasi-statically at this point.

Here in this case the performance of auxetic specimens is found to be lower than the positive Poisson's ratio specimens, this is because of the back face failure that has increased the severity and the damage is accomplished by fibre breakage with small but more concentrated delamination region. Hence, this back face damage has considerably reduced the load carrying capability of the auxetic laminate. The degraded performance under residual loading in the auxetic specimens is assumed to be indicative of the nature of the damage created. This damage is unique in two ways, and each of these contributes to this apparently poor residual performance.

Firstly, there are few delaminations in the impacted auxetic specimens, unlike the positive Poisson's ratio specimens in which energy is exhausted through the creation of large areas of damage far away from the impact site. Auxetic damage appears instead to be created directly under the impactor nose region; this is

typically in the form of shear cracks and fibre breakage. A similar effect was also found in through-thickness specimens in the previous section.

Secondly, the damage discussed above is particularly accompanied by the back surface damage even at relatively low impact energy levels; this has possibly the most prominent effect on the residual strength. However, in conjunction with the localised delamination, back surface damage is definitely one of the characteristics of the failure mechanisms of the auxetic composite laminates, which greatly affect the residual strength directly under the indentor nose region.

6.7 High Velocity Impact Resistance of Through-thickness Specimens

High velocity impact (HVI) investigation was performed to examine the impact response of the through-thickness laminate to assess whether the auxetic behaviour observed during low velocity impact event is still evident. For more precise analysis two energy levels were focused to study the impact response. A careful investigation at velocities 90m/sec and 110m/sec of the recorded data revealed that both the auxetic and the positive Poisson's ratio specimen exhibit almost similar trends in terms of the rebound velocity and loss of energy when allowed to undergo high velocity impact.

The fractographic analysis of both types of specimens revealed a shallow damaged area, which is also limited to a smaller extent. The extent of the damage is shorter at the bottom side of the damage profile compared to the surface of the specimens. However, the damage area in the auxetic specimens is a slightly more crushed region and it is difficult to segregate the laminating layers. This severity is less pronounced in the positive Poisson's ratio specimens. This can be concluded here that both types of the through-thickness specimens were not found very different in terms of the extent of damage and energy absorption from each other, when subjected to tests at high velocity impact.

7 CONCLUSIONS & FURTHER WORK

7.1 Conclusions

There have been many features to this research into the low velocity impact, post impact, post indentation, high velocity impact and in-plane behaviour, of auxetic composites. The overall objective was a detailed investigation of the impact, post-impact, indentation, post-indentation resistance of the auxetic laminate configuration in comparison to the behaviour of the positive Poisson's ratio laminate configurations chosen to have particularly different values of the through-thickness and in-plane Poisson's ratio specimens.

This goal was achieved by testing the composite laminates under and away from the indentor nose region because previous studies do not explain the behaviour of axuetic laminates in response to multiple impact events. The reason behind such testing condition was to assess the effect of the auxetic through-thickness Poisson's ratio on the performance of composite laminate under multiple indentation events. It was important to test under and away from the indentor nose region to assess the effect of multiple indentations on auxetic behaviour and also replicate the real in service conditions. The laminates with greater anisotropy than conventional carbon laminates is used in the present work. This is to achieve

greater difference among positive and negative Poisson's ratio values of both the through-thickness and in-plane specimens.

Throughout this work three test locations; centre of the square laminate, 20mm away from the centre in the direction of damage and also opposite to the damage direction; of each square specimens were of prime focus for indentation tests. These sites were exposed to multiple indentation events to assess the response of the laminate after the initial indentation. In negative through-thickness specimens, auxetic behaviour was not only observed at first failure point but also well into the failure process i.e. peak load during the quasi-static indentation event. This development in the auxetic character was also found at higher value of the energy even away from the initial test site. Hence, the auxetic laminates are easily repairable due to confined region of damage.

An impact testing program was launched after the quasi-static indentation investigation in an attempt to duplicate each stage of the failure process and to compare each type of specimen in terms of damage behaviour. For this, quasi-static indentation results were used to calculate the values for the energy absorption to define the required impact test and support conditions. In this way each relevant stage of the failure process was captured successfully and it was

possible to compare directly the results of each specimen corresponding to the quasi-static indentation test.

The experimental data achieved for the auxetic specimens under indentation testing program was very similar to that achieved for the impact tests. In both cases, the negative Poisson's ratio specimens presented auxetic behaviour compared to the positive Poisson's ratio specimens by showing very confined damage which is limited to the impact site. It was important to assess the damage present within the specimens after the comprehensive test program was over. This was the best way to pinpoint and assess the real differences in specimen behaviour and to find a justification for the auxetic character. However, fractographic technique made it possible not only to compare the amount of the damage created but to also to describe in detail the damage present and hence compared it across the different types of specimens and test conditions.

This investigation; into the damage for both the quasi-static indentation and the low velocity impact tests; acknowledged a definite difference in the behaviour of the auxetic and the positive Poisson's ratio specimens. Delamination in the auxetic specimens is always observed very confined to the test site and hence leaves minimum effect in the surrounding region. Despite this, the positive Poisson's ratio specimens consume all of the supplied energy in creating large

delaminations even far apart from the test location, which affects the whole test specimen in terms of strength after an indentation event. Thus auxetics laminates can be considered easier to repair in comparison with the positive Poisson's ratio specimens because a smaller area is required to be replaced.

Findings of the above discussed through-thickness specimens were also confirmed in a different predictive way by conducting dynamic analysis of the laminates. The main purpose of this kind of linear and non-linear analysis is to reassure the results upon multiple indentation and impacts, under the nose region or away from the initial test site. Auxetic effect is clearly observed due to the better performance of the specimen's plots, which resembles very close to the predicted curves. This prediction for the positive Poisson's ratio specimens is limited to centre indentation event only. This is due to the reason that in all other cases presence of large delaminations are responsible the lower performance observed for the laminates.

A preliminary investigation was also launched into the in-plane laminates to study the quasi-static indentation for detailed analysis with the same test set up. Similarly, impact tests were carried out on all the specimens to replicate the various stages of the failure process as observed in the indentation test. The experimental data obtained after the impact tests was much closer for the auxetic

and positive Poisson's ratio specimens. The auxetic specimens are found to have better resistance to penetration events and also have enhanced energy absorption characteristics, which is up to 27% compared to the positive Poisson's ratio specimens

All the through-thickness specimens were also investigated in a preliminary study on the high velocity impact response. These specimens were tested at two different energy levels. The test data and fractographic analysis revealed that the auxetic specimens do not appear to behave differently, when allowed to undergo high velocity impact event. The only slight difference between the two types of specimens was found in fractography, where the damage region in the auxetic specimens is more crushed and difficult to find laminating layers otherwise both type of specimen show almost similar extent of damage and energy absorption. It can be assumed here, this effect diminishes due to the reason of short interaction between the laminates and steel ball during an impact event.

Multiple impact events in the vicinity of the initial impact site are not well documented in quasi-isotropic laminates. The damage induced in auxetic laminates by low velocity impact is compared with the approximately matched modulus quasi-isotropic laminates of 24-plies and other comparable parameters. A detailed insight into the fractoghrapic analysis of auxetic laminate and failure

index of each ply suggest that quasi-isotropic laminates have more severe ply failure [191] after the mid ply and resulted in rapid strength decay, due to back-face damage laminate [192] whereas auxetic laminate shows minimal ply failures after the mid ply and also the damage of auxetic laminate appears more confined.

Qausi-isotropic laminates are designed to have more dispersed ply orientations and the damage spreads away along each ply under goes failure along its principle axis and higher stresses are produced in quasi-isotropic laminates[193]. It is reported in[6], [174], that the area of auxetic laminate in terms of computed damage areas as a percentage of the total plate size, the results show less internal damage within the auxetic specimens; the percentage damage area being 7%, indicating that damage is more localized directly under the loading nose in this case and exhibit a response which leads to suppression of the length of delamination growth compared to other matched modulus laminates[194]. This effect may be considered due to a combination of enhanced shear modulus leading to an improved material response and allowing a wider distribution of strain, and the mismatch between individual lamina layers for auxetic specimen leading to an orderly progression of damage and a greater communication of shear strain, giving higher resistance to delaminate lamina layers results in the occurrence of interlaminar stresses which in turn give rise to delaminations[64], [195].

The reason for these differences is thought to be due to the interaction of the plies within the auxetic lay-up. This leads to the conclusion that the auxeticity of the laminate creates a densification mechanism suppressing delamination growth creating highly localised damage. This is a feature of the laminate stacking sequence consisting of only layers within a narrow orientation range and symmetrically balanced. In this way under compression loading in which conventional quasi-isotropic lay-ups are severely prone to delaminations, the auxetic laminates, or the preferable mismatch of such a laminate leads to an auxetic effect which in turn leads to much less damage. As more delaminations are evident in qausi-isotropic laminates compared to the auxetic laminate at the same impact load. It has been reported increasing damage zone resulted inverse relationship to the residual strength and damage zone[194].

The comparative testing in this Thesis has been carried out on matched modulus composites following the work of Evans et al, Alderson et al and Ward et al [6], [47], [50], [171], [174], [195]–[199]. It would be interesting to conduct tests to compare directly the properties of the industry standard quasi-isotropic laminates and auxetic laminates but at this stage, it was important to isolate the auxetic effect by matching the through thickness modulus. In this way, enhancements observed could be directly attributed to the sign of the Poisson's

ratio. Future work should devise auxetic laminates using the existing computer programmes to match in properties as far as possible[35], [63], [200]–[202] with quasi-isotropic laminates; this would not optimise the Poisson's ratio as has been done here but would provide a closer comparison with composites in general use today. Theoretical studies are already on going for carbon, Kevlar and glass reinforced composites and experimental work following on from and building on this study would be a useful next stage.

Here a comprehensive insight into this study can be given at the end to understand the outcome of the work. This has been confirmed repeatedly by testing data that the through-thickness auxetic laminates exhibit very small damage area in response of multiple impact events and thus are easy to repair compared to the positive Poisson's ratio laminates. Quasi-static indentation resistance of in-plane auxetic laminates are also found better compared to the positive Poisson's ratio laminates in this study, at high velocity impact condition, auxetic effect is not observed to be well pronounced for through the thickness laminates

7.2 Further Work

The recommendations made here are to further develop the research into through-thickness and in-plane auxetic laminate and to truly exploit their potential. Recommendations for the future work are given below;

It is recommended to apply non-contact strain measurement by video extensometer to precisely measure the non-contact strains in the composite laminates in particular for the measurement of the in-plane strain and to identify failures under tensile loading. It would also be useful to measure the through-thickness and in-plane Poisson's ratios of each specimen with the help of non-contact strain measurements, which will give a good comparison with the contact strain measurement by the strain gauge method.

It is further recommended to study the smart hybrid laminate with auxetic properties, such as glass or Kevlar fibres, to assess if similar damage mechanisms are possible as observed in the carbon epoxy system. Glass-epoxy pre-pregs have been previously modelled as auxetic materials; as described in the literature review. They can be tested to compare in terms of their mechanical performance to endorse the findings of this investigation and can be alternative good candidate materials for applications that demand better impact resistance.

It is also recommended that finite element techniques are applied to study and utilize the finding of this work, for instance within a structure such as stiffened panels. This may help to evaluate the benefits not only of the enhanced damage resistance, which is confirmed experimentally, but also the relative advantage or disadvantage of both type of Poisson's ratio. This can be helpful in designing applications with the auxetic composites.

High velocity impact testing program can be redesigned effectively by replacing a flat support on the back of the specimen with a hollow back support at the centre of the specimen. This will give more room in bending the specimen for realistic results and to compare the difference with solid back support plate.

The through-thickness specimens were allowed to undergo high velocity impacts in order to observe the auxetic enhancements after an impact event. Similarly, in-plane Poisson's ratio specimens can also be studied to find if any auxetic enhancement sustains in response of high velocity impact testing and their damage mechanism can be compared to find the more realistic inside picture of the specimens.

The in-plane Poisson's ratio laminates are preliminarily investigated in this research for their auxetic character and are assumed to be better performers even

away from the centre of indentation. This predicted investigation can be further extended to assess their behaviour in response of the multiple impact events not only under the indentor nose region but also away from the initial damage site, in the direction of damage and opposite to the damage direction.

In high velocity impact tests, the use of fairly large specimen of at least $80mm^2$ is recommended to provide more options in the testing program; for instance multiple impacts can be formed at various sites and also residual testing can be incorporated to assess the strength after an impact event.

A test program with the use of strain gauges is recommended for both the low velocity impact and the indentation tests on specimens with an array of logically positioned gauges, which would undoubtedly offer the best results. Similarly, if strain gauges are used during the residual testing program, they can provide more realistic results to assess the performance of auxetic specimen after a failure event and to compare with other laminate sequences with a more conventional damage profile.

8 REFERENCES

[1] G. DeFrancisci, Z. Chen, and J. Rhymer, "Impact Damage Formation on Composite Aircraft Structures," *depts.washington.edu*.

[2] K. Evans, M. Nkansah, I. Hutchinson, and S. Rogers, "Molecular network design," *Nature*, no. 124, p. 353, 1991.

[3] Q. Liu, "Materials with Negative Poisson's Ratios and Potential Applications to Aerospace and Defence," DTIC Document, 2006.

[4] L. Munteanu, V. Chiroiu, D. Dumitriu, and M. Beldiman, "On the characterization of auxetic composites," *Proc.of Rom. Acad. Ser. A Math. Physics, Tech. Sci. Inf. Sci.*, vol. 9, no. 1, pp. 33–40, 2008.

[5] A. Christoforou, "Impact dynamics and damage in composite structures," *Compos. Struct.*, vol. 52, no. 2, pp. 181–188, 2001.

[6] K. L. Alderson and V. L. Coenen, "The low velocity impact response of auxetic carbon fibre laminates," *Phys. Status Solidi Basic Res.*, vol. 245, no. 3, pp. 489–496, 2008.

[7] J. Lee and D. Dhital, "Review of flaws and damages in space launch vehicle: Structures," *… Intell. Mater. Syst. Struct.*, 2013.

[8] C. Herakovich, "Mechanics of composites: A historical review," *Mech. Res. Commun.*, 2012.

[9] N. Jackson, E. Born, A. Dooley, A. Isildar, and G. Jackson, "Alternative Materials for FDOT Sign Structures: Phase I Literature Review," 2012.

[10] S. C. Materials and F. C. Campbell, "Introduction to Composite Materials," pp. 1–30, 2010.

[11] George and Marsh, "Composites lift off in primary aerostructures," *Reinf. Plast.*, vol. 48, no. April, pp. 22–27, 2004.

[12] M. Hinton, A. Kaddour, and P. Soden, *Failure criteria in fibre reinforced polymer composites: The World-Wide Failure Exercise*. 2004.

[13] P. Toensmeier, "Advanced composites soar to new heights in Boeing 787," *Plast. Eng.*, 2005.

[14] B. Griffiths, "Boeing sets pace for composite usage in large civil aircraft," *High Perform. Compos.*, 2005.

[15] J. Teresko, "The Boeing 787: A Matter of Materials," *Ind. Week-clevel. OHIO-*, 2007.

[16] S. Kotha and R. Nolan, "Boeing 787: the dreamliner," *Harvard Bus. Sch.*

Case …, 2005.

[17] F. Arago, *Œuvres complètes*. Paris ; Gide et J. Baudry ;, 1854.

[18] P. Karasudhi, "Foundations of solid mechanics," p. 353, 1991.

[19] F. P. Beer, E. R. Johnston, and J. T. DeWolf, *Mechanics of materials*, no. 1. McGraw-Hill, 1992.

[20] R. S. Lakes, "Foam structures with a negative Poisson's ratio," *Science (80-.).*, no. 235, pp. 1038–1040, 1987.

[21] K. E. Evans, "Auxetic polymers: a new range of materials," *Endeavour*, vol. 15, no. 4, pp. 170–174, 1991.

[22] C. T. Herakovich, "Composite Laminates with Negative Through-the-Thickness Poisson's Ratios," *J. Compos. Mater.*, vol. 18, no. 5, pp. 447–455, 1984.

[23] Almgren R. F, "An isotropic three-dimensional structure with Poisson's ratio=-1," *J. Elast.*, vol. 15, pp. 427–430, 1985.

[24] Y. Liu and H. Hu, "A review on auxetic structures and polymeric materials," *Sci. Res. Essays*, 2010.

[25] Bathurst R. J. and Rothenburg L, "Note on a random isotropic granular material with negative Poisson's ratio," *Int. J. Eng. Sci.*, vol. 26, no. 4, pp. 373–383, 1988.

[26] W. Yang, Z.-M. Li, W. Shi, B.-H. Xie, and M.-B. Yang, "Review on auxetic materials," *J. Mater. Sci.*, vol. 39, no. 10, pp. 3269–3279, 2004.

[27] K. E. Gaspar, N., Ren, X. J., Smith, C. W., Grima, J. N., & Evans, "Novel honeycombs with auxetic behaviour," *Acta Mater.*, vol. 53, pp. 2439–2445, 2005.

[28] T. Hughes, A. Marmier, and K. Evans, "Auxetic frameworks inspired by cubic crystals," *Int. J. Solids …*, vol. 47, no. 11–12, pp. 1469–1476, Jan. 2010.

[29] A. Alderson, K. L. Alderson, D. Attard, K. E. Evans, R. Gatt, J. N. Grima, W. Miller, N. Ravirala, C. W. Smith, and K. Zied, "Elastic constants of 3-, 4- and 6-connected chiral and anti-chiral honeycombs subject to uniaxial in-plane loading," *Compos. Sci. Technol.*, vol. 70, no. 7, pp. 1042–1048, 2010.

[30] K. E. E. B D Caddock and, "Microporous materials with negative Poisson's ratios. I. Microstructure and mechanical properties," *Journal of Physics D: Applied Physics*, vol. 22, no. 12. p. 1877, 1989.

[31] R. S. Lakes, "Deformation mechanisms in negative Poisson's ratio materials: structural aspects," *J. Mater. Sci.*, vol. 26, pp. 2287–2292, 1991.

[32] Rothenburg L., B. A. A., and and B. R. J., "Microstructure of isotropic materials with negative Poisson's ratio," *Nature*, vol. 354, pp. 470 – 472, 1991.

[33] G. W. Milton, "Composite materials with poisson's ratios close to — 1," *J. Mech. Phys. Solids*, vol. 40, no. 5, pp. 1105–1137, 1992.

[34] Prall D. and Lakes R. S., "Properties of a Chiral Honeycomb with a Poisson's Ratio of -1," *Int. J. Mech. Sci.*, vol. 39, no. 3, pp. 305 – 314, 1997.

[35] K. E. Evans and A. Alderson, "Auxetic materials: Functional materials and structures from lateral thinking!," *Adv. Mater.*, vol. 12, no. 9, pp. 617–628, 2000.

[36] K. E. Evans, "The design of doubly curved sandwich panels with honeycomb cores," *Compos. Struct.*, vol. 17, no. 2, pp. 95–111, 1991.

[37] Choi J. B. and Lakes R. S., "Design of a Fastener Based on Negative Poisson's Ratio Foam. Cellular Polymers," *Cell. Polym.*, vol. 10, no. 3, pp. 205–212, 1991.

[38] A. Spadoni, "Application of Chiral Cellular Materials for the Design of Innovative Components," 2008.

[39] I. Sokolnikoff, *Higher mathematics for engineers and physicists*,. New York;London: McGraw-Hill book company inc., 1934.

[40] J. Poirier, *Introduction to the Physics of the Earth's Interior*. 2000.

[41] Y. . Fung, *Foundations of Solid Mechanics*. Prentice-Hall, 1968.

[42] J. T. Beer, F.P., Johnston, E.R., Jr. and DeWolf, F. P. Beer, E. R. Johnston, and J. T. DeWolf, *Mechanics of Materials*, no. v. 1. McGraw Hill, 2001.

[43] S. Timoshenko and J. N. Goodier, *Theory of Elasticity*, vol. 49, no. 2. Butterworth-Heinemann, 1986.

[44] Hertz H., "Uber die Berührung fester elastischer Körper," *J. für die reine und Angew. Math.*, vol. 92, pp. 156–171, 1881.

[45] K. E. Chan, N. and Evans, "Indentation resilience of conventional and auxetic foams," *J. Cell. Plast.*, vol. 34, pp. 231–162, 1998.

[46] K. J. Lakes, R.S. and Elms, "Indentability of conventional and negative Poisson's ratio foams," *J. Comp. Mat.*, vol. 27, pp. 1193–1202, 1993.

[47] V. Coenen, K. Alderson, P. Myler, and K. Holmes, "The indentation response of auxetic composite laminates," in *6th Int. Conf. Deformation and Fracture of Composites*, 2001, vol. Manchester.

[48] K. L. Alderson, A. P. Pickles, P. J. Neale, K. E. Evans, and N. P. and E. K. Alderson KL, Pickles AP, "Auxetic polyethylene: the effect of a negative Poisson's ratio on hardness," *Acta Met*, vol. 42, no. 7, pp. 2261–2266, 1994.

[49] R. Lakes, "Advances in negative Poisson's ratio materials," *Adv. Mater.*, vol. 5, no. 4, pp. 293–296, 1993.

[50] K. E. K. Evans, J. P. Donoghue, and K. L. Alderson, "The Design, Matching and Manufacture of Auxetic Carbon Fibre Laminates," *J. Compos. Mater.*, vol. 38, no. 2, pp. 95–106, Jan. 2004.

[51] G. Greaves, A. Greer, R. Lakes, and T. Rouxel, "Poisson's ratio and modern materials," *Nat. Mater.*, 2011.

[52] Irwin G. R., "Analysis of Stresses and Strains Near the End of a Crack Traversing a Plate," *J. Appl. Mech.*, vol. 24, no. 361–364, 1957.

[53] Choi J. B. and Lakes R. S., "Fracture toughness of re-entrant foam materials with a negative Poisson's ratio: experiment and analysis," *Int. J. Fract.*, vol. 80, pp. 73–83, 1996.

[54] H. M. Deuschle, *3D Failure Analysis of UD Fibre Reinforced Composites: Puck's Theory within FEA*. 2010.

[55] S. Tsai and H. Hahn, "Introduction to Composite Materials," 1980.

[56] J. P. Donoghue, "Negative Poisson's ratio effects on the Mechanical performance of composite laminates," University of Liverpool, 1992.

[57] K. A. KE Evans, JP Donoghue, "The design, matching and manufacture of auxetic carbon fibre laminates," *J. Compos. …*, 2004.

[58] M. Miki and Y. Morotsu, "The peculiar behavior of the Poisson's ratio of laminated fibrous composites," *JSME Int. J.*, vol. 32, pp. 67–72, 1989.

[59] R. Zhang, H.-L. Yeh, and H.-Y. Yeh, "A preliminary study of negative Poisson's ratio of laminated fiber reinforced composites," *J. Reinf. Plast. Compos.*, vol. 17, no. 18, pp. 1651–1664, 1998.

[60] H. Yeh, H. Yeh, and R. Zhang, "A study of negative Poisson's ratio in randomly oriented quasi-isotropic composite laminates," *J. Compos. Mater.*, vol. 33, no. 19, pp. 1843–1857, 1999.

[61] S. Abrate, *Impact on Composite Structures*. 2005.

[62] W. W. J. Bjeletich. J. G., Crossman. P. W., "Failure In Composites," *Metall. Soc*, no. IV, pp. 118–137, 1977.

[63] E. Hadi Harkati, A. Bezazi, F. Scarpa, K. Alderson, and A. Alderson, "Modelling the influence of the orientation and fibre reinforcement on the Negative Poisson's ratio in composite laminates," *Phys. status solidi*, vol. 244, no. 3, pp. 883–892, 2007.

[64] V. L. Coenen and K. L. Alderson, "Mechanisms of failure in the static indentation resistance of auxetic carbon fibre laminates," *Phys. status solidi*, vol. 248, no. 1, pp. 66–72, 2011.

[65] J. F. Clarke, R. A. Duckett, P. J. Hine, I. J. Hutchinson, and I. M. Ward, "Negative Poisson's ratios in angle-ply laminates: theory and experiment,"

Composites, vol. 25, no. 9, pp. 863–868, 1994.

[66] K. L. Alderson, V. R. Simkins, V. L. Coenen, P. J. Davies, A. Alderson, and K. E. Evans, "How to make auxetic fibre reinforced composites," *Phys. Status Solidi Basic Res.*, vol. 242, no. 3, pp. 509–518, 2005.

[67] J. Chaudhuri and Q. Jang, "Effect of Special Orientation on the Fracture Behavior of Graphite/Epoxy Laminates," in *Proceedings of the American Society for Composites 3rd tech. conf.*, 1988, p. 701.

[68] A. Bezazi and F. Scarpa, "Mechanical behaviour of new non conventional materials having a negative Poisson ' s ratio (Auxetic)," 1945.

[69] C. T. Sun and S. Li, "Three-dimensional effective elastic constants for thick laminates," *J. Compos. Mater.*, vol. 22, pp. 629–639, 1988.

[70] Lempriere B. M, "Poisson's ratio in orthotropic materials.," *AIAA J.*, vol. 6, no. 11, pp. 2226–2227, 1968.

[71] Al-Khalil. M. F. S, "Strength of Filament wound structures under complex stresses," University of Manchester, 1990.

[72] "Messphysik: Messphysik Videoextensometer Package, Aborgerrite Ges. M. B. H., Furstenfeill. Austria." .

[73] A. Love, *A treatise on the mathematical theory of elasticity*. 2013.

[74] A. Love, *A Treatise on the Mathematical Theory of Elasticity*, vol. 4. Cambridge: Cambridge University Press, 1927.

[75] G. Greaves, "Poisson's ratio over two centuries: challenging hypotheses," *Notes Rec. R. …*, 2013.

[76] H. Kimizuka, H. Kaburaki, and Y. Kogure, "Mechanism for Negative Poisson Ratios over the α-β Transition of Cristobalite, SiO_ {2}: A Molecular-Dynamics Study," *Phys. Rev. Lett.*, 2000.

[77] H. Kimizuka, H. Kaburaki, and Y. Kogure, "Molecular-dynamics study of the high-temperature elasticity of quartz above the α-β phase transition," *Phys. Rev. B*, 2003.

[78] A. M. Garber, "Pyrolytic Materials for Thermal Protection. Systems," *Aerosp. Eng.*, vol. 22, pp. 126–137, 1963.

[79] H. Kimizuka, S. Ogata, and Y. Shibutani, "Atomistic characterization of structural and elastic properties of auxetic crystalline SiO2," *Phys. status solidi*, 2007.

[80] L. Gibson and M. Ashby, *Cellular solids: structure and properties*. 1999.

[81] G. S. S. and C. I. R. L. J. Gibson, M. F. Ashby, "The mechanics of two-dimensional cellular materials," *… Soc. London …*, vol. 382, pp. 25–42, 1982.

[82] J. B. Friis, E. A., Lakes, R. S., and Park, "Negative Poisson's ratio polymeric and metallic materials," *J. Mater. Sci.*, vol. 23, pp. 4406–4414, 1988.

[83] K. Alderson and V. Simkins, "Auxetic materials," *US Pat. 6,878,320*, 2005.

[84] Y. Prawoto, "Seeing auxetic materials from the mechanics point of view: A structural review on the negative Poisson's ratio," *Comput. Mater. Sci.*, vol. 58, no. 0, pp. 140–153, 2012.

[85] A. Spadoni, M. Ruzzene, S. Gonella, and F. Scarpa, "Phononic properties of hexagonal chiral lattices," *Wave Motion*, 2009.

[86] A. Spadoni and M. Ruzzene, "Elasto-static micropolar behavior of a chiral auxetic lattice," *J. Mech. Phys. Solids*, 2012.

[87] and P. S. Scarpa F., Yates J. R., Ciffo L. G., "Dynamic crushing of auxetic open-cell polyurethane foam," *Proc. Inst. Mech. Eng. Part C-Journal Mech. Eng. Sci.*, vol. 216, no. 12, pp. 1153–1156, 2002.

[88] R. S. Choi, J.B and Lakes, "Nonlinear properties of metallic cellular materials with a negative Poisson's ratio," *J. Mater. Sci.*, vol. 27, no. 19, pp. 5373–5381, 1992.

[89] R. S. Choi, J.B and Lakes, "Nonlinear properties of polymer cellular materials with a negative Poisson's ratio," *J. Mater. Sci.*, vol. 27, no. 19, pp. 5373–5381, 1992.

[90] J. DIRRENBERGER, "Doctorat ParisTech THÈSE," *hal-ensmp.archives-ouvertes.fr*.

[91] Lipsett A.W. and Beltzer A. I., "Reexamination of Dynamic Problems of Elasticity for Negative Poisson's Ratio," *J. Acoust. Soc. Am.*, vol. 84, no. 6, pp. 2179–2186, 1988.

[92] R. S. Chen, C.P. and Lakes and Chen C. P. and Lakes R. S., "Micromechanical analysis of dynamic behavior of conventional and negative Poisson's ratio foams," *J. Eng. Mater. Technol., ASME*, vol. 118, no. 3, 1996.

[93] and S. F. Chekkal I., Bianchi M., Remillat C., Becot F.-X., Jaouen L., "Vibro-Acoustic Properties of Auxetic Open Cell Foam: Model and Experimental Results," *Acta Acust. united with Acust.*, vol. 96, pp. 266–274, 2010.

[94] A. Alderson and K. L. Alderson, "Auxetic materials," *Proc. Inst. Mech. Eng. Part G J. Aerosp. Eng.*, vol. 221, no. 4, pp. 565–575, 2007.

[95] R. Baughman and J. Shacklette, "Negative Poisson's ratios as a common feature of cubic metals," *Nature*, 1998.

[96] A. Alderson, K. L. Alderson, P. J. Davies, and G. M. Smart, "The effects of processing on the topology and mechanical properties of negative Poisson's

ratio foams," in *2005 ASME International Mechanical Engineering Congress and Exposition, IMECE 2005*, 2005, vol. 70 AD, pp. 503–510.

[97] M. Avellaneda, "Calculating the performance of 1–3 piezoelectric composites for hydrophone applications: An effective medium approach," *J. Acoust. Soc. Am.*, vol. 103, no. 3, p. 1449, Mar. 1998.

[98] M. Nakamura, "Fundamental properties of intermetallic compounds," *Mater.Res. Soc.*, vol. 20, no. XX, pp. 33–39, 1995.

[99] P. J. Avellanads, M and Swart, "Calculating the performance of 1-3 piezo composites for hydrophone applications: An effective medium approach," 1998.

[100] R. Caspe, V. Coenen, A. Nesbitt, and A. Wilkinson, "Through-thickness melding of advanced cfrp for aerospace applications," *iccm-central.org*.

[101] R. Caspe, "Through-thickness melding of advanced carbon fibre reinforced polymers," 2011.

[102] R. Hill, *The mathematical theory of plasticity*. 1998.

[103] K. A. Aveston J, Cooper G, "Single and Multiple Fracture. In The Properties of Fibre Composites," *Natl. Phys. Lab. IPC Sci. Technol. Press Ltd., Surrey,* pp. 15–26, 1971.

[104] M. E. Tuttle, *Structural Analysis of Polymeric Composite Materials, Second Edition*. CRC Press, 2012, 2012.

[105] Tsai S., "Strength Theories of Filamentary Structures," *Wiley Intersci.*, pp. 3–11, 1968.

[106] S. Tsai and E. Wu, "A general theory of strength for anisotropic materials," *J. Compos. Mater.*, 1971.

[107] A. Puck., "Should Fibre-Plastics Composites be designed with Strain or Stress Criteria," *Kunststoffe - Ger. Plast.*, vol. 82, no. 5, pp. 431–434, 1992.

[108] B. Schleh¨ofer and A. Mattern, "Research of the suitability of GRP pipes for long distance hot water transportation," *Fernw¨arme Int.*, vol. 10, no. 4, pp. 194–198, 1981.

[109] J.W. Kopp., "Contribution to the Stress and Strength Analysis of Unidirectionally Fibre Reinforced Plastics. PhD thesis," RWTH Aachen, Institut f¨ur Kunststoffverarbeitung (IKV), 2000.

[110] and D. E. W. Michaeli, M. Knops, O. Fischer, "Investigations on the fiber fracture behaviour of carbon fiber reinforced plastics," *Proc. Intern. SAMPE Symp. Exhib. Long Beach, CA,* 2002.

[111] O. Fischer., "Fibre Fracture Behaviour in Fibre Reinforced Plastics. PhD thesis," RWTH Aachen, Institut f¨ur Kunststoffverarbeitung (IKV), 2003.

[112] M. Mannigel., "Influence of Shear Stresses on the Fibre Failure Behaviour in Carbon Fibre Reinforced Plastics (CFRP). PhD thesis," RWTH Aachen, Institut f¨ur Kunststoffverarbeitung (IKV), 2007.

[113] Wang A, "An Overview of the Delamination Problem in Structural Composites," *Key Eng. Mater.*, vol. 37, pp. 1–20, 1989.

[114] Armanios E, "Interlaminar Fracture in Graphite/Epoxy Composites," *Key Eng. Mater.*, vol. 37, pp. 85–102, 1989.

[115] R. T. HAFTKA and R. LE RICHE, "Optimization of laminate stacking sequence for buckling load maximization by genetic algorithm," *AIAA J.*, vol. 31, no. 5, 2012.

[116] P. Francescato, A. Gillet, D. Leh, and P. Saffré, "Comparison of optimal design methods for type 3 high-pressure storage tanks," *Compos. Struct.*, 2012.

[117] N. Mathivanan and J. Jerald, "Experimental investigation of woven E-glass epoxy composite laminates subjected to low-velocity impact at different energy levels," *… Miner. Mater. Charact. …*, 2010.

[118] T. Lowe and D. Sandstrom, "Control of deformation-induced imperfections to enhance strength of metals and alloys," *US Pat. 20,130,078,139*, 2013.

[119] D. Zheng and W. K. Binienda, "Effect of permanent indentation on the delamination threshold for small mass impact on plates," *Int. J. Solids Struct.*, vol. 44, no. 25–26, pp. 8143–8158, 2007.

[120] W. J. Cantwell and J. Morton, "Comparison of the low and high velocity impact response of cfrp," *Composites*, vol. 20, no. 6, pp. 545–551, 1989.

[121] P. O. Sjoblom, J. T. Hartness, and T. M. Cordell, "On low-velocity impact testing of composite materials," *J. Compos. Mater.*, vol. 22, no. 1, pp. 30–52, 1988.

[122] A. P. Christoforou and A. S. Yigit, "Characterization of impact in composite plates," *Compos. Struct.*, vol. 43, no. 1, pp. 15–24, 1998.

[123] Swanson SR., "Limits of quasi-static solutions in impact of composite structures," *Comp Eng.*, vol. 2, pp. 261–267, 1992.

[124] J. Whitney and R. Nuismer, "Stress fracture criteria for laminated composites containing stress concentrations," *J. Compos. Mater.*, 1974.

[125] M. De Freitas and L. Reis, "Failure mechanisms on composite specimens subjected to compression after impact," *Compos. Struct.*, 1998.

[126] G. A. O. Davies and X. Zhang, "Impact damage prediction in carbon composite structures," *Int. J. Impact Eng.*, vol. 16, no. 1, pp. 149–170, 1995.

[127] S. Reid and G. Zhou, "Impact Behaviour of Fibre-Reinforced Composite

Materials," 2000.

[128] A. Christoforou and S. Swanson, "Analysis of impact response in composite plates," *Int. J. Solids …*, 1991.

[129] Y. Zhang, P. Zhu, and X. Lai, "Finite element analysis of low-velocity impact damage in composite laminated plates," *Mater. Des.*, 2006.

[130] M. Richardson and M. Wisheart, "Review of low-velocity impact properties of composite materials," *Compos. Part A Appl. Sci. …*, 1996.

[131] L. C. Winggenraad, J. F. M. and Ubels, "Impact damage and failure mechanisms in structure relevant composite specimens," 1997.

[132] K. Malekzadeh, M. Khalili, R. Olsson, and A. Jafari, "Higher-order dynamic response of composite sandwich panels with flexible core under simultaneous low-velocity impacts of multiple small masses," *Int. J. …*, 2006.

[133] J. Paul, S. Galea, and R. Jones, "Residual strength of composites with multiple impact damage," 1994.

[134] Galea S.C., Sanderson S., and Shah L.P., "The effect of multiple damage in composite structures: A theoretical investigation," *null*, vol. null, no. null, p. null.

[135] W. De Morais, S. Monteiro, and J. D'Almeida, "Evaluation of repeated low energy impact damage in carbon–epoxy composite materials," *Compos. Struct.*, 2005.

[136] W. De Morais, S. Monteiro, and J. D'Almeida, "Effect of the laminate thickness on the composite strength to repeated low energy impacts," *Compos. Struct.*, 2005.

[137] H. Razi and A. Kobayashi, "Delamination in cross-ply laminated composite subjected to low-velocity impact," *AIAA J.*, 1993.

[138] G. Appleby-Thomas, P. Hazell, and G. Dahini, "On the response of two commercially-important CFRP structures to multiple ice impacts," *Compos. Struct.*, 2011.

[139] B. C. Foos, "Damage progression in composite plates due to low velocity impact," The Ohio State University, 1990.

[140] S. Tsai, *Theory of composites design*. 1992.

[141] E. Barbero, *Finite element analysis of composite materials*. 2008.

[142] L. Malvern and R. Sierakowski, "Impact failure mechanisms in fiber-reinforced composite plates," *… Veloc. Deform. …*, 1978.

[143] N. Cristescu, "Failure Mechanisms in Composite Rates Impacted by Blunt-Ended Penetrators," *Foreign Object Impact …*, 1975.

[144] J. Nairn, "Matrix microcracking in composites," *Polym. matrix Compos.*, 2000.

[145] J. Nairn, "Fracture mechanics of composites with residual stresses, imperfect interfaces, and traction-loaded cracks," *Compos. Sci. Technol.*, 2001.

[146] M. O. W. Richardson and M. J. Wisheart, "Review of low-velocity impact properties of composite materials," *Compos. Part A Appl. Sci. Manuf.*, vol. 27, no. 12, pp. 1123–1131, 1996.

[147] S. Abrate, "Matrix cracking in laminated composites: A review," *Compos. Eng.*, vol. 1, no. 6, pp. 337–353, Jan. 1991.

[148] W. J. Cantwell and J. Morton, "The impact resistance of composite materials — a review," *Composites*, vol. 22, no. 5, pp. 347–362, 1991.

[149] Olsson R., "A review of impact experiments at FFA during 1986 to 1998."

[150] R. Olsson and L. Asp, "A review of some key developments in the analysis of the effects of impact upon composite structures," *ASTM Spec. …*, 2001.

[151] D. Liu, "Impact-induced delamination—a view of bending stiffness mismatching," *J. Compos. Mater.*, 1988.

[152] N. Rilo and L. Ferreira, "Experimental study of low-velocity impacts on glass-epoxy laminated composite plates," *Int. J. Mech. Mater. …*, 2008.

[153] C. Cho and G. Zhao, "Effects of Geometric and Material Factors on Mechanical Response of Laminated composites due to low velocity impact," *J. Compos. Mater.*, 2002.

[154] Z. Aslan, R. Karakuzu, and B. Okutan, "The response of laminated composite plates under low-velocity impact loading," *Compos. Struct.*, 2003.

[155] M. Aktaş, C. Atas, B. İçten, and R. Karakuzu, "An experimental investigation of the impact response of composite laminates," *Compos. Struct.*, 2009.

[156] D. Liu and L. Malvern, "Matrix cracking in impacted glass/epoxy plates," *J. Compos. Mater.*, 1987.

[157] E. Nilsson, "Residual Strength Prediction of Composite Laminates Containing Impact Damage," *Interface*, 2005.

[158] E. Guynn and T. O'Brien, "The influence of lay-up and thickness on composite impact damage and compression strength," *… 26th Struct. Struct. Dyn. Mater. …*, 1985.

[159] H. Y. Choi, H.-Y. T. Wu, and F.-K. Chang, "A New Approach toward Understanding Damage Mechanisms and Mechanics of Laminated Composites Due to Low-Velocity Impact: Part IIâ€"Analysis," *J. Compos. Mater.*, vol. 25, no. 8, pp. 1012–1038, Jan. 1991.

[160] C. Jih and C. Sun, "Prediction of delamination in composite laminates

subjected to low velocity impact," *J. Compos. Mater.*, 1993.

[161] Sjögren A, "Fractographic characterization of impact damage in carbon fiber/epoxy laminates," 1999.

[162] G. Dorey, "Impact damage in composites—development, consequences and prevention," *Sixth Int. Conf. Compos. Mater. …*, 1987.

[163] W. J. Cantwell, P. T. Curtis, and J. Morton, "An assessment of the impact performance of CFRP reinforced with high-strain carbon fibres," *Compos. Sci. Technol.*, vol. 25, no. 2, pp. 133–148, 1986.

[164] S. Abrate, "Impact on laminated composite materials," *Appl. Mech. Rev.*, vol. 44, no. 4, pp. 155–190, 1991.

[165] M. Mitrovic, H. T. Hahn, G. P. Carman, and P. Shyprykevich, "Effect of loading parameters on the fatigue behavior of impact damaged composite laminates," *Compos. Sci. Technol.*, vol. 59, no. 14, pp. 2059–2078, 1999.

[166] W. Elber, "Failure Mechanics in Low-Velocity Impacts on Thin Composite Plates.," 1983.

[167] V. L. Coenen, "Auxetic Composite Laminates with Enhanced Impact Resistance," University of Bolton, 2001.

[168] Hexcel Composites Publication, "Data Sheet HexPly® 8552 Hexcel Carbon Fibre Products," FTA 072e, 2013.

[169] "ASTM International, 'Standard Test Methods for Properties of Continuous Filament Carbon and Graphite Fiber Tows' ASTM D4018 - 11." .

[170] Q. Chandhuri, J. and Jang, "Effect of Special Orientation on the Fracture Behaviour of Graphite/Epoxy Laminates," *Proc. Am. Soc. Comps. 3rd Tech. Conf*, p. 701, 1980.

[171] J. P. Donoghue, K. L. Alderson, and K. E. Evans, "The fracture toughness of composite laminates with a negative Poisson's ratio," *Phys. Status Solidi Basic Res.*, vol. 246, no. 9, pp. 2011–2017, 2009.

[172] "BS EN ISO 527-4:1997, BS 2782-3:Method 326F:1997 - Plastics. Determination of tensile properties. Test conditions for isotropic and orthotropic fibre-reinforced plastic composites – BSI British Standards." .

[173] "EN 2561-1990 aerospace series. carbon-thermosetting resin unidirectional laminates. tensile test parallel to the fibre direction." .

[174] V. L. Coenen and K. L. Alderson, "Mechanisms of failure in the static indentation resistance of auxetic carbon fibre laminates," *Phys. status solidi*, vol. 248, no. 1, pp. 66–72, 2011.

[175] "ASTM International, 'Standard test method for Measuring the Damage Resistance of a Fibre-Reinforced Polymer Matrix Composite to a Drop-

Weight Impact Event' ASTM D7136/7136M - 12." .

[176] G. R. Fowles, G. E. Duvall, J. Asay, P. Bellamy, F. Feistmann, D. Grady, T. Michaels, and R. Mitchell, "Gas Gun for Impact Studies," *Rev. Sci. Instrum.*, vol. 41, no. 7, 1970.

[177] "ASTM International, 'Standard test method for Compressive Residual Strength Properties of Damaged Polymer Matrix Composite plates' ASTM D7137/D7137M - 12." .

[178] X.-F. Wu, G. Ghoshal, M. Kartashov, Z. Aslan, J. A. Turner, and Y. A. Dzenis, "Experimental characterization of the impact-damage tolerance of a cross-ply graphite-fiber/epoxy laminate," *Polym. Compos.*, vol. 29, no. 5, pp. 534–543, 2008.

[179] V. Kostopoulos, A. Baltopoulos, P. Karapappas, A. Vavouliotis, and A. Paipetis, "Impact and after-impact properties of carbon fibre reinforced composites enhanced with multi-wall carbon nanotubes," *Compos. Sci. Technol.*, vol. 70, no. 4, pp. 553–563, 2010.

[180] K. N. Shivakumar, W. Elber, and W. Illg, "Prediction of Impact Force and Duration Due to Low-Velocity Impact on Circular Composite Laminates," *J. Appl. Mech.*, vol. 52, no. 3, p. 674, Sep. 1985.

[181] W. De Morais, S. N. Monteiro, J. R. M. d'Almeida, and W. A. De Morais, "Evaluation of repeated low energy impact damage in carbon–epoxy composite materials," *Compos. Struct.*, vol. 67, no. 3, pp. 307–315, 2005.

[182] G. Caprino, "Residual Strength Prediction of Impacted CFRP Laminates," *J. Compos. Mater.*, vol. 18, no. 6, pp. 508–518, Jan. 1984.

[183] G. Belingardi and R. Vadori, "Low velocity impact tests of laminate glass-fiber-epoxy matrix composite material plates," *Int. J. Impact Eng.*, vol. 27, no. 2, pp. 213–229, 2002.

[184] Z. Zou, S. R. Reid, S. Li, and P. D. Soden, "Application of a delamination model to laminated composite structures," *Compos. Struct.*, vol. 56, no. 4, pp. 375–389, 2002.

[185] K. L. Alderson and K. E. Evans, "Dynamic analysis of filament wound pipes undergoing low velocity transverse impact," *Compos. Sci. Technol.*, vol. 45, no. 1, pp. 17–22, 1992.

[186] S. Abrate, *Impact engineering of composite structures*. 2011.

[187] A. Christoforou, S. Swanson, and B. S. Christoforou AP, Swanson SR, Ventrello SC, "Impact damage in carbon/epoxy composite cylinders," *32nd Int. SAMPE Symp.*, pp. 964–73, 1987.

[188] G. Minak, S. Abrate, D. Ghelli, R. Panciroli, and A. Zucchelli, "Residual torsional strength after impact of CFRP tubes," *Compos. Part B …*, vol. 41,

no. 8, pp. 637–645, 2010.

[189] Michael Lindell, "The Laminator." 1997.

[190] U. Farooq and P. Myler, "Finite element simulation of carbon fibre-reinforced composite laminates subjected to low velocity impact using damage induced static load-deflection methodology," *Thin-Walled Struct.*, vol. 97, pp. 63–73, Dec. 2015.

[191] U. Farooq and P. Myler, "Efficient computational modelling of carbon fibre reinforced laminated composite panels subjected to low velocity drop-weight impact," *Mater. Des.*, vol. 54, pp. 43–56, Feb. 2014.

[192] U. Farooq, P. Myler, and B. Kandola, "Prediction of barely visible impact damage in composite panels subjected to blunt nose impact.," Jan. 2009.

[193] U. Farooq and P. Myler, "Prediction of load threshold of fibre-reinforced laminated composite panels subjected to low velocity drop-weight impact using efficient data filtering techniques," *Results Phys.*, vol. 5, pp. 206–221, 2015.

[194] U. Farooq and P. Myler, "Finite element simulation of buckling-induced failure of carbon fibre-reinforced laminated composite panels embedded with damage zones," *Acta Astronaut.*, vol. 115, pp. 314–329, Oct. 2015.

[195] V. L. Coenen and K. L. Alderson, "The effect of indentor geometry on the indentation resistance of auxetic carbon fibre laminates."

[196] W. Miller, P. B. Hook, C. W. Smith, X. Wang, and K. E. Evans, "The manufacture and characterisation of a novel, low modulus, negative Poisson's ratio composite," *Compos. Sci. Technol.*, vol. 69, no. 5, pp. 651–655, 2009.

[197] W. Zhang and K. E. Evans, "Design of laminates with specified mechanical-properties," in *2nd international conf on computer aided design in composite material technology*, 1990, pp. 69–81.

[198] K. L. Alderson, A. Alderson, P. J. Davies, G. Smart, N. Ravirala, and G. Simkins, "The effect of processing parameters on the mechanical properties of auxetic polymeric fibers," *J. Mater. Sci.*, vol. 42, no. 19, pp. 7991–8000, 2007.

[199] I. M. Ward and J. Sweeney, *Mechanical Properties of Solid Polymers*. Chichester, UK: John Wiley & Sons, Ltd, 2012.

[200] E. H. Harkati, A. Bezazi, W. Boukharouba, and F. Scarpa, "Influence of carbon fibre on the through-the-thickness NPR behaviour of composite laminates," *Phys. status solidi*, vol. 246, no. 9, pp. 2111–2117, 2009.

[201] A. Spadoni, "An Isotropic Auxetic Structural Network with Limited Shear Stiffness," 2011.

[202] A. Rahmane, A. Bezazi, N. Ouelaa, and F. Scarpa, “Stacking sequence effect over the modal damping ratios in auxetic composite laminates.”